The elastic and nonlinear acoustic vibrational properties of vitreous SiO2 and rare earth phosphate glasses

Hassan, Senin Bin

Award date:
1994

Awarding institution:
University of Bath

THE ELASTIC AND NONLINEAR ACOUSTIC VIBRATIONAL PROPERTIES OF VITREOUS SiO_2 AND RARE EARTH PHOSPHATE GLASSES

submitted by

SENIN BIN HASSAN

for the degree of PhD

of the University of Bath

1994

Copyright

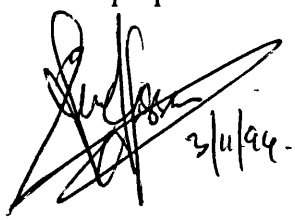

ProQuest LLC
789 East Eisenhower Parkway
P.O. Box 1346
Ann Arbor, MI 48106-1346

ACKNOWLEDGEMENTS

It is a great pleasure to acknowledge the guidance and encouragement of my supervisor Prof. George A. Saunders. I have been fortunate to have the opportunity at times to work closely with him and share his knowledge of glasses. His way of guiding, leading by doing, is the best source of advice and is the most effective.

I would also like to express my thanks to Dr. P.J. Ford for advice on the manuscript and to Dr. Q. Wang for assistance in the experiments. I am grateful to Mr. Bob Draper, for help in building the coating jig for indium bonding, during the preparation of glasses and advice on the manuscript; to Mr. E. Lambson, for technical assistance and to Mrs. W. Lambson, for cutting and polishing the samples. I would also like to thank Mr. H. Perrott and Dr. G. Love (Centre for Electron Optical Studies) for technical assistance during sample analysis.

Special thanks must go to Prof. G. Carini (University of Messina, Italy) who allowed me to use his data, Dr. J. Keartland (University of Witwatersrand, South Africa), Prof. B. Rainford (University of Southampton), Dr. M. Cankurtaran (Haceteppe University, Turkey) and to Dr. H.A.A. Sidek (University Pertanian Malaysia) for assistance and useful discussions. It is also my pleasure to thank my colleagues in the Solid State Group for their friendship and assistance.

I am very grateful to the Government of Malaysia and University Pertanian Malaysia for financial support and study leave. Special thanks are also to Dr. S. Bartlett (Johnson Matthey Technology Centre) and Mr. S. Takel (DRA Maritime Division) for support of the programme of work on rare earth phosphate glasses.

My great appreciation goes to my wife, Juliana Justin and daughter, Faridah for sharing this adventure with me. They have endured the hardships necessary for me to complete this work. Without their loving patience, this research would have been much more difficult to carry out. My father and relatives in Malaysia have given me endless love, my gratitude to them is beyond words.

ABSTRACT

Phosphate glasses containing high concentrations of rare earths: Ce, Pr, Nd, Eu, Gd, Tb, Dy, Ho and Er have been made. These glasses are transparent and have a variety of colours. The compositions of these glasses, determined using electron probe microanalysis, are close to that corresponding metaphosphate.

To provide an overall picture of the acoustic vibrational properties of these glasses, measurements have been made of their ultrasonic wave velocities and attenuation as a function of temperature and pressure. At low temperatures, the velocities continue to increase and the attenuation is characterised by a broad peak, properties which are consistent with thermally activated relaxations of two-level systems. The ultrasonic wave velocities propagated in Eu^{3+}, Tb^{3+}, Dy^{3+}, Ho^{3+} and Er^{3+} phosphate glasses decrease under pressure: the hydrostatic pressure derivatives $(\partial C_{IJ}^{S}/\partial P)_{T,P=0}$ of the second order elastic stiffnesses C_{IJ}^{S} and $(\partial B^{S}/\partial P)_{T,P=0}$ of the bulk modulus B^{S} are negative. When compressed, these glasses, like vitreous Sm^{3+} phosphates and SiO_2, show the interesting property of becoming easier to squeeze. However, glasses containing La^{3+}, Ce^{4+}, Pr^{3+} and Nd^{3+} display normal elastic behaviour under pressure; Gd^{3+} phosphate glasses display intermediate effects.

Measurements, using a pulse superposition technique, of the effect of uniaxial stress on ultrasonic wave velocities have been used to determine the third order elastic stiffness tensor components C_{IJK} (TOEC) of vitreous SiO_2 and Sm^{3+}, Eu^{3+}, Gd^{3+} and Tb^{3+} phosphate glasses between 77K and 293K.

For vitreous SiO_2, the TOEC (except the smallest C_{456}) are anomalously positive: consistent with the negative hydrostatic pressure derivatives $(\partial C_{IJ}^{S}/\partial P)_{T,P=0}$. The acoustic mode Grüneisen parameters are negative: application of pressure induces

a decrease in the long-wavelength phonon frequencies. The TOEC increase as the temperature is reduced: pressure-induced acoustic mode softening becomes enhanced at lower temperatures. $(\partial C_{11}{}^{S}/\partial P)_{T,P=0}$, is larger than $(\partial C_{44}{}^{S}/\partial P)_{T,P=0}$ over the whole temperature range, and the longitudinal Grüneisen parameter, $|\gamma_L|$, is larger than that, $|\gamma_S|$, of the shear wave: the longitudinal mode softens more with pressure than the shear mode. The mean Grüneisen parameter γ^{el} increases to a larger negative value than previously suspected on the basis of the assumption of temperature independent TOEC.

For Sm^{3+} and Eu^{3+} glasses, the TOEC are mostly positive, for La^{3+} and Nd^{3+} glasses they are mostly negative. Intermediate behaviour is shown by Gd^{3+} and Tb^{3+} glasses. Strong temperature dependences of the C_{IJK} and $(\partial C_{IJ}{}^{S}/\partial P)_{T,P=0}$ have been observed in Sm^{3+} and Eu^{3+} phosphate glasses. As the temperature is reduced, the pressure-induced mode softening becomes enhanced. Similar, but less pronounced softening effects, are displayed by Gd^{3+} and Tb^{3+} phosphate glasses.

CONTENTS

CHAPTER 1

RESEARCH OVERVIEW

1.1 INTRODUCTION

The properties of glasses containing rare earth ions are of considerable interest for applications in optical data transmission, detection, sensing and laser technologies. Certain trivalent lanthanide ions such as Nd^{3+}, Er^{3+}, Ho^{3+} and Tm^{3+} in phosphate glasses are predominantly used as active ions in glass laser materials (Weber 1990, Marion and Weber 1991). Rare earth phosphate glasses normally have strong and sharp electronic absorptions in the ultraviolet to near infrared region and thus they can be useful as fibre lasers and optical signal couplers (Sun and Risen 1985). Aluminophosphate glasses containing low concentrations of Nd^{3+} ions are used in high power laser fusion facilities (Jiang et al. 1986, Toratani et al. 1987). A lead-iron phosphate glass has been found to be suitable as a stable medium for storage of high-level nuclear waste (Sales and Boatner 1984). In addition, phosphate glasses doped with silver have high ionic conductivities and find application in batteries (Ravaine 1985).

Despite a number of investigations on the various physical properties of binary phosphate glasses containing a variety of different modifying ions during the last twenty years, the information on the elastic, anelastic and nonlinear acoustic properties are limited. Most work has been concentrated on electrical and optical properties (see for example, Harani and Hogarth 1986, Morgan et al. 1987, Ananthamohan and Hogarth 1990, Arzeian and Hogarth 1991, Nga et al. 1991). Not much previous work was done on their elastic properties under pressure and temperature which are necessary parameters for designing solid state devices and other applications.

As part of a comprehensive plan to study the properties of rare earth phosphate glasses, this thesis reports an ultrasonic study as a function of temperature, pressure and frequency carried out on these glasses. These ultrasonic measurements provide

details of the elastic and nonlinear acoustic vibrational properties such as ultrasonic wave velocities, the ultrasonic attenuation, the second order elastic stiffness tensor components C_{IJ}^S (SOEC), the temperature dependences of the SOEC, the hydrostatic pressure derivatives $(\partial C_{IJ}^S/\partial P)_{T,P=0}$ of the SOEC C_{IJ}^S and $(\partial B^S/\partial P)_{T,P=0}$ of the bulk modulus B^S. To quantify further the anharmonicity of the atomic vibrations of these glasses, the long-wavelength acoustic mode Grüneisen parameters and higher order elasticity such as the third order elastic stiffness tensor components (TOEC) C_{IJK} have been evaluated. The main objective is to gain a more complete picture of the acoustic vibrational properties of phosphate glasses down to much lower temperatures than studied previously. Before the ultrasonic studies on phosphate glasses were made, the elastic and nonlinear acoustic vibrational properties of vitreous SiO_2 were first examined from room temperature (293K) down to 77K. Vitreous SiO_2 was chosen as a reference material because of its established anomalous elastic and thermal properties and its great technological importance. However, its well-known remarkable acoustic mode softening has not been studied previously at low temperatures and the new information gained about this glass is also presented here.

This chapter provides a brief overview of the ultrasonic wave propagation in binary rare earth phosphate glasses carried out during this research. The relationship between elastic and nonlinear acoustic properties and vibrational anharmonicity of the inter-atomic forces will be explained first. The soft mode behaviour, a behaviour which is associated with the decrease of the ultrasonic wave velocities under pressure, an extraordinary and interesting behaviour, which initially motivated this study will then be described briefly. The observations of the anomalies in the acoustic and thermal behaviour of glasses at low temperatures, which stand at the forefront of glass studies will then be described. Finally, the organisation of the chapters in this thesis will be presented.

1.2 ELASTIC AND NONLINEAR ACOUSTIC PROPERTIES OF AN ISOTROPIC SOLID

In the elastic region, the mechanical properties represented by Hooke's law are given by the elastic stiffness which is based on the linear relationship between stress and strain for small deformations. The elastic stiffness is related to the interatomic binding forces which cause long-range attraction and short-range repulsion. In theoretical investigations of the acoustic vibrational properties of solids, an elastic stiffness defines the slope of an acoustic branch of the phonon dispersion curves near the long-wavelength zone centre. In the long-wavelength limit ($\lambda \gg a$, where a is atomic spacing), a solid material can be treated as continuum media for elastic wave propagation.

For the development of the opto-electronic devices utilising phosphate glasses, there is a need to know the higher order elasticity and their temperature dependences. This investigation leads us to the determination of the vibrational anharmonicity, a concept related to the nonlinearity of interatomic forces with respect to atomic displacements. When nonlinear terms come into play, Hooke's law is no longer strictly obeyed.

In general a solid medium is nonlinear. Thermal expansion and heat conduction, the temperature and pressure dependences of the elastic stiffnesses all depend upon either anharmonic theory for their microscopic description or nonlinear theory for their macroscopic description. The description of nonlinearity is made in terms of higher order elastic stiffness tensor components which are the primary interest of the present study. The TOEC play an important role in accounting for anharmonic and nonlinear elastic properties of solids and in some situations they alone suffice to describe the nonlinear behaviour. Using the TOEC data, the hydrostatic pressure derivatives of the SOEC can be determined and consequently can be used to analyse the properties such as the volume compression. For more detailed interpretations, fourth order elastic

stiffness tensor components (FOEC) C_{IJKL}, or even higher order, elastic stiffnesses need to be evaluated.

The available TOEC data for the isotropic materials are limited to Pyrex glass (Hughes and Kelly 1953), vitreous SiO_2 (Bogardus 1965, Shull 1969), a-As (Brassington et al. 1980), a-As_2S_3 (Brassington et al. 1981a), a-TeO_2 (Benbattouche et al. 1989), and for the only phosphate glass containing iron (Brassington et al. 1981b). Most of these data are at or around room temperature (293K). The temperature dependences of the complete sets of the TOEC have not been measured down to low temperatures. It is the main aim of the present work to fill this gap.

The temperature dependences of the TOEC provide important additional knowledge of the anharmonicity of lattice vibrations, especially at low temperatures. The nonlinear elastic properties are useful in determining the thermal expansion coefficients through the Grüneisen parameters of the long-wavelength components which can be determined from the effect of pressure. Thermal expansion is caused by the fact that lattice vibration increases as the temperature rises. Because of the anharmonic terms, the mean positions of the atoms change. As a result, the whole solid expands to the volume at which the free energy is minimum. Hence all the mode frequencies change in proportion to the change in volume. These values can then be used to calculate the shift of the mode energies with compression and characterize the acoustic mode vibrational anharmonicity which quantifies the strain dependences of the lattice vibrational frequencies.

1.3 DETERMINATION OF THE TOEC USING AN ULTRASONIC METHOD

In general, the experimental determinations of the temperature dependences of the TOEC are sparse because measuring the pressure dependences of ultrasonic wave velocities as a function of temperature is rather difficult, especially at low temperatures. Using ultrasonic techniques, the normal practice used to obtain a complete set of TOEC

is to measure the effects of hydrostatic pressure and uniaxial stress on the velocity of ultrasonic waves propagated in the sample. Emphasis is usually placed on making as many measurements under hydrostatic pressure as possible because the effects induced are larger, and easier to measure with accuracy when compared to those obtained from the application of uniaxial stress. However, hydrostatic pressure measurements have been restricted between 253K and 400K; at low temperatures the liquids used as pressure transmitting media freeze, making it difficult to measure the effects of pressure on ultrasonic wave velocity or even to ensure that the applied pressure is truly hydrostatic. Although it is possible to use gaseous systems to apply hydrostatic pressure, this is best avoided, for safety reasons. This presented an obstacle in determining the TOEC down to 77K. However, it is possible to obtain all three independent components of the TOEC for a glass by making ultrasonic wave velocity measurements solely under uniaxial stress (Prof. G. A. Saunders, private communication), a possibility which does not seem to have been explored before. This method has proved to be the best experimental approach that can be used to obtain the complete sets of TOEC which are needed to quantify the nonlinear acoustic properties at much lower temperatures than before. This approach has been used in the determination of the complete sets TOEC of rare earth phosphate glasses and for vitreous SiO_2 at lower temperatures.

1.4 SOFT MODE BEHAVIOUR IN GLASSES

In general the effects of pressure on the elastic behaviour of glasses can be divided into two distinct categories.

The first category of glasses, whose elastic behaviour under pressure is more normal (that is, the ultrasonic wave velocities increase when hydrostatic pressure is applied) includes: amorphous arsenic (Brassington et al. 1980) and As_2S_3 (Brassington et al. 1981a), fluorozirconate glass (Brassington et al. 1981c), vitreous TeO_2 (Benbattouche et al. 1989) and also phosphate glasses containing iron (Brassington et al.

1981b), molybdenum (Comins et al. 1987) and lanthanum (Sidek et al. 1988). The hydrostatic pressure derivatives $(\partial C_{11}^S/\partial P)_{T,P=0}$ and $(\partial B^S/\partial P)_{T,P=0}$ are positive. These glasses show normal behaviour in the sense that the long-wavelength acoustic modes stiffen under high pressures.

In the second category of glasses, for example Pyrex glass (Hughes and Kelly 1953), fused silica (Bogardus 1965, Shull 1969) and samarium phosphate glasses (Mierzejewski et al. 1988a,b, Sidek et al. 1988), the ultrasonic wave velocities are reduced under pressure, a feature now known to be consistent with soft mode behaviour (Brassington and Saunders 1982). Thus, these glasses show anomalous elastic behaviour under pressure; the hydrostatic pressure derivatives $(\partial C_{11}^S/\partial P)_{T,P=0}$ and $(\partial C_{44}^S/\partial P)_{T,P=0}$ of the elastic stiffnesses are negative: the long-wavelength acoustic mode Grüneisen parameters are negative. Hence the long-wavelength acoustic phonons soften under pressure. The concept of long-wavelength acoustic mode softening in glasses is now well established. Anomalous pressure dependences of ultrasonic wave velocities are also observed in crystalline solids which have soft acoustic phonons modes. Soft mode behaviour was observed in crystalline SmS by Tu Hailing et al. (1984) in which material it is associated with valence instability.

The physical origin of the diversity in the behaviour of acoustic mode vibrational anharmonicity in glasses is still not fully understood. In the case of samarium phosphate glasses, it was speculated previously that the soft mode behaviour is related to the valence instability (Mierzejewski et al. 1988a,b, Sidek et al. 1988) similar to that shown by crystalline SmS (Tu Hailing et al. 1984). However, this is not the case for samarium phosphate glasses (Farok et al. 1992); mixed valence is not the cause of the soft mode behaviour. Another possible source is the motion of the bridging oxygens; this has been postulated for vitreous SiO_2 (Sato and Anderson 1980). The difficulty explaining the soft mode behaviour in samarium phosphate glasses has motivated us to carry out further

comparative investigation with other vitreous phosphates which contain different rare earth ions as network modifiers. It is also the aim to establish where rare earth phosphate glasses fit in the two categories.

1.5 ANOMALOUS VIBRATIONAL PROPERTIES AT LOW TEMPERATURES

Anomalies in a wide range of physical properties at low temperatures due to frozen-in supplementary degrees of freedom are a dominant feature of glasses. The most characteristic features are the linear behaviour of the specific heat and the T^2 dependence of the thermal conductivity in the temperature region below 1K, which are well accounted for by the phenomenological tunnelling model of two-level systems (Anderson et al. 1972, Phillips 1972).

The same effect of the topological disorder in amorphous structures is observed by the introduction of supplementary degrees of freedom, giving rise to anomalies in the thermal (Pohl 1981), acoustic, dielectric (Hunklinger and Schickfus 1981) and optical (Jäckle 1981) properties. This excess of degrees of freedom is normally attributed to the localised structural defects or particles which have a different mobility from the rest of the host structure and which are subjected to thermally activated local motion at high temperatures and to tunnelling motions at very low temperatures. Besides the acoustic phonons, the existence of additional vibrational states must be included in order to explain the anomalous excess of specific heat and the plateau in the thermal conductivity in the region between 1 and 30K.

It is likely that there is a common origin for these effects together with those observed in low-frequency Raman (Nemanich 1977, Carini et al. 1994b) and inelastic neutron scattering spectra (Buchenau et al. 1988, Malinovsky et al. 1990). Several models have been proposed to account for the universal form of the excess of density-of-vibrational states; the two most attractive and general are the phonon-fracton

cross-over model (Alexander and Orbach 1982, Orbach 1986) and the soft-potential model (Karpov et al. 1983, Parshin 1993).

Neutron scattering measurements support a common interpretation of the low-frequency vibrational states in vitreous SiO_2 arising from local motions of coupled SiO_4 tetrahedra (Buchenau et al. 1988). Whether this finding extends to rare earth phosphate glasses is still under question. Since the addition of modifier ions to phosphate glasses alters the coupling constant between the PO_4 tetrahedra, it can be expected to influence the density of relaxing particles: a major source of ultrasonic attenuation. It is possible that eventual identification of the microscopic groups involved in local motions could come from study of the glassy systems in which the number or the kind of structural units present in the network, is altered by varying the composition and the type of modified ion (in the present case those in the rare earth series).

1.6 CHAPTER ORGANISATION

The thesis is organized as follows. Chapter 2 describes some aspects of glasses which include their structure and the universal anomalous properties at low temperatures. The descriptions of two-level systems, the soft-potential model and phonon-fracton cross-over model are presented in that Chapter. Chapter 3 describes the theoretical aspects of elastic properties and nonlinear acoustic properties of an isotropic material. The related expressions that are required for determination of the SOEC and TOEC are given together with the expressions for the hydrostatic pressure derivatives and the long-wavelength acoustic mode Grüneisen parameters. Chapter 4 describes the production of a large number of rare earth phosphate glasses using a high temperature programmable electric furnace.

Chapter 5 is concerned with the ultrasonic pulse echo techniques. The pulse echo overlap technique has been used to determine the absolute value and the hydrostatic pressure dependences of the ultrasonic wave velocities, whereas the pulse superposition

technique determines the uniaxial stress effects on the ultrasonic wave velocities.

The discussion on the experimental results begins in Chapter 6, with a description of the elastic and nonlinear acoustic vibrational properties of vitreous SiO_2 over the temperature range between 77K to 293K. In Chapter 7, the elastic properties of rare earth phosphate glasses such as the density, ultrasonic wave velocities, SOEC and other physical properties such as bulk modulus, fractal dimension and Debye temperature are given. The temperature dependences of the ultrasonic wave velocities and attenuation propagated through the various rare earth phosphate glasses are presented and interpreted in terms of a thermally activated relaxation process of two-level systems.

Chapter 8 presents complete sets of the TOEC and their temperature dependences for various binary rare earth phosphate glasses. The hydrostatic pressure derivatives $(\partial C_{IJ}^{S}/\partial P)_{T,P=0}$ of the SOEC and $(\partial B^{S}/\partial P)_{T,P=0}$ of the bulk modulus at room temperature, and their temperature dependences are given. The compressions $V(P)/V_0$ extrapolated to high pressures are estimated at room temperature and 77K, using the measured ultrasonic data. The long-wavelength acoustic mode Grüneisen parameters, which quantify the vibrational anharmonicity of these glasses, are presented. Included, as a natural addition in Chapter 9, to the results obtained during the present research, are the results and interpretation of the investigation on the different influences of lanthanide modifiers in phosphate glasses (much of that work is being carried out at the University of Messina, Italy). In Chapter 10, the conclusions of the present findings of the elastic and nonlinear acoustic vibrational properties of vitreous SiO_2 and rare earth phosphate glasses are presented, also in this chapter, work currently in progress and ideas for future investigation are indicated.

CHAPTER 2

THE STRUCTURES AND VIBRATIONAL PROPERTIES OF GLASSES

2.1 INTRODUCTION

The term glass can be applied to a number of amorphous solids that can be manufactured by quenching from the melts sufficiently fast to avoid crystallization. This process leads to non-crystalline solids where the structural disorder of the liquid is retained. The absence of long range order or periodicity in glasses has made it an interesting area for investigating the atomic arrangement and molecular interactions.

Most of the commonly used glasses are silicates. Traditional glass remains an essential material for architecture, transport, packaging and lighting. More technological glasses have been developed for use in optics, electronics and optoelectronics (such as lasers, optical fibres, integrated micro-electronics, energy conversion devices, etc) and also in medicine. Phosphate glasses find applications, such as glass lasers (Weber 1990, Marion and Weber 1991), optical fibres etc (Stokowski et al. 1980). In these applications several properties such as luminescence of rare earth ions and refractive indexes in the phosphate glasses, which are higher than silicate glasses, are utilized. These properties can be associated with local electronic states of structural units present in the glasses.

Many glasses of different chemical composition such as dielectric, semiconducting and metallic glasses are known. Glassy SiO_2, B_2O_3, P_2O_5 and binary rare earth phosphate glasses R_2O_3-P_2O_5, are examples of dielectric glasses. Semiconducting glasses include chalcogenide glasses, As_2S_3, GeSe and *a*-Se. There are a large number of glassy metals, which are complex compounds of metals and non-metals.

During the last two decades, numerous experimental investigations of the different properties of glasses have been performed. One result of this work has been the discovery

of a set of universal properties that are almost independent of specific chemical composition of the glass. These properties have been called anomalous: they include low-temperature specific heat, thermal conductivity, thermal expansion and also the acoustic properties (Figure 2.1). Early attempts to provide a theoretical explanation of the experimentally observed anomalous properties of glasses failed, and progress was achieved only after the introduction of important postulates concerning localised atomic and electronic states, proposed by Anderson et al. (1972) and Phillips (1972). They assume that there exist two-level systems (TLS) associated with local tunnelling atomic states in double-well potentials. However, above about 1K, properties such as the plateau in the thermal conductivity and the peak in the temperature dependence of $C_p(T)/T^3$, cannot be accounted for by the tunnelling model. Additional low-frequency excitations, which co-exist with sound waves, contribute a large excess heat capacity in the temperature range 2 to 20K (Buchenau et al. 1986, Carini et al. 1994b). Several theories have been proposed to explain the anomalous behaviour in this region. One of the more successful and topical phenomenological approaches is a development of the soft-potential model (Karpov et al. 1983) which augments the tunnelling model by a high density of soft anharmonic localised vibrational modes (Buchenau et al. 1992, Gil et al. 1993). At about the same time, Alexander and Orbach (1982) assumed that the glasses are fractal and proposed that a band of fractons - the localised vibrations of a fractal object - is responsible for the plateau. It is feasible that strong anharmonic interactions of acoustic phonons with such localised modes might markedly affect the vibrational anharmonicity of the long-wavelength acoustic waves and hence the higher order elastic stiffness tensor components.

In the present chapter, a brief description of the atomic structure of vitreous SiO_2 and phosphate glasses will be given, as well as the vibrational properties of glasses at low temperatures. Vitreous SiO_2 has been chosen as a reference because it provides the

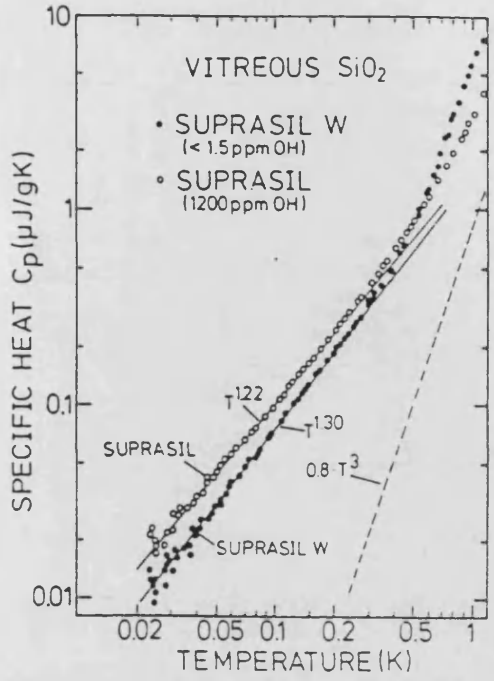

(a)

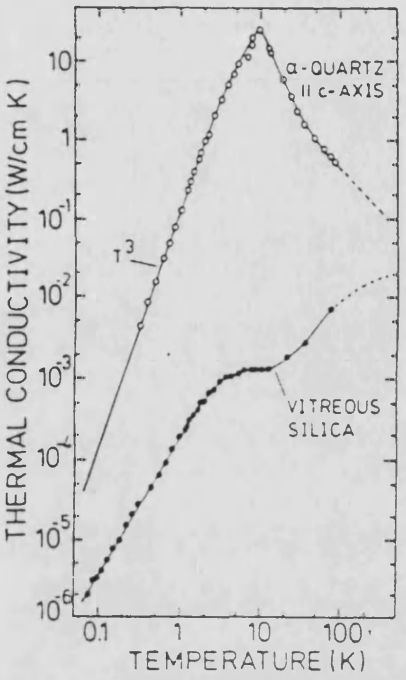

(b)

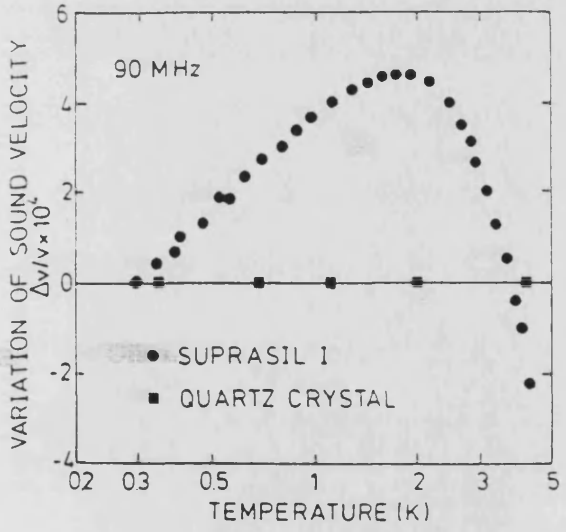

(c)

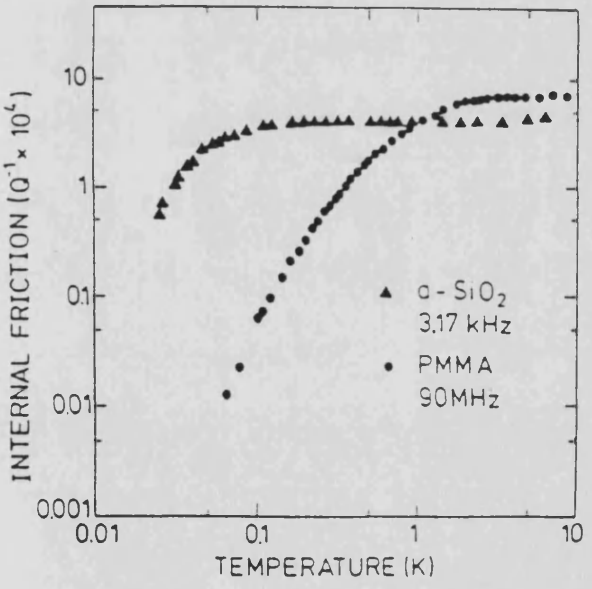

(d)

Figure 2.1. (a) Specific heat (after Lasjaunias et al. 1975), (b) thermal conductivity (after Zeller and Pohl 1971), (c) relative variation of longitudinal sound velocity (after Hunklinger 1977) and (d) internal friction (after Federle and Hunklinger 1984) as a function of temperature for vitreous SiO_2.

largest amount of experimental data on which to discuss the theoretical explanations. It is planned to use the description of the tunnelling model of two-level systems in discussing the anomalous acoustic behaviour in phosphate glasses as a function temperature and pressure.

2.2 THE MELT - GLASS TRANSITION

The difference between a glass and the corresponding liquid or supercooled liquid, may be appropriately demonstrated by a volume-temperature relationship of the type shown in Figure 2.2. On cooling from a temperature **T**, a liquid which normally does not form a glass to the melting point $\mathbf{T_m}$ of the crystal form, the path **a** is followed. By contrast, in the absence of crystallization, the volume-temperature relationship may be described by the path **b** to give a supercooled liquid. On further cooling to a glass transition temperature $\mathbf{T_g}$, the viscosity of the supercooled liquid reaches 10^{13} -10^{14} poise, a transition of state seems to occur. Below this region the non-crystalline material is termed a glass and path **c** is followed.

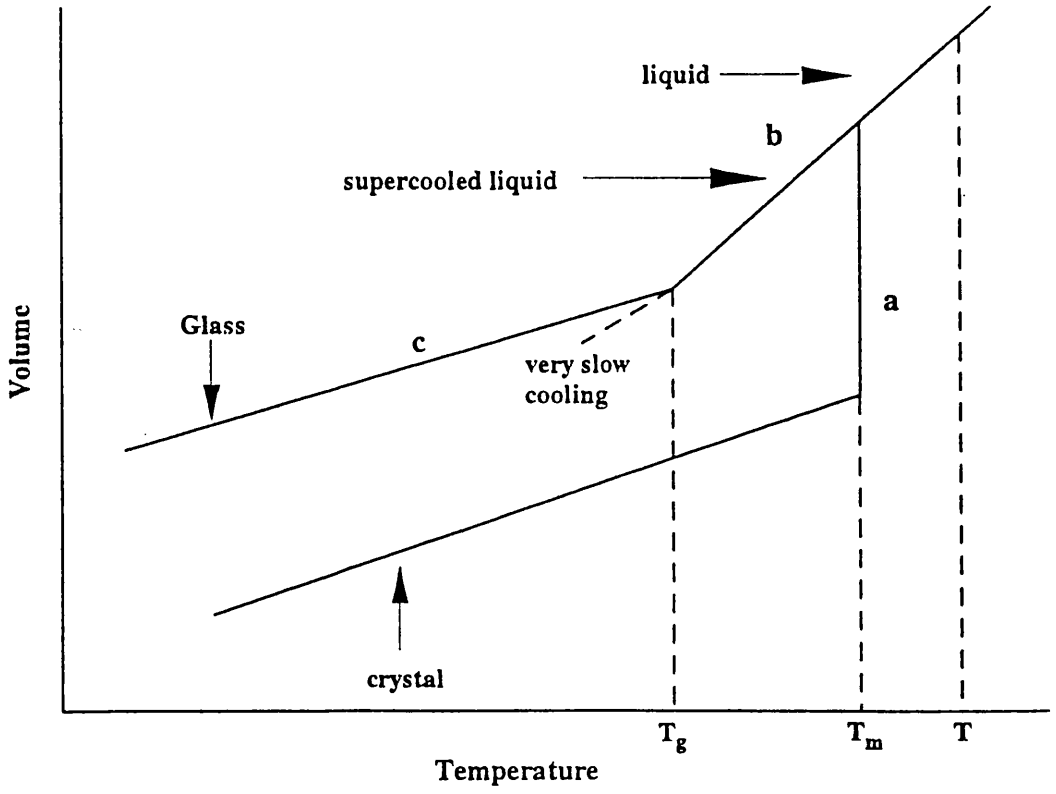

Figure 2.2. Volume-Temperature characteristics of a glass forming system.

2.3 THE STRUCTURE OF GLASSES

It is more difficult to determine the precise structure of a glass than that of a crystalline solid. Much work has been carried out on the investigation of the structure of glasses during the past fifty years, by X-ray and neutron diffraction, and by spectroscopic methods. Infrared and Raman spectroscopy have been widely used to probe the nature of the bond between the metal cation and its surrounding oxygens. In addition, new methods have also been developed for use as a probe to investigate the structure of glasses. Computer modelling methods (Soules 1990) and the discrete variational-Xα (DV-Xα) cluster method (Kowada et al. 1993) have been used recently to study the electronic states and chemical bonding in phosphate glasses.

The current knowledge of glass structure is based on a partial synthesis of the information obtained by many methods. The structure of glass lacks translational symmetry so that it is impossible to define a unit cell. The absence of periodicity and symmetry in glass distinguishes it from a crystal. The isotropic vibrational properties of glass are a consequence of the absence of symmetry and the atomic arrangement should be statistically the same in all directions. Zarzycki (1991) proposed two ways of describing a glass. First, the whole system is considered as a giant molecule, which means that the exact coordinates and the nature of each atom have to be specified. Second, the system is described statistically, expressing the probability of finding an atom at a specified position from another atom. Recently, Wright (1990) and Elliott (1990), have described the medium- and long-range structural features around any specified reference atom.

2.3.1 Random Network Theory

Many of the properties of the technologically important glasses can be discussed in terms of the continuous random network model proposed originally by Zachariasen

(1932). The atomic structures of the glass-forming oxides such as SiO_2, GeO_2, B_2O_3 and P_2O_5 have been proposed and subsequently confirmed by Warren and Biscoe (1938), using X-ray diffraction. However, due to rapid progress in the study of glasses some additional features have to be considered, such as the changes of the co-ordination numbers of some network forming elements (Rawson 1991).

The most important glass-forming oxides are characterized by relatively small cations such as B^{3+}, Si^{4+} and P^{5+}, each surrounded by either three or four oxygen atoms. The basic unit of structure is a triangle or tetrahedron. In the pure oxide, the units are joined together at their corners only and each oxygen atom is shared by two cations. This arrangement is a common feature of the corresponding crystalline materials. Thus Zachariasen's (1932) proposed that a particular glass would have a structure built from the similar units to those found in its crystalline counterpart. However, in glasses sufficient randomness in bond angles and bond length is introduced to destroy any long range periodicity in the lattice, and from this, he derived four rules for oxide structure that indicate which oxides tend to form glasses. The rules are:

1. No oxygen atom may be linked to more than two glass-forming atoms.
2. The coordination number of the glass-forming atoms is small.
3. The oxygen polyhedra share corners with each other, not edges or faces.
4. The polyhedra are linked in a three-dimensional network.

The subsequent experimental work of Warren and Biscoe (1938) included both two-and three components glasses, in which metal oxides containing relatively large cations were introduced. An example is the system Na_2O-SiO_2. In vitreous SiO_2, the additional oxygen ions are accommodated by the breaking of Si-O-Si bridges which link the tetrahedra. Figure 2.3 shows schematic structures of a two-dimensional oxide represented as a crystal, a glass, and a glass modified with a metal cation, such as

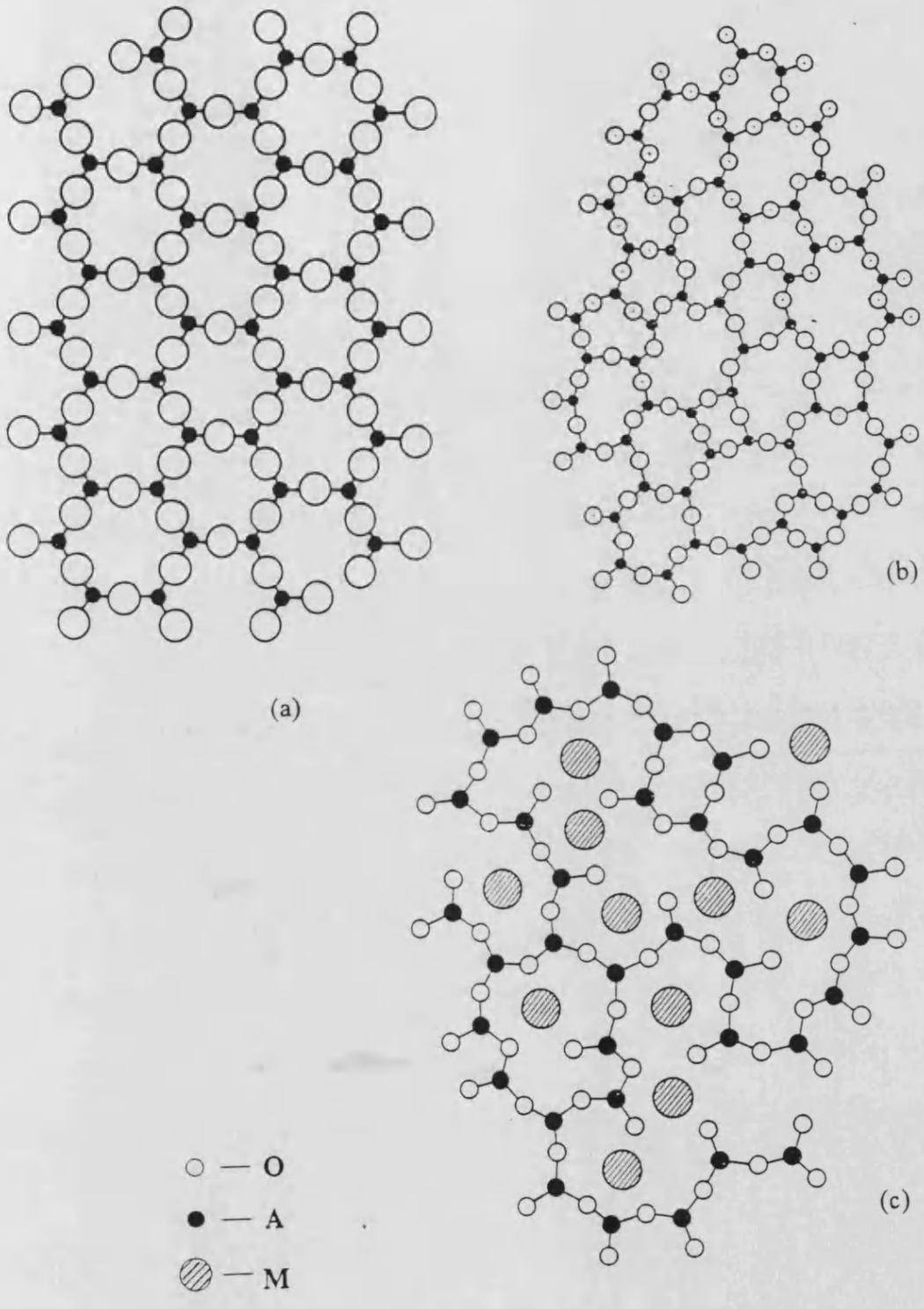

Figure 2.3. Structure of an imaginary two-dimensional oxide A_2O_3, (a) as a crystal, (b) as a glass (after Zachariasen 1932) and (c) as a binary glass of A_2O_3 and M_2O, where M is a metallic cation (after Warren and Biscoe 1938).

sodium, which forms singly charged ions. Here the glass-forming oxide is represented as oxygen triangles, instead of tetrahedra, in order to make a two-dimensional representation of the glass structure. According to Zachariasen model, it is suggested that the formation of binary glass is based on the rupture of the Si-O-Si bonds in the SiO_4 tetrahedra. The Si-O-Si bridge rupture mechanism leads to a loosened network structure with two types of oxygens: an oxygen bonded to two Si atoms is called a bridging oxygen and an oxygen bonded to one Si atom is called non-bridging. For each additional oxygen introduced, two non-bridging oxygen atoms are formed. The sodium atoms are accommodated in the relatively large holes in the network, surrounding themselves with, on average, six oxygen atoms (Figure 2.3c). The negative charge of the additional oxygen atom is localised mainly on the two non-bridging oxygen atoms that have been formed. In this way the positive charge of the sodium ion is locally neutralised.

2.3.2 Vitreous SiO_2

The simplest of the silicate glasses is vitreous SiO_2. It is a colourless glass with a refractive index of 1.46 (Galeener and Lucovsky 1976). In crystalline SiO_2 the coordination number of silicon-to-oxygen ions is four; thus the silicon-oxygen tetrahedron is the basic building block for silicate structures. Similarly, the basic structural unit of vitreous SiO_2 is also the SiO_4 tetrahedron, with a Si cation at its centre and oxygen anions at the vertices. On the basis of the Zachariasen's random network theory (1932), the tetrahedral units are linked together to form a continuous, irregular, three-dimensional network. The randomness in the structure of vitreous SiO_2 is based on the variation of the Si-O-Si angle ranges from 120° to 180°, with a mean of approximately 147°. The O-Si-O basically does not change from the ideal tetrahedral angle of 109.5°. A slight variation of Si-O length is also proposed (Bell et al. 1968).

There is a wealth of experimental data in the literature relating to the atomic structure of vitreous SiO_2. The earlier investigation of the structure for vitreous SiO_2 by Warren and Biscoe (1938), using X-ray diffraction, was consistent with the form of Zachariasen's random-network theory. Later work of Mozzi and Warren (1969) has confirmed this agreement. The pair-distribution function curve measured by Mozzi and Warren (1969) is shown in Figure 2.4. The pair-distribution function allows the interatomic distances to be calculated directly from the peak positions, and the areas under the peaks give the number of neighbouring atoms. The first peaks correspond to an Si-O distance of 1.62Å, and the second corresponds to an O-O distance of 2.65Å. These distances are consistent with those found in crystalline silicates. The width of these peaks are similar with a tetrahedral distribution of O atom around each Si atom, as shown by the calculated peaks in the Figure 2.4 (dotted line). The third peak corresponds to the Si-Si distance of 3.12Å, and is much broader than the other two peaks because of the distribution in Si-O-Si bond angle. The fourth peak, at 4.15Å, is the Si-2nd O contribution, and the fifth peak, at about 5.1Å, is a combination of the O-2nd O and Si-2nd Si peaks. A sixth peak, at about 6.4Å, could result from the Si-3rd O contribution. No more peaks would be expected from random network theory, and none were observed experimentally. Using extended X-ray absorption fine structure (EXAFS), Greaves et al. (1981) have also found that their results are in substantial agreement with the work of Mozzi and Warren (1969).

The shapes of the third, fourth and fifth peaks were fitted by assuming a distribution in the Si-O-Si bond angle, as shown in Figure 2.5 (Mozzi and Warren 1969). The maximum of the distribution curve is at 144°, with a maximum angle of 180° and a minimum angle of 120°. The distribution of the Si-O-Si bond angle is wide enough to distinguish the structure clearly from a crystalline arrangement.

The original Zachariasen picture of the local structure of alkali and alkaline earth

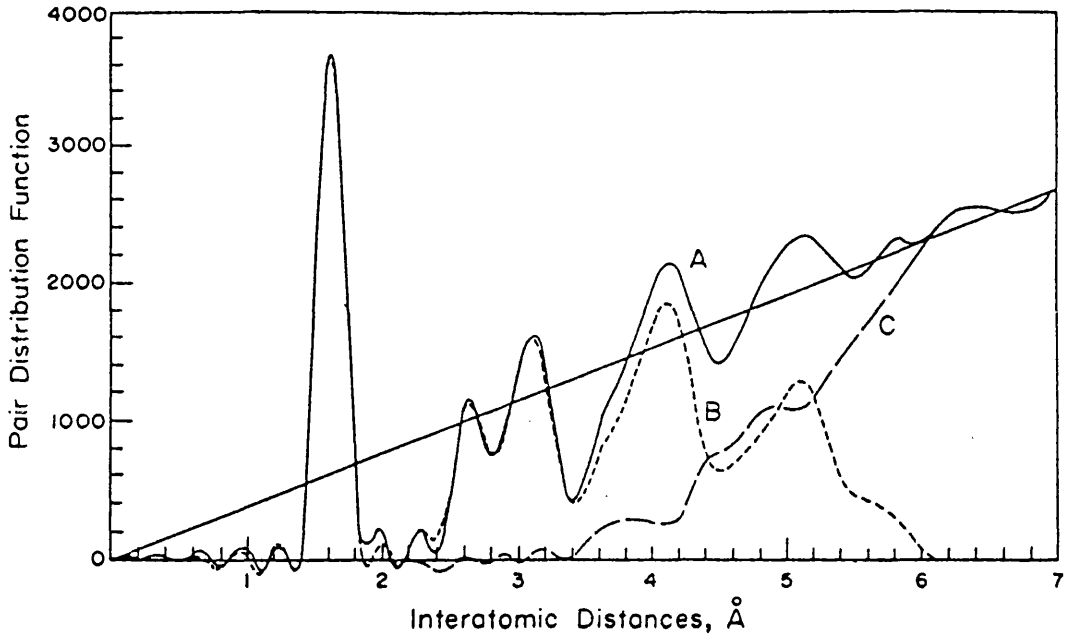

Figure 2.4. The pair distribution function for fused silica. **A** is the measured curve. **B** is the sum of the calculated curves for the first six contributions: Si-O, O-O, Si-Si, Si-2nd O, O-2nd O and Si-2nd Si. **C** is the difference between **A** and **B** (after Mozzi and Warren 1969).

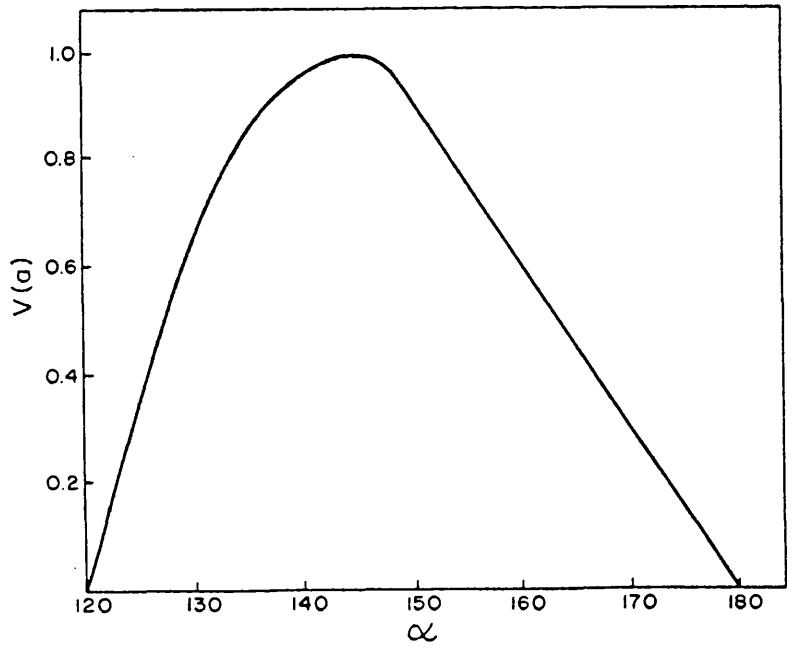

Figure 2.5. The distribution of Si-O angles in fused silica. The function V(α) is the fraction of bonds with angle α (after Mozzi and Warren 1969).

cations is left unspecified; they occupy a statistical distribution of holes in the three-dimensional covalent network. The work of Mozzi and Warren 1969 has provided an atomic structural picture of vitreous SiO_2; however, they were unable to deduce anything definite about the oxygen ligands surrounding modifying cations (Greaves et al. 1981). A model developed by Bell and Dean (1972) has introduced single covalent interatomic interactions, and in some instances attempts have been made to introduce the effects of Van der Waals interactions (Long et al. 1976, Greaves et al. 1979). However, the ionic interactions between those of modifying cations and oxygen atom are more appropriate to the covalently network structure (Greaves et al. 1981).

In the investigation of the atomic vibration of vitreous SiO_2, Simon (1957) has given the first composite infrared and Raman spectra for the glass down to about $200cm^{-1}$, and some neutron scattering results have also been obtained for the low-frequency region (Bell et al. 1968). The spectral positions of the peaks at about $410cm^{-1}$, $800cm^{-1}$ and $1040cm^{-1}$ calculated on the basis of the model derived by Bell et al. (1968) correspond quite well with those observed at $465cm^{-1}$, $800cm^{-1}$ and $1100cm^{-1}$ in the experimental infrared spectrum of Simon (1957). Bell et al. (1968) assigned the band at 1040 cm^{-1} to a bond-stretching vibration, in which the bridging oxygen atoms move in the opposite direction to their Si neighbours, and roughly parallel to the Si-O-Si lines. The peak at $730cm^{-1}$ was assigned to a bond bending vibration, in which the oxygens move approximately at right angles to the Si-O-Si lines and similarly at 410 cm^{-1} was assigned to vibration, in which the oxygen atoms move roughly perpendicular to the Si-O-Si lines. In general, each of the vibrational modes responsible for these peaks involves both stretching and bending vibration of the silicon-oxygen bond.

2.3.3 Crystalline and vitreous P_2O_5

In the random network theory of Zachariasen (1932), the structural units of a glass are considered to be the same as those for its corresponding crystal. The crystalline structure of P_2O_5 is well known; it was first studied by de Decker and MacGillavry (1941). Basically, phosphorus pentoxide P_2O_5 has three crystalline forms, all having structures based on the PO_4 tetrahedron. Crystals of the hexagonal form P_2O_5 melt at 422°C; the liquid formed consists of a three-dimensional network of P_4O_{10} rings (Wells 1975). The orthorhombic form of P_2O_5 melts at 580°C to produce a very viscous liquid which can readily be superheated to temperatures well above the melting point. However, melting at only a slightly lower temperature 560°C (Van Wazer 1958), is another orthorhombic crystalline form, which consists of a three-dimensional network of P_4O_{10} rings; the glass formed consists of a layer of P_6O_6 hexagons (Wells 1975). Owing to these two melting temperatures of the orthorhombic form, it is difficult to choose either structure in preference to the other as an analogue of the glass. Bridge et al. (1983) have suggested that the structure of vitreous P_2O_5 consists mainly of P_nO_n rings with n averaging about six.

To introduce the structure of binary phosphate glasses, let us begin with a description of the structure of pure P_2O_5 glass. Pure P_2O_5 glass is an extremely hygroscopic colourless glass, with a refractive index of about 1.55 in the visible region (Galeener and Mikkelsen 1979). Based on random network theory (Zachariasen 1932), each phosphorus atom is surrounded by four oxygen atoms, one double-bonded to the phosphorus (Figure 2.6). The other three oxygens are bridging to neighbouring PO_4 units in a disordered network of PO_4 tetrahedra, as shown in Figure 2.7 (Sales 1990). In contrast to vitreous SiO_2, the doubly bonded oxygen atom does not participate in the network bonding scheme.

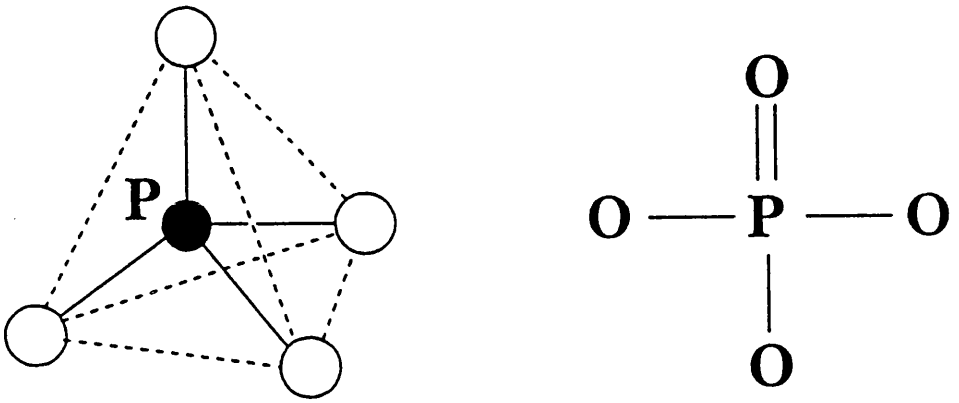

Figure 2.6. Schematic illustration of the PO_4 tetrahedra.

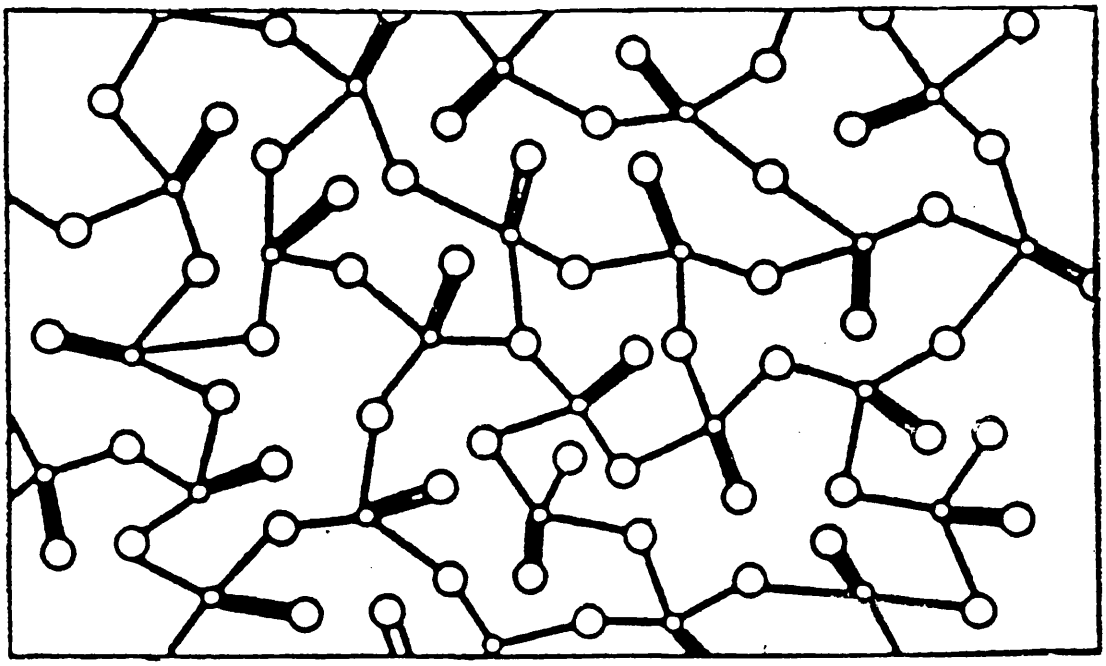

Figure 2.7. Schematic illustration of the pure P_2O_5 glass. (after Sales 1990).

Structural studies of pure P_2O_5 glass are sparse, due to its volatile and hygroscopic nature. However, some aspects of its structure have been deduced from studies of P_2O_5 alloyed into other glass formers (Doremus 1973). Wong and Angell (1976) have reported an infrared transmission spectrum for thin film of P_2O_5 prepared by techniques of chemical vapour deposition. There has been no X-ray radial distribution study on pure P_2O_5 glass (Doremus 1973). The first Raman spectroscopy structural studies of P_2O_5 glass was reported by Bobovich (1962) in a study of $(1-x)CaO.(x)P_2O_5$. The most recent and more correct Raman spectrum of pure P_2O_5 glass is that obtained by Galeener and Mikkelsen (1979); they suggested that the Raman spectrum of Bobovich (1962), contains significant bands that can be attributed to either alkali or alkaline earth contamination. Figure 2.8 shows the Raman spectra for pure P_2O_5 glass at 530°C, and also of gaseous P_4O_{10} (Galeener and Mikkelsen 1979).

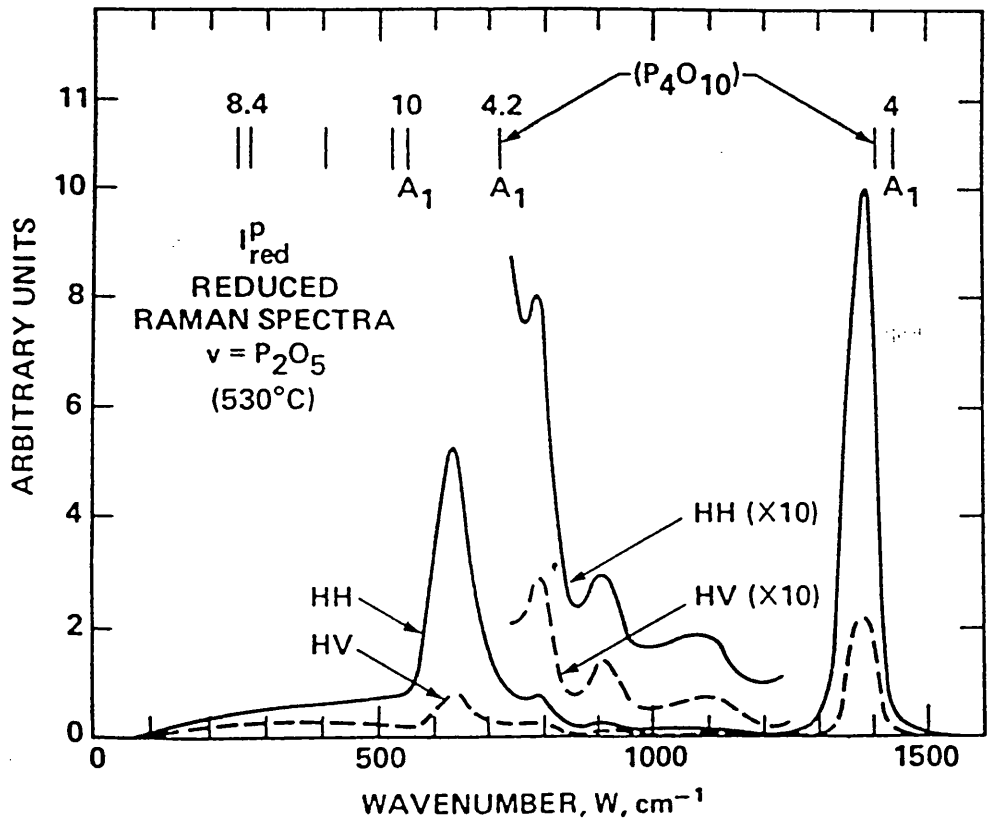

Figure 2.8. The Raman spectra of pure P_2O_5 glass compared with the observed Raman lines in gaseous P_4O_{10} (after Galeener and Mikkelsen 1979).

Raman spectra are related to vibrational motions of structural units; the intense band at about 1390cm^{-1} is attributed to the strong P=0 stretching mode, while the second band at about 640cm^{-1} is due to the symmetric stretching of all the bridging oxygen atoms. From the Raman spectra, Galeener and Mikkelsen (1979) confirmed that the structure of pure P_2O_5 glass is consistent with the proposed model of random network theory, with each phosphorus is surrounded by four oxygen atoms (Zachariasen 1932). Figure 2.8 also shows the Raman spectrum of gaseous P_4O_{10} and the assumption that the glass might consist of P_4O_{10} molecules, as does the crystalline form of P_2O_5, is puzzling (Gallener and Mikkelsen 1979): some aspects of the P_4O_{10} molecular structure are retained in pure P_2O_5 glass.

2.4 RARE EARTH ELEMENTS OR LANTHANIDES

The rare earth elements, known as lanthanides, are a group of 14 elements that run from cerium (atomic number 58) to lutetium (atomic number 71) inclusively. Often included as lanthanides are certain elements with valence 3 in the d-transition series: scandium (atomic number 21), yttrium (atomic number 39) and lanthanum (atomic number 57). The exclusion of lanthanum from the lanthanide group itself is based upon the absence of 4f electrons. The electronic configuration of the lanthanides is based on the xenon core, ($1s^2 2s^2 2p^6 3s^2 3p^6 3d^{10} 4s^2 4p^6 4d^{10} 5s^2 5p^6$), denoted as [Xe], plus three electrons in the higher energy 5d and 6s orbitals. The *4f* level is progressively filled from cerium [Xe]$4f^1 5d^1 6s^2$ to lutetium [Xe]$4f^{14} 5d^1 6s^2$. The presence of the three outer electrons accounts for the +3 oxidation state.

The *4f* electrons are inner electrons and thus play a minor role in determining the chemical properties of the elements which hardly vary with atomic number. The close resemblance between their chemical and physical properties ensures that the rare earth elements occur together in individual minerals, and also accounts for the considerable

difficulties in separating them from one another. Because of similar atomic and ion sizes and the same chemical valences, one rare earth ion can readily be replaced in a crystal lattice by another rare earth ion with little strain. The rare earths have very different and striking magnetic properties; the reason for this lies in the existence of electrons in the inner shell *4f* states.

2.4.1 Lanthanide contraction

The lanthanide contraction is a result of the imperfect shielding of one *4f* electron by another *4f* electron (Jørgensen 1955). As the nuclear charge, and thus the *4f* electron population, increases, the imperfect shielding induced by the directed nature of these orbitals causes each *4f* electron to experience added electrostatic attraction by the nucleus. The result is a decrease in the size of the entire $4f^n$ arrangement, and therefore in the sizes of atom and ions, with increasing atomic number. The variations of ionic and atomic radii of lanthanides as a function of atomic number are shown in Figure 2.9.

2.4.2 Valence instability

An important feature of lanthanides is that there is no significant difference in the binding energy of a *4f* electron and a *5d* valence electron. A *4f* electron may be promoted to the *5d* valence shell to make a tetravalent ion, such as Ce, Pr and Tb or a *5d* valence electron may be demoted to the *4f* shell to create a divalent ion as in Sm, Eu, Tm and also Yb. The lanthanides that exhibit this phenomena of valence instability can show intermediate valence states. Application of pressure to divalent samarium crystalline compounds can induce a transition via an intermediate valence state towards a trivalent state (Jayaraman et al. 1970). An example is SmS. The transition from the electronic

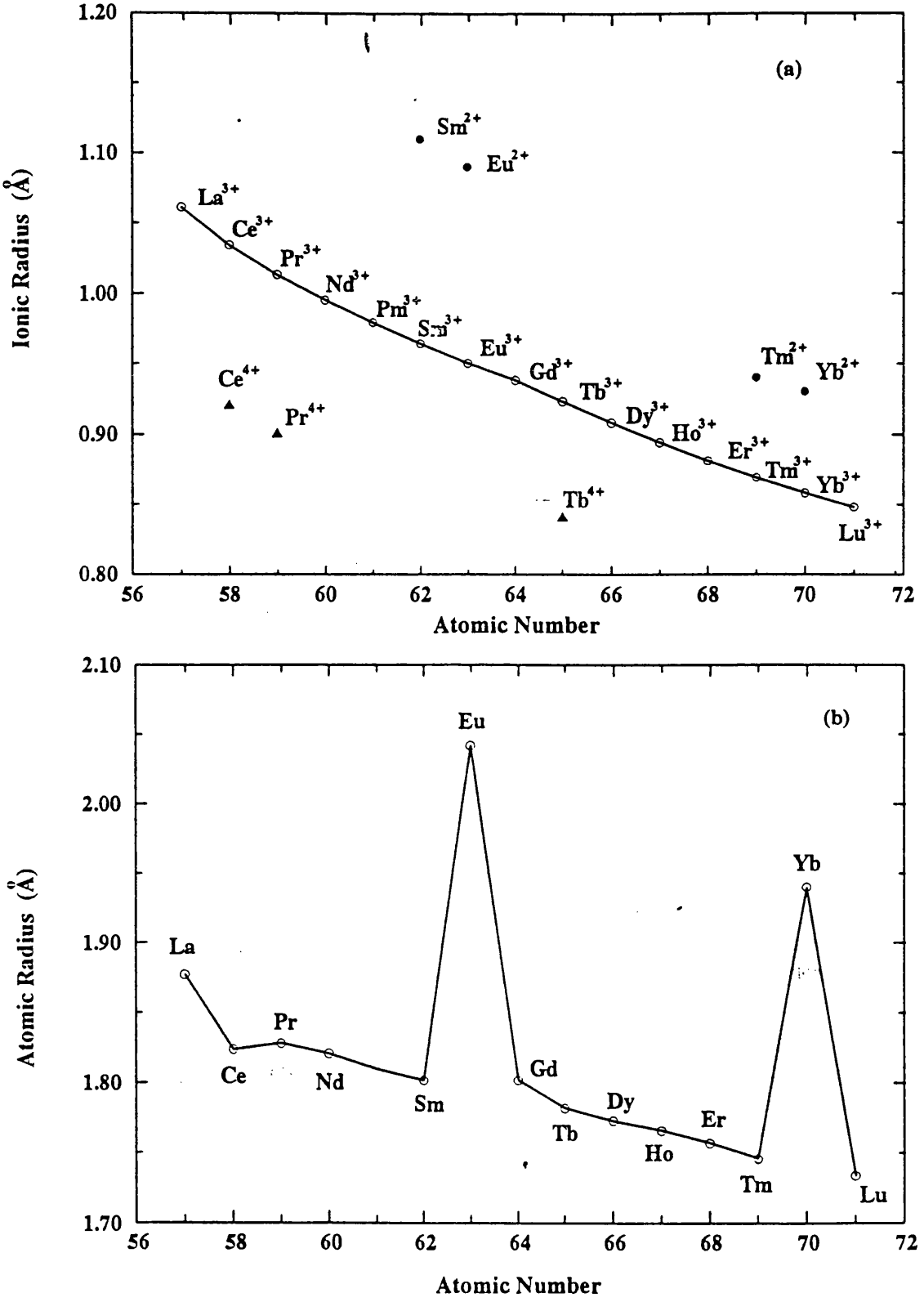

Figure 2.9. Variation in ionic and atomic radii of the lanthanides (after Moeller 1973).

configuration $4f^6 5d^0$ (2^+) to time sharing with $4f^5 5d^1$ (3^+) involves a marked size reduction of the samarium ions, and as a result crystalline SmS shows the unusual decrease of elastic stiffness under pressure (Tu Hailing et al. 1984). A similar behaviour of mixed valent state of rare earth ions under pressure, such as SmS, where the 2+ component is reduced at the expense of 3+, and the ions occupy a smaller volume, may also occur in the rare earth phosphate glasses (Mierzejewski et al. 1988a,b, Sidek et al. 1988).

2.5 RARE EARTH PHOSPHATE GLASSES

The structure of binary phosphate glasses have been investigated intensively over the past five decades after the pioneering work of Zachariasen (1932). To date, most of the studies on these systems have been focused on glasses in which the network modifier is either monovalent or divalent (Kordes 1939, Biscoe et al. 1941, Westman 1960). Books such as by those Van Wazer (1958) and Corbridge (1974) give full details concerning phosphorus and its compounds. Structural studies of phosphate glasses containing Pr^{3+} and Dy^{3+} have been carried out by Sun and Risen (1986) using infrared, far infrared and Raman spectroscopy. In addition, Morgan et al. (1987) have measured the Raman spectra of binary CeO_2-P_2O_5 and Pr_2O_3-P_2O_5 glasses. However, these studies are not complete, do not provide a clear picture of the structure and vibrational properties of rare earth phosphate glasses. The present work focus part of a systematic study of the structure and properties of binary phosphate glasses.

Phosphate can be defined those compounds of phosphorus of which each atom of phosphorus is surrounded by four oxygen atoms arranged at corners of a tetrahedron. By sharing oxygen atoms between tetrahedra, chains, rings and branched polymers of interconnected PO_4 tetrahedra can be produced. This means that there are numerous building units from which phosphate can be made. One of them is the PO_4 unit in which

three oxygen atoms are shared with neighbouring PO_4 units. This is called a *branching unit*. Another is the *middle unit* in which two oxygen atoms are shared with neighbouring PO_4, and there is one negative charge which is neutralised by a cation. Then, we have the *end group* in which one oxygen is shared with another PO_4, and there are two negative charges. A schematic illustration of these basic building units of phosphates is given in Figure 2.10.

By arranging in all possible ways, the above elementary structural units of phosphates consisting of branching, end and middle units, a large number of hypothetical phosphate groups can be derived including those shown in Figure 2.11 (Van Wazer 1958).

The usual combinations are as follows:

i. Ortho- monophosphate	n = 1	$[PO_4]^{3-}$
ii. Pyro- or diphosphate	n = 2	$[P_2O_7]^{4-}$
iii. Triphosphate	n = 3	$[P_3O_{10}]^{5-}$
iv. Tetraphosphate	n = 4	$[P_4O_{13}]^{6-}$
v. Polyphosphate	n = x	$[(PO_3)_x.H_2O]^{x-}$

2.5.1 The structure of binary phosphate glasses

Phosphorus pentoxide P_2O_5 is an excellent glass former, but is extremely unstable in moist air. The addition of rare earth oxides to pure P_2O_5 improves the chemical durability and hence their physical properties (Mierzejewski et al. 1988a,b, Sidek et al. 1988). The atomic structure of binary phosphate glasses consists of polymeric chains of PO_4 tetrahedra bonded to adjacent tetrahedra via bridging oxygens. These poly-phosphate chains are linked together by the interaction between the metal cation of the network modifier and the non-bridging oxygens of the network former.

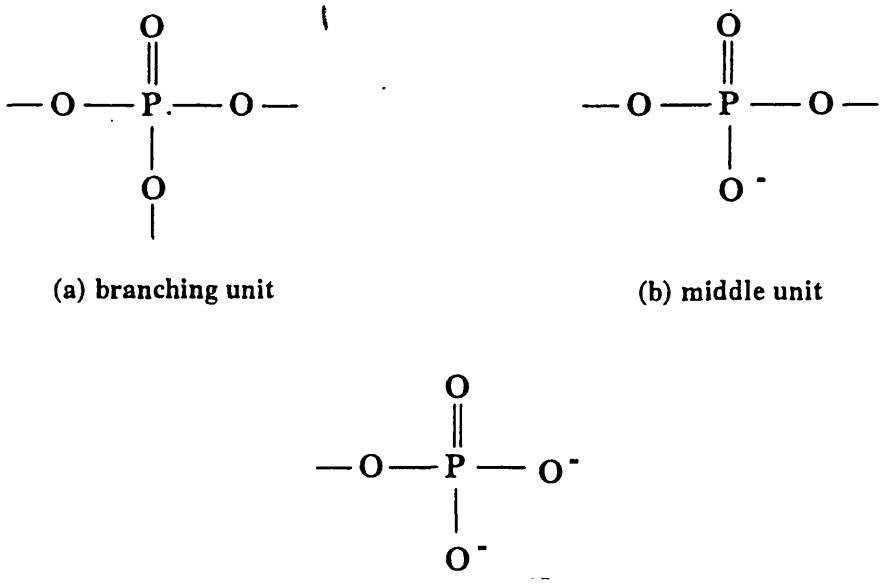

Figure 2.10. Schematic illustration of the elementary building units of the PO_4 tetrahedra (after Van Wazer 1958)..

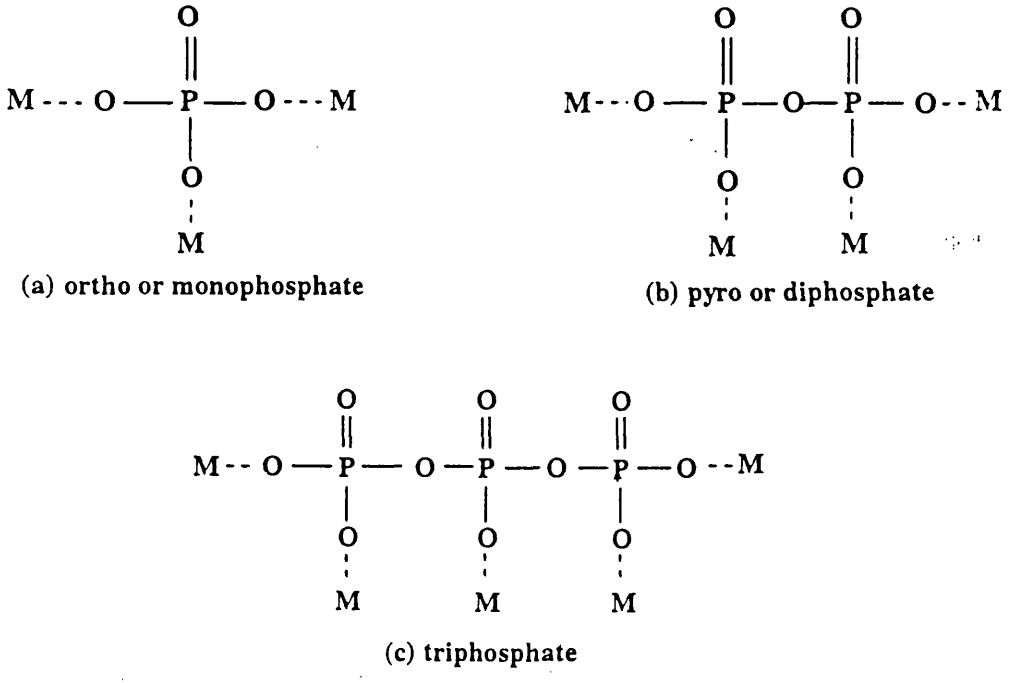

Figure 2.11. Schematic illustration of some examples of the phosphate groups present in phosphate glasses (after Van Wazer 1958).

It appears that Kordes et al. (1939, 1941, 1949 and 1953) were the first to consider the formation of non-bridging oxygens in phosphate glasses. In their models, they assumed that the doubly bonded oxygens remain so, and that a one-to-one correspondence exists between the number of alkali cations added and the number of non-bridging oxygens created. At that time, however, only bulk physical property data were available with which to confirm the correctness of these assumptions. Using modern techniques, such as MASS-NMR, X-ray absorption fine structure (EXAFS), high performance liquid chromatography (HPLC), Mössbauer absorption and Raman scattering, it is possible to provide detailed information about the local environment around particular atoms in phosphate glasses.

Generally, there are several structural divisions, based on Van Wazer's (1958) Reorganisation Theory, which can be developed for phosphate glasses. Examples of these are orthophosphate, pyrophosphate, metaphosphate, polyphosphate and ultraphosphate. These structural divisions are based on a ratio R between the metal oxide to phosphorus pentoxide, where the metal oxide can be, for example an alkali metal, alkaline earth, transition metal, rare earth or actinide. According to the ratio R, the structure of metal phosphate glasses changes from a continuous cross-linked PO_4 tetrahedra three-dimensional network into a polymer type of PO_4 chain with a distribution of chain length as the phosphate content decreases. This is due to the glass composition changing from ultraphosphate ($0<R<1$) to the polyphosphate ($1<R<2$). The ultraphosphate glasses are very difficult to prepare and are known to be very unstable in humid conditions (Van Wazer 1958); hence, very little is known about these glasses. This is explained by the existence of the branch structure in the ultraphosphate glasses which are constructed with a phosphorus atom with one non-bridging oxygen and three bridging oxygens (Kowada et al. 1993).

Binary phosphate glasses with the stoichiometry $M(PO_3)_x$, where M is a metal

cation of valence x, are called metaphosphates. For metaphosphate glasses, R is equal to 1; these are the glasses studied in the present work. Metaphosphate glasses are thought to consist of long chains of PO_4 tetrahedra linked to adjacent tetrahedra by bridging oxygen atoms and considered the most stable of glasses (Van Wazer 1958, Sales et al. 1986, Mierzejewski et al. 1988a,b)

Although there have been no detailed atomic structural investigations of the rare earth phosphate glasses, there is some pertinent knowledge of the structure of other vitreous phosphates, such as lead-iron phosphate glasses (Sales et al. 1986, Sales 1990) and those formed from alkali oxides (Martin 1991). The structure of lead-iron phosphate glasses has been investigated by Sales et al. (1986). Their work suggests that, as the metal cations are added to the structure, non-bridging oxygen bonds are created to preserve charge balance, breaking up the network of PO_4 tetrahedra. If enough metal cations are added to the glass, each fourfold coordinated phosphorus has one doubly bonded and singly bonded oxygen and two bridging oxygens to neighbouring PO_4 tetrahedra. The metaphosphate (1:1) come into this regime. A schematic illustration of lead metaphosphate is shown in Figure 2.12 (Sales 1990). The chains are interconnected via somewhat weaker bonds (ionic bonds) to the metal cations. With still higher metal-to-phosphorus ratios, the average length of the phosphorus chains become shorter until the glass network consists primarily of isolated pyrophosphate dimers embedded in a 'sea' of metal cations (Figure 2.13). Phosphate glasses with larger metal-to-phosphorus ratios are difficult to prepare due to the tendency of the melts to crystallize on cooling.

The structure of binary rare earth phosphates glasses may be similar since most binary phosphate glasses can share the same basic structure regardless of the metal cation. As the metal modifier content is increased, the PO_4 tetrahedra change configuration. The additional oxygens participate in the network and cause the rupture of

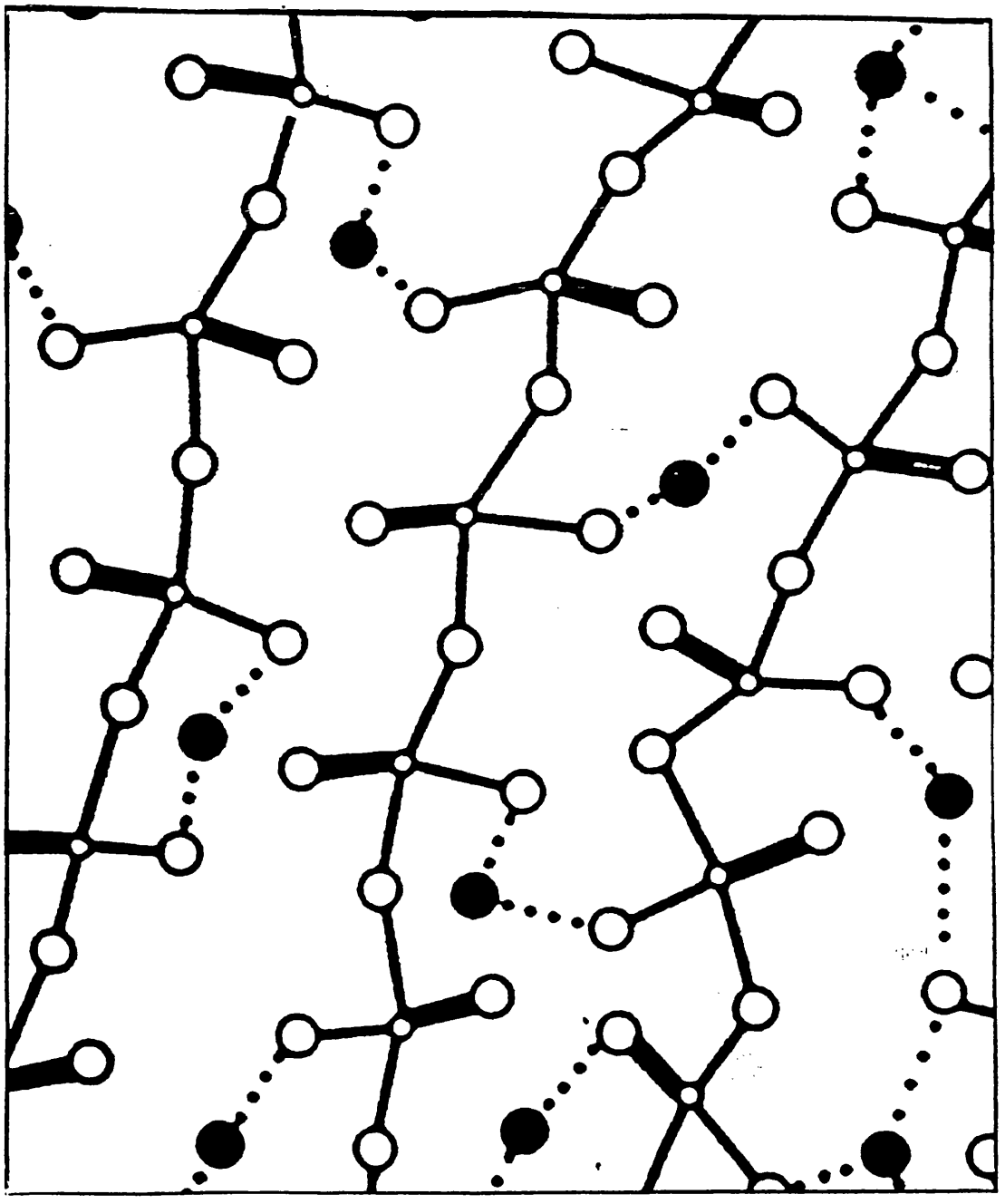

Figure 2.12. Schematic illustration of the structure of lead metaphosphate glass (after Sales 1990).

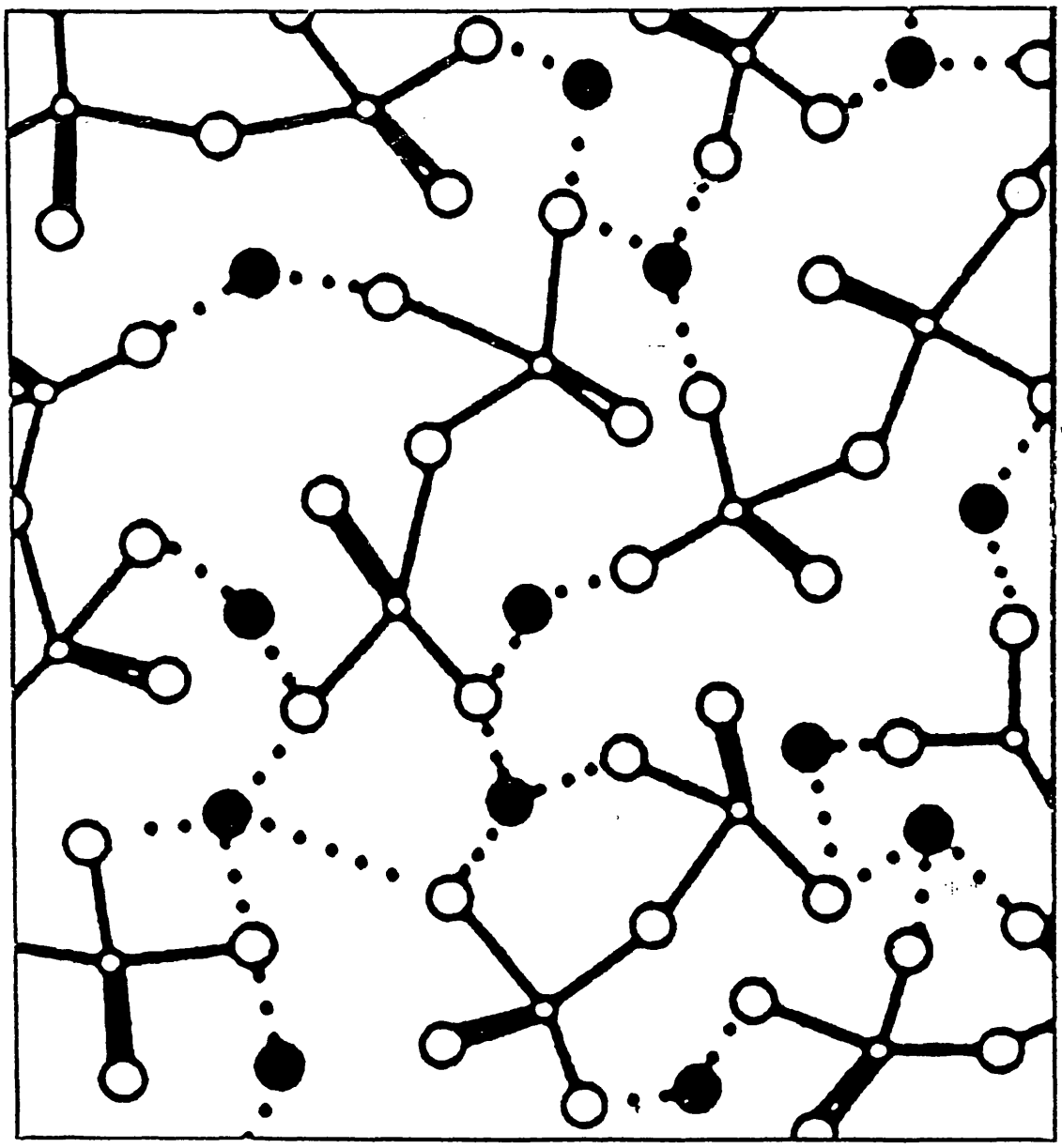

Figure 2.13. Schematic illustration of the structure of lead pyrophosphate glass (after Sales 1990).

a specific number of bonds. A P-0-P bond is broken and the added oxygen saturates the unsatisfied bond of one P and two $P\text{-}O^-$ are formed. The two negative charges on the oxygens are compensated by the nearby presence of cations ensuring the electrostatic neutrality of the ensemble. In the case of fusion which leads to glass formation, the primitive network of PO_4 is thus progressively broken - depolymerized - and the cations lodge in the neighbourhood of the broken bonds. Metaphosphate glasses tend to form long chains of PO_4 tetrahedra, which are connected at two corners and have two non-bridging oxygen atoms. For the trivalent rare earth R^{3+} ions the metaphosphate composition is $R(PO_3)_3$.

It is interesting to note that the rare earth phosphate glasses studied in the present work are particularly resistant to water absorption. It is possible that metal cations which have a valence of two or more can form a cross bond between non-bridging oxygen of the tetrahedra in adjacent chains (Van Wazer 1958). The formation of these cross-links demonstrates why some phosphate glasses containing the higher-valence network modifiers, such as lead-iron-phosphate glasses (Sales et al. 1985) are more chemically durable. Based on their conclusions, the addition of iron oxide dramatically decreases the average length of the polyphosphate chains forming the backbone of the glass structure. The Fe^{3+} ions appear to be located in octahedral sites and improve the durability of the glasses by strengthening the cross-bonding between the polyphosphate chains (Sales et al. 1985). It is possible that the rare earth ions could also provide a stronger crosslink between the polyphosphate chains in rare earth phosphate glasses.

2.6 STRUCTURAL INVESTIGATIONS OF RARE EARTH PHOSPHATE GLASSES

As yet no structural studies made on our rare earth phosphate glasses have been reported in the literature. However, some studies of phosphate glasses have been carried

out using diffraction methods. X-rays diffraction studies have been made by Biscoe et al. (1941) on $CaO-P_2O_5$ glasses, by Brady (1958) on $NaPO_3$ glass and by Musinu et al. (1990) on lead-iron phosphate glasses. Using a neutron diffraction technique, Matsubara et al. (1988) have studied alkaline earth and zinc metaphosphate glasses. Suzuki and Ueno (1985) and Matz et al. (1988) have used the same approach to study the $NaPO_3$ and alkaline earth metaphosphate glasses. More recently, X-ray scattering techniques have been used for structural studies of metaphosphate glasses, $R(PO_3)_2$, with R = Mg, Ca, Zn, Sr or Ba (Walter et al. 1990).

The radial distribution functions determined by Biscoe et al. (1941), for two different samples of $CaO-P_2O_5$ glasses, on the ultraphosphate side of the metaphosphate composition, with the CaO/P_2O_5 mole ratios being equal to 0.731 and 0.964, respectively, are shown in Figure 2.14. They have interpreted the first peak at about 1.57Å as corresponding to the P-O distance, with an average of 4.2 oxygen atoms around each phosphorus atom for both glasses. The second peak on the distribution curve, occurring at about 2.3-2.4Å, has been interpreted as resulting from the O-O and Ca-O distances, with about 6-8 oxygen atoms surrounding each calcium ion. The third peak is attributed to the P-P distance of about 2.94 Å, corresponding to an P-O-P angle of about 140°.

2.6.1 Vibrational Spectroscopy of Phosphate Glasses

There have been a number of structural studies of binary phosphate glasses based on vibrational spectroscopy. Infrared and Raman spectroscopy have been widely used to probe the vibrational nature of the bond between the metal cation and surrounding oxygen atoms for metaphosphate glasses (Bobovich 1962, Miller 1979, Nelson and Exarhos 1979, Sales et al. 1986, Morgan et al. 1987, Mierzejewski et al. 1988a, Nga et al. 1991). These workers have interpreted the vibrational spectra of several metaphosphate glasses and suggest that their structures consist primarily of chains of

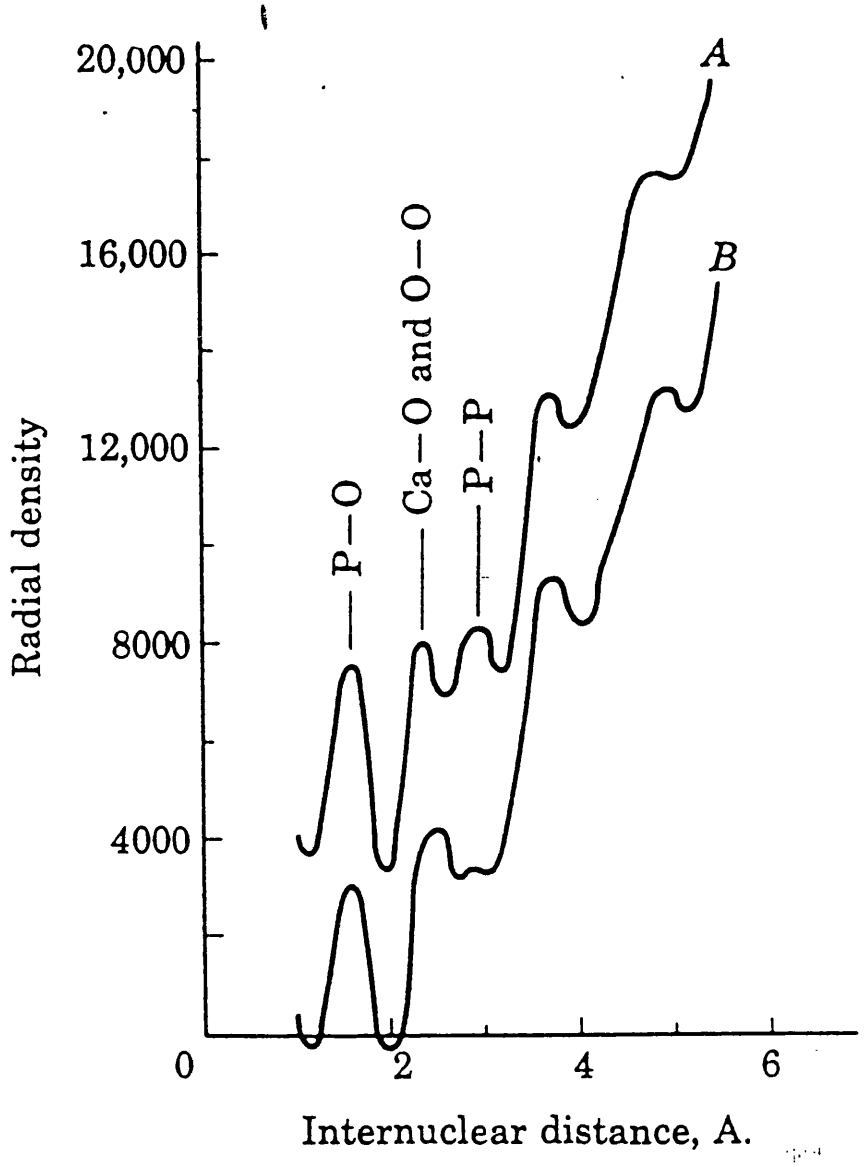

Figure 2.14. The radial distribution functions for $CaO\text{-}P_2O_5$ glasses. Curves A and B represent the CaO/P_2O_5 mole ratios of 0.731 and 0.964, respectively (after Biscoe et al. 1941).

corner sharing PO_4 tetrahedra. Metal cations are presumed to be located randomly among the disordered chains, providing charge balance of the non-bridging oxygens on the chain tetrahedra. Mierzejewski et al. (1988a) have demonstrated that the Raman spectra of samarium phosphate glasses are almost analogous with those for previously studied

metal metaphosphate glasses. This similarity is due to the general feature that the metal cation interacts weakly via ionic bonding with the bridging oxygens forming the poly-phosphate chains (Nelson and Exarhos 1979).

The possible vibrational modes of the PO_4 tetrahedra in metaphosphate glasses are shown schematically in Figure 2.15 (Emsley and Hall 1976).

The experimental results published in the literature for metal metaphosphate glasses give rise to the proposal that there are four frequency regions of the Raman spectra that characterize the metaphosphate glasses.

1. A band above 1200cm^{-1} corresponds to the P-O asymmetric stretching vibrations.
2. A 1000-1200cm^{-1} band corresponds to the P-O symmetric stretching vibrations.
3. A 600-800cm^{-1} band corresponds to the P-O-P symmetric stretching and bending vibrations.
4. Nga et al. (1991) have ascribed that a band below 600cm^{-1} corresponds to deformation vibrations, but it is not clear what that implies.

In the case of $(Sm_2O_3)_{0.248}(P_2O_5)_{0.752}$ glass (Mierzejewski et al. 1988a), the Raman lines are situated at about 1231 cm^{-1}, 1190 cm^{-1}, 703 and 329 cm^{-1}, respectively. They have interpreted that, the bands at about 1231 cm^{-1} and 1190 cm^{-1} are associated with the O-P-O antisymmetric and symmetric stretching vibrations, respectively. While, the band at about 703 cm^{-1} is corresponding to symmetric stretching of the P-O-P vibrations. Thus, these experimental observations of the Raman spectra for samarium phosphate glasses are consistent with those of earlier studies of vibrational spectra of other metaphosphate glasses. The broad band in the 800-1200 cm^{-1} region of the Raman spectra of phosphate glasses indicates that a wide distribution of types of non-bridging oxygen ions are present in these glasses (Kohli et al. 1993)

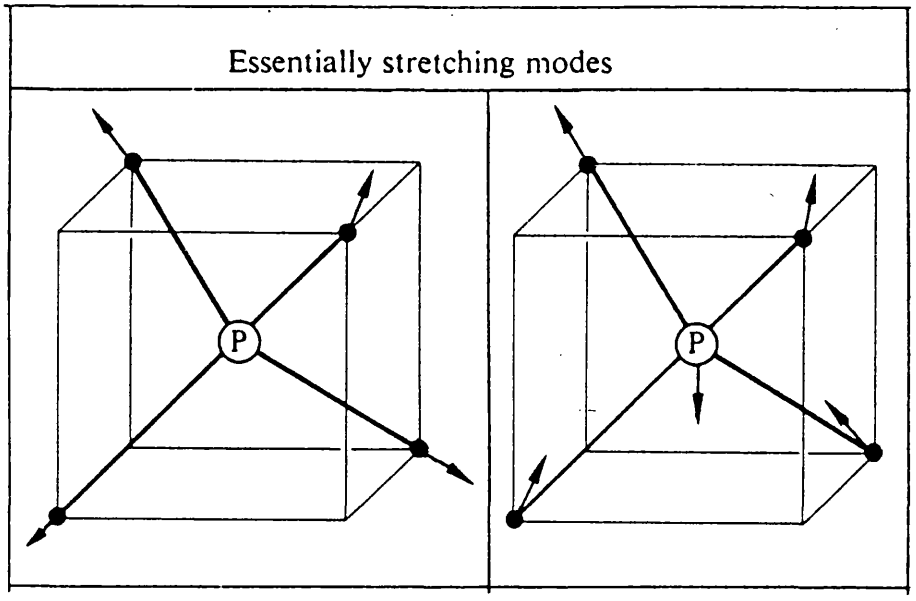

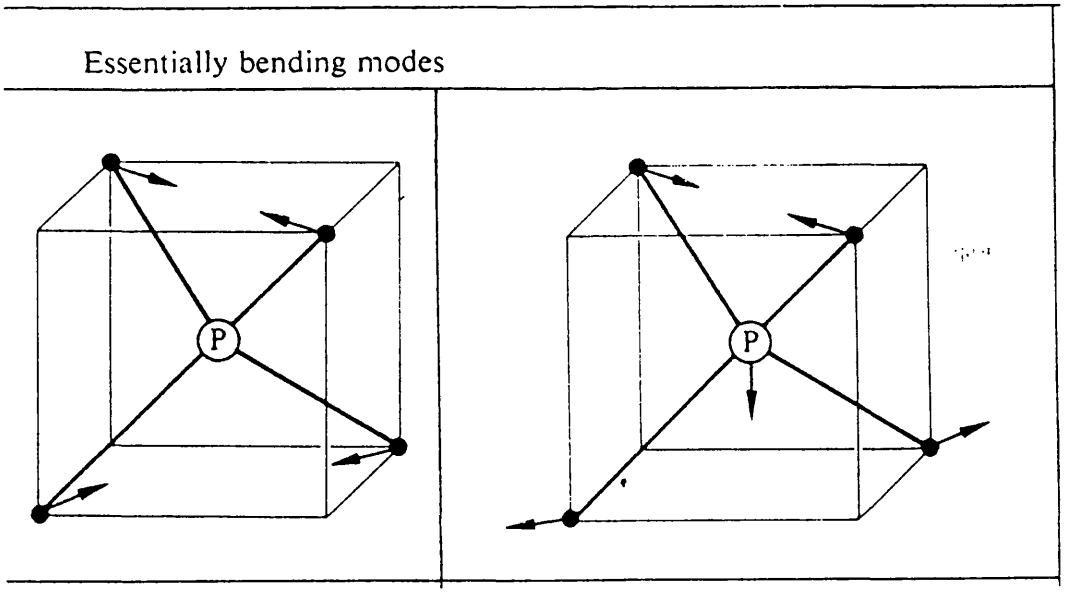

Figure 2.15. Schematic representation of possible stretching and bending vibrational modes for the PO_4 tetrahedra (after Emsley and Hall 1976).

The IR spectra of phosphate glasses have been investigated by Exarhos et al. (1974) and by Nelson and Exarhos (1979). Sales et al. (1985) have studied the IR spectra for lead-iron phosphate glasses. The infrared spectra of the metaphosphate glasses may also be divided into four groups of stretching frequencies (Exarhos et al. 1974). Based on this work, the four groups are generally assigned as: ν_{as}(O-P-O) at about 1240-1310 cm^{-1}, ν_s(O-P-O) at 1170-1090 cm^{-1}, ν_{as}(P-O-P) at 1050-850 cm^{-1}, ν_s(P-O-P) at 790-690 cm^{-1}. Here ν_{as} and ν_s correspond to asymmetric and symmetric vibrational modes, respectively. The broad band at 530 cm^{-1} is a low frequency shoulder arising from the bending modes of the metaphosphate chain. These features are also present in the IR spectra of other metaphosphate glasses and shift only slightly as the metal cation is varied.

2.6.2 Extended X-ray absorption fine structure (EXAFS)

EXAFS is a another key technique for determining aspects of the structure of glass. Because the environment of modifying cations is extremely sensitive to the morphology of the glassy network. EXAFS can be used to locate differences in overall topology that result from different glass configurations. Each atom has its own characteristic X-ray edge absorption (such as K, L ...). When an X-ray excited, a photo-electron is subject to the scattering from the surrounding atoms, its light emission interferes with the scattered photo-electronic wave, which makes the photo-electron absorption cross section vary periodically with the energy of the incident X-ray, leading to an X-ray absorption fine structure. Thus, unlike X-ray diffraction whose radial distribution function is a statistical average of all atoms, EXAFS can reveal information on a particular atom, so this technique can be used to determine the chemical bonding and local structure of a given atomic constitution in glass.

Greaves et al. (1988) have shown that the environments of modifying cations like Na or Ca are extremely sensitive to the overall morphology of the adjacent network. A model which incorporates the specific local structure of modifying cations and non-bridging oxygens within the framework of a continuous random network (CRN) is set up. This modified random network (MRN) is characterized by percolation paths or channels of modifying cations (Greaves 1985). Using MRN, Greaves et al. (1988) have explained qualitatively many of the physical and diffusion related properties of glasses.

Greaves et al. (1988) appear to be the first workers to have applied EXAFS to construct the MRN model for phosphate glasses. EXAFS can allow determination of inter-atomic distances with considerable precision and information on the coordination number of phosphorus atoms, and it can be used for examining the detailed structure of glasses prepared in different ways. With EXAFS, Greaves et al. (1988) showed that it is possible to construct a more accurate picture of the role of iron and lead in cross-linking of the polyphosphate chains in metaphosphate glasses. This is illustrated schematically in Figure 2.16 for a lead-iron phosphate glass using a MRN model; the PO_4 groups are shown as edge-sharing for convenience; the lead and iron network modifier cations are shown systematically as large and small circle, respectively. The 'slack' in the structure generated by disorder in the $(PO_4)_n$ chains is taken up by the lead sites, with the iron sites occupying more regular environments as demonstrated by the EXAFS results. It is clear, from Figure 2.16, that the morphology of the modified regions complement the polyphosphate chain structure, forming channels that bifurcate through the structure. Moreover, because iron is more tightly bound than lead, it can form knots in the structure. Furthermore, by increasing the metal cation content, the polyphosphate chains in metaphosphate glasses can be reduced in size. Liquid chromatography measurements confirm this, but, more importantly, yield the distribution of chain sizes

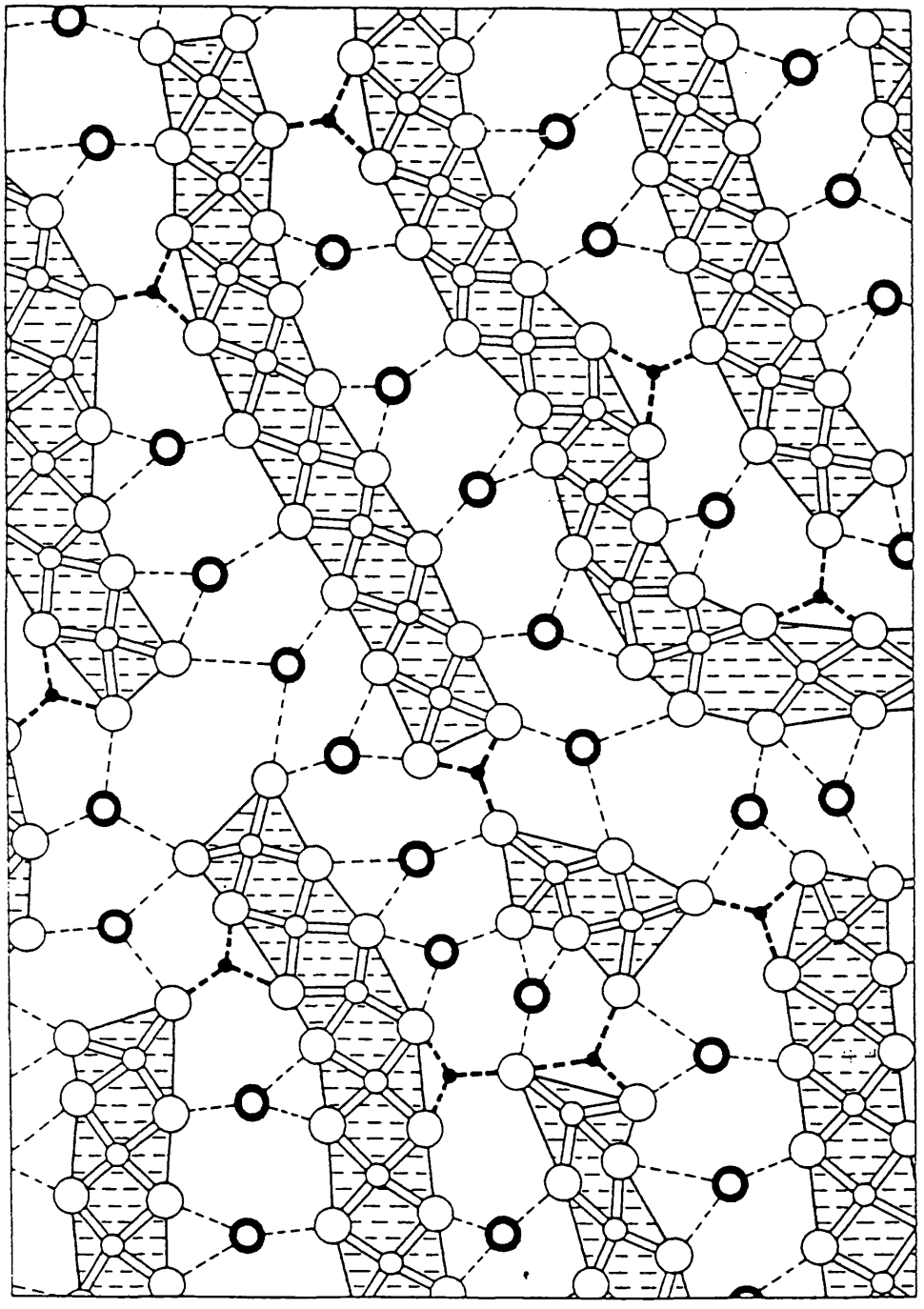

Figure 2.16. Modified random network (MRN) model for iron-lead-phosphate glasses. Polyphosphate chains are cross-linked by lead atoms (open circles) and iron atoms (smaller filled circles), the latter forming 'knot' in the percolation networks which will restrain cation diffusion (after Greaves et al. 1988).

(Sales et al. 1986). Thus, EXAFS measurements have shown that the iron in lead-iron phosphate glass occupies well defined octahedral sites, as compared to lead, where the environment is far more disordered. The combination of restricted cation diffusion and insoluble orthophosphate at the surface serves to endow lead-iron phosphate glasses with their unusually high chemical durability. Structural investigations of rare earth phosphate glasses manufactured at this university using EXAFS are planned for the near future.

2.6.3 Optical absorption and fluorescence spectra

The 4f electron states in trivalent rare earth ions in crystals produce characteristic absorption spectra, and in some cases strong fluorescence (Runciman 1958). Related effects are found in glasses; a comprehensive survey of the early experimental data on optical absorption and fluorescence spectra for glasses has been given by Weyl (1959) and extended later by Bamford (1977), Wong and Angell (1977), Elliott (1990) and Fuxi (1992).

Optical absorption spectra and laser-induced fluorescence measurements have proved to be a powerful way for examining the valence state of the rare earth ions in crystals and glasses. The first measurements using laser-induced fluorescence spectra on rare earth phosphate glasses containing samarium ions were reported by Farok et al. (1992). The results show that only Sm^{3+} ions are present, Sm^{2+} ions are not present in measurable quantities. Measurements on the optical absorption and fluorescence spectra have been carried out recently for europium phosphate glasses (Farok et al. 1994). These spectra also do not show any obvious sign of divalent europium ions, only trivalent europium ion fluorescence being observed. Room temperature absorption spectra of these glasses also show only the absorption bands of trivalent europium.

Studies of the absorption and fluorescence spectra of other rare earth phosphate

glasses are in progress in the University of Bath.

2.7 LOW TEMPERATURES VIBRATIONAL PROPERTIES OF GLASSES

At low temperatures, the thermal properties of solids are determined by phonons of long-wavelength. Phonons are characterized by the elastic behaviour of the medium averaged over a distance comparable with their wavelength. Typically, at temperatures below 1K, the wavelength of the dominant phonons is of the order of 1000Å, which is several hundred times larger than the interatomic distance in glass (Hunklinger and Raychaudhuri 1986). Therefore, at first sight no difference in long-wavelength phonon propagation effects between the irregular network of a glass and the regular lattice of a crystal should be noticeable. However, Zeller and Pohl (1971) found that the specific heats and thermal conductivities of vitreous and crystalline SiO_2 are essentially different. Of the various models originally proposed to account for anomalous behaviour of thermal properties, the one most widely and successfully used has been the phenomenological two-level system tunnelling model (Anderson et al. 1972, Phillips 1972). According to this model, atoms or groups of atom have more than one site in a disordered lattice, and these sites are separated by energy barriers. At low temperatures, atoms or groups of atoms can tunnel through the potential wells separating their possible sites, leading to splitting of the ground state of the two-level systems.

2.8 THE TWO-LEVEL SYSTEMS

In a perfect crystal, each atom is constrained by symmetry to occupy only a single potential minimum. Many defects can be represented microscopically as interstitial or substitutional impurity atoms or molecules moving in a multi-minima potential provided by the neighbouring atoms. At low temperatures a quantum mechanical description is necessary, and tunnelling of atoms from one minimum to another gives

rise to a very small energy splitting. A similar situation of tunnelling at very low temperatures is supposed to exist in the glassy state. In glassy networks, a certain number of atoms or small groups of atoms can occupy two or even more potential minima of nearly equal energy. However, only a small fraction of the total number of atoms will have this degree of freedom, while the remainder vibrate in single well potentials and are therefore essentially immobile at very low temperatures. A schematic illustration of a double-well potential is shown in Figure 2.17. At very low temperatures, a quantum tunnelling process through the barrier will be dominant, while at high temperature the atoms comprising the two-level systems will change configuration by means of a thermally activated process by hopping over the barrier.

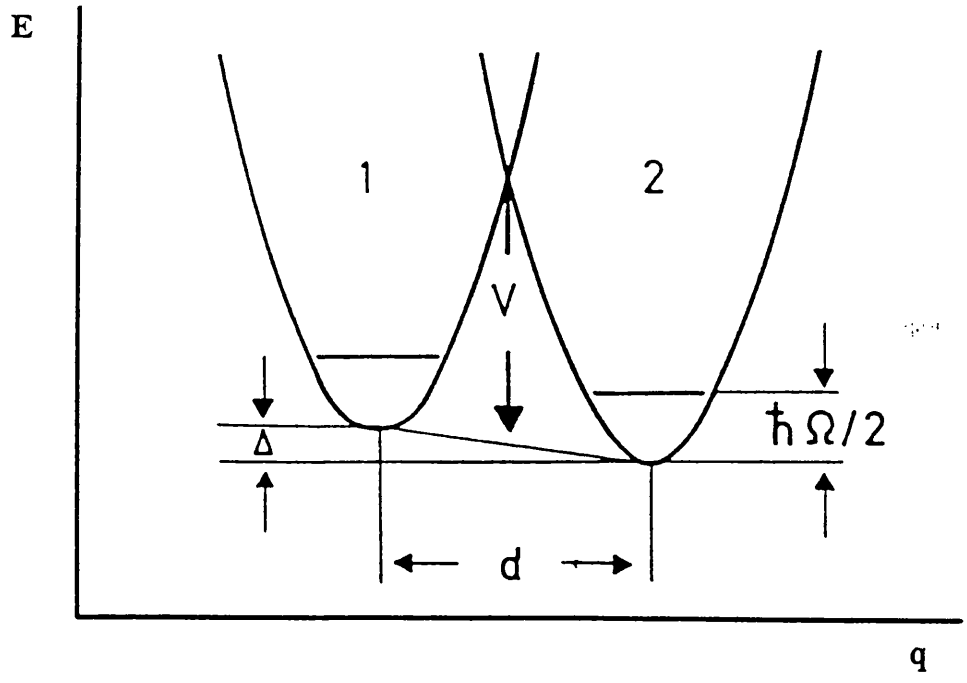

Figure 2.17. Schematic illustration of the double-well potential characterizing a two-level system plotted as a function of configurational coordinate **q**. The parameter Δ is the asymmetry energy and V is the barrier height (after Elliott 1990).

In the tunnelling model, the two wells of a double-well potential, separated by a distance d, are assumed to be parabolic and identical (Figure 2.17). There is an energy difference Δ between the depths of the wells so the two-level system is asymmetric; the barrier height is denoted by V. The ground state energy is $\hbar\Omega/2$. The configurational coordinate q, describes a combination of coordinates of a number of atoms (Phillips 1987).

At low temperatures only the vibrational ground state will be populated. If tunnelling occurs, the common ground state will not only be split due to Δ but also experience a tunnelling splitting Δ_0 given by

$$\Delta_0 = \hbar\Omega_0 e^{-\lambda} \tag{2.1}$$

where Ω is the vibrational frequency of each atom in a single well potential. The tunnelling parameter λ is given by

$$\lambda = d\left(\frac{2mV_0}{\hbar^2}\right)^{\frac{1}{2}} \tag{2.2}$$

where m is the mass of the tunnelling particle. In a random glassy network, the environment of the particle can be different at the two sites, leading to an energy difference Δ between the depths of the potential wells. The energy splitting E of the two eigenstates which represent the two-level system is then given by (Phillips 1981):

$$E = (\Delta^2 + \Delta_0^2)^{\frac{1}{2}} \tag{2.3}$$

An appropriate distribution of the parameters of the tunnelling states has to be introduced in the tunnelling model. Both Δ and λ are assumed to be independent of each other and uniformly distributed owing to the random disorder of glass structure (Hunklinger and Schickfus 1981). The generally accepted assumption is that :

$$P(\Delta,\lambda)d\Delta d\lambda = \overline{P}d\Delta d\lambda \tag{2.4}$$

where the distribution $\overline{P}$ is a constant. This assumption leads to a constant vibrational density of tunnelling states $n(E)$ and a very wide distribution of relaxation times.

This model can account for the low-temperature thermal properties since the atomic tunnelling offers a mechanism by which low excitation energies can be generated in the range of 10^{-5}eV<E<10^{-4}eV which correspond to a temperature between 0.1 and 1K. In the tunnelling states, the dominant process is resonant scattering of acoustic phonons, which controls the mean free path and hence the thermal conductivity, and also the ultrasonic attenuation. Thus below 1K, one finds a linear dependence of specific heat and thermal conductivity increases as T^2. This phenomenological model has turned out to be most successful, and explains quite well the universal low-temperature properties of glasses, especially below 1K (see for example, Phillips 1981, Hunklinger and Schickfus 1981, Hunklinger and Raychaudhuri 1986, Phillips 1987).

The higher-temperature, thermally activated configurational changes associated with the TLS can be detected through the observation of relaxational effects in which loss attenuation peak is manifested in ultrasonic wave attenuation measurements. This attenuation peak has been attributed to relaxation by thermally activated processes due to motion of oxygen atoms (Anderson and Bömmel 1955). A theoretical treatment of the relaxation process of two-level systems in glasses has been given by Jäckle (1972). This relaxation is supported by the observation that the shifts of the peak temperature P_{max} with changes in the frequency are in accord with an Arrhenius type law. For example in vitreous SiO_2, the peak maximum P_{max} of the ultrasonic wave attenuation is about 30K for the frequency of 1kHz, and shifted to about 100K at a driving frequency of 10^{10} Hz (Buchenau 1987). A mean activation energy of about 0.04eV was deduced from these processes. This value is consistent with a mean activation energy previously calculated by Hunklinger (1974) by assuming that there is a wide distribution of activation energies. A similar behaviour of thermally activated process has been

observed recently in phosphate glasses which have been made for this present study (Carini et al. 1994a).

The conventional relaxation spectroscopy experiments provide no information about the nature of this relaxation process. On the basis of neutron scattering experiments, it was suggested by Buchenau et al. (1988) that the structural relaxational in vitreous SiO_2 involved coupled rotational jumps of SiO_4 tetrahedra through distances of about 0.5Å (Figure 2.18). The motion involved is similar to that of low-frequency harmonic vibrations, found in calculations of low-frequency modes in a relaxed structure of vitreous SiO_2 (Guttmann and Rahman 1985).

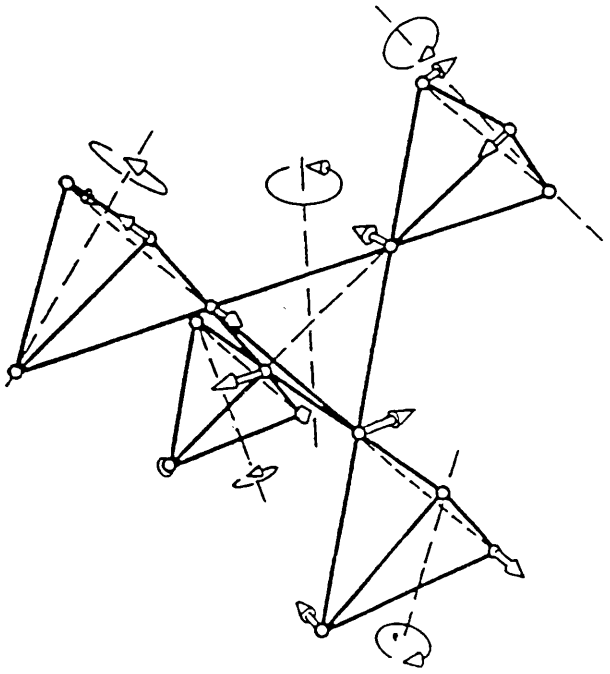

Figure 2.18. Local vibrational mode of five coupled SiO_4 tetrahedra (after Buchenau et al. 1984).

2.9 THE SOFT-POTENTIAL MODEL

Above 1K, the universal properties of glasses deviate from the predictions of tunnelling in the two-level systems model. The specific heat C_p rises more strongly than the Debye T^3-term (Lasjaunias et al. 1975), the thermal conductivity shows a plateau (Zeller and Pohl 1971), the sound velocity increases (Hunklinger and Arnold 1976) and the sound attenuation shows a plateau (Federle and Hunklinger 1982). At still higher temperatures, there is a peak in $C_p(T)/T^3$ (Jäckle 1981, Carini et al. 1994b) and a second increase of the thermal conductivity (Zeller and Pohl 1971, Freeman and Anderson 1986). It is in this temperature region that, the sound velocity decreases linearly and the sound absorption increases with increasing temperature (Hunklinger and Raychaudhuri 1986, Carini et al. 1994a). Buchenau et al. (1986) interpreted this behaviour as being related to a maximum in $g(\nu)/\nu^2$, where $g(\nu)$ is the low frequency vibrational density of states with a frequency ν. The low-frequency modes which contribute to the specific heat, co-exist with sound waves and show effects in neutron (Buchenau et al. 1986) and Raman scattering (Shuker and Gammon 1970, Winterling 1975, Malinovsky and Sokolov 1986), and in numerical work on model glass (Laird and Schober 1991, Schober and Laird 1991). Inelastic-neutron scattering measurements have shown these additional vibrational states to be soft harmonic vibrations, localised to about 10 or more atoms (Buchenau et al. 1986, 1988). The density of vibrational states obtained from the measurements of different properties for various glasses is found to have a universal character in the energy region of about 2 to 10 meV (Malinovsky et al. 1990). It is plausible to assume that both the two-level systems and these soft harmonic vibrations have a similar structural origin: they have the same vibrational structure (Grace and Anderson 1989, Brand and Löhneysen 1991).

A mathematical theory based on the idea of this soft harmonic configurations was developed by Karpov et al. (1983) using a soft-potential model (SPM). In this model,

both the tunnelling and the soft vibrational states appear as very similar localised modes with only slightly different potential parameters, the difference being ascribed to the local variation of atomic surroundings. The localised modes are assumed to have small force constants which can be positive or negative, but are stabilised by a positive fourth order term. The origin of the configurational coordinate x is chosen such that the third-order term of the potential vanishes.

According to the soft-potential model of Karpov et al. (1983), the potential of the soft localised modes with an effective mass M in terms of the dimensionless displacement x and a stabilising fourth-order term can be written as

$$V(x) = W\left[D_1\left(\frac{x}{d}\right) + D_2\left(\frac{x}{d}\right)^2 + \left(\frac{x}{d}\right)^4 \right] \tag{2.5}$$

where W is the binding energy given by

$$W = \frac{\hbar^2}{2Md^2} \tag{2.6}$$

Here d is a distance of the order of the interatomic spacing. The coefficients D_1 and D_2 are independent parameters which describe the soft mode. These two coefficients determine whether one deals with a tunnelling state, a soft vibration or relaxational state at even higher temperatures. Figure 2.19 shows the single- and double-well region of potential of Eq. (2.5) in the D_1 and D_2 plane. The inserts show the potential and the level of a typical tunnelling state (left) and of a typical vibrational state (right) (Buchenau 1993, Ramos et al. 1993).

Using the soft-potential model, it has been possible to explain the maximum in $C_p(T)/T^3$, the plateau in the thermal conductivity,(Figure 2.20), as well as the rapid rise of the acoustic absorption around 10K (Buchenau et al. 1992, Ramos et al. 1993, Buchenau 1993), a linear temperature dependence of the sound velocity below 100K (Carini et al. 1994a) and a number of relaxation and heat release phenomena (Parshin and Sahling 1993).

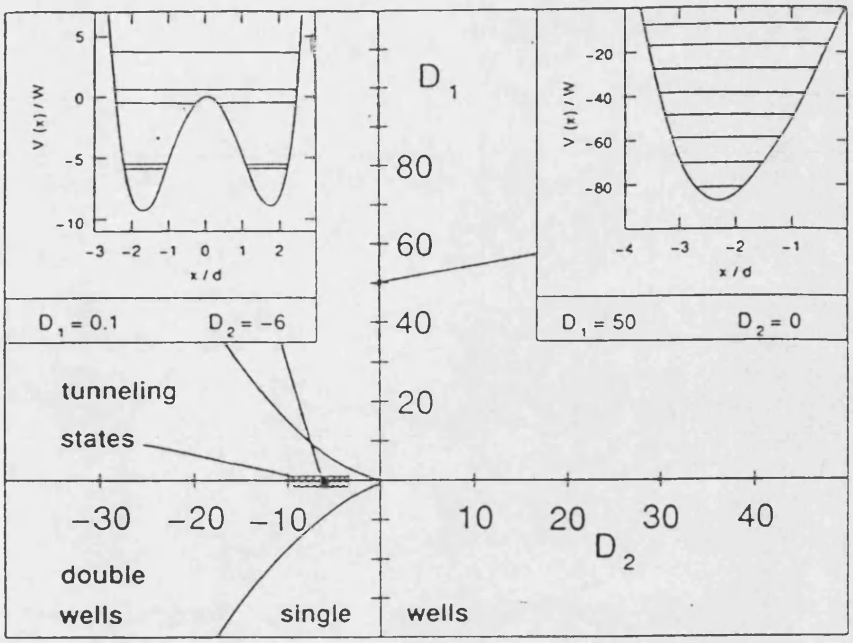

Figure 2.19. Single and double-well regions in the D_1-D_2 plane of the soft-potential model. Inserts: potentials and levels of a typical tunnelling state (left) and a typical vibrational state (right) (after Buchenau 1993).

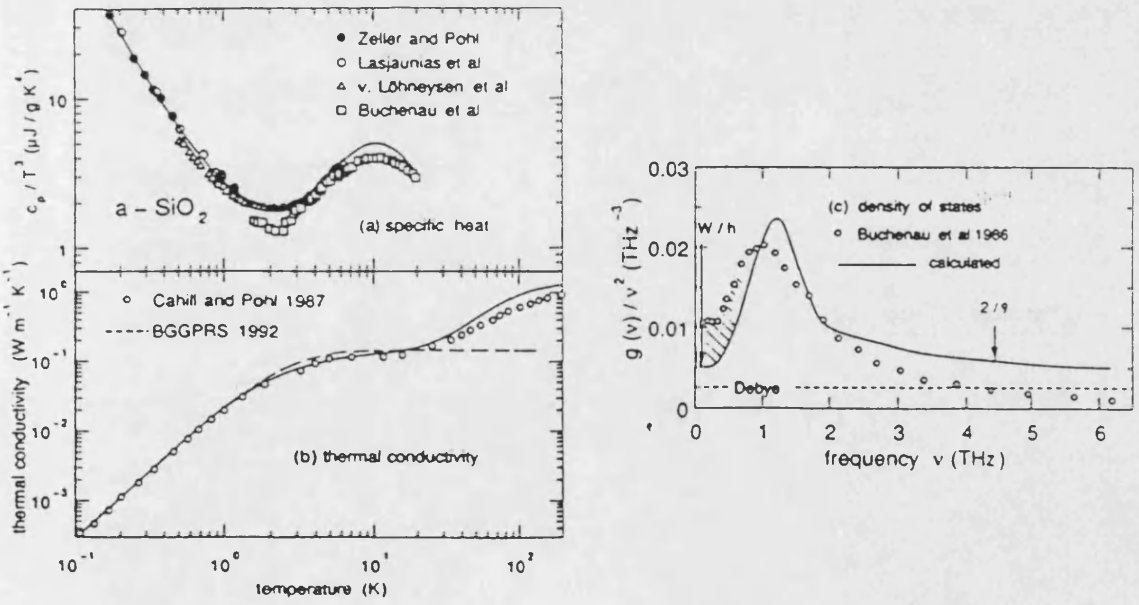

Figure 2.20. Comparison of the soft-potential model calculations (continuous lines) with those of experimental data for vitreous silica: (a) specific heat, (b) thermal conductivity and (c) density of vibrational states (after Gil et al. 1993).

2.10 LOCALISED VIBRATIONAL FRACTON MODES.

The soft-potential model discussed above provides a unified description of both the tunnelling and the low-frequency vibrational states. In an attempt to account for the deviation of the tunnelling model of the two-level systems above 1K, Alexander and Orbach (1982) introduced a fracton model, using the concept of fractals, first introduced by Mandelbrot (1977). Possible explanation for the enhanced low-frequency vibrational density of states $g(\nu)$ as compared to the Debye density of states $g_D(\nu)$ in amorphous materials is crossover from sound waves at low-frequencies to vibrations of crystallites or fractals. Thus this model is a consequence of the presence of localised vibrations which arise from the possible fractal structure of glasses (Alexander et al. 1983). It was suggested by Alexander et al. (1983) that one regard glassy materials as having a random force-constant structure at short length scales. A fractal connectivity was assumed for the masses which participate in the vibrational dynamics at length scales smaller than some characteristic length ζ. In analogy to percolation networks, the materials look homogeneous at larger length scales. In aerogels of silica, where such a crossover from fractal to homogeneous structure has been experimentally observed in neutron scattering (Codden et al. 1989, Vacher et al. 1989), the fractal structure is thought to exist in a mesoscopic length scale regime. When the smaller distances are probed, the microstructure from which the gel is constructed (silica spheres of radius between 6 and 10Å) begin to appear. In this length regime the fractal structure appropriate to mesoscopic length scales no longer applies. In denser media, such as vitreous silica, Alexander et al. (1983) assumed that a similar demarcation exists between a homogeneous and a fractal regime for the network which generates the elastic compliance. Alexander et al. (1983) also point out that the mass density does not have to be fractal, rather, the mass which is participating in the vibrational dynamics is assumed to be vibrationally connected via a network of bonds which possesses fractal

geometry on sufficiently short length scales. The picture of the structure of a glass as having vibrational dynamics associated with a force-constant fractal structure at short length scales can be motivated by the observation that, although the mass density may be uniform on the average in a disordered network, the vibrational connectivity between sites could be random and self-similar. This leads to a fractal structure insofar as the connectivity and elastic properties are concerned (Jagannathan et al. 1989).

The phonon-fracton cross-over model of Orbach (1986) is associated with the existence of a characteristic length scale ζ, beyond which the medium appears to be homogeneous (Euclidean) and allows propagation of extended phonons modes. This length scale can be translated into a crossover frequency for the medium ω_{co} given by (Aharony et al. 1985)

$$\omega_{co} \propto \zeta^{-D/\bar{d}} \tag{2.6}$$

where D is the fractal dimension and $\bar{d}$ is the fracton dimension. Here, the fracton frequencies are greater than ω_{co} and phonon frequencies are less than ω_{co}. The variation of the vibrational density of states $N(\omega)$ associated with a vibrating fractal network can be seen in Figure 2.21 (Aharony et al. 1985). It suggests a bump-like structure in the vicinity of ω_{co}.

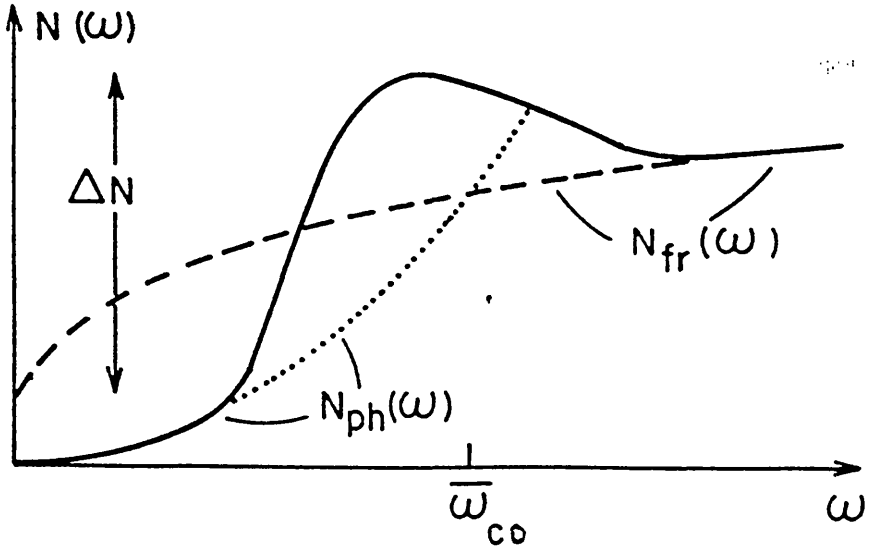

Figure 2.21. Crossover of the density of vibrational states (solid line). The dotted (dashed) lines represent the continuation of the phonon (fracton) asymptotic behaviour into the crossover regime (after Aharony et al. 1985).

The localised character of fracton excitations can have profound implications, such as in the thermal conductivity and the specific heat of a fractal network (Orbach 1986). At temperatures well below that of the plateau region, the thermal conductivity has a T^2 dependence (Zeller and Pohl 1971, Anderson 1981) that can be understood as arising from the scattering of phonons off two-level systems in glassy medium (Anderson et al. 1972, Phillips 1972). The long length scale (low-energy) vibrational excitations are phonons and able to carry heat from one spatial region to another. However, as the temperature increases, higher energy vibrations will be excited, phonon scattering due to other processes become important, giving rise to a steeply falling phonon mean free path as a function of increasing temperature. This regime is caused by a combination of strong elastic scattering of the phonons from the strong spatial force-constant fluctuations, caused when the phonon wavelength shortens to the length scale ζ, and inelastic scattering resulting from anharmonicity of the localised vibrational excitations. When the phonon wavelength reduces to a length scale ζ, crossover occurs to localised vibrational excitations. Phonons of wavelengths shorter than this characteristic length scale, or of frequency greater than the so-called crossover frequency, will be localised. When ω is approximately equal to ω_{co}, higher temperatures will excite fractons and not phonons (Figure 2.21). However, fractons cannot carry heat from one spatial region to another because they are localised. This means that kT will be much greater than the energy of those vibrational states that can carry heat (the phonons). Assuming a temperature-independent mean free path for the phonons implies a thermal conductivity independent of temperature. Such a plateau in the thermal conductivity is common to nearly all amorphous solids (Zeller and Pohl 1971). When the temperature is further increased, eventually the thermal conductivity is seen to increase. A new channel for heat conduction comes into effect. This is a hopping contribution to thermal conductivity κ of the localised vibrational excitations assisted by the phonons to which

they are coupled via vibrational anharmonicity interactions (Alexander et al. 1986, Orbach 1986). The thermal conductivity is predicted to increase linearly with temperature, which is consistent with experimental observations (Zeller and Pohl 1971).

Similarly, the fracton model has been tested by many authors in descriptions of the experimental data. Good agreement has been obtained to explain the maximum in $C_p(T)/T^3$ (Aharony et al. 1985, Avogadro et al. 1986, 1987, Carini et al. 1994b), the plateau in the thermal conductivity (Jagannathan et al. 1989, Posselt et al. 1991), and also the temperature and frequency dependence of the sound velocity in vitreous silica (Jagannathan and Orbach 1990). However, the application of the fractal concept of phonon-fracton crossover especially to denser glasses can still be questioned and is not fully supported by the experimental observation (Graebner et al. 1986, Posselt et al. 1991, Ahmad and Hutt 1991).

In the present experimental observations of the acoustic and thermal properties of rare earth phosphate glasses, the velocity and attenuation data have been interpreted (Carini et al. 1994a) successfully using the soft-potential model (Parshin 1993), with the dominant relaxation mechanism involves the soft single well potentials or harmonic oscillators. In the case of interpretation of the specific heat data for samarium phosphate glasses (Carini et al. 1994b), the phonon-fracton cross-over model (Orbach 1986) provides more consistent results similar to those of other oxide glasses. However the effects of pressure on the elastic behaviour of glasses have not yet been treated in the context of the soft-potential model or fracton model.

CHAPTER 3

THE THEORY OF ELASTICITY FOR ISOTROPIC MATERIALS

3.1 INTRODUCTION

Elasticity is the property whereby a body, when deformed, automatically recovers its normal configuration as the deforming forces are removed. The fundamental quantities in elasticity are second-rank tensors: the deformation is represented by the strain tensor and the forces are represented by the stress tensor. In the present study, two areas of acoustic vibrational properties of an isotropic material have been investigated: the linear and nonlinear elastic properties. Beyond the elastic limit, the medium deforms permanently; this is plastic deformation. Figure 3.1 shows the regions of linear and nonlinear elastic deformation of stress-strain relation for a solid material.

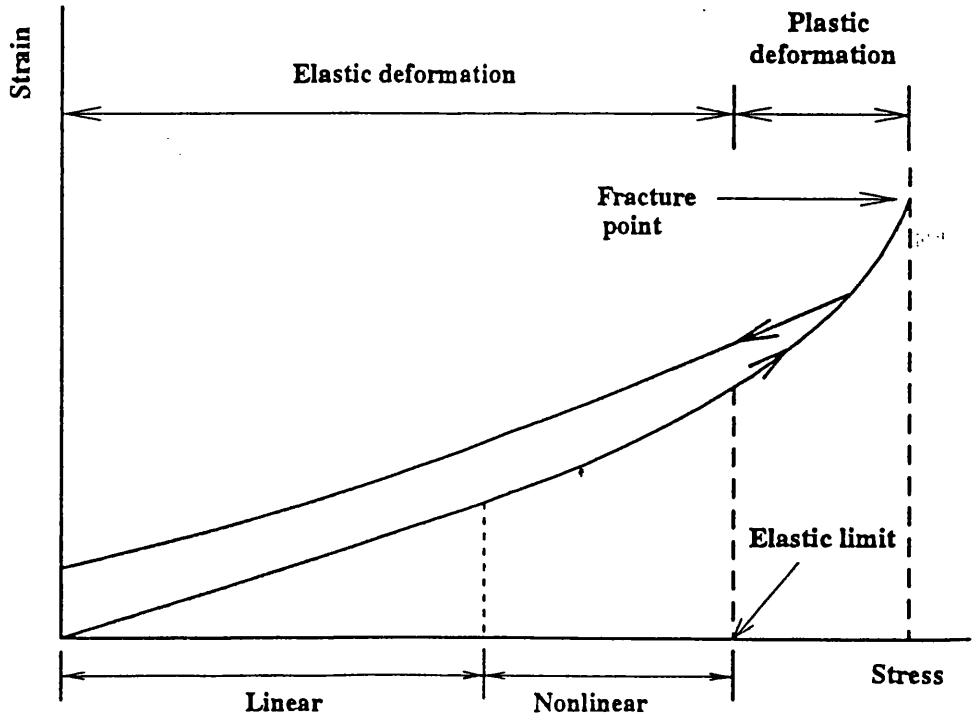

Figure 3.1. Stress-strain behaviour of a solid material.

In the linear elastic region, the only deformation that is considered is that the stress is linearly related to strain. This is Hooke's law. The proportional constant relating stress and strain is the elastic stiffness, more precisely, the second order elastic stiffness (SOEC), a fourth rank tensor property with components C_{IJ}. As the deformations are increased further, the relation between strain and stress becomes nonlinear. However, when the stress is removed, the body still returns to its original state. In the nonlinear deformation region, a quantitative assessment of the nonlinear behaviour requires the third and higher order elastic stiffnesses.

The nonlinearity of the interatomic forces with respect to atomic displacement relates to the anharmonicity of the interatomic vibration, that is, the vibrational anharmonicity. These nonlinear terms are responsible for anharmonic effects such as thermal expansion, which depend upon thermal atomic motion and the interaction of waves with each other. Knowledge of the higher order elasticity such as third (TOEC) and fourth (FOEC) order elastic stiffness tensor components allows one to evaluate the nonlinear terms in the equation of motion. As such, the TOEC and FOEC provide detailed information on the elastic behaviour under pressure. The SOEC and TOEC data can be used to calculate the hydrostatic pressure derivatives $(\partial C_{IJ}^{S}/\partial P)_{T,P=0}$ of the SOEC and $(\partial B^{S}/\partial P)_{T,P=0}$ of the bulk modulus B. To quantify the vibrational anharmonicity of the glasses in the long-wavelength limit, the acoustic mode Grüneisen parameters are evaluated. In the following sections, a description of the theory of elasticity of solids with particular reference to an isotropic material is given.

3.2 STRESS, STRAIN AND HOOKE'S LAW

When an ultrasonic wave propagates in a solid material, it disturbs the particles of the medium from their equilibrium positions. Internal restoring forces and particle

inertia can cause vibrations of the medium and elastic wave propagation ensues. Any solid material which is acted on externally by such a system of forces is in a state of stress. The elastic stiffnesses are defined in term of the response of a solid material to an applied stress.

The stress tensor σ_{ij} represents the components of force per unit area acting on an element of area in the material (Figure 3.2). Because of symmetry conditions arising from the assumed absence of torques, the stress tensor is symmetric, that is $\sigma_{i,j} = \sigma_{j,i}$. Thus there are only six independent components of stress. The nine possible stress components may be written in the form of a matrix

$$\begin{bmatrix} \sigma_{11} & \sigma_{12} & \sigma_{13} \\ \sigma_{21} & \sigma_{22} & \sigma_{23} \\ \sigma_{31} & \sigma_{32} & \sigma_{33} \end{bmatrix} \tag{3.1}$$

The strain tensor $\varepsilon_{k,l}$ represents the components of deformation which a body undergoes when subjected to a stress (Figure 3.3). The strain tensor $\varepsilon_{k,l}$ can be written as (Nye, 1985):

$$\varepsilon_{k,l} = \frac{1}{2}(\varepsilon_{k,l} + \varepsilon_{l,k}) = \frac{1}{2}\left(\frac{\partial S_k}{\partial x_l} + \frac{\partial S_l}{\partial x_k}\right) \quad with \quad k,l = 1,2,3 \tag{3.2}$$

where S_k is the displacement of a point within the body and x_l is a coordinate of the reference frame. The strain tensor $\varepsilon_{k,l}$ is symmetric, that is $\varepsilon_{k,l} = \varepsilon_{l,k}$. Again, of the possible nine components of the strain tensor, only six components are independent.

$$\begin{bmatrix} \varepsilon_{11} & \varepsilon_{12} & \varepsilon_{13} \\ \varepsilon_{21} & \varepsilon_{22} & \varepsilon_{23} \\ \varepsilon_{31} & \varepsilon_{32} & \varepsilon_{33} \end{bmatrix} \tag{3.3}$$

Hooke's Law forms the basis for describing the linear relation between stress and strain for a small deformation:

$$\sigma_{ij} = C_{i,j,k,l}\varepsilon_{k,l} \tag{3.4}$$

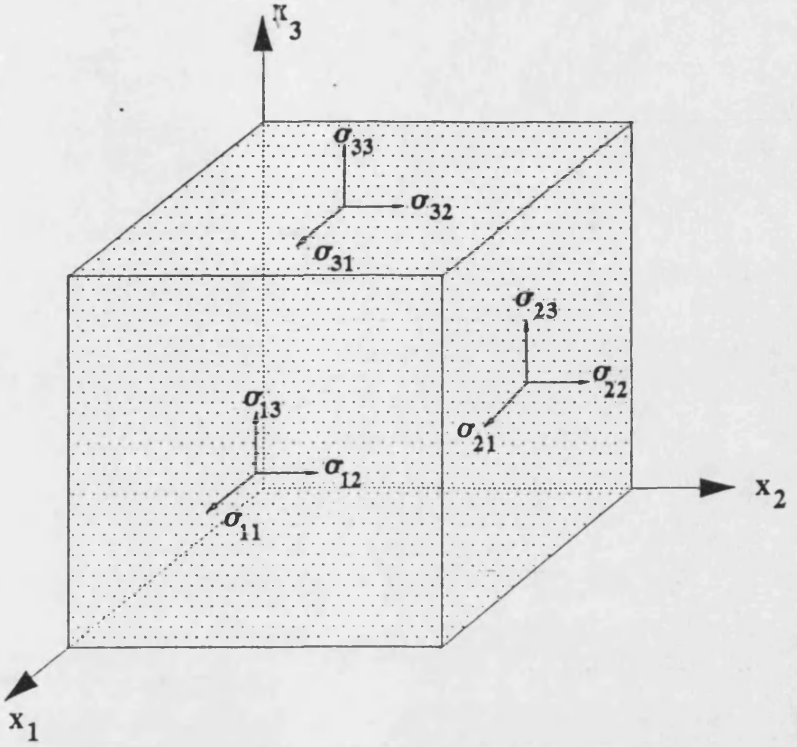

Figure 3.2. Definitions of the stresses acting on a rectangular parallelpiped sample.

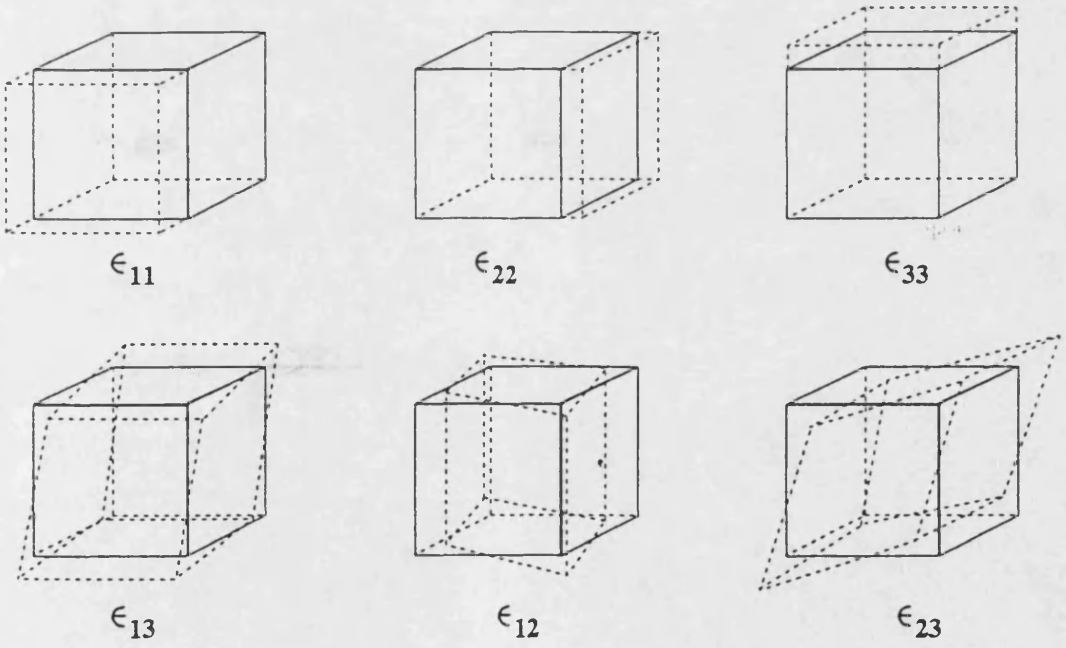

Figure 3.3. Definitions of the strains produced in a rectangular parallelpiped sample.

where the components $C_{i,j,k,l}$ are the 81 elastic stiffness tensor coefficients of a solid material. However, since the stress and strain tensors are symmetric, the number of coefficients is reduced from 81 to 36, that is,

$$C_{i,j,k,l} = C_{i,j,l,k} = C_{j,i,k,l} \tag{3.5}$$

The other symmetry requirement is that there should be an elastic potential (the medium being elastic) having strain energy as a function of state and independent of the path by which the state is reached. This imposes further the symmetry relation:

$$C_{i,j,k,l} = C_{j,i,k,l} = C_{i,j,l,k} = C_{k,l,i,j} \tag{3.6}$$

This symmetry condition has the effect of reducing the number of independent elastic stiffness tensor components for any medium from 36 to 21 (Huntington 1958). For solids of higher symmetry, the necessary independent elastic stiffness tensor components become fewer in number.

Taking into account the symmetry of the tensor $\sigma_{i,j}$, $\varepsilon_{i,j}$ and $C_{i,j,k,l}$, one can adopt another, frequently more convenient system of labelling, which replaces two indices by one and four indices by two, that is, $C_{i,j,k,l} \rightarrow C_{IJ}$. The scheme of replacement is as follows:

Tensor Notation *i,j*	11	22	33	23 , 32	13 , 31	12 , 21
Matrix Notation *I,J*	1	2	3	4	5	6

Then Hooke's law takes the matrix form with 21 elastic stiffnesses

$$\begin{bmatrix}\sigma_1\\ \sigma_2\\ \sigma_3\\ \sigma_4\\ \sigma_5\\ \sigma_6\end{bmatrix} = \begin{bmatrix}C_{11} & C_{12} & C_{13} & C_{14} & C_{15} & C_{16}\\ C_{12} & C_{22} & C_{23} & C_{24} & C_{25} & C_{26}\\ C_{31} & C_{32} & C_{33} & C_{34} & C_{35} & C_{36}\\ C_{41} & C_{42} & C_{43} & C_{44} & C_{45} & C_{46}\\ C_{51} & C_{52} & C_{53} & C_{54} & C_{55} & C_{56}\\ C_{61} & C_{62} & C_{63} & C_{64} & C_{65} & C_{66}\end{bmatrix} \begin{bmatrix}\varepsilon_1\\ \varepsilon_2\\ \varepsilon_3\\ \varepsilon_4\\ \varepsilon_5\\ \varepsilon_6\end{bmatrix} \tag{3.7}$$

where $C_{I,J} = C_{J,I}$.

For an isotropic solid, the three coordinate axes, *x, y, z* and the three coordinate planes *yz, xz, xy* are equivalent. Consequently, the response of the medium must be the same for a longitudinal stress applied along any axis. This condition leads to

$$C_{11} = C_{22} = C_{33}$$

$$C_{12} = C_{13} = C_{23} \tag{3.8}$$

Similarly, the shear strain produced in a coordinate plane by a shear stress applied in that plane must be the same for all coordinate planes,

$$C_{44} = C_{55} = C_{66} \tag{3.9}$$

Next, suppose that a longitudinal stress σ_1 applied along the *x* axis produces a shear strain ε_6 in the *xy* plane. Since the medium is isotropic, an equally valid solution to the applied stress problem is one in which the medium is rotated through 180° about the x axis. This reverses the sign of ε_6, which can therefore only be zero. As a consequence,

$$C_{16} = 0 \quad . \tag{3.10}$$

Similarly

$$C_{14} = C_{15} = C_{24} = C_{25} = C_{26} = C_{34} = C_{35} = C_{36} = 0 \tag{3.11}$$

and

$$C_{45} = C_{46} = C_{56} = 0 \tag{3.12}$$

Thus, the second order elastic stiffness tensor components matrix for an isotropic material is written as:

$$C_{I,J} = \begin{bmatrix} C_{11} & C_{12} & C_{12} & 0 & 0 & 0 \\ C_{12} & C_{11} & C_{12} & 0 & 0 & 0 \\ C_{12} & C_{12} & C_{11} & 0 & 0 & 0 \\ 0 & 0 & 0 & C_{44} & 0 & 0 \\ 0 & 0 & 0 & 0 & C_{44} & 0 \\ 0 & 0 & 0 & 0 & 0 & C_{44} \end{bmatrix} \tag{3.13}$$

with

$$C_{12} = C_{11} - 2C_{44} \tag{3.14}$$

From (3.13) and (3.14), it follows that an isotropic medium has only two independent stiffness components; often called the *Lamé constants* and written as λ and μ, where $\lambda = C_{12}$ and $\mu = C_{44}$; thus $C_{11} = \lambda + 2\mu$. The elastic stiffnesses C_{11} and C_{44} are more preferable in the present work, because they are related directly to the longitudinal and shear ultrasonic waves velocities. These elastic stiffnesses are also analytically related to the other elastic parameters such as the bulk (B) , Young's (E) moduli and Poisson's ratio σ (see below).

3.3 EQUATIONS OF MOTION

The SOEC have been determined experimentally by measuring the velocities of ultrasonic elastic waves propagating through a sample. The wave motion is assumed to be adiabatic causing only infinitesimal displacements of volume elements in the media. The equations of motion are obtained by equating the resultant force due to internal stresses to the product of acceleration and mass per unit volume. Newton's equation of motion in a continuous medium can be written as:

$$\frac{\partial \sigma_{ij}}{\partial x_j} = \rho_0 \frac{\partial^2 u_i}{\partial t^2} \tag{3.15}$$

where ρ_0 is the density, t is the time and u is the displacement vector. Using Hooke's Law:

$$C_{ijkl}\frac{\partial \varepsilon_{kl}}{\partial x_j} = \rho_0 \frac{\partial^2 u_i}{\partial t^2} \quad with \quad i = 1,2,3 \tag{3.16}$$

The equations of motion can be solved using the *Christoffel equation* (see for example, Mason 1958, Maynell 1972, Pollard 1977). For an isotropic material, the solution consists of one longitudinal and two identical shear waves. In summary, ultrasound wave propagation in an isotropic medium is characterized by the following:

1. There are three velocities corresponding to three plane waves.
2. The longitudinal mode corresponds to C_{11} and has a velocity of v_L equal to $\sqrt{C_{11}/\rho}$.
3. The two shear modes are degenerate with the same velocity for all directions of propagation. The shear wave velocity is given by v_S equal to $\sqrt{C_{44}/\rho}$.
4. The velocities of the three modes remain the same for all directions of propagation; that is, as a consequence of the isotropy condition:

$$2C_{44} = C_{11} - C_{12} \quad .$$

The measured experimental values of ultrasonic wave velocities and the density of the sample are used to determine the values of the adiabatic SOEC, and their related elastic behaviour by the following expressions:

SOEC	$C_{11}^S = \rho v_L^2$
	$C_{44}^S = \rho v_S^2$
Bulk modulus	$B^S = \rho(3v_L^2 - 4v_S^2)/3$
Fractal dimension	$F = 4C_{44}/B^S$
Young's modulus	$E^S = \rho v_S^2 \frac{(3v_L^2 - 4v_S^2)}{(v_L^2 - v_S^2)}$

Poisson's ratio

$$\sigma^s = \frac{(v_L^2 - 2v_S^2)}{2(v_L^2 - v_S^2)} \tag{3.17}$$

3.4 ULTRASONIC WAVE ATTENUATION

If a solid medium obeyed Hooke's Law strictly, there would be no acoustic absorption. However, in a real medium there are viscous damping forces and nonlinearities, which cause energy to be extracted from the wave in the form of heat. Ultrasonic wave attenuation is defined as the rate of decay of a mechanical wave at ultrasonic frequency as it propagates through the sample. The rate of decay of the wave can be expressed as:

$$A = A_0 e^{(-\alpha z)} e^{i(\omega t - kz)} \tag{3.18}$$

where α is the attenuation of the wave travelling in the z-direction with propagating constant k ($= (2\pi)/\lambda$) and wavelength λ. The wave is defined as infinite in extent and of uniform amplitude A in the x- and y-direction. Its angular frequency is ω, which is 2π times the frequency f in hertz.

In the present work, ultrasonic wave attenuation is determined using the pulse echo method by measuring relative amplitudes of ultrasonic signals propagated through the sample and is calculated from the equation:

$$\alpha = 20 \log\left[\frac{A_1}{A_2}\right] \quad \text{dB} \tag{3.19}$$

where A_1 and A_2 are the amplitude of adjacent echoes.

The attenuation α is usually expressed in units dB/cm or Np/m where 1Np is equal to 8.7 dB.

3.5 LATTICE VIBRATIONAL ANHARMONICITY

Lattice vibrations in crystalline solids are treated as quasi-particles called phonons. These phonons are responsible for many physical properties such as elasticity, thermal

expansion, specific heat, thermal conductivity etc. Based on the lattice dynamic model, the restoring forces between atoms and hence their potential energy are generally considered to be a function of atomic displacement from equilibrium positions.

In the purely harmonic approximation (Figure 3.4), the series of potential energy as a function of the atomic displacement is terminated at the quadratic term which is equivalent to Hooke's law. In this harmonic approximation, phonons are treated as a superposition of independent harmonic vibrations. As a consequence of this approximation, the elastic stiffnesses would be independent of both temperature and pressure (see for example, Ashcroft and Mermin 1976, Brüesch 1982). However, in real solids the harmonic approximation is not valid, since temperature and pressure dependences of the elastic stiffnesses are observed. In order to obtain a correct interpretation of the lattice vibrations in solids, the anharmonic vibrational effects have to be taken into consideration.

In the quasiharmonic approximation proposed by Leibfried and Ludwig (1961), the power series of the potential energy is also terminated in the quadratic term. However, in this approximation, the force constants are dependent on the interatomic distance, that is, the phonon frequencies are considered to be volume dependent. Even though this model has been used to explain the thermal behaviour of solids, it is not accurate enough to explain many important thermodynamic properties. To acquire a complete description of anharmonicity of lattice vibrations in solids, the power series of the interatomic potential energy should include the higher order terms which describe the asymmetry of the lattice potential energy (Figure 3.4). These terms are related closely to the higher order elastic stiffness tensor components studied in the present work and which describe the vibrational anharmonicity of the long-wavelength acoustic phonons.

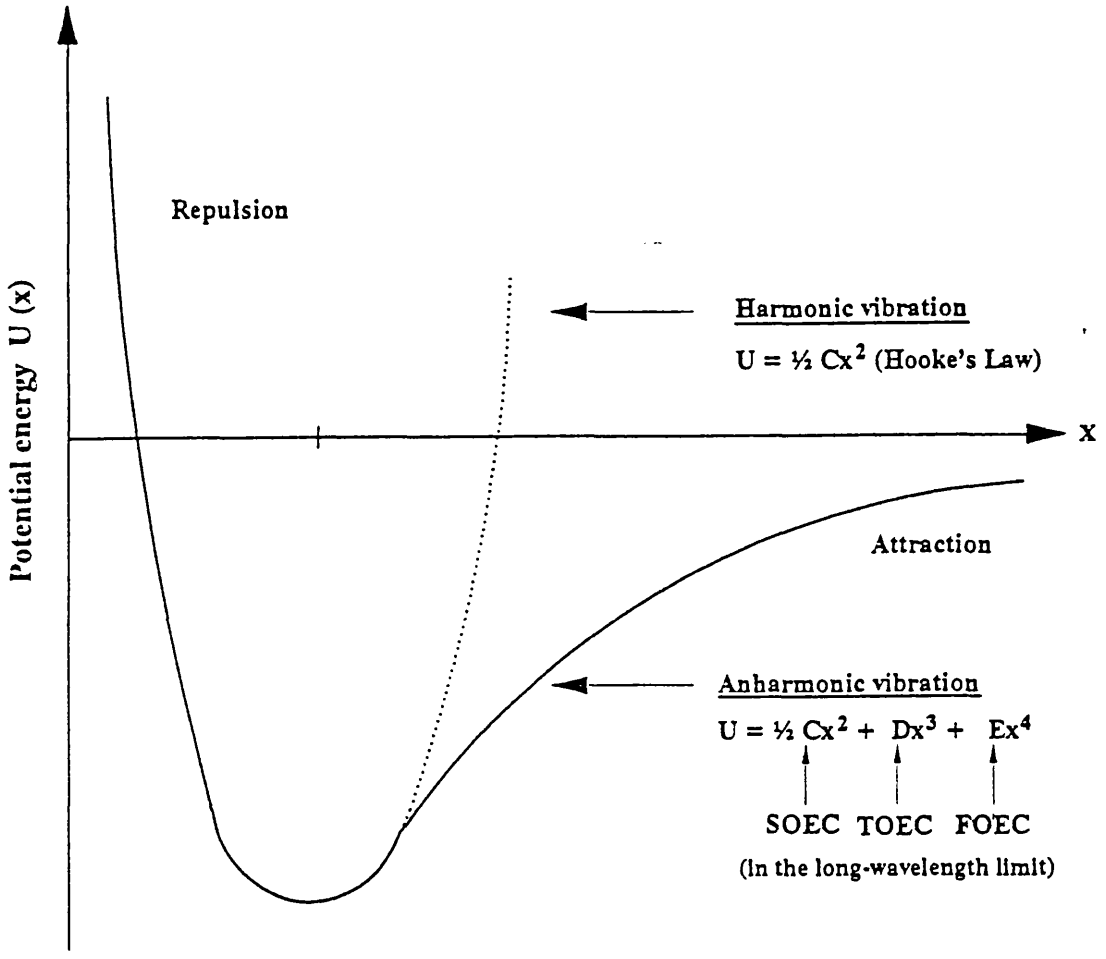

Figure 3.4. Interatomic potential U(x) as a function of atomic displacement of harmonic and anharmonic lattice vibrations in a solid material.

The strain-energy density of a solid material is given by the power series expansion in Langrangian

$$\rho_0 U(\eta) = \frac{1}{2} C^S_{\alpha\beta\gamma\delta}\eta_{\alpha\beta}\eta_{\gamma\delta} + \frac{1}{6} C^S_{\alpha\beta\gamma\delta\varepsilon\zeta}\eta_{\alpha\beta}\eta_{\gamma\delta}\eta_{\varepsilon\zeta}$$

$$+\frac{1}{24} C^S_{\alpha\beta\gamma\delta\varepsilon\zeta\nu\theta}\eta_{\alpha\beta}\eta_{\gamma\delta}\eta_{\varepsilon\zeta}\eta_{\nu\theta} + \cdots\cdots \qquad \eta_{\gamma\delta}\eta_{\varepsilon\zeta}$$

$$+\frac{1}{24} C^S_{\alpha\beta\gamma\delta\varepsilon\zeta\nu\theta}\eta_{\alpha\beta}\eta_{\gamma\delta}\eta_{\varepsilon\zeta}\eta_{\nu\theta} + \cdots\cdots \tag{3.20}$$

where $U(\eta)$ is the strain energy per unit mass and ρ_0 is the density at atmospheric pressure. The Langrangian strain $\eta_{\alpha\beta}$ is defined in terms of the deformation gradient from the natural to the strained state $\mathbf{F}=\partial\mathbf{x}/\partial\mathbf{X}$ (X_α and x_i being the coordinates of material particles in the natural and strained states) by

$$\eta_{\alpha\beta} = \frac{1}{2}(F_{i\alpha}F_{i\beta} - \delta_{\alpha\beta}) \tag{3.21}$$

The coefficients of the terms in the strain-energy expansion (Eq. 3.20) are the thermodynamic second-, third-, and fourth-order isentropic (superscript S, adiabatic) stiffness tensor (Brugger 1964)

$$C^S_{\alpha\beta\gamma\delta} = \rho_0\left(\frac{\partial^2 U(S,\eta)}{\partial\eta_{\alpha\beta}\partial\eta_{\gamma\delta}}\right)_{S;\eta=0}$$

$$C^S_{\alpha\beta\gamma\delta\varepsilon\zeta} = \rho_0\left(\frac{\partial^3 U(S,\eta)}{\partial\eta_{\alpha\beta}\partial\eta_{\gamma\delta}\partial\eta_{\varepsilon\zeta}}\right)_{S;\eta=0}$$

$$C^S_{\alpha\beta\gamma\delta\varepsilon\zeta\nu\theta} = \rho_0\left(\frac{\partial^4 U(S,\eta)}{\partial\eta_{\alpha\beta}\partial\eta_{\gamma\delta}\eta_{\varepsilon\zeta}\eta_{\nu\theta}}\right)_{S;\eta=0} \tag{3.22}$$

which form tensors of the fourth, six and eighth ranks respectively.

The TOEC and FOEC are the coefficients of the cubic and quartic terms, respectively, in the Hamiltonian as a function of strain and so measure the long-wavelength anharmonicity of the vibrational states (up to fourth power in strain), that is, the nonlinearity of the atomic forces with respect to atomic displacements. The knowledge of TOEC and FOEC provides quantitative understanding of thermal expansion hence the nonlinear acoustic vibrational behaviour. Using ultrasonic tech-

niques, a determination of the TOEC is associated with the measurements of finite strains produced by propagating the elastic waves through a medium which is subjected to static stress.

Some physical properties such as the temperature dependence of the SOEC result from thermal motion which relates to vibrational anharmonicity can be interpreted quantitatively when the higher order elastic stiffness tensor components are known.

3.6 TEMPERATURE DEPENDENCE OF THE SOEC

The temperature dependence of the SOEC is an example of the anharmonic character of the interatomic potential energy in solid materials. Theoretical studies of this problem were made by Born and Huang (1954) and by Leibfreid and Ludwig (1961).

The temperature dependences of the velocities of longitudinal and shear ultrasonic waves propagated in phosphate glasses normally do not follow the behaviour expected from vibrational anharmonicity, namely a linear increase with decreasing temperature and a zero slope at low temperatures. The steepening rise as temperature is lowered, which has been observed, bears some resemblance to behaviour observed in the temperature dependence of the velocities of ultrasonic waves propagated in vitreous SiO_2 (Piché et al. 1974, Hunklinger 1982, Raychaudhuri and Hunklinger 1984), although it commences at a rather higher temperature. At very low temperatures, the ultrasonic velocity propagated in vitreous SiO_2 reaches a maximum at a temperature T_m below which it decreases as a result of a resonant interaction. Above T_m there is a relaxation effect arising from the energy splitting of the two-level systems in the ultrasonic strain field. Measurements have been made on the phosphate glasses at temperatures well above T_m which corresponds to the relaxation interaction regime. Evidence for this is provided by the ultrasonic attenuation between 10K and about 250K, which is characterised by a broad peak typical of a spectrum of thermally

activated structural relaxations of the two-level systems (Carini et al. 1990a,b).

In the present study, to assess the magnitude of the relaxation contribution to the ultrasonic wave velocities, the more usual anharmonic effects have been extracted on the basis of the Debye model coupled with an anharmonic oscillator. The temperature dependence of each elastic stiffness has been approximated by the conventional model for vibrational anharmonicity using (Lakkad 1971):

$$C_{IJ} = C_0\left[1 - KF\left(\frac{T}{\Theta_D}\right)\right] \tag{3.23}$$

with

$$F\left(\frac{T}{\Theta_D}\right) = 3\left(\frac{T}{\Theta_D}\right)^4 \int_0^{\Theta_D/T} \frac{x^3 dx}{e^x - 1} \tag{3.24}$$

where C_0 is the elastic stiffness at zero Kelvin, Θ_D is the Debye temperature and a constant K have been chosen to fit the elastic stiffness data at high temperatures where the relaxation is negligible.

The relaxation contribution to each mode velocity can be obtained from the relative difference in velocity $\Delta v/v_0$ between the experimentally measured values and that after the anharmonic contribution has been extracted. Raychaudhuri and Hunklinger (1984) suggested that the relaxation interaction to the velocity can be described logarithmically:

$$\frac{\Delta v}{v} = -A \ln\left[\frac{T}{T_0}\right] \tag{3.25}$$

where T_0 is an arbitrary temperature and A is a constant. However, the Eq. (3.25) does not describe adequately the effect on the velocity of the spectrum of thermally activated relaxations indicated by the temperature dependence of the ultrasonic attenuation.

The temperature derivatives $(\partial C_{IJ}/\partial T)$ of the SOEC can be determined using a quasiharmonic continuum model of Garber and Granato (1975) which have been extended to isotropic materials by Claytor and Sladek (1978). At room temperature,

the $(\partial C_{IJ}/\partial T)$ for an isotropic material can be calculated using the following expression (Thurston 1964):

$$\frac{\partial C_{IJ}}{\partial T} = C_{IJ}^{T}\left[\frac{2}{f_0}\left(\frac{\partial f}{\partial T}\right) - \frac{\alpha_V}{3}\right] \tag{3.26}$$

where f_o is the measured overlap frequency and α_V is the volume thermal expansion coefficient. These values have been used here to estimate the magnitude of the fourth order elastic stiffness tensor components (FOEC) in glasses.

3.7 EXPERIMENTAL CONFIGURATIONS FOR DETERMINATION OF THE TOEC OF AN ISOTROPIC MATERIAL

An isotropic material has the following TOEC:

$$\begin{gathered} C_{123} \\ C_{456} \\ C_{111} = C_{222} = C_{333} \\ C_{144} = C_{255} = C_{366} \\ C_{112} = C_{233} = C_{133} = C_{113} = C_{122} = C_{233} \\ C_{155} = C_{244} = C_{344} = C_{166} = C_{266} = C_{355} \end{gathered} \tag{3.27}$$

Of these only three are independent; in accordance to *Lamé coefficients* they can be written as:

$$\begin{aligned} \nu_1 &= C_{123}, \\ \nu_2 &= C_{144}, \\ \nu_3 &= C_{456} \end{aligned} \tag{3.28}$$

The remaining non-zero tensor components are then given by linear combinations of these three parameters:

$$C_{112} = \nu_1 + 2\nu_2$$

$$C_{155} = \nu_2 + 2\nu_3$$

$$C_{111} = \nu_1 + 6\nu_2 + 8\nu_3. \qquad (3.29)$$

The TOEC, which are sixth rank tensor components C_{uvprqs}, can be obtained from the stress derivatives $(\rho_o W^2)'_{P=O}$ evaluated at zero stress (Brugger 1965):

$$-(\rho_o W^2)'_{P=O} = (\mathbf{N}.\mathbf{M})^2 + 2wF_{UC} + G_{UC}, \qquad (3.30)$$

with

$$w = (\rho_o W^2)_o = (\rho v^2)_o = C^S_{pqrs} N_p N_q U_r U_s,$$

$$F_{UC} = S^T_{abrs} M_a M_b U_r U_s,$$

$$G_{UC} = S^T_{abuv} C_{uvprqs} M_a M_b N_p N_q U_r U_s. \qquad (3.31)$$

where W is the natural velocity, v is the measured velocity, **N** and **U** are unit vectors along the wave propagation and polarisations directions respectively; **M** is a unit vector along the applied stress direction; C^S_{IJ} and S^T_{IJ} are isentropic stiffness and isothermal compliance tensor components respectively. The solutions, obtained using the procedure of Thurston and Brugger (1964), for the effect of uniaxial stress on the velocity of ultrasonic modes propagated in an isotropic material are given in Table 3.1. Using these ultrasonic mode configurations, the three independent TOEC for vitreous SiO_2 and some of the rare earth phosphate glasses have been determined.

Table 3.1. The Thurston-Brugger relations (1964) for an isotropic material under uniaxial stress: mode 1 (longitudinal), 2 (shear) and 3 (shear). The propagation direction N is perpendicular to stress.

Mode No.	Displacement direction	w	$\left[\frac{d(\rho_0 W^2)}{dP}\right]_{P=0}$
1	// to N	C_{11}	$\frac{1}{E}[\sigma(2w+8\nu_3)+\nu_1(2\sigma-1)+\nu_2(8\sigma-2)]$
2	$\perp$ to stress	C_{44}	$\frac{1}{E}[\sigma(2w+4\nu_3)+\nu_2(2\sigma-1)]$
3	// to stress	C_{44}	$\frac{1}{E}[-2w+\nu_2(2\sigma-1)+2\nu_3(\sigma-1)]$

In allowing for a change in the dimensions of the sample resulting from applied stress, it is necessary to calculate the value of ρv^2 by translating the measured transit time into a velocity. Similarly, the change in density has to be calculated. This problem has been solved by Thurston and Brugger (1964) by a method which was developed to eliminate the necessity of this operation. In their paper, the expressions are given, for different modes for the quantity

$$(\rho_0 W^2)'_{P=0} = \left[\frac{d(\rho_0 W^2)}{dP}\right]_{P=0} \tag{3.32}$$

where ρ_0 is the density in the unstressed state, and P is the magnitude of applied stress. W is known as the natural velocity, it is referred to original dimensions given by $W = (l_0/T_P)$ where l_0 is the unstressed path length and T is the transit time under stress. By using the Thurston and Brugger (1964) equation:

$$\left[\frac{d(\rho_0 W^2)}{dP}\right]_{P=0} = 2\rho_0 W_0 \left[\frac{dW}{dP}\right]_{P=0},$$

$$\left[\frac{d(\rho_0 W^2)}{dP}\right]_{P=0} = 2\rho W_0^2 \left[\frac{d((W/W_0)-1)}{dP}\right]_{P=0} \tag{3.33}$$

can be found and then

$$\left[\left(\frac{1}{W}\right)\frac{dW}{dP}\right]_{P=0} = \left[\frac{d((W/W_0)-1)}{dP}\right]_{P=0} \tag{3.34}$$

The uniaxial pressure derivatives $\{(1/W)dW/dP\}_{P=0}$ is the gradients of the measured pressure dependence of the relative change $\Delta W/W_0$ in the natural velocities. These results for $\{(1/W)dW/dP\}_{P=0}$ have been transformed to $\{d(\rho_0 W^2)/dP\}_{P=0}$ using

$$\left\{\frac{d(\rho_0 W^2)}{dP}\right\}_{P=0} = 2\rho_0 W_0^2 \left\{\left(\frac{1}{W_0}\right)\frac{dW}{dP}\right\}_{P=0} = 2\rho_0 v_0^2 \left\{\left(\frac{1}{f_0}\right)\frac{df}{dP}\right\}_{P=0} \tag{3.35}$$

Hence $\{d(\rho_0 W^2)/dP\}_{P=0}$ is directly related to the initial slope and intercept of the measured frequency f_0 versus pressure P curve of ultrasonic transit time measurements. The $\{d(\rho_0 W^2)/dP\}_{P=0}$ obtained for all three mode configurations are used to determine the TOEC using the mode equations given in Table 3.1 and solved using a computer program written in FORTRAN 77 listed in Appendix I.

Measurement of the change in ultrasonic wave velocity induced by application of a constant stress produces mixed adiabatic (S) and isothermal (T) TOEC moduli ($C_{IJK}^{S,T}$) (this has been written without superscripts S and T throughout this thesis), making it necessary to know the corrections required to determine adiabatic TOEC C_{IJK}^{S}. Following the techniques described by Shull (1969), it can be shown that the relationship giving the difference between the measured $C_{111}^{S,T}$ and the adiabatic quantity C_{111}^{S}, is (Saunders et al. 1993)

$$(C_{111}^{S} - C_{111}^{S,T}) = - \left\{ \frac{B^S}{B^T} - 1 \right\} \left[\frac{(\partial C_{11}/\partial T)_P}{3\alpha} - \left(\frac{C_{111} + 2C_{112}}{3} \right) \right] \quad . \qquad (3.36)$$

where α is the linear thermal expansion coefficient. The difference $(C_{111}^{S} - C_{111}^{S,T})$ has been calculated by Saunders et al. (1993), and is substantially less than the experimental error. The magnitudes of this correction $(C_{IJK}^{S} - C_{IJK}^{S,T})$ are the same for other TOEC. Therefore the data for the TOEC given in the present work can be taken as being the purely adiabatic TOEC when they are required for computational purposes.

3.8 THE HYDROSTATIC PRESSURE DERIVATIVES OF SOEC

The variation of the SOEC with external pressure is one of the more important anharmonic effects which can be used to measure interatomic repulsive forces: the hydrostatic pressure derivatives $(\partial C_{IJ}^{S}/\partial P)_{T,P=0}$ of the SOEC C_{IJ}^{S} and $(\partial B^S/\partial P)_{T,P=0}$ of the bulk modulus B^S provide detailed information on the acoustic mode vibrational

anharmonicity of solid materials.

The hydrostatic pressure derivatives of the SOEC and bulk modulus for an isotropic material can be determined from the SOEC and TOEC data using the following relations (Lambson et al. 1985):

$$\left(\frac{\partial C_{11}^S}{\partial P}\right)_{T,P=0} = -\frac{1}{9B}(C_{111}+6C_{122}+2C_{123}) - \frac{2}{9B}(6C_{11}-6C_{44}+C_{111}-C_{123}) \tag{3.37}$$

$$\left(\frac{\partial C_{44}^S}{\partial P}\right)_{T,P=0} = \left[-\frac{1}{6B}(6C_{11}-6C_{44}-C_{111}-C_{123})\right] \tag{3.38}$$

$$\left(\frac{\partial B^S}{\partial P}\right)_{T,P=0} = \left[-\frac{1}{9B}(C_{111}+6C_{112}+2C_{123})\right] \tag{3.39}$$

The hydrostatic pressure derivative $(\partial B^S/\partial P)_{T,P=0}$ of the bulk modulus can then be calculated and used to examine the elastic behaviour under pressure. The bulk modulus is related to the first order term in pressure P by

$$B(P) = B_0 + P(\partial B/\partial P)_{T,P=0} \tag{3.40}$$

Usually the bulk modulus becomes larger as pressure is increased, this is a normal elastic behaviour under pressure. However, if the bulk modulus becomes smaller as pressure is increased, the long-wavelength soften under pressure, the material is easier to squeeze under pressure.

3.9 THE COMPRESSION V(P)/V_0 EXTRAPOLATED TO HIGH PRESSURES

It is a common practice to use ultrasonic velocity data to extrapolate the compression V(P)/V_0 of a material up to high pressures by recourse to an equation-of-state (Murnaghan 1944, Birch 1952 and Anderson 1966). It is interesting to examine how the sign of $(\partial B^S/\partial P)_{T,P=0}$ influences this procedure. Based upon the

assumption that the bulk modulus varies linearly with pressure, Murnaghan (1944) derived a widely used equation-of-state

$$P = \frac{B_0^T}{B_0'}\left[\left(\frac{V_0}{V}\right)^{B_0'} - 1\right] \quad , \tag{3.41}$$

which in logarithmic form (Anderson 1966) is

$$\ln\left(\frac{V_0}{V}\right) = \frac{1}{B_0'}\ln\left[B_0'\left(\frac{P}{B_0^T}\right) + 1\right] \quad . \tag{3.42}$$

Here, B_0^T is the isothermal bulk modulus and $B_0' = (\partial B_0^T/\partial P)_{P=0}$. Birch (1952) has given another commonly used equation-of-state

$$P = \frac{3B_0^T}{2}\left[\left(\frac{V_0}{V}\right)^{7/3} - \left(\frac{V_0}{V}\right)^{5/3}\right]\left\{1 - \left(3 - \frac{3B_0'}{4}\right)\left[\left(\frac{V_0}{V}\right)^2 - 1\right]\right\} \quad . \tag{3.43}$$

Anderson (1966) developed yet another equation-of-state in the form of a quartic polynomial, requiring the second and third order pressure derivatives of the bulk modulus. However, only the first pressure derivative $(\partial B/\partial P)_{T,P=0}$ is available from the present ultrasonic measurements. By assuming that

$$B_0^T\left(\frac{\partial^2 B^T}{\partial P^2}\right)_{P=0} \ll 1 \quad \text{and} \quad (B_0^T)^2\left(\frac{\partial^3 B^T}{\partial P^3}\right)_{P=0} \ll 1 \tag{3.44}$$

the quartic polynomial can be simplified to a first order approximation to a quadratic or a cubic polynomial containing only B_0' (Anderson 1966):

$$\frac{V}{V_0} = 1 - \frac{P}{B_0^T} + m\left(\frac{P}{B_0^T}\right)^2 \quad ,$$

$$\frac{V}{V_0} = 1 - \frac{P}{B_0^T} + m\left(\frac{P}{B_0^T}\right)^2 + n\left(\frac{P}{B_0^T}\right)^3 \quad , \tag{3.45}$$

where

$$m = \frac{1}{2}(1 + B_0')$$

$$n = \frac{1}{6}[1 + 3B_0' + 2(B_0')^2] \quad . \tag{3.46}$$

For a number of solids, which have a positive $(\partial B/\partial P)_{T,P=0}$, the compressions extrapolated to high pressures using both Murnaghan's and Birch's equations-of-state fit well with available high pressure experimental data up to more than 100GPa (Anderson 1966, McWhan 1967). Anderson (1966) used the quadratic and cubic polynomial forms for solids with a positive $(\partial B/\partial P)_{T,P=0}$. However, the equations-of-state have not been applied to materials with negative $(\partial B/\partial P)_{T,P=0}$ to any extent. To compute the compression when $(\partial B/\partial P)_{T,P=0}$ is negative, Murnaghan's equation-of-state (Eqn. 3.41) can be written in the form

$$\frac{V(P)}{V_0} = \left[B_0' \left(\frac{P}{B_0^T} \right) + 1 \right]^{-1/B_0'} \quad . \tag{3.47}$$

To determine accurately the compression $V(P)/V_0$ by use of the equations-of-state, the input data should be transformed to the isothermal form, requiring the thermal Grüneisen parameter γ^h or specific heat C_P, which are not available for most phosphate glasses. However, the differences between adiabatic and isothermal data are very small (Wang et al. 1992) and the use of adiabatic data provides a reasonable approximation.

It was shown that the Birch equation-of-state is not valid at pressures above 2GPa (Senin et al. 1993). The compression computed from Murnaghan's equation-of-state drops down to zero when the value of $P(\partial B^S/\partial P)_{T,P=0}$ approaches that of B_0^S (=3.92GPa). This arises from use of the linear approximation of the bulk modulus under pressure, given in Eq. (3.40). This implies that the bulk modulus of

a solid with a negative $P(\partial B^S/\partial P)_{T,P=0}$ continues to decrease with increasing pressure until it becomes zero at the pressure P_m satisfying the condition

$$P_m\left(\frac{\partial B^S}{\partial P}\right)=-B_0 \quad , \tag{3.48}$$

This situation is not consistent with experimental observation. For vitreous SiO_2, there is a reversal of the slope of the bulk modulus at about 3.5GPa (Murnaghan 1944). It has been shown that Birch's equation-of-state fails to give an acceptable estimate of the compression of vitreous SiO_2 at high pressure (Senin et al. 1993). For Murnaghan's equation-of-state, the quadratic polynomial and the cubic polynomial each fit the experimental data well below 2GPa, but above 3.5GPa, the computed compression deviates from the experimental data. This is due to the change of the sign of the pressure dependence of the bulk modulus so that higher order pressure derivatives dominate the pressure variation of the bulk modulus. This behaviour can be expected for materials with a negative $(\partial B^S/\partial P)_{T,P=0}$.

Therefore, the preferred option for estimation of the compression at high pressures for a glass having a negative $(\partial B^S/\partial P)_{T,P=0}$ is Anderson's quadratic polynomial in the range of $P<P_m$. Murnaghan's equation-of-state is suitable for glasses with a positive $(\partial B^S/\partial P)_{T,P=0}$.

3.10 ACOUSTIC MODE VIBRATIONAL ANHARMONICITY AND GRÜNEISEN PARAMETERS

Physical properties such as thermal expansion or phonon-phonon interactions, which depend upon thermal motion are much influenced by anharmonicity, the nonlinearity of interatomic forces with respect to atomic displacements. The experimental measurements of the second and third order elastic stiffness tensor components, and their hydrostatic pressure derivatives enable determination of the vibrational anhar-

monicity of the long-wavelength acoustic phonons.

In the quasiharmonic approximation, where the phonon frequencies are assumed to change with temperature only through lattice dimension, the vibrational anharmonicity of atomic vibration is usually described in terms of the thermal Grüneisen parameters γ^{th}. A thermodynamic expression of the vibrational anharmonicity is usually described in terms of an average thermal Grüneisen parameter (Slater 1939):

$$\gamma^{th} = \frac{3\alpha V}{\kappa^S C_P} = \frac{3\alpha V}{\kappa^T C_V}, \tag{3.49}$$

where α is the coefficient of linear coefficient of thermal expansion, V is the volume, κ is the compressibility and C is the specific heat capacity. The thermal Grüneisen parameter is the weighed average of the mode Grüneisen parameters γ_i, that is, the contribution of all excitations from each phonon mode including the long-wavelength acoustic mode (Slater 1939):

$$\gamma^{th} = \frac{\sum_i (\gamma_i c_i)}{\sum_i c_i}, \tag{3.50}$$

where c_i is the Einstein specific heat associated with the i-th mode and can be written as (Slater 1939)

$$c_i = k\left(\frac{h\nu_i}{kT}\right)^2 \frac{e^{h\nu_i/kT}}{(e^{h\nu_i/kT} - 1)^2} \tag{3.51}$$

Here ν_i is the phonon frequency, k is Boltzmann's constant and h is Planck's constant.

The effect of pressure on the mode vibrational frequencies can be quantified by the Grüneisen parameter γ_i of an individual mode of vibration which expressed the volume V dependence of the normal mode frequency ω_i:

$$\gamma_i = -\frac{\partial \ln \omega_i}{\partial \ln V} \tag{3.52}$$

The negative sign indicates that in normal circumstances the phonon frequencies decrease as lattice expands. As a consequence, when a solid material is compressed, it becomes harder; restoring forces become greater, and vibrational frequencies increase so that each ω_i increases with decreasing volume, a normal behaviour for a phonon; hence the Grüneisen parameters are positive. However, in certain circumstances, the Grüneisen parameters can have negative values (that is true for some of the glasses studied here). In this case the phonon frequencies and energies decrease when the volume is reduced; the acoustic modes soften under pressure. This behaviour is known as phonon mode softening. A negative Grüneisen parameter means that the contribution to thermal expansion coefficient would be expected to be negative.

The acoustic mode Grüneisen parameters, determined from ultrasonic measurements, express the contribution of the modes of long-wavelength acoustic phonons to lattice vibrational anharmonicity. The SOEC and TOEC provide a measure, which can be expressed by acoustic mode Grüneisen parameters, of the anharmonicity of the long-wavelength acoustic modes alone. These Grüneisen parameters quantify the first-order anharmonicity (the cubic term in Langrangian strain) of the zone centre acoustic modes. For glass, which is an isotropic material, there are only two components of the acoustic mode Grüneisen parameter at the long-wavelength limit: longitudinal γ_L, shear γ_S Grüneisen parameters. These two parameters can be obtained from the experimental values of the SOEC and TOEC data using (Brugger and Fritz 1967)

$$\gamma_L = -\left[\frac{1}{6C_{11}}(3B + 2C_{11} + C_{111} + 2C_{112})\right] \tag{3.53}$$

and

$$\gamma_S = -\left[\frac{1}{6C_{44}}\left(3B + 2C_{44} + \frac{1}{2}(C_{111} + 2C_{123})\right)\right] \tag{3.54}$$

At low temperatures, the specific heat in Eq. (3.50) may be replaced by a v^{-3} weighting, where v is the wave velocity. The mean acoustic mode Grüneisen parameter calculated on the basis of the Debye continuum model is then given by

$$\gamma^{el} = \left(\frac{\gamma_L}{v_L^3} + \frac{2\gamma_S}{v_S^3}\right) \Big/ \left(\frac{1}{v_L^3} + \frac{2}{v_S^3}\right), \tag{3.55}$$

At room and higher temperature, the Debye model yields the mean long-wavelength acoustic mode Grüneisen parameter γ^{el}

$$\gamma^{el} = \frac{\gamma_L + 2\gamma_S}{3} \tag{3.56}$$

The temperature dependences of the thermal Grüneisen parameter come from two sources (Eq. 3.50), namely the mode Grüneisen parameter γ_i and the weighting factor (or mode specific heat) c_i. At low temperatures, the specific heat due to lattice vibrations in a crystalline solid, obeys the Debye law, $c_v \propto T^3$; that is, the specific heat tends to zero as T tends to zero. In glasses, at low temperatures when the excited phonon population includes a high proportion of long-wavelength acoustic modes, the values of the elastic γ_L^l and thermal γ_L^{th} Grüneisen parameters would be expected to become equal. But this is not the case, the specific heat is dominated by the high density of states of two-level systems, which also contribute to the thermal expansion (Phillips 1981) and to the ultrasonic wave velocities and attenuation (Piché et al. 1974). Recent specific heat measurements have shown that the rare earth phosphate glasses worked on here do have such an excess specific heat (Carini et al. 1994b). In the present work, the long-wavelength acoustic mode Grüneisen parameters have been determined from the SOEC and TOEC data. These data are strongly temperature dependent. Hence the temperature dependence of the acoustic mode Grüneisen parameter γ^{el} is a consequence of the temperature dependence of all mode Grüneisen parameters and mode specific heats.

3.11 THE FOURTH ORDER ELASTIC STIFFNESS TENSOR COMPONENTS (FOEC)

Information about higher order elastic stiffness tensor components is extremely useful for understanding the nature of short-range repulsive forces in solids. This information is most readily obtainable through study of anharmonic properties such as in the present study. To extend the determination of the higher order elasticity, the fourth order elastic stiffness tensor components C_{ijkl} has to be estimated. The FOEC is the coefficient of the quartic terms in the Hamiltonian as a function of strain and so measures the anharmonicity of the vibrational states up to fourth power in strain.

Glass, which is an isotropic material, has four independent adiabatic FOEC which may be taken as τ_1, τ_2, τ_3 and τ_4. The complete set of FOEC can be written as (Shull 1969):

$$
\begin{aligned}
C_{1111} &= \tau_1 + 12\tau_2 + 32\tau_3 + 12\tau_4; \\
C_{1112} &= \tau_1 + 6\tau_2 + 8\tau_3; \\
C_{1144} &= \tau_2 + 2\tau_4; \\
C_{1122} &= \tau_1 + 4\tau_2 + 4\tau_4; \\
C_{1123} &= \tau_1 + 2\tau_2; \\
C_{1166} &= \tau_2 + 4\tau_3 + 2\tau_4; \\
C_{1266} &= \tau_2 + 4\tau_3; \\
C_{1244} &= \tau_2 + 4\tau_3; \\
C_{1456} &= \tau_3; \\
C_{4444} &= 3\tau_4; \\
C_{4455} &= \tau_4.
\end{aligned}
\tag{3.57}
$$

In order to estimate the complete set of the FOEC, the knowledge of TOEC, the $\partial C_{IJ}/\partial T$ of the temperature and the second pressure derivatives $\partial^2 C_{IJ}/\partial P^2$ of the SOEC are necessary. The second pressure derivatives of the SOEC have been evaluated by

differentiating the modulus equation twice (Hart 1983):

$$C_{IJ} = \rho v^2 = \rho_0 W^2 \tag{3.58}$$

Hence

$$\left(\frac{\partial^2 C_{IJ}}{\partial P^2}\right) = \left(\frac{\partial^2(\rho_o W^2)}{\partial P^2}\right) + \frac{2}{3B^T}\left(\frac{\partial(\rho_o W^2)}{\partial P}\right) + \frac{C_{IJ}}{9B_T^2} - \frac{C_{IJ}}{3B_T^2}\left(\frac{\partial B_T}{\partial P}\right) \tag{3.59}$$

where

$$\left[\frac{d^2}{dP^2}(\rho_0 W^2)\right] =$$

$$2\rho_0 W_0^2 \left(\left[\frac{d}{dP}\left(\frac{\Delta W}{W_0}\right)^2\right]_{P=0-} + \left[\frac{d^2}{dP^2}\left(\frac{\Delta W}{W_0}\right)\right]_{p=0}\right) \tag{3.60}$$

By assuming that the difference between the adiabatic B^S and isothermal B^T is very small (Wang et al. 1992), the adiabatic data can be used as an approximation. The required relations for determination of the FOEC have been developed previously by Brassington et al. (1980) and can be written as:

$$9\tau_1 + 48\tau_2 + 64\tau_3 + 20\tau_4 = 9B^2\left(\frac{\partial^2 C_{11}}{\partial P^2}\right)_{[T,P=0]} - (1 + 3\frac{\partial B}{\partial P})C_{11}$$

$$-(4 + 3\frac{\partial B}{\partial P})(C_{111} + 2C_{112}) \tag{3.61}$$

$$9\tau_2 + 24\tau_3 + 6\tau_4 = 9B^2\left(\frac{\partial^2 C_{44}}{\partial P^2}\right)_{[T,P=0]} - (1 + 3\frac{\partial B}{\partial P})C_{44}$$

$$-(4 + 3\frac{\partial B}{\partial P})(C_{144} + 2C_{155}) \tag{3.62}$$

$$\frac{1}{2C_{11}}(3\tau_1+16\tau_2+32\tau_3+16\tau_4)+\frac{1}{C_{44}}(3\tau_2+8\tau_3+6\tau_4=\frac{3}{k\rho N}\left(\frac{\partial C_{11}}{\partial T}\right)_V$$

$$+6(\gamma_L^{11})^2+12(\gamma_S^{11})^2-\frac{1}{2C_{11}}(5C_{111}+2C_{112})$$

$$-\frac{1}{C_{44}}(C_{111}+2C_{112}+4C_{155}) \qquad (3.63)$$

$$\frac{1}{2\omega_L}[3\tau_2+8\tau_3+8\tau_4]+\frac{1}{4\omega_S}[5\tau_2+16\tau_3+25\tau_4]=\frac{3}{k\rho N}\left(\frac{\partial C_{44}}{\partial T}\right)_V$$

$$+6(\gamma_L^{23})^2+12(\gamma_S^{23})^2-\frac{1}{2\omega_L}(2C_{144}+7C_{155}+C_{456})$$

$$-\frac{1}{2\omega_S}(C_{144}+9C_{155}+4C_{456}) \qquad (3.64)$$

where

$$\omega_L=\frac{1}{2}(C_{11}+C_{12}+2C_{44})=C_{11}$$

$$\omega_S=\frac{1}{4}(C_{11}+3C_{44}),$$

$$\gamma_L^{11}=-\frac{1}{6C_{11}}(3B+2C_{11}+C_{111}+2C_{112})$$

$$\gamma_S^{11}=-\frac{1}{6C_{44}}(3B+2C_{44}+C_{144}+2C_{155})$$

$$\gamma_L^{23}=-\frac{1}{6\omega_L}(C_{44}+\omega_L+2C_{155})$$

$$\gamma_S^{23}=-\frac{1}{6\omega_S}\left(C_{44}+\omega_S+C_{166}+\frac{1}{2}C_{144}+\frac{3}{2}C_{456}\right) \qquad (3-65)$$

The above equations (Eqs. 3.61 - 3.64) are solved by using the data of N (the number of vibrational unit per unit mass), the SOEC, TOEC and their related pressure derivatives $(\partial^2 C_{11}/\partial P^2)_{T,P=0}$, $(\partial^2 C_{44}/\partial P^2)_{T,P=0}$, $(\partial C_{11}/\partial T)_V$ and $(\partial C_{44}/\partial T)_V$, using a computer program written in FORTRAN 77 listed in Appendix II. Generally, the absolute values of FOEC are much bigger compared to those of the SOEC and TOEC.

CHAPTER 4

MANUFACTURE OF THE RARE EARTH PHOSPHATE GLASSES

4.1 INTRODUCTION

This chapter describes the procedure for the production and preparation of the different rare earth phosphate glasses for the ultrasonic and other investigations. These glasses are denoted by the formula $(R_2O_3)_x(P_2O_5)_{1-x}$, where R represents the nine rare earth elements Ce, Pr, Nd, Eu, Gd, Tb, Dy, Ho and Er, and x is the mole fraction. Laboratory Analar grade of phosphorus pentoxide P_2O_5 and Analar grade rare earth (R) oxide of 99.9% purity are used in the preparation of these rare earth phosphate glasses. In general the preparation method for each glass is similar. Nevertheless, there are subtle differences in the manufacture due to the fact that some heavier oxides have higher melting temperatures.

4.2 PREPARATION DETAILS

A stoichiometric mixture of rare earth oxide and phosphorus pentoxide P_2O_5, weighing about 50g is mixed together in an alumina crucible of 100 cm^3 capacity. The chemicals are weighed on an electronic balance to an accuracy of ± 1 mg. During weighing and subsequent handling of the chemicals, plastic goggles and a mouth dust protector are worn because the chemicals used are hazardous, especially phosphorus pentoxide, which reacts violently with water and is very corrosive. For each preparation, the phosphorus pentoxide is weighed out first and then covered by the rare earth oxide to minimise water absorption. The contents of the crucible are well mixed to ensure homogeneity by stirring with an alumina rod. The mixture, which is normally called a batch, is heated in a closed alumina crucible in a high temperature electric muffle furnace (Carbolite, UK) to form a homogeneous molten liquid (Figure 4.1).

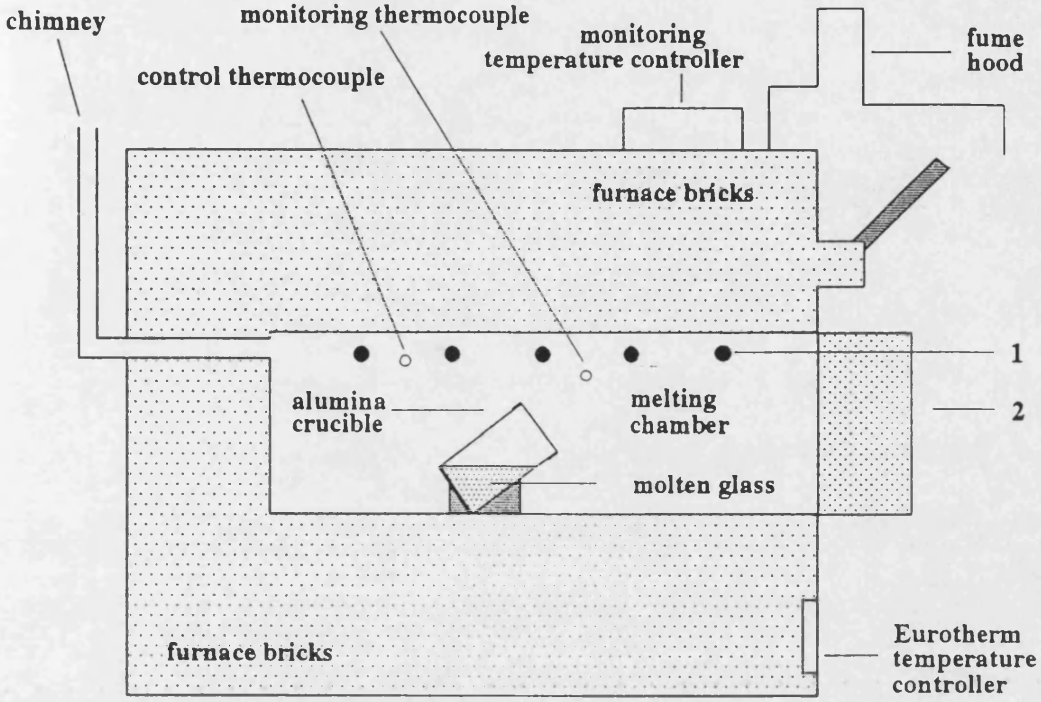

Figure 4.1. The electrical furnace used for producing glass. 1 - silicon carbide heating elements, 2 - opening for charging the glass batch.

The melting temperature of these glasses is normally in the range 1300-1800°C - the exact temperature depending on the type of rare earth oxide used. The approximate melting point and annealing temperature for each of these glasses are tabulated in Table 4.1. Phosphorus pentoxide has a low melting temperature of 580°C and it sublimes at 395°C under atmospheric pressure. This means that care must be taken to minimise

Table 4.1. A comparison of the melting and the annealing temperatures of rare earth phosphate glasses. The estimated experimental errors are mole fraction ±0.005, melting temperature ±50K and annealing temperature ±25K.

Glasses (Colour)	Mole fraction	Melting temperature (K)	Annealing temperature (K)
Cerium (Orange) Standard:Ce coil	0.226 0.235 0.245 0.254 0.257	1400 1400 1400 1440 1450	450 450 450 500 500
Praseodymium (Dark green) Standard:PrP_5O_{14}	0.216 0.254 0.256	1350 1400 1400	400 500 500
Neodymium (pink) Standard:$NdAl_2$	0.191 0.194 0.196 0.234 0.254	1400 1450 1500 1550 1650	500 500 550 600 600
Europium (pink) Standard:EuS	0.186 0.200 0.208 0.218 0.252	1350 1400 1500 1520 1550	400 500 550 550 600
Gadolinium (colourless) Standard:$GdAl_2$	0.222 0.226 0.229 0.245 0.250	1350 1400 1400 1450 1450	400 450 450 500 500
Terbium (colourless) Standard:$Tb_3Fe_5O_{12}$	0.226 0.247 0.263 0.271	1600 1650 1650 1680	600 600 600 650
Dysprosium (colourless) Standard:Dy_3F	0.225	1660	600
Holmium (dark salmon pink) (yellow under the sun light) Standard:Ho_3F	0.208 0.220 0.231	1700 1800 1850	650 650 700
Erbium (light pink) Standard:Er_3F	0.239	1620	500

loss of phosphorus pentoxide and this is achieved by having three separate manufacturing stages using three different electrical muffle furnaces. The furnaces are maintained at different temperatures to allow the procedures to be carried out rapidly and hence minimise the loss of P_2O_5. However, a small loss of phosphorus pentoxide does occur during preparation in some cases, and this may be significant for the higher percentages of rare earth oxide when the melting temperature is greater.

The three manufacturing stages are as follows:

1. The mixture is heated in an electric furnace at a temperature of 500°C for about 1 h. This allows the phosphorus pentoxide to decompose and react with the rare earth oxide.

2. The mixture is then taken out and placed, without cooling, into a second, preheated furnace at a temperature of 1000°C and held for another hour during which the temperature is progressively raised from 1000°C to 1400°C. This is done in order to thoroughly melt and mix the glass.

3. For glasses with higher melting points (more than 1400°C), the mixture is transferred to the third furnace which is set to 1400°C, and the temperature is then increased until the mixture is molten.

Usually the molten glass is not homogeneous; it may contain numerous gas bubbles from dissociation of compounds, reaction with refractories and furnace atmosphere which are trapped in the high viscosity mixture. To reduce the number of these inclusions, a process of refining has to be carried out. This process consists of raising the temperature of the molten glass to a higher temperature (+100°C) than the melting point, to reduce the viscosity. The bubble ascension rate, that is, the

proportion of the air bubbles which depart to the surface, is increased and thus, homogeneity is normally enhanced; the presence of air bubbles in the glass sample is reduced. Therefore, to ensure the homogeneity of the melt, the furnace temperature is firstly decreased and then increased to about 100°C below and above the melting point for about 15 minutes each, before finally setting it again at its melting temperature.

In the third furnace, the furnace controller supplied had an upper temperature limit of 1400°C. This is not a high enough temperature to melt all the rare earth oxide mixtures. The furnace elements and insulation are capable of reaching higher temperatures so that the control thermocouple emf is 'backed off' using an external millivolt source and higher temperatures can be obtained. The circuit diagram for the electronic connection is given in Figure 4.2. With this method the furnace temperature could reach

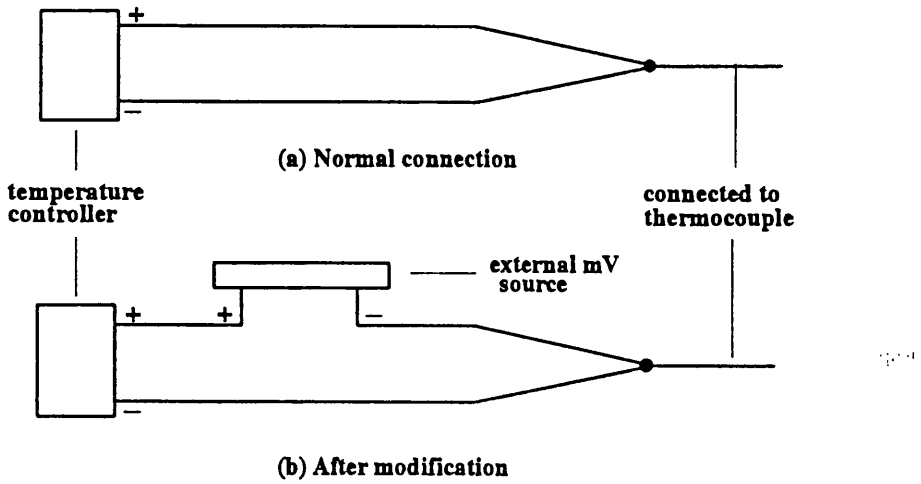

Figure 4.2. Circuit connection for backing off thermocouple emf.

a maximum of 2000°C, though with a reduced furnace element lifetime. The melting temperature of the furnace elements, which consist of SiC, is 2700°C. To monitor this temperature, an additional thermocouple (platinum-13% rhodium/platinum) is installed in the furnace chamber and connected to a digital thermometer with an accuracy of

±5°C. The temperature of the furnace is checked by comparing the reading of the thermocouple emf with the temperature calibration chart. The difference is normally in the range of the experimental error.

To handle the hot alumina crucibles in the furnace, metal tongs are required. In addition, safety wear are vital to protect the face and eyes, including a pair of heavy duty gloves, a special high temperature reflective jacket, and a safety visor equipped with darkened glass to enable direct viewing into a high temperature furnace. After checking the melt, it is then cast into a hot steel split cylindrical mould 10 mm inside diameter and 40 mm long (Figure 4.3) which has previously been heated in an annealing furnace held at the temperature at which the glass produced is subsequently to be annealed.

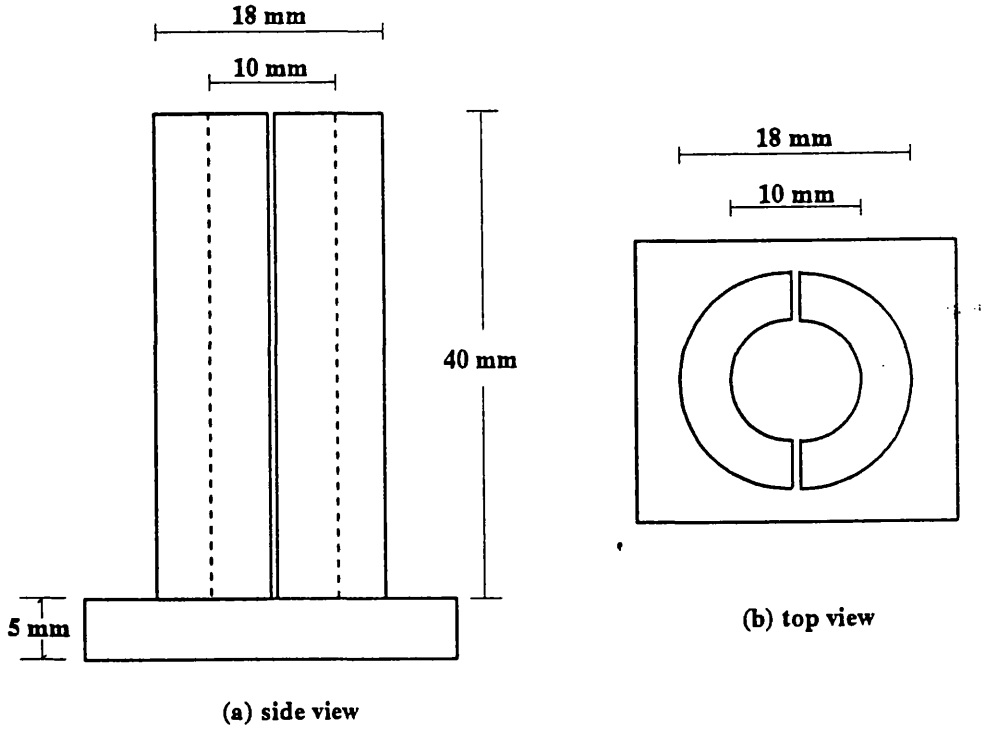

Figure 4.3. Stainlees steel cylindrical split mould for casting glass sample.

The temperature of the heated mould should be approximately 0.3 of the melt temperature. This is required to minimize the thermal stresses on solidifying the melt. The process of pouring the molten glasses into the hot steel moulds must be carried out very fast and efficiently to avoid the melt solidifying before reaching the mould. After casting, the glass is immediately transferred to an annealing furnace and kept there for 24 hours, so as to undergo thermal treatment which relieves the residual stresses. The residual stress is related to the variations in properties and cause the glasses to be very brittle. In particular, the glass must not contain any appreciable residual stress which is likely to cause breakage during cutting and polishing. Since the furnace capacity greatly exceeds the mould volume, it is assumed that there is a negligible temperature gradient across the sample. At the end of this process, the furnace is switched off and the glasses left to cool down to room temperature gradually by controlled thermal treatment at a cooling rate of 0.5 °C/min.

4.3 GENERAL PHYSICAL PROPERTIES AND STORAGE OF GLASS SAMPLES

The resulting glass samples are transparent glass cylinders approximately 10 mm long and 10 mm in diameter. The glasses obtained are free from cracks and air bubbles. They have a variety of colours (Table 4.1) due to the large number of different optical transitions which can occur in the rare earth ions. The nature and amount of strain present in the glasses can be determined by examining them in a beam of polarised light using a strain viewer. Normally, the glass obtained using the above production method is homogeneous as shown by the good quality pulse echo patterns produced by each sample. Once prepared, the samples are stored in a desiccator. They have a rather hard texture and take a rather long time to polish.

4.4 CUTTING AND POLISHING

The sample faces between which the ultrasonic waves are reflected must be flat and parallel; otherwise, interference will occur between different regions of the transducer, because of slight variations in the path length travelled by the ultrasonic waves through the sample. This would lead to an apparent non-exponential loss and affect the precision of the measured echo transit times. Hence, to make a glass sample that is suitable for the ultrasonic measurements and also for quantitative analysis, in the determination of their chemical compositions, they are carefully cut and polished to have high quality optically flat and parallel surfaces.

For the cutting and polishing of the samples, a slow speed (600 rpm) peripheral diamond saw has to be used for maximum precision cuts and minimum surface damage. The Anshaw Instruments Radial Arm Disc Saw (Figure 4.4) has been found to be suitable for cutting these rare earth phosphate glasses. The procedure is that one of the faces of the glass sample is glued to the cutting platform and two parallel faces are cut. To obtain a rectangular parallelepiped sample, the cutting platform is then turned through 90° relative to the saw and two more faces are cut. The sample is then removed from the platform and glued, using cyanoacrylate adhesive, to a Logitech PP5 precision polishing jig, similar to that shown in Figure 4.5. 20 cm diameter lapping plates are normally suitable for use with this jig. The jig can slide smoothly on the lapping plate and rotate gently on its own axis using a Logitech PM2 precision polishing machine. Samples are generally ground flat using a slurry of 600 grit carborundum on a flat cast iron polishing plate. The glasses are then polished on soft metal plates made of solder using diamond paste, typically to a 6μm finish. The polishing of the specimen is continued until satisfactory finish and flatness is achieved normally with a distinctly mirror-like appearance. The sample is then separated from the precision polishing jig by soaking in acetone and another cut face is prepared using the same procedure. The

(a)

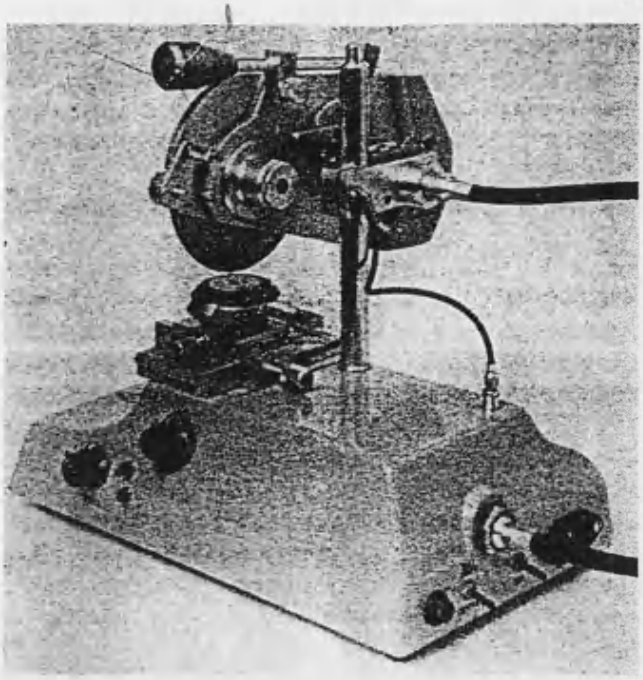

(b)

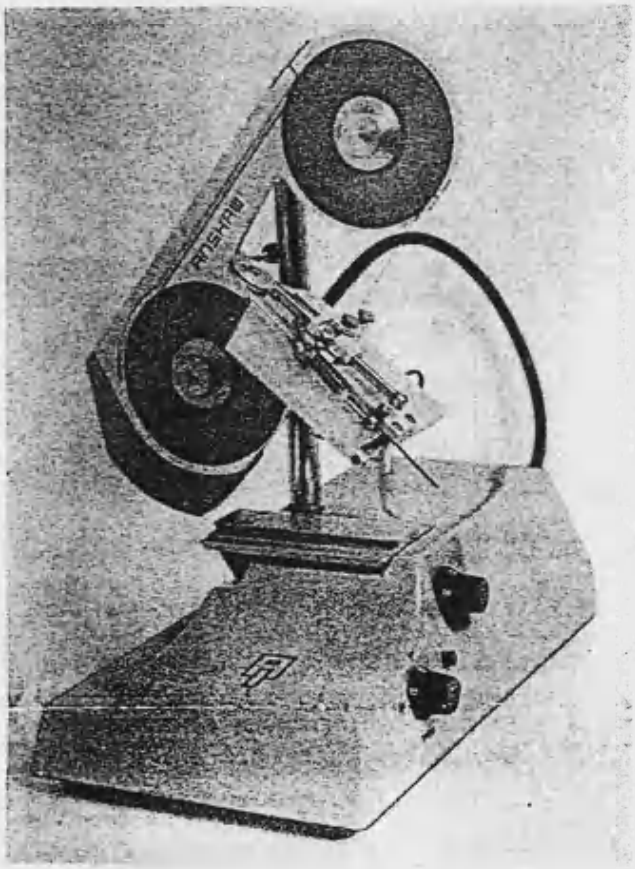

Figure 4.4. (a) Disc saw with cutting head turned through 90° and (b) wire saw with disc and cylinder cutting attachment.

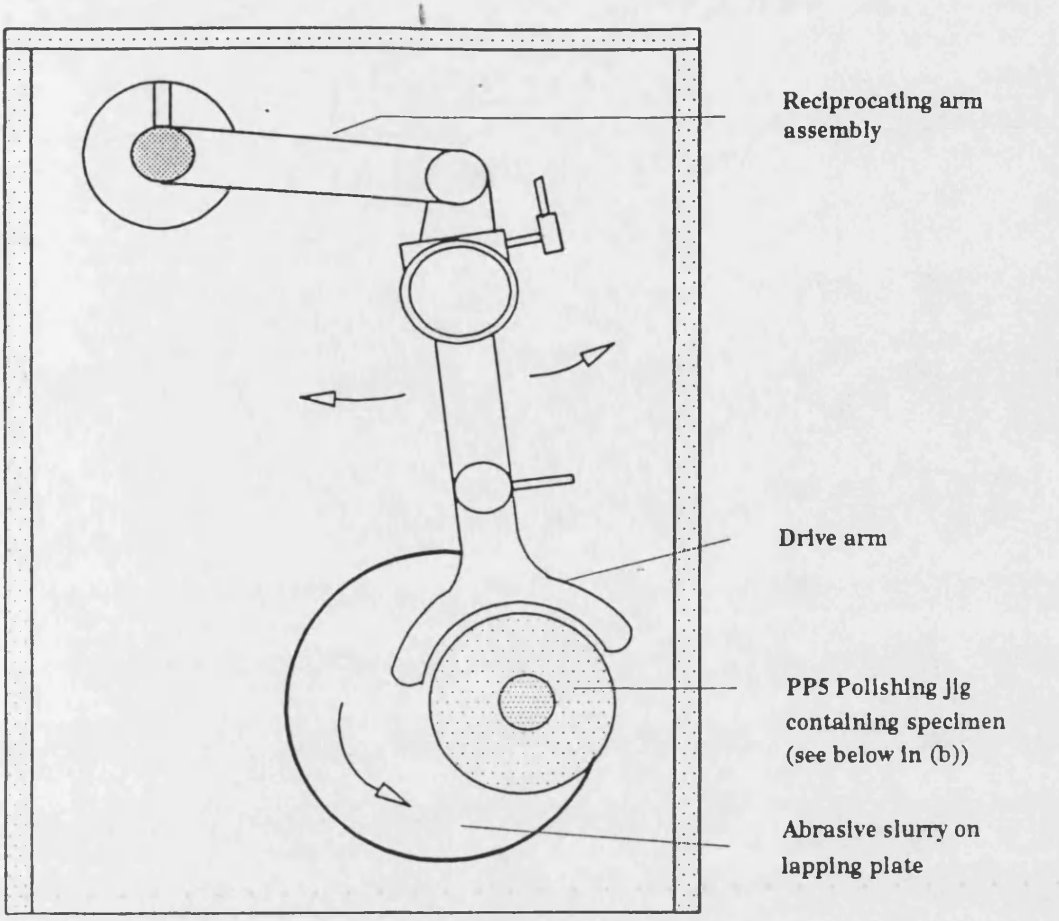

(a) Top view

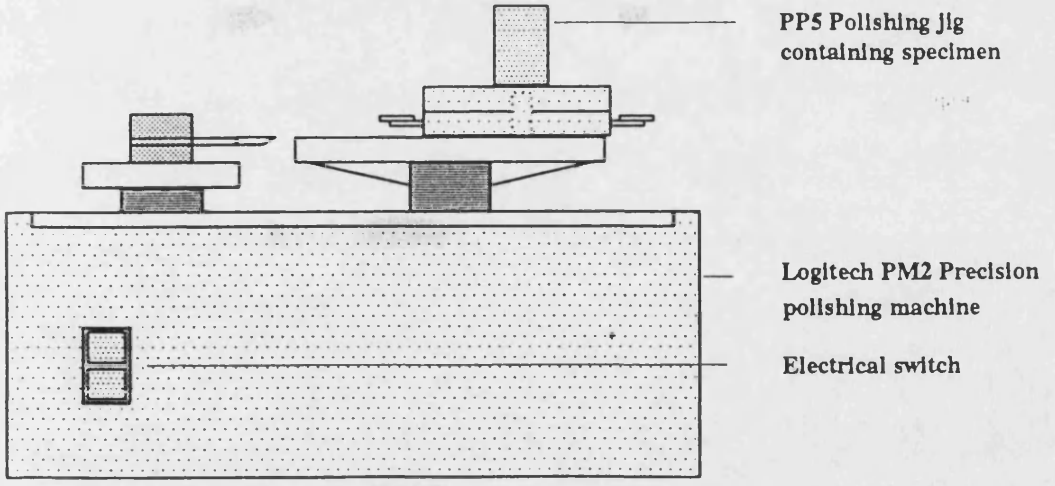

(b) Side view

Figure 4.5. General arrangement for lapping and polishing.

available equipment enables the surfaces to be prepared to a flatness of one-tenth of an optical light wavelength and a parallelism of 2" of arc for a sample with a thickness of about 5 mm.

4.5 QUANTITATIVE ANALYSIS OF THE SAMPLE COMPOSITIONS

The composition of the glasses manufactured in our laboratory has been analysed by quantitative analysis using the JEOL JXA 8600M electron-probe microanalyzer (EPMA), which is essentially a purpose-built analytical microscope of the scanning electron microscope (SEM) type (Figure 4.6). The qualitative analysis is performed by bombarding the specimen with a finely focused electron beam, and measuring the wavelength and intensity of the characteristic X-ray emitted. Secondary electrons and back scattered electrons are used to obtain the images of the sample surface that to be analyzed.

The EPMA is fitted with a wavelength-dispersive spectrometer (WDS) which gives accurate quantitative analysis results. The principle of the WDS is that the X-radiation coming from the sample is filtered so that only certain X-rays of a chosen wavelength (usually the characteristic wavelength of the element of interest) are allowed to fall onto the detector. The filtering is achieved by a crystal spectrometer which employs diffraction to separate the X-rays according to their wavelength. Measurements of how many X-rays of any type are emitted enables us to find out which elements are present in the sample. The JXA 8600M can be used in the manual mode or it can be computer controlled. A detailed account of electron probe microanalysis is given by Scott and Love (1983) and also in a review article on recent progress in electron probe microanalysis by Mackenzie (1993).

In the present quantitative analysis, used of a cubic sample is best; however a sample with two parallel faces may also be employed. Since the sample is an insulating glass, it needs to be coated with a very thin layer of conducting carbon using a vapour

deposition. A very thin carbon layer is used because it is less absorbent for X-ray emission. In a quantitative analysis routine, the use of standard samples containing the element in question in an exactly known form is required. These standards can be pure elements or compounds. The standards are required because the intensity of the X-ray gives a direct measure of the concentration. The standards used to analyse the content of phosphorus, oxygen and aluminium in the glass samples are GaP, $MgAl_2O_4$ and Al respectively and those used for rare earth elements have been given in Table 4.1.

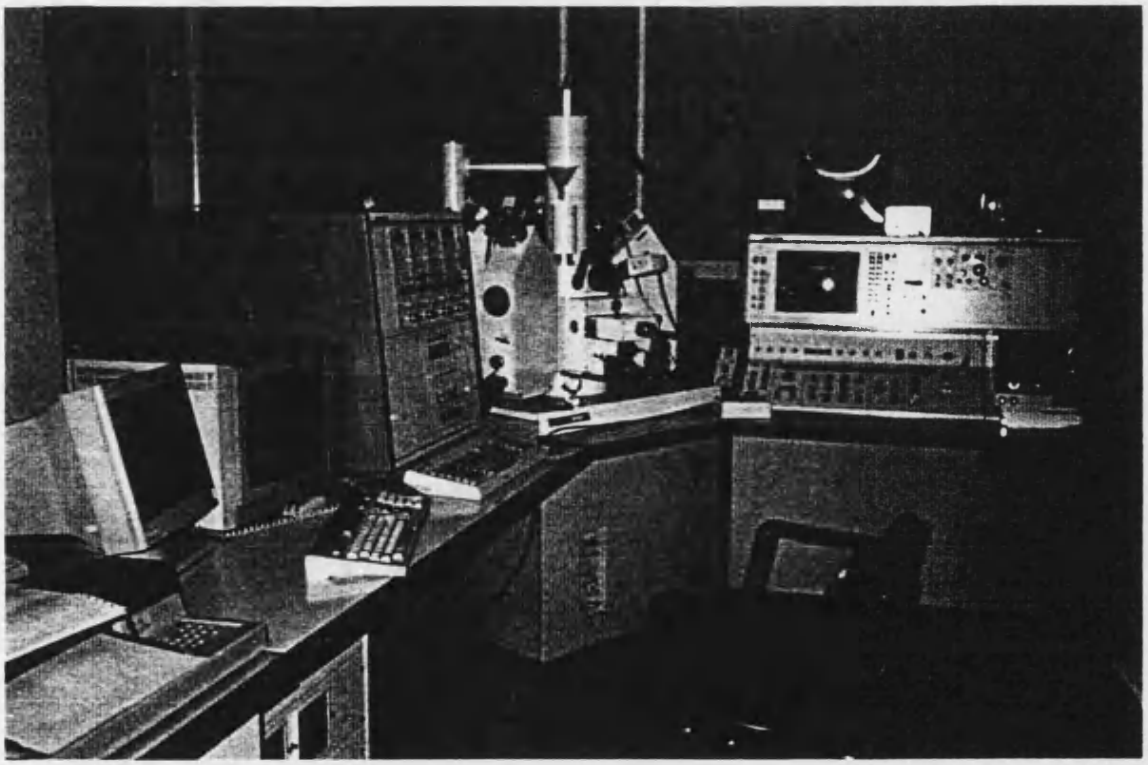

Figure 4.6. A photograph of the electron-probe microanalyser

CHAPTER 5

EXPERIMENTAL TECHNIQUES

5.1 INTRODUCTION

In this chapter, the ultrasonic experimental method used to make measurements of the elastic and nonlinear acoustic properties of rare earth phosphate glasses and vitreous SiO_2 will be described. This involved the basic experimental technique of measuring the ultrasonic wave velocities, the ultrasonic wave attenuation and the changes of the ultrasonic wave velocity as a function of pressure or temperature.

In particular, two different ultrasonic pulse techniques have been used: the pulse echo overlap technique (May 1958 and Papadakis 1964, 1966, 1967), the pulse superposition technique (McSkimin 1961, 1965 and McSkimin and Andreatch 1962). The former technique was used to measure the absolute values of the elastic stiffnesses, attenuation and the changes of the elastic stiffnesses under hydrostatic pressure, while the latter was used to measure the extremely small changes in the elastic stiffnesses induced by the application of uniaxial pressure. The measurements have been made using frequencies which are in the MHz region; thus the elastic stiffnesses obtained are essentially adiabatic.

This chapter begins with the description of wave propagation in solids. This is followed by a description of the sample preparation for the ultrasonic measurements. The operation of the pulse echo overlap technique together with the hydrostatic equipment and pulse superposition system along with the uniaxial stress apparatus will be presented. The methods used for making the measurements at low and high temperatures will be then explained. Finally, a brief description of the experimental errors resulting from the measurements is given.

5.2 WAVE PROPAGATION IN GLASS

In an isotropic solid like a glass, there are two different types of ultrasonic waves that can be propagated independently. The first type is the longitudinal wave, in which the glass particles vibration is parallel to the direction of propagation and the second is the shear wave, where the particle vibration is perpendicular to the direction of propagation.

The ultrasonic waves can be induced into a sample by applying a high voltage rf pulse, to a transducer acoustically bonded to one of the sample faces. The ultrasonic wave travels through the sample at the velocity of sound to the opposite face. Reflection occurs at the other face of the sample; the wave then returns to the initial face where a small amount of sound energy is transferred back to the same transducer and an electrical signal is developed. The reflection of the ultrasonic waves between two flat and parallel faces continues until the energy is dissipated in the sample as it travels through it. The received pulses are detected and displayed on the screen of an oscilloscope where the echo heights decrease exponentially with time (Figure 5.1).

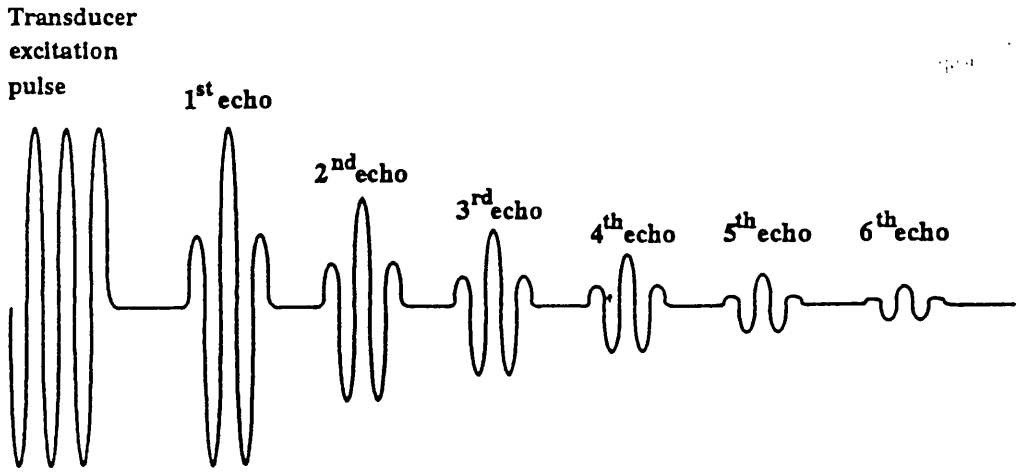

Figure 5.1. Pulse echo pattern display on the oscilloscope screen.

The ultrasonic wave velocity is determined from the pulse transit time while the attenuation is determined from the relative heights of the successive echos.

5.3 TRANSDUCERS

A gold plated piezoelectric quartz transducer is attached to one of the sample faces with a suitable bonding material. This transducer is used as both transmitter and receiver of the ultrasonic waves. The transducer converts mechanical energy into electrical energy or vice versa at ultrasonic frequencies by the piezoelectric effect or its converse. Two types of quartz transducer were used: X-cut for generating longitudinal waves and Y-cut for generating shear modes (Figure 5.2(a)). To differentiate between them, the Y-cut transducer had a flat edge parallel to the polarisation direction, as illustrated in Figure 5.2(b). One side of the transducer was coated coaxially with gold to form two electrodes; the middle gold electrode was used for the high voltage connection. The outer ring was connected to the other face of the transducer which was plated with gold over its entire area, which was used as an earth connection.

The fundamental resonant frequency of the transducers used for this work were in the range of 10 to 60 MHz. The thickness of the transducer is equal to half the wavelength of the sound wave in quartz. Hence in the case of a 10MHz transducer, the thicknesses are 0.29 ± 0.02 mm for the longitudinal mode and 0.19 ± 0.02 mm for the shear mode.

The transducer acts as a piston source and generates a wave which is essentially plane with a width equal to the diameter of the piston up to a distance d given by:

$$d = \frac{r^2}{\lambda} \tag{5.1}$$

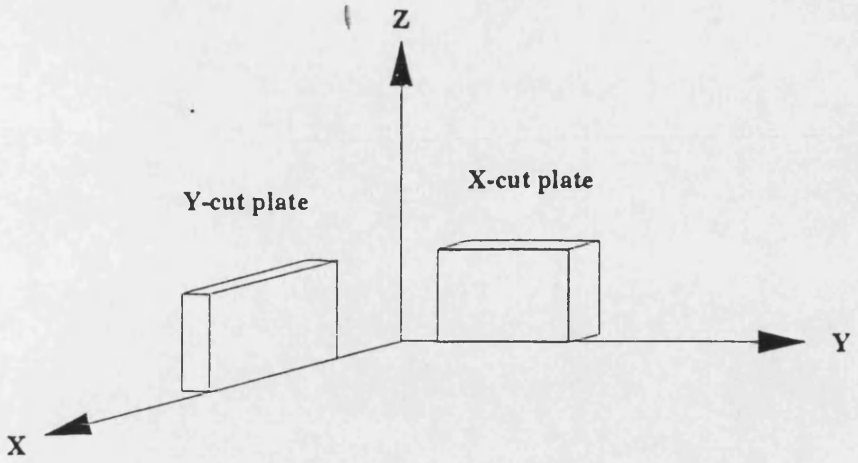

(a) Quartz crystal and pure mode transducer cuts

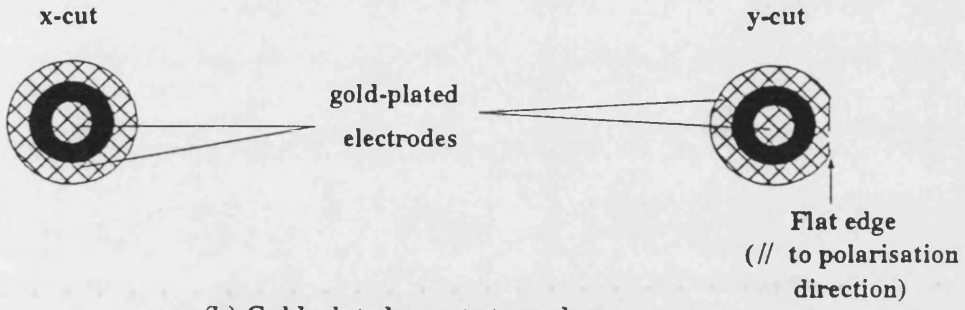

(b) Gold-plated quartz transducer

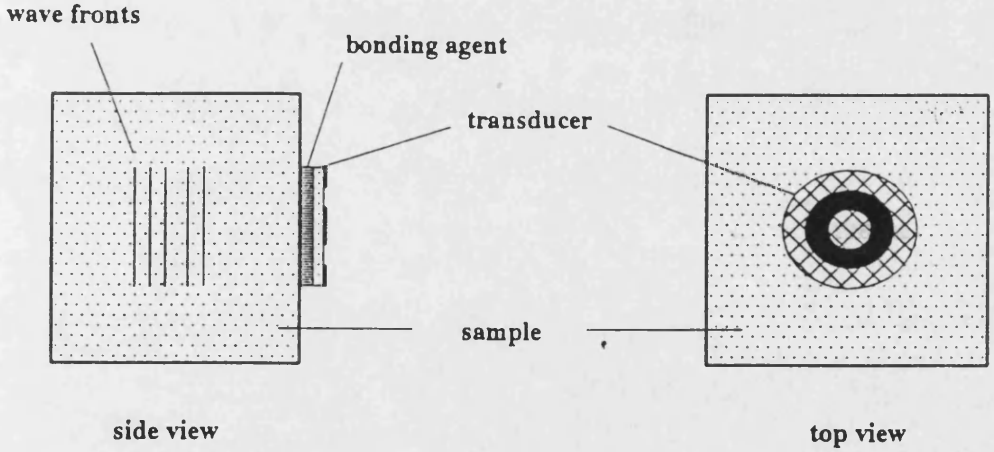

(c) bonding the transducer to sample

Figure 5.2. The quartz tranducer and bonding of the ultrasonic sample.

where r is the radius of the transducer and λ is the wavelength of the vibration in the sample. Transducers with a diameter of 4 mm and 6 mm respectively were used throughout. In order to restrict side-wall reflections (Waterman 1959), the diameter of the transducers used should be less than the sample diameter. The quartz transducers were essentially phase sensitive devices and hence it was necessary for the sample faces to be parallel.

5.4 TRANSDUCER-SPECIMEN BONDING

In order to reduce the large losses of acoustic energy generated by the quartz transducer due to reflection at the transducer-sample interface, the transducer was bonded to the sample using a suitable bonding agent (Figure 5.2(c)). The bond thickness had to be very small compared to the acoustic wavelength. To obtain a good, uniform and thin bond, both bonding material and the sample surface had to be free of dirt and the bonding material should not damage or react chemically with either the sample surface or the transducer. When dirt was detected, the transducer was removed and the surfaces cleaned with a suitable solvent such as acetone.

A variety of materials have been tested as bonding materials: these include Dow Resin, Nonaq stopcock grease, Q.D. colloidal silver paste, vacuum grease, glycerine, silicon oil and also indium. An extensive discussion of the bonding materials is given by Bateman (1966) or Farley (1973).

The present work has employed several of these bonding materials. In the case of the rare earth phosphate glasses, Nonaq stopcock grease (Fisher Scientific Co.) was used for the ultrasonic measurements of the longitudinal waves throughout the range of temperature from 10K to 400K. For the experiments with shear waves, Dow resin 276-V9 (Dow-Corning Corp.) was used from room temperature down to about

200K; below this temperature Nonaq stopcock grease was used.

The procedure involved in bonding the transducer to sample using Dow resin 276-V9 is as follows..A very small drop of bonding agent is first placed on the sample face, which is then heated to about 333-353K with a hot air blower until the normally viscous resin begin to flow easily. The transducer is then placed on the sample and pressed down with a finger to squeeze out any excess resin. A similar procedure is also applied to Nonaq stopcock grease but without the process of heating since this bonding material is already viscous at room temperature.

For measurements with a shear wave propagation, Q.D. colloidal silver paste (Du Pont UK Ltd) was found to be a suitable as a bonding agent from room temperature up to 400K. The procedure to bond the transducer to the sample using silver paste involve the following: 1) attach the transducer with silver paste to one of the sample face, 2) to set the bonding, bake the sample bonded with the transducer at 353K for 24 hours and 3) leave the sample to cool down naturally to room temperature.

After the bonding of the transducer to the sample is completed, the sample is then placed in a test jig and the quality of the echo pattern is checked. If the echo pattern shows an exponential decay, then the sample is ready for the ultrasonic measurements.

5.4.1 Indium bonding

In the case of vitreous SiO_2, Nonaq Stopcock grease can only give a good coupling between the transducer and sample in the temperature range of 293K down to about 150K. This limiting temperature range has been overcome by using a cold-weld indium bonding technique for attaching the transducer to the sample (James 1987). With this technique, a very thin layer of uniform thickness of indium is produced

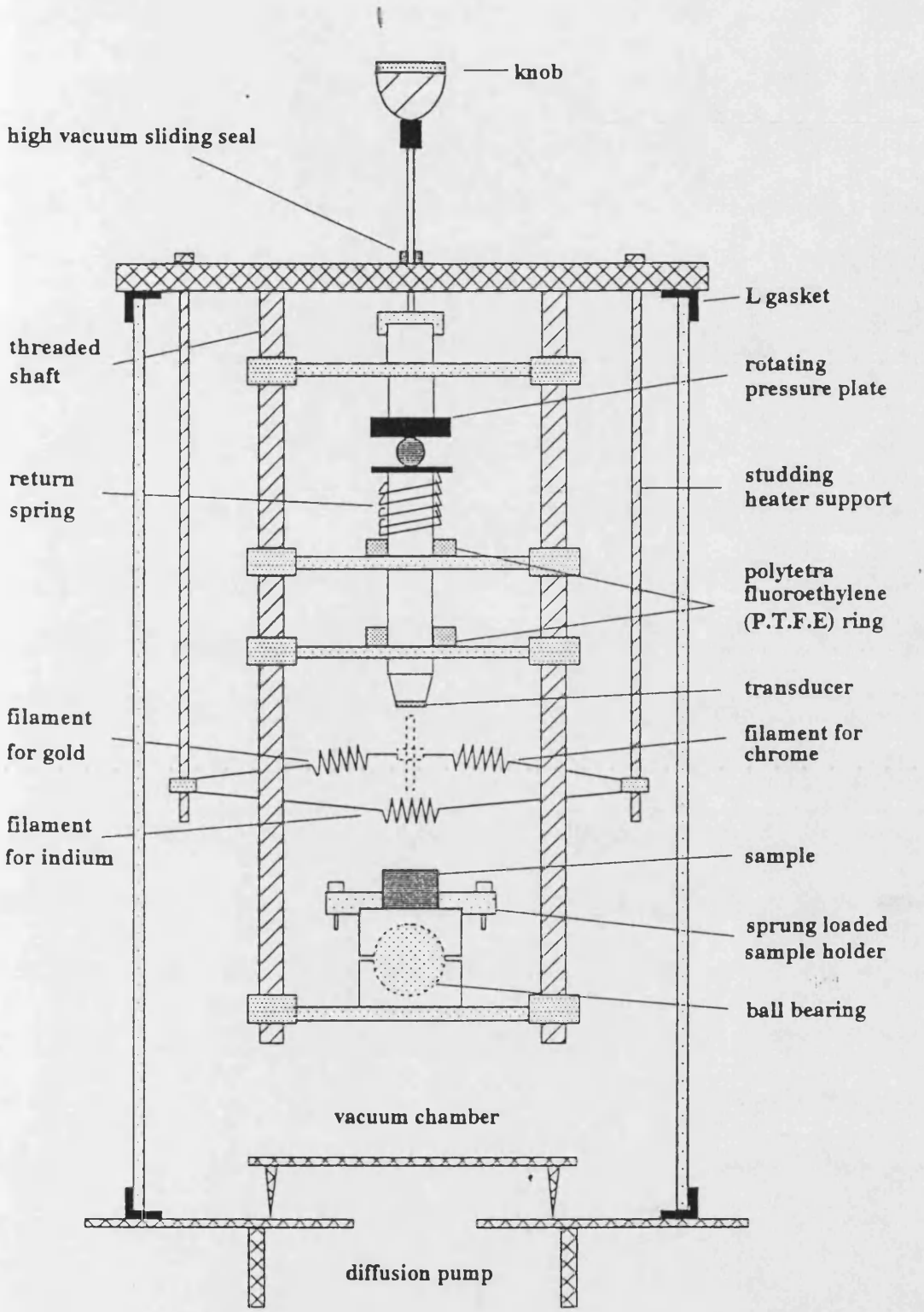

Figure 5.3. Schematic representation of the coating jig for indium bonding.

and this provides a suitable bond for both longitudinal and shear waves. The bond characteristics have been found not to vary appreciably over the temperature range of 300K down to 10K.

The bonding process was performed in a vacuum chamber where a coating of indium (99.9% purity) could be deposited evenly on both the sample and the transducer. The apparatus designed and built for this process is sketched in Figure 5.3. Before any evaporation was made, thorough cleaning of the coating jig and the filament were carried out using acetone in order to remove dust and grease from the transducer and sample. To evacuate the chamber, the apparatus was placed on top of a diffusion pump which produced a vacuum better than 10^{-4} torr. The filaments were first heated for about 15 to 20 seconds in the vacuum chamber to remove any residual elements that may be present from previous evaporations. A precleaned tweezer was used to place the chromium, gold and indium in their respective filaments. The transducer was placed at the bottom of the plunger and fixed with a small amount of epoxy resin. The distance of the filaments to the transducer and the sample needed to be the same, so that equal thicknesses of the deposited films could be obtained. To aid adhesion, a very thin layer of chromium was first deposited onto the sample; it was then followed by a layer of gold and finally a layer of indium was deposited. These layers of bonding produced a total thickness of about 1 micron. Immediately after the evaporation was completed, the plunger was then screwed down onto the sample. A constant force was used to stick the transducer to the sample. The sample was taken out and cleaned with acetone to remove the grease and residues, when the temperature of the bond had cooled down.

An examination of the quality of the bond was made to ensure that the indium bonding was uniform and could produce good exponential echoes. After an ultrasonic

measurement had been performed, the transducer was removed from the sample and another transducer having a different vibrational mode could then be fixed. The block diagram of the coating unit Speedivac model 6E2, which was used for the evaporation of indium onto the sample is shown in Figure 5.4.

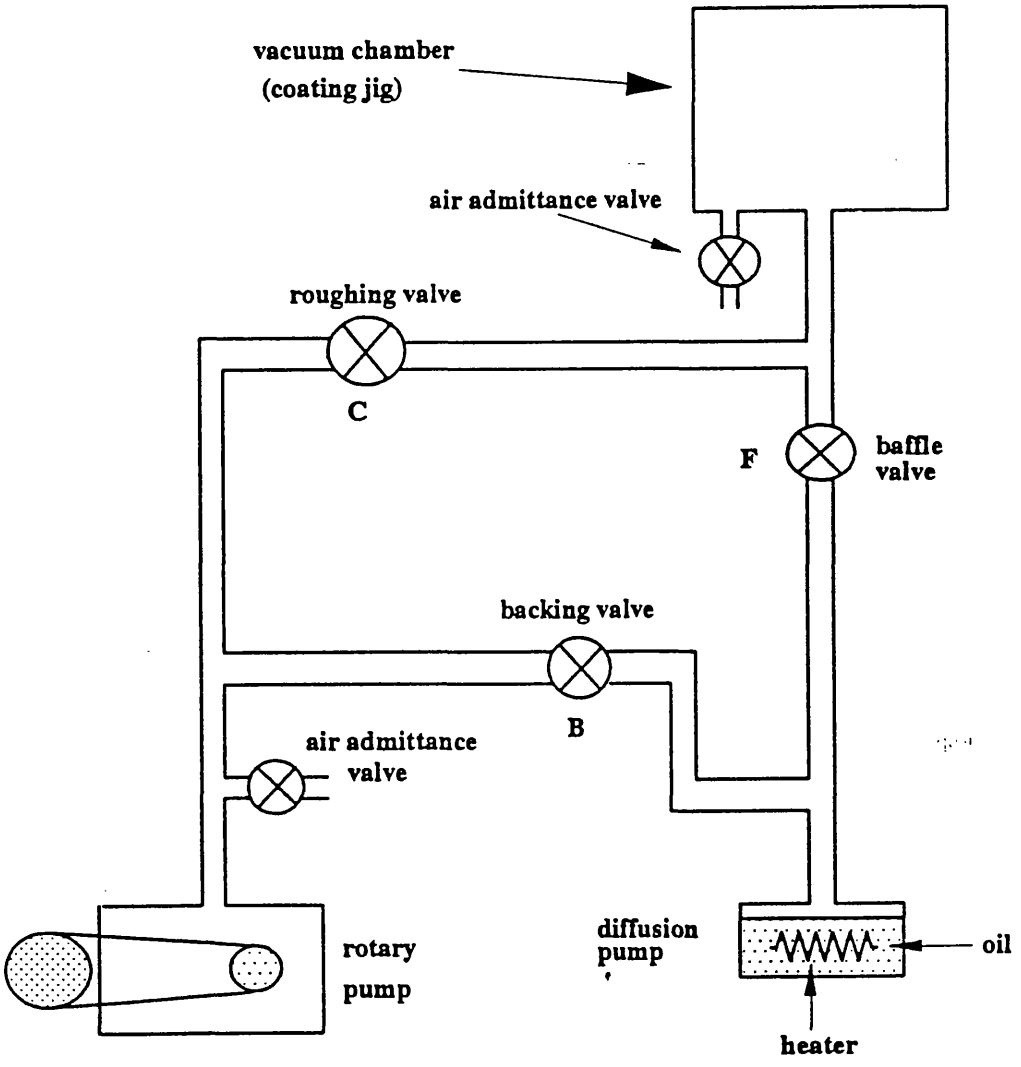

Figure 5.4. The vacuum pump system.

5.5 PULSE ECHO OVERLAP TECHNIQUE

The pulse echo overlap technique used to measure the transit time of ultrasonic pulses, based on the overlapping of two selected echoes, was first proposed by May (1958) and developed by Papadakis (1964, 1966, 1967). The pulse echo overlap system detects the changes in ultrasonic transit time with a sensitivity of 1 part in 10^5. The block diagram of the equipment used is shown in Figure 5.5.

The operation of the pulse echo overlap technique was as follows. A square wave synchronising signal (Figure 5.6(a)) was generated by a high resolution frequency source (Matec- Model 110). This signal was then used to trigger the rf pulse generator in the modulator/receiver (Matec- Model 6600). The carrier frequency of the rf pulse generator was set to the resonant frequency of the transducer and a series of a short duration high voltage rf pulses were produced. These pulses of about 3μs time duration and maximum magnitude of 630 volt peak-to-peak were used to excite the quartz transducer.

The rf pulse generator had to be triggered at a low repetition frequency, which allowed all the echoes from the one rf pulse to die away before the next ultrasonic pulse was generated. Thus, a complete set of echoes was observed (Figure 5.6(d)). Using a decade divider (Matec- Model 122B), the low triggering frequency was obtained by dividing the output signal of the high resolution frequency source by a factor of 1000 (Figure 5.6(b)). When the rf pulse, shown diagrammatically in Figure 5.6(c), was applied to the transducer bonded to the sample, the electrical signal was converted to a mechanical vibration which passed through the sample. This vibration was reflected back and forth between the faces of the sample and produced a train of ultrasonic echoes. These mechanical vibrations were converted by the transducer into

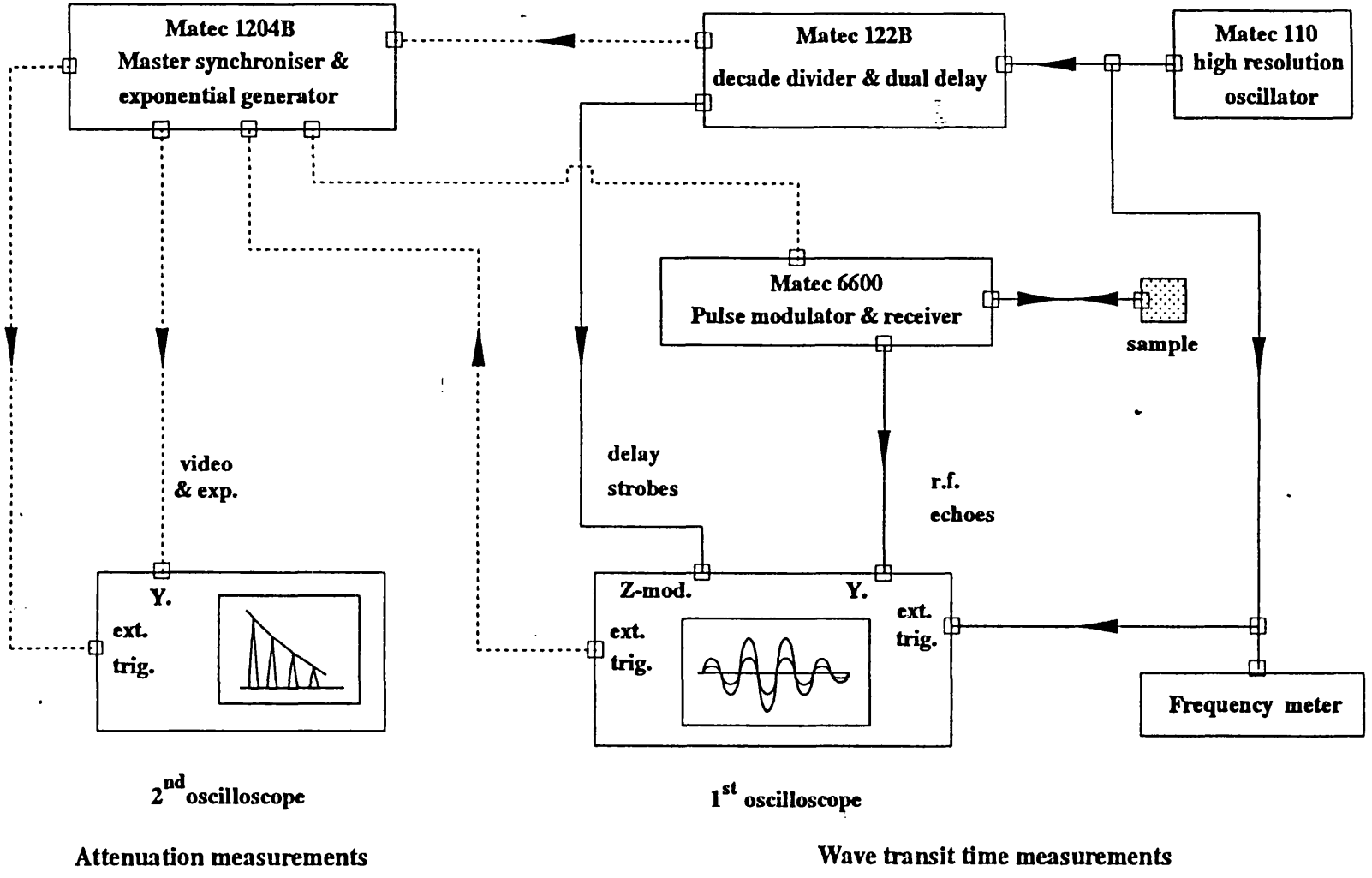

Figure 5.5. Block diagram of the pulse echo overlap system.

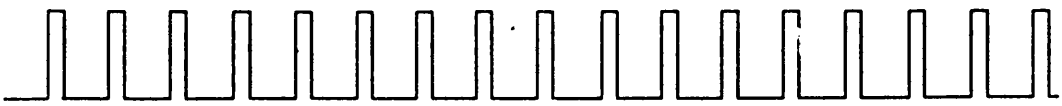

(a) Master sync. from high resolution oscillator

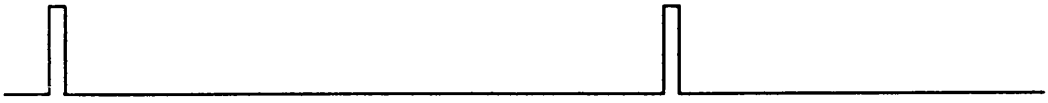

(b) Divided synchroniser (/1000)

(c) Radio frequency (rf) pulses to transducer

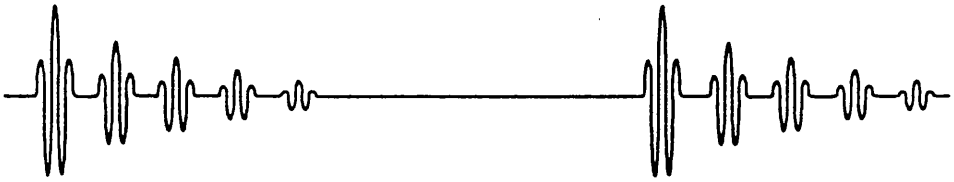

(d) Radio frequency echoes

(e) Z modulation - intensification of echoes 1 and 2

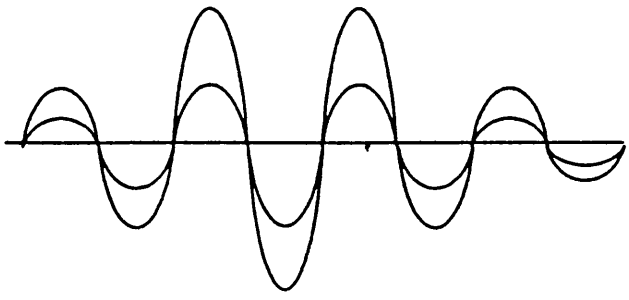

(f) Overiap of echoes 1 and 2

Figure 5.6. Signal at various points in the pulse echo overlap system.

an electrical signal, which was then fed to the amplifier in the receiver. The output from the amplifier was observed on an oscilloscope and the display appeared as depicted in Figure 5.6 (d).

To make transit time measurements, the strobe generator was triggered by the output signal from the decade divider to produce a pair of square wave pulses (Figure 5.6(e)). These pulses were fed into the Z-modulation of the oscilloscope to intensify two selected echoes. The oscilloscope brightness was reduced until only two intensified echoes were visible on the screen. The oscilloscope was triggered using pulses from the synthesizer, the frequency of which was highly stable, typically to better than 1 part in 10^7 per day. The frequency of the synthesizer was adjusted until it was approximately the same as the reciprocal of the time delay between the two selected echoes. Adjustment of the time base of the oscilloscope allowed the two intensified echoes to appear overlapped on the display (Figure 5.6(f)). Critical adjustment of the high resolution oscillator frequency then produced a cycle-to-cycle matching within the echoes. The echo transit time was calculated using the reciprocal of the oscillator frequency. This frequency was measured using a frequency meter.

The echo pulse shapes were distorted due to phase shifts occurring on each interface reflection within the sample (Eros and Reitz 1958). As a consequence, it was difficult to match the corresponding cycles in successive echoes. To overcome this difficulty, a cycle near to the centre of the first echo was chosen and overlapped over the equivalent cycle in the second echo. Should this overlap condition have been in error by say one cycle, then the mismatch would have become more apparent as the strobe pulse was moved to other echoes in the train.

For the measurements of the ultrasonic wave attenuation, an electronically generated exponential curve was superimposed on the display of the rectified echo

train on the second oscilloscope. This was done using the Matec Model 1204B (Figure 5.5). The exponential curve was fitted to the echo pattern and the attenuation was then obtained from the time constant of the exponential curve.

The measurement of the ultrasonic wave velocity and attenuation of rare earth phosphate glasses were carried out between 10-300K using a close-cycle liquid helium cryostat. A Cryophysics Model 22C cryodyne refrigeration system was used. It consisted of a compressor of Model SC, a cold head of Model 22 and a temperature controller. The operation of this system was described earlier in detail by Chang Fanggao (1992). The temperatures of the sample were monitored and stabilised using a temperature sensor and an electric heater and these were recorded to an accuracy of ± 0.1K. The temperature of the sample was changed very slowly due to its low thermal conductivity, such that for every temperature setting, a time period of at least 10 minutes was allowed for the sample temperature to stabilize before each measurement was made.

5.6 THE HYDROSTATIC PRESSURE APPARATUS

A hydrostatic pressure rig, based in essence on the designs by Bridgman (1958), Wentorf (1962) and Bradley (1969), was used to measure the pressure dependences of the ultrasonic wave velocity as shown in Figure 5.7. The system consisted of a steel piston-cylinder, which contains the sample in an oil-filled cavity between two end pistons. 'Dow Corning' 200/1000 cs silicone oil was used as the pressure transmitting medium. It was possible to work in the temperature range 243K to 450K without freezing or igniting this silicone oil. Although the system capability was of reaching a maximum pressure of 1 GPa, the highest pressure used was 0.15GPa.

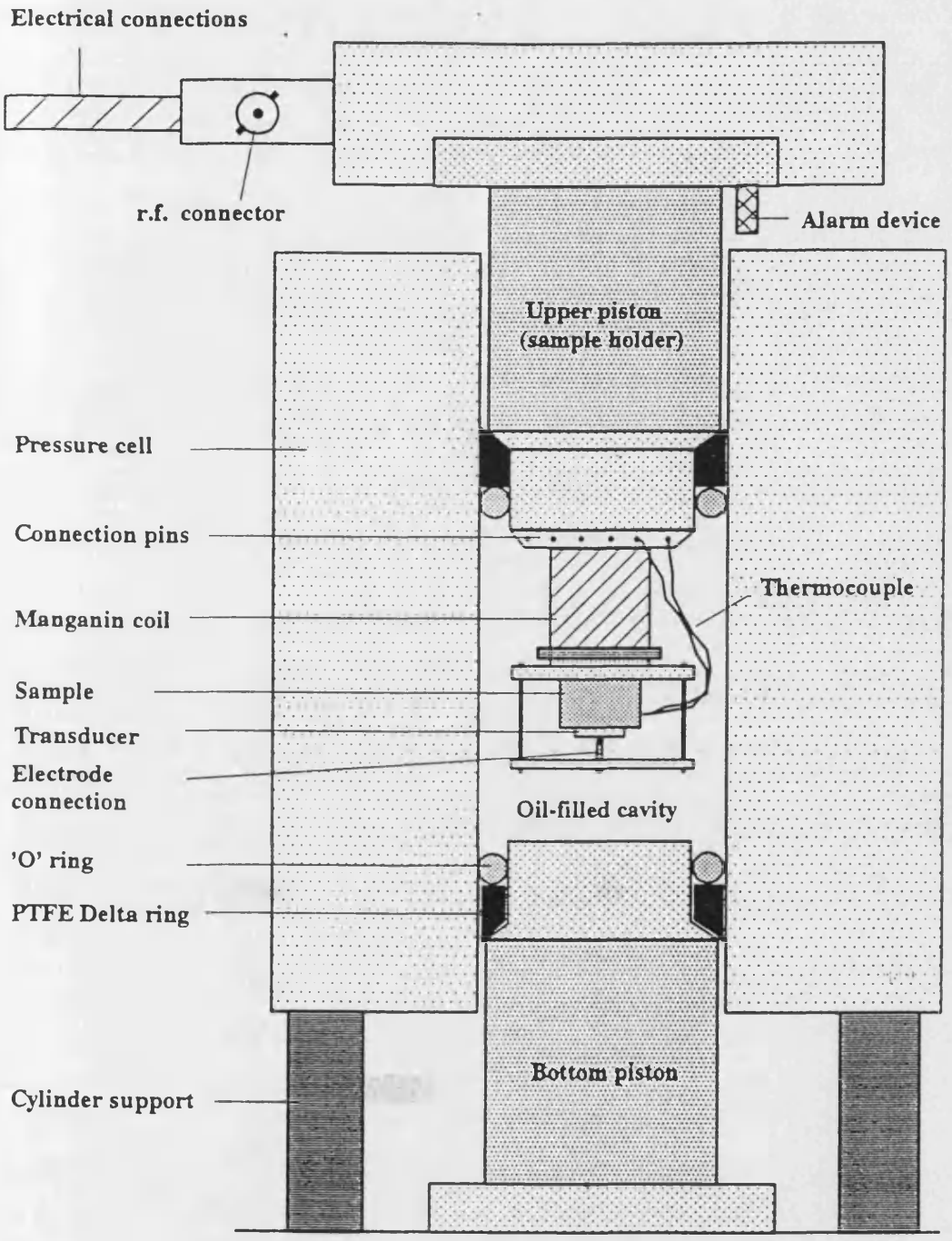

Figure 5.7. The hydrostatic pressure apparatus.

The pistons and cylinder were made from EN26 nickel alloy carbon steel. The cylinder was 11.5 cm high, 12.7 mm diameter with a bore of 2.54 cm diameter. Seals between the pistons and the internal cylinder walls were formed by a rubber O-ring and PTFE delta ring for each piston which provide satisfactory sealing within the working temperature range. To measure the internal pressure, the sample holder and manganin coil gauge were mounted on top of the upper plunger. The top piston was forced towards the bottom one within the pressure cell to create the hydrostatic pressure on the sample through the liquid medium. To measure the electrical resistance of the manganin coil under pressure, a 'Thurlby' multimeter with a sensitivity of 1 mΩ was used. The resistance data was converted to pressure using the following relation

$$P = \frac{((R/R_o) - 1)}{2.4x10^{-3}} \quad (kbar) \tag{5.2}$$

where R and R_0 are the resistance under arbitrary pressure P and initial pressure P_0 respectively. The constant $2.4x10^{-3}(kbar)^{-1}$ is the pressure coefficient of resistance, as measured by Samara and Giardini (1964). The temperature within the cell was measured by an internal NiCr/NiAl thermocouple with a Digitron digital thermometer having a sensitivity of 0.2K. The pressure was generated by a 50 ton hydraulic press which was constructed by Bishop Lifting Services, Bristol, UK. The press and pressure cell were enclosed in a 7 mm thick steel cabinet, in the interest of safety.

As soon as the pressure cell was sealed, the pressure was usually increased to the maximum value required, to check for leaks and to set the bonding of the quartz transducer. After releasing this initial applied pressure, the system was left for a period of time for it to regain thermal equilibrium. The collection of the data could then take place. During the experiment, the pressure was increased in steps of approximately

0.01-0.02GPa. Changes in applied pressure generated a temperature rise in the pressure cell. Hence, before any measurements were made, thermal equilibrium of the system had to be attained.

5.6.1 The temperature dependences of ultrasonic wave velocities under hydrostatic pressure

The measurements of the small changes of the transit time under hydrostatic pressure were carried out between 293K-400K. The temperature of the whole pressure cell was increased by passing an electric current through a cylindrical heating element tightly clamped around the external wall of the pressure cylinder. The external wall temperature of the pressure cell was held at a reasonably steady temperature by using an Eurotherm Mini 17-90B temperature controller. The sensor for the temperature controller was a NiCr/NiAl thermocouple held between the heating element and the pressure cell. When the temperature registered by this thermocouple fell below a value preset on the Eurotherm controller, the relay would close and the heater energised. The electric current of the heating element was controlled by a variac. Using this system, the external temperature of the pressure cell was held steady to within a few Kelvin. Temperature oscillations at the external surface of the pressure cell were damped considerably by the thermal mass of the cylinder walls so that temperature at the centre of the cell was constant to within 0.3K.

The operation of the system was as follows. The Eurotherm controller was set to the desired temperature and the variac set to give an adequate current to the heating element. When the required temperature of the external cell was attained, the heater current was reduced since only heat losses had then to be overcome. The hydrostatic pressure experiment was then performed in the usual way; that is, when the pressure was increased, the temperature of the system was left to return to its equilibrium value before an echo transit time measurement was made. Although the pistons of the pressure

cell were insulated to some extent from the press by plastic packing, heat losses to the press did increase as pressure was applied. To counteract this effect, the heater current had to be occasionally increased slightly.

5.7 THE PULSE SUPERPOSITION TECHNIQUE

The major aim of the present work has been to determine all the three independent values of the TOEC for an isotropic material from 77K to 293K. The hydrostatic pressure measurements cannot give all the information needed for the calculation of the complete set of TOEC. However, it is possible to determine all three independent values of the TOEC for an isotropic solid by making measurements solely under uniaxial pressure. Since only extremely small changes in ultrasonic wave velocities are induced by the application of a relatively small uniaxial compression, a highly accurate method for measuring the velocity of ultrasonic waves is required. Hence, a pulse superposition technique was used.

The pulse superposition technique was developed by McSkimin (1961, 1965) and McSkimin and Andreatch (1962) and subsequently improved by Holder (1970) using an automatic gated carrier pulse technique. This was a modified version of the pulse interference method first described by Williams and Lamb (1958). The pulse superposition technique has been improved further by Yogurtcu et al. (1980) to a stage where changes in ultrasonic wave transit time can be measured with a precision of 1 part in 10^7. The system developed and built by Yogurtcu et al. (1980) used an automatic frequency-controlled gated-carrier pulse superposition technique. The block diagram of this apparatus is shown in Figure 5.8.

In this technique, the transit time measurement was based on the time delay between superimposed 'in-phase' pulses. The repetition rate of the pulses was adjusted to be either equal to the reciprocal of the round-trip transit time in the sample or to

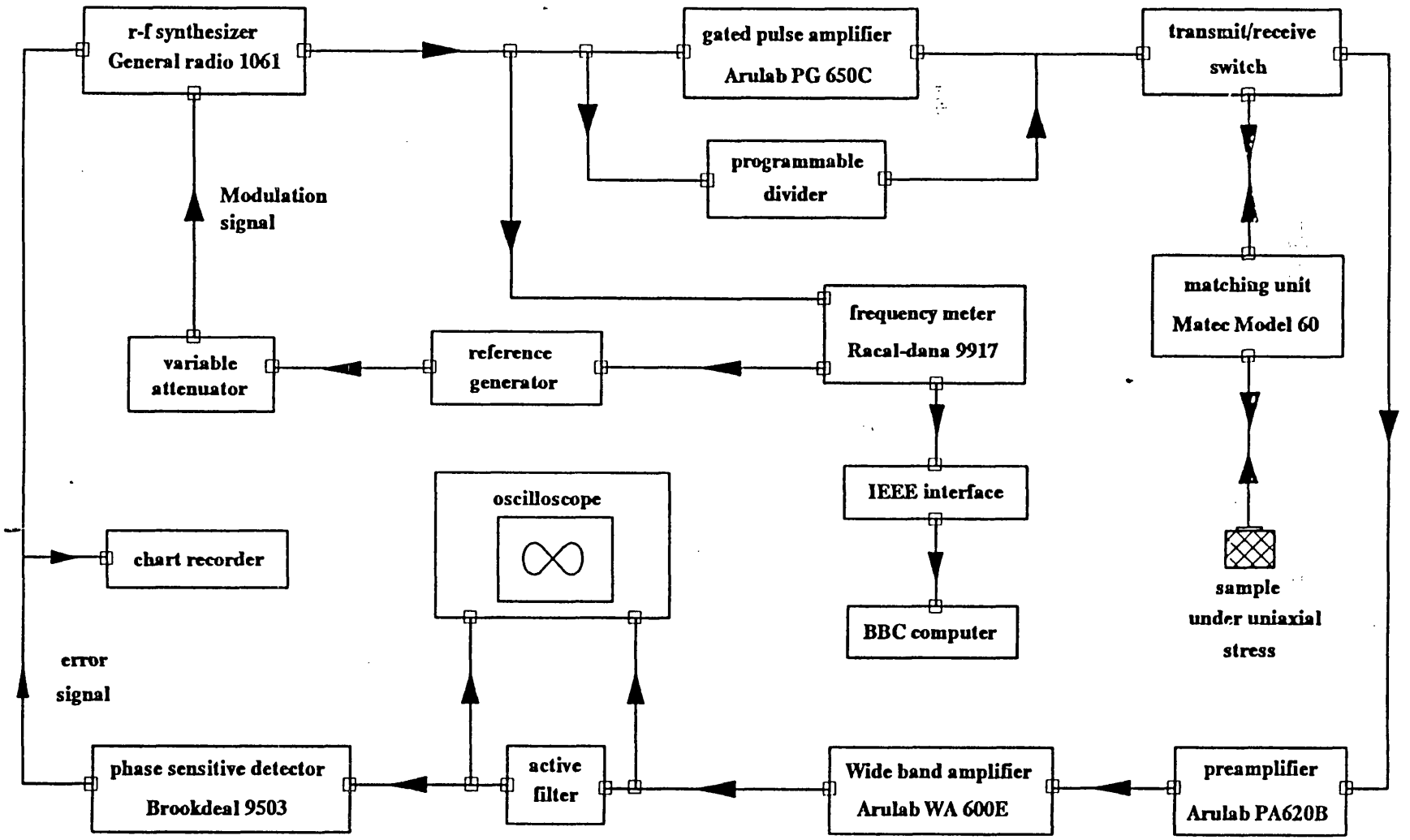

Figure 5.8. Block diagram of an automatic frequency-controlled gated-carrier pulse superposition technique.

submultiples of that rate. In contrast to the pulse echo overlap technique, the successive rf pulses applied generate ultrasonic waves in the sample before the earlier generated waves decayed. Figure 5.9 shows the ultrasonic pulses excited by the transducer and the echo trains to be superimposed upon one another and the ultrasonic wave velocity can be determined by the following relationship

$$v = \frac{2pl}{T} \tag{5.3}$$

where l is the thickness of the sample, T is the transit time between two echoes and p is an integer given as a multiple of the round-trip delay time.

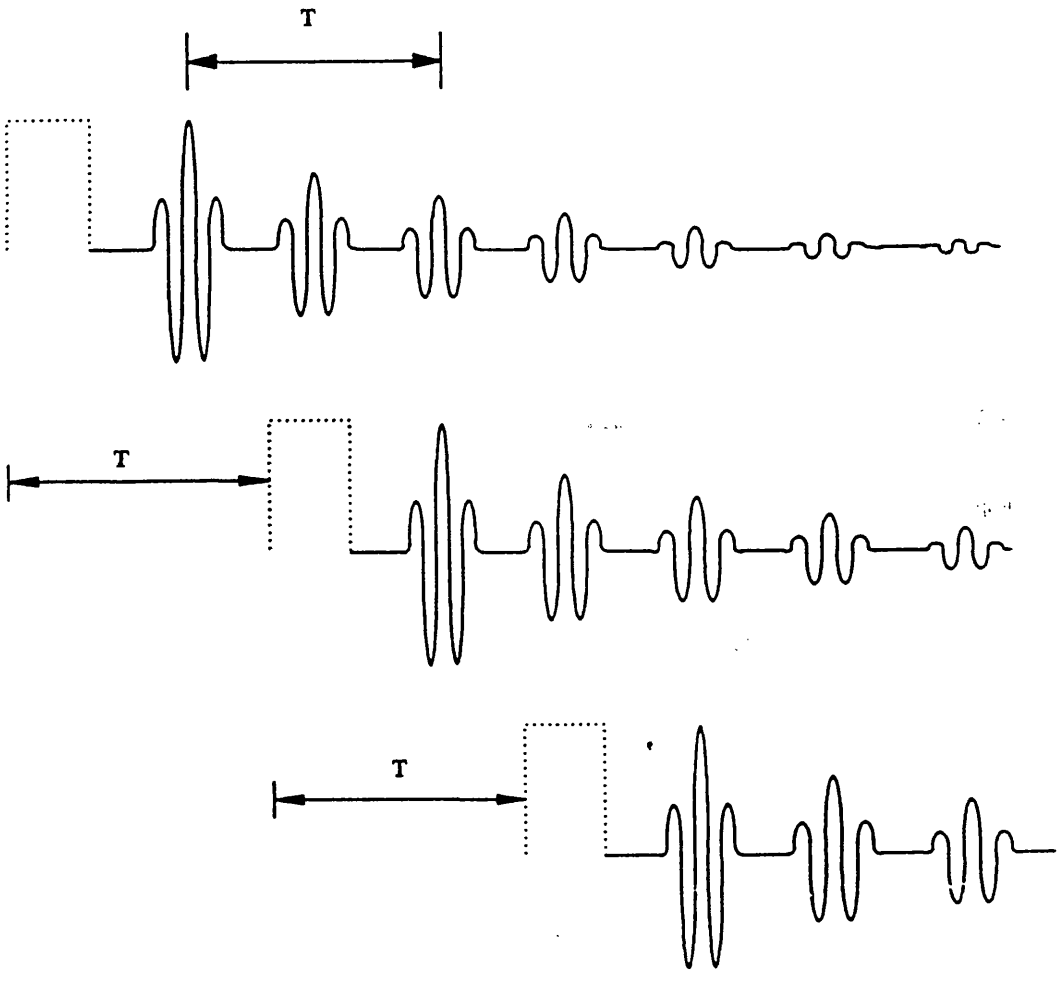

Figure 5.9. Wave pockets in a sample, showing superposition of echoes for p=2.

The superposition of the pulses was indicated by a maximum in the echo amplitude being observed on the oscilloscope. A full description of the operation of this pulse superposition technique is well documented by Lambson (1988).

5.8 THE UNIAXIAL STRESS APPARATUS

The uniaxial stress apparatus is shown in Figure 5.10. It is capable of providing an accurate, homogeneous uniaxial pressure to a rectangular parallelepiped sample.

This apparatus was manually controlled. The pressure was applied through a finely threaded screw shaft, transmitted into a calibrated proving ring and through a thrust rod onto the sample. To ensure that no twisting forces were applied to the proving ring, a thrust bearing was attached to the screw shaft. The thrust rod was centralised in the reaction tube by two sets of PTFE sleeve bearing fixed in the tube, to ensure that the tube moved vertically and with as little friction as possible. Two springs were used to release the pressure, when the screw was released. The reaction to the thrust was provided by the outer steel tube and the frame of the uniaxial stress apparatus.

The calibrated proving ring was used in its elastic deformation range of 0 to 2kN. A micrometer dial gauge was used to measure the deformation of the diameter of this proving ring, when the stress was applied. The dial gauge had a resolution of 2 micron per division which gave a resolution of 50N in the applied force. The reading indicated by this gauge was directly proportional to the force applied to the sample. The pressure P (in units of bars) at a certain deflection R of the dial gauge was calculated using the following expression:

$$P = \frac{R}{A}(6.35 - 1.25x10^{-4}R)x10^{-5} \qquad (5.4)$$

where A is the stressed sample area in units of m^2.

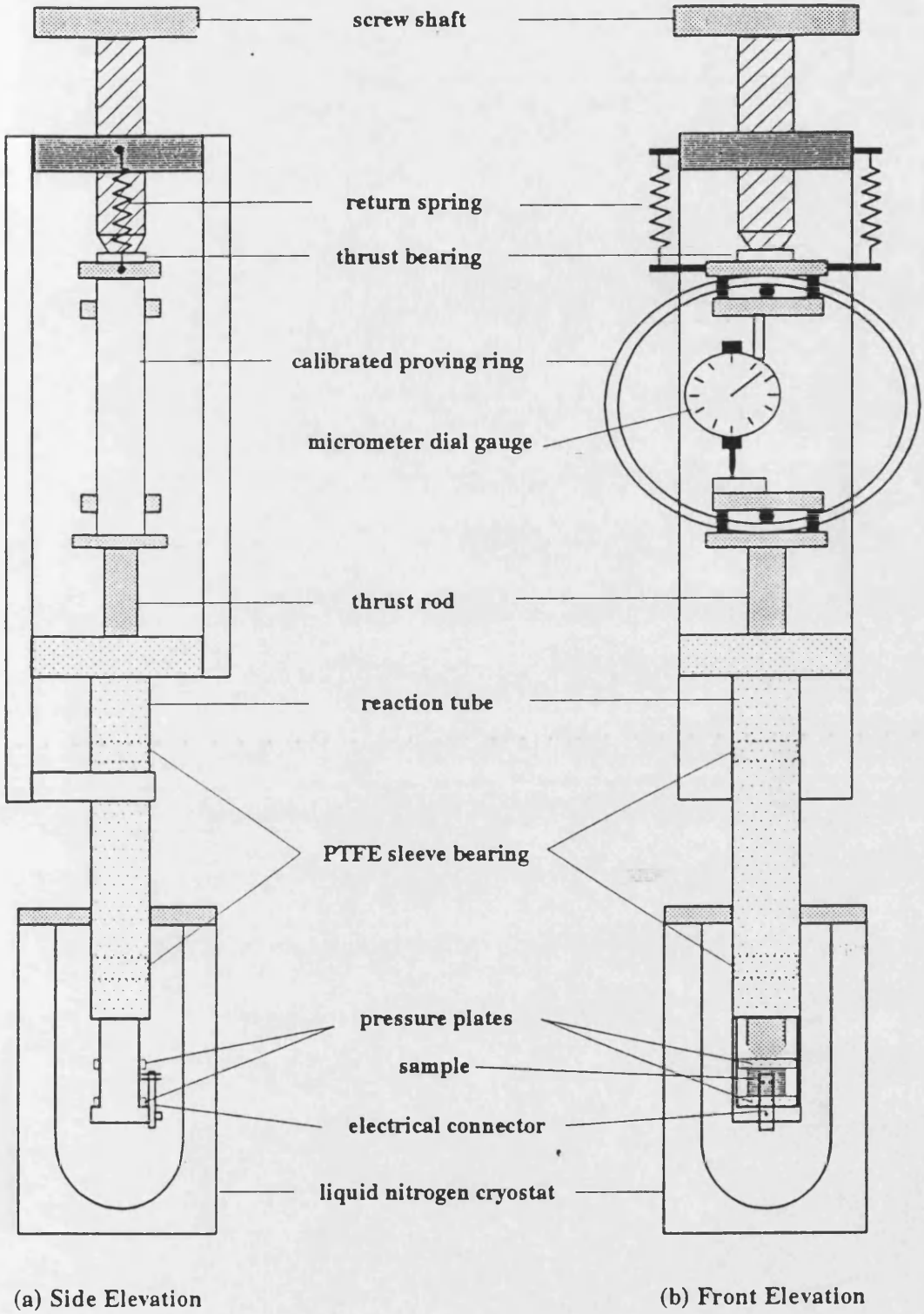

Figure 5.10. Diagrams of the uniaxial stress apparatus.

A ball bearing, attached to the end of the thrust rod, pressed upon one of two optically flat stainless steel plates between which the sample was mounted. The electrical connection to the transducer, which had been previously bonded to the sample, was made using two spring probes. These probes were fixed onto a perspex plate screwed onto the reaction tube.

5.8.1 The temperature dependences of ultrasonic wave velocities under uniaxial stress

The temperature dependence of the effect the uniaxial stress on ultrasonic wave velocities was determined above room temperature using an electrical heating system and below room temperature using a liquid nitrogen cryostat.

For measurements between 293K and 400K, the temperature of the sample was increased and controlled by passing an electric current through a heater wire wound around a cylindrical copper former which surrounded the sample and was clamped to the reaction tube of the uniaxial stress apparatus. The temperature of the heater was held steady by using a Harwell temperature controller. The sample temperature was monitored by attaching a NiCr/NiAl thermocouple to it and the temperature was displayed by a 'Digitron' thermometer. The sample temperature was controlled to within ± 0.1K.

For measurements below room temperature down to 77K, a liquid nitrogen cryostat was used. This system consisted of a vented dewar containing liquid nitrogen. The temperature was adjusted by varying the distance between the sample and the surface of liquid nitrogen. To measure the temperature, a 0.07% gold-iron/chromel thermocouple was placed it in contact with the surface of the sample. The temperature of the sample was displayed by a Thurlby digital 1905a multimeter with resolution

of $\pm$0.1K.

For measurements close to room temperature, dry ice or ice/water mixture was used instead of liquid nitrogen. To obtain measurements at a fixed temperature of 77K, the sample was immersed in the liquid nitrogen.

5.9 OPERATING PROCEDURES

The operating procedures for using the automatic frequency-controlled gated-carrier pulse superposition technique and uniaxial stress apparatus were as follows:

1. The sample with a transducer bonded to it was placed between the parallel plates of the uniaxial stress and the quality of echo pattern was checked.

2. A small pressure was applied to the sample and the stress distribution was checked using cross polaroids. To ensure that the stress within the sample was homogeneous, it was necessary that the fringe displacements were uniform throughout the sample and that the colour of these fringes changed from the centre of the sample outwards as stress was applied.

3. The rf synthesizer was set to the resonant frequency of the transducer and the switch divider to a large division ratio, say 1000. This allowed the complete sets of echo trains to be observed without interfering with each other. The video output from the wideband amplifier was monitored on the oscilloscope, and as the high voltage of the gated amplifier was increased, echoes were seen as depicted in Figure 5.11(a).

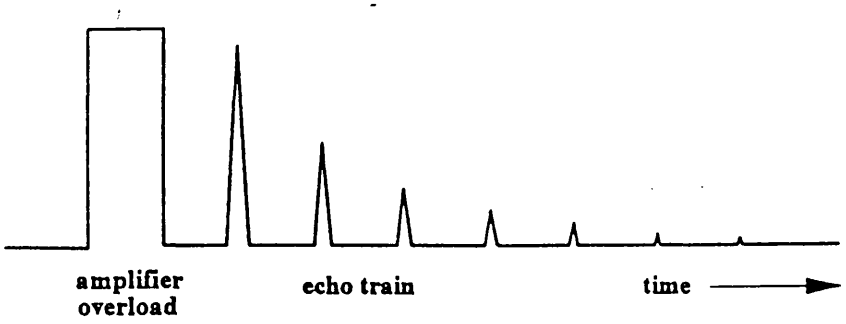

(a) Video output from the wideband amplifier for a large division ratio.

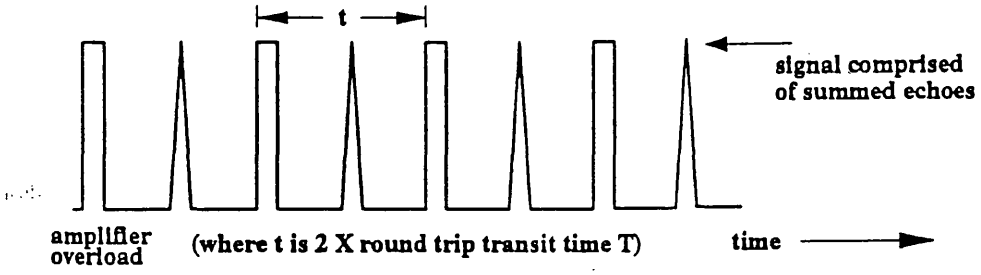

(b) Video output from the wideband amplifier for a small division ratio.

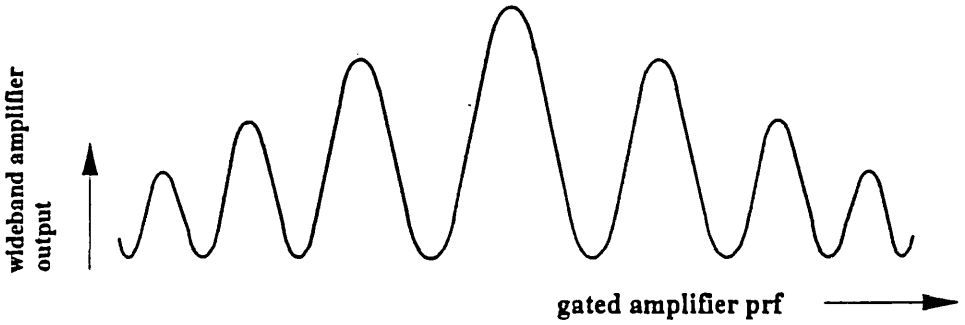

(c) Resonance peaks produced, when the pulse repetition frequency (prf) is varied.

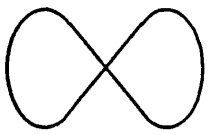

(d) Lissajous figure

Figure 5.11. Signal at various points in the pulse superposition system.

4. The synthesizer frequency, the tuning of the gated amplifier and the matching unit were adjusted for maximum echo amplitude. By reducing the programmable divider ratio, the transducer excitation pulse was made to coincide with alternate received echoes (Figure 5.11(b)).

5. The divider output was used to trigger the oscilloscope, so that the trace remained stable as the division ratio was changed. The output from the rf synthesizer was frequency modulated by using the search-sweep facility, and initially a wide frequency sweep was used by depressing the *x100* kHz button and increasing the modulation input voltage. The modulating voltage was applied to the *x* input of the oscilloscope, the timebase being switched off and a series of resonance peaks were observed. When the division ratio was set to its optimum value, a series of peaks with a maximum sharpness were obtained, with a decreasing amplitude and symmetrically spaced (Figure 5.11(c)).

6. The amplitude of the modulation input to the rf synthesizer was reduced. Using the rotary frequency control, the central peak was selected, and the frequency at which it occurs was taken. The synthesizer digits were set to this frequency and a smaller search sweep range was selected. The oscilloscope timebase was switched to normal operation. A slow sweep speed and the output from low pass active filter could then be monitored. When the modulating voltage was set to its maximum, the oscilloscope input sensitivity was increased. A waveform containing a large second harmonic content of the modulating frequency at 444 Hz could then be seen.

7. As the rf frequency was slowly changed, the waveforms altered. On each side of the superposed echo resonance peak, a 222 Hz, a sinusoidal waveform was produced with a phase difference of 180° between the two waves. Using the

modulating voltage as the *X* input, this signal was displayed on the oscilloscope as a Lissajous figure (Figure 5.11(d)) which appeared as a figure of eight at the peak of superimposed echo resonance curve. This showed that the doubling of the modulating frequency was taking place at this point. On either side of the resonance peak, a tilted ellipse was produced with the angle of tilt moving through 90° when the signal changed from the in-phase to the anti-phase condition.

8. This signal was connected to the input of the phase sensitive detector and the feedback loop was completed. The apparatus was set to its maximum sensitivity by observing this figure of eight, whilst increasing the output time constant. The optimum settings were achieved just before the figure became unstable, indicating that the system was just about to break into self-sustained oscillation.

9. The system was then connected to the IEEE interface and the process of data taking using the 'BBC' computer could begin. To ensure that the sample temperature was stable, normally a waiting period of 30 minutes was required for a single temperature measurement.

5.10 EXPERIMENTAL ERRORS AND CORRECTIONS

The precision in determining the SOEC and TOEC depends predominantly upon the accuracy with which the absolute ultrasonic wave velocities and the relative changes in ultrasonic wave velocities can be measured. Experimental error can arise through measurements of the sample dimensions, density and the pulse echo transit time. The temperature fluctuation of the sample and slight changes in the bonding material during cooling or heating have also contributed some inaccuracies in the measured data. Difficulty may also arise in correct positioning of the sample in the uniaxial

press to obtain a uniform stress in the sample. Although, some of these difficulties may be partially corrected, their effects can only be estimated. A brief discussion on the various types of error and the steps taken to rectify them is as follows.

5.10.1 Measurements of sample dimensions and density

The path length of ultrasonic pulses is equal to twice the length (l_0) of the sample in the propagation direction. The dimensions of the samples were measured using a digital micrometer to a precision of 1 μm. Several measurements were made at different points on the relevant face of each sample and the mean of these measurements was used to calculate the ultrasound path length. Typical standard deviations in the measurements of the sample dimension were of the order of 0.02%. This error contributes directly to the error in the derived velocity and this leads to an error of approximately 0.04% in the resultant SOEC.

The density of the glasses was measured at room temperature by Archimedes' principle using toluene (density = 0.868 gcm^{-3} at 20°C) as a flotation fluid. Toluene was used instead of distilled, de-ionised water, because the phosphate glasses could have been slightly hydroscopic. An analytical balance was used to weigh the sample in air and in toluene to an accuracy of ±1 mg. The density of the sample ρ_s was calculated using the following expression:

$$\rho_S = \rho_T \left[\frac{(M_A)}{(M_A - M_T)} \right] \tag{5.5}$$

where ρ_T is the density of toluene and M_A and M_T are the mass of the sample in air and toluene respectively. The measurements were repeated several times within an accuracy of ±0.01%. The density of each sample was corrected for ambient temperature. The accuracy with which each glass density could be determined depended

on the size of the sample. Since the SOEC are determined from an equation of the general form $C_{IJ} = \rho v^2$, an error in the density measurement contributes directly to the error in the calculated SOEC.

5.10.2 Measurements of transit time

In ultrasonic pulse echo methods, the prime potential source of error arises from the measurements of an absolute pulse transit times. When the ultrasonic wave from the sample is incident onto a transducer-sample boundary, the wave is partly transmitted to the transducer and partly reflected to the sample. The transmitted wave is reflected back and forth within the transducer and a delay is introduced into the echo transit times as a result of these multiple internal reflections.

The correction of the error due to transit time measurements was based on the estimation of the reflection coefficient R of the following expression:

$$R = \frac{Z_T - Z_S}{Z_T + Z_S} \tag{5.6}$$

where Z_T and Z_S are the characteristic impedances of the transducer and sample, respectively. The algorithm for this calculation was given previously by Brassington (1982), using a method for correction of the time delay by Kittinger (1977). The estimated corrections for this transit time measurement were approximately 0.5 to 2.0%.

5.10.3 Diffraction and non-parallelism

Even though the transducer is regarded as a piston source for generating plane ultrasonic waves, some radiated energy may still be lost from the sides of the cylindrical region of acoustic flux. This is because the transducer is finite in extent and has a diffraction field which can cause errors in transit time measurements. A detailed theoretical explanation can be found in Truell et al. (1959). The diffraction field is characterized by the dimensions of the transducer and the properties of the propagation

medium. Since glasses are isotropic, this error is very small and could be disregarded. A method to calculate the diffraction field and the correction for the transit time measurements has been given by Papadakis (1966).

To avoid the effect of non-parallelism, the sample faces were polished flat and parallel to optical precision as described in Section 4.4.

5.10.4 Errors due to temperature fluctuations

It was found that there were a strong temperature dependences of the ultrasonic waves velocities for phosphate glasses, especially in the low temperature region. When measuring relative velocity changes due to applied pressure, it was important to ensure that the temperature was stable. During measurement, the temperature of the sample was monitored by the thermocouple in contact with it. The temperature controller in the hydrostatic pressure system was found to be able to stabilise the temperature of the sample to within $\pm$0.3K.

In the case of measurements under the effect of the uniaxial stress, extremely small changes of transit time were induced by the low pressure applied, and hence a small changes in sample temperature would affect the measurements. This temperature fluctuation was minimised by insulating the sample from its surroundings using a copper former enclosing the sample. Using this method, the temperature could normally be stabilised within $\pm$0.1K.

CHAPTER 6

THE TEMPERATURE DEPENDENCES OF TOEC AND ACOUSTIC MODE VIBRATIONAL ANHARMONICITY OF VITREOUS SiO_2

6.1 INTRODUCTION

It has been established that the nonlinear acoustic vibrational properties of vitreous SiO_2 are singularly anomalous as compared to those of its crystalline counterparts, quartz and cristoballite. The temperature dependences of the sound velocities in vitreous SiO_2 differ markedly from those which would be expected on the basis of the vibrational anharmonicity, which would be a nearly linear behaviour with a negative slope at high temperatures becoming flat when the temperature is lowered down to 0K (Fine et al. 1954, Anderson and Bömmel 1955, Krause and Kurkjian 1968, Krause 1971 and Kurkjian et al. 1972). The observed temperature dependence of the ultrasonic wave velocity propagated in vitreous SiO_2, can be divided into three different regions (Hunklinger and Schickfus 1981), as shown in Figure 6.1. At very low temperatures, the ultrasonic wave velocity increases linearly with decreasing temperature until it reaches a maximum T_{max} at about 1K. Below 1K, the linear temperature dependence of sound velocity is due to the resonant scattering of phonons, and has been successfully accounted for in terms tunnelling model of two-level systems (Anderson et al. 1972, Phillips 1972). In the vicinity of 1K and above, relaxational scattering comes into play, leading to a decrease in sound velocity with increasing temperature (Hunklinger and Arnold 1976). The temperature dependence is predicted to be logarithmic (with the sign reversed with respect to the resonant scattering regime) and this is observed experimentally (Raychaudhuri and Hunklinger 1984). With continuing increase in temperature, the sound velocity exhibits a stronger temperature dependence. It is in this region, above 10K or so, that the interaction of ultrasonic wave and two-level system via thermally activated

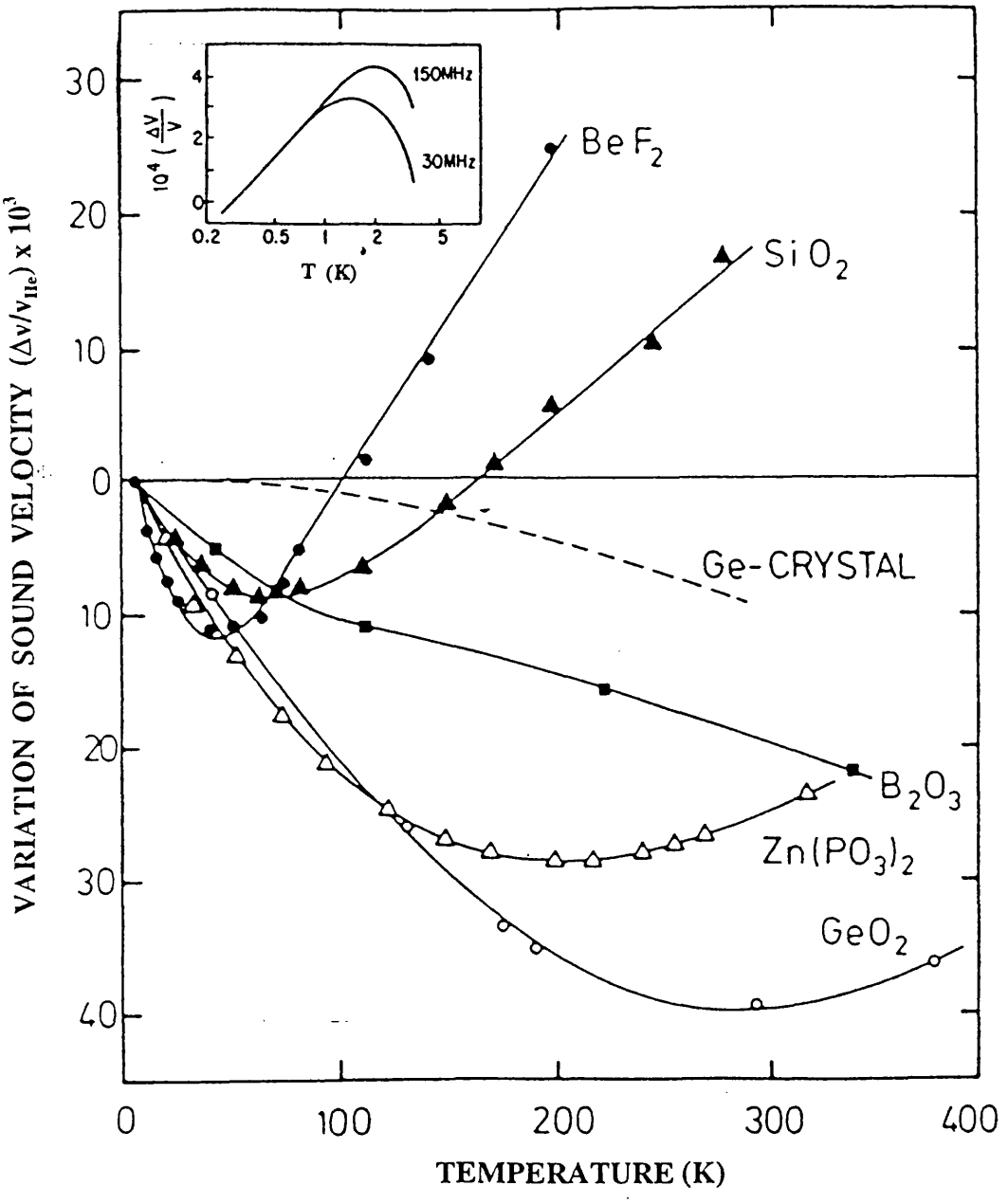

Figure 6.1. Temperature dependence of the velocity of 20 MHz, longitudinal sound waves for vitreous SiO_2 and several other glasses. The velocity of crystalline germanium at 25 MHz is included for comparison. The inset shows as enlarged plot of the typical behaviour at very low temperatures for two different frequencies. v_{He} is the velocity at liquid helium temperature (Hunklinger and Schickfus 1981).

processes becomes dominant. The sound velocity of vitreous silica decreases to a minimum at about 60K, then increases again with increasing temperature. The behaviour is this region cannot be explained by the two-level system model (Tielbürger et al. 1992). It seems to be a characteristic of glasses with a tetrahedral structure similar to vitreous silica (Krause and Kurkjian 1968, Kurkjian et al. 1972, Hunklinger and Schickfus 1981). Several models have been brought forward to interpret this increase, such as density fluctuations (Kul'bitskaya et al. 1974, Hunklinger and Schickfus 1981), but without satisfactory and sensible explanation, until recently using the soft-potential model (section 2.9).

The hydrostatic pressure dependences are negative: when subjected to pressure, vitreous silica becomes easier to squeeze (Bridgman 1948, Bogardus 1965, Peselnick et al. 1967, Shull 1969). This extraordinary behaviour also occurs in other tetrahedrally coordinated glasses, such as GeO_2 and BeF_2 (Kurkjian et al. 1972). While the elastic moduli of fused quartz decrease under moderate applied pressure, normal behaviour is assumed at higher pressures. In his early compression studies Bridgman (1948) first observed that the bulk modulus decreases with increasing pressure until a reversal of slope at about 3GPa. This was confirmed by ultrasonic measurements as a function of high pressure which showed a nonlinear decrease of the elastic stiffnesses and the bulk modulus to a minimum value at about 2.3±0.2GPa, and thereafter an increase with increasing pressure; elastic behaviour was observed up to pressures of 3GPa (Kondo et al. 1981).

Bogardus (1965) first obtained a set of mixed adiabatic-isothermal TOEC for fused silica at room temperature from measurements using the ultrasonic pulse superposition technique as a function of both hydrostatic and uniaxial pressure. He found that each TOEC, except the smallest C_{456}, has a positive value consistent with the anomalous negative sign of the hydrostatic pressure derivatives $(\partial C_{IJ}^S/\partial P)_{P=0}$ of

the second order elastic stiffness tensor components (SOEC). Bogardus (1965) observations of the anomalous nonlinear acoustic vibrational properties of vitreous SiO_2 have attracted many workers to verify the anomalous elastic behaviour under pressure. Using the pulse superposition method of McSkimin (1961, 1965), Shull (1969) determined the complete set of TOEC at room temperature and extended the determination to higher order elasticity in the estimation of the complete set of fourth order elastic stiffness tensor components C_{IJKL} (FOEC). Subsequently, Yost and Breazeale (1973) obtained a complete set of truly adiabatic TOEC of GE type 151 fused SiO_2, using their calculated results derived from ultrasonic second harmonic generation and with those of ultrasonic beam mixing of Dunham and Huntington (1970). Cantrell and Breazeale (1978) have determined the temperature dependence of the adiabatic TOEC C^S_{111} alone between 3K and 300K from measurements of the second harmonic generation from the fundamental of longitudinal ultrasonic waves. Recently, the pressure dependence of the longitudinal sound wave velocity in vitreous silica has been measured using high resolution Brillouin spectroscopy between 50K and 300K and pressure up to 3GPa (Tielbürger et al. 1992); the reduction of ultrasound velocity by application of pressure was found to occur throughout this temperature range.

Negative hydrostatic pressure derivatives $(\partial C^S_{IJ}/\partial P)_{T,P=0}$ of the SOEC and $(\partial B^S/\partial P)_{T,P=0}$ of the bulk modulus, and positive temperature dependences $(\partial C^S_{IJ}/\partial T)_{T,P=0}$ of the SOEC and positive TOEC C_{IJK} reveal anomalous effects in the acoustic vibrational anharmonicity: the frequencies of the long-wavelength acoustic modes decrease under pressure so that the acoustic mode Grüneisen parameters

$$\gamma(p,\underline{q}) = -(\partial \ln \omega(p,\underline{q})/\partial \ln V)_{T,P=0}$$

$$= -V\left(\frac{\partial \ln \omega(p,\underline{q})}{\partial P}\right)_{T,P=0}\left(\frac{\partial P}{\partial V}\right)_{T,P=0}$$

$$= B^T\left(\frac{\partial \ln \omega(p,\underline{q})}{\partial P}\right)_{T,P=0} \qquad (6.1)$$

are negative. Here $\omega(p,\underline{q})$ is the vibrational frequency of a mode p of wavevector $\underline{q}$, P is the applied pressure, V is the volume of the solid and B^T is the isothermal bulk modulus which is defined as

$$B^T = -V\left(\frac{\partial P}{\partial V}\right)_T. \qquad (6.2)$$

In addition to being responsible for nonlinear acoustic properties, vibrational anharmonicity is the source of thermal expansion. Those glasses which show the anomalous elastic behaviour under pressure or with temperature can also exhibit a negative thermal expansion at low temperature (Kurkjian et al. 1972), where contributions from the long-wavelength, low frequency acoustic modes play a dominant role. Therefore knowledge of the acoustic mode Grüneisen parameters is a prerequisite for understanding the thermal expansion at low temperatures. Although the acoustic mode Grüneisen parameters have been determined for vitreous silica at room temperature (Brugger and Fritz 1967, Kurkjian et al. 1972, Kondo et al. 1981), their temperature dependences were not known - one aim of the present work has been to fill this gap. Acoustic mode Grüneisen parameters can be determined from measurements of either the hydrostatic pressure derivatives of the second order elastic constants or the TOEC. Therefore TOEC data, and the acoustic mode Grüneisen parameters, determine the vibrational anharmonicity of the long-wavelength acoustic modes to cubic order in strain.

In this chapter, the experimental results of the linear and nonlinear acoustic

properties of vitreous SiO_2 will be presented. To achieve the objectives, Wang et al. (1992) used solely a uniaxial stress onto a rectangular parallelepiped sample of vitreous SiO_2 with dimensions of about 1 cm^3 with three pairs of orthogonal faces polished flat and parallel to optical precision. A complete set of TOEC have been evaluated and a significant temperature dependence has been observed.

6.2 THE CHARACTERIZATION AT ROOM TEMPERATURE

The experimental results of elastic and nonlinear acoustic properties of vitreous SiO_2 measured at room temperature are given in Table 6.1. The data are compared with those of Bogardus (1965), Shull (1969) and Yost et al. (1973). Considering the different source of material, frequency ranges and the experimental techniques being used, the results obtained are in reasonable agreement with previously reported data. With the exception of the smallest and negative C_{456}, each of the TOEC is anomalously positive, with C_{111} having the largest magnitude. The effects on the longitudinal mode are much greater than on the shear mode. In addition, the third order Cauchy relationships

$$C_{123} = C_{144} = C_{456} \tag{6.3}$$

are not obeyed, implying a large non-central force contribution to the vibrational anharmonicity.

The hydrostatic pressure derivatives $(\partial C_{IJ}/\partial P)_{P=0}$ of the SOEC C_{IJ} and $(\partial B/\partial P)_{P=0}$ of the bulk modulus B have been calculated from the TOEC data. The hydrostatic pressure derivatives $(\partial C_{IJ}/\partial P)_{P=0}$ are negative, with $(\partial C_{11}^S/\partial P)_{T,P=0}$ being much greater than $(\partial C_{44}^S/\partial P)_{T,P=0}$ (Table 6.1). The anomalous negative sign of the hydrostatic pressure derivatives $(\partial C_{IJ}/\partial P)_{T,P=0}$ reveals softening of the long-wavelength acoustic modes under pressure. The pressure dependence is greater for the longitudinal than for the shear mode: there is a volume rather than a shear effect.

The hydrostatic pressure derivative $(\partial B/\partial P)_{T,P=0}$ of the bulk modulus is negative

Table 6.1. Comparison of elastic and nonlinear acoustic properties of vitreous SiO_2 at room temperature with previous published data (density = 2203 kg/m^3).

Property	Present results	Bogardus (1965)	Shull (1969)	Yost et al. (1973)
SOEC (GPa)				
C_{11}^S	78.6 ± 0.1	78.4	77.5	78.5
C_{44}^S	30.7 ± 0.2	31.3	31.2	31.2
Elastic Moduli (GPa)				
B^S	37.7 ± 0.1	36.7	36.0	36.9
E^S	72.4 ± 0.1	73.1	72.6	73.0
Poisson's Ratio σ	0.180 ± 0.001	0.168	0.164	0.170
TOEC (GPa)				
C_{111}	467 ± 10	526	620	648
C_{112}	233 ± 20	239	261	537
C_{123}	85 ± 5	54	72	428
C_{144}	74 ± 6	93	95	54
C_{166}	59 ± 1	72	90	28
C_{456}	-8 ± 0.6	-11	-2.5	-13
Pressure derivatives				
$(\partial C_{11}/\partial P)_{T,P=0}$	-9.95 ± 0.03	-10.84	-12.30	-17.2
$(\partial C_{44}/\partial P)_{T,P=0}$	-2.96 ± 0.02	-3.42	-3.83	-2.27
$(\partial B/\partial P)_{T,P=0}$	-6.00 ± 0.03	-6.28	-7.19	-14.2
Grüneisen parameters				
γ_L	-2.51 ± 0.06	-2.70	-3.02	-4.22
γ_S	-1.98 ± 0.02	-2.17	-2.38	-1.51
$\gamma^{el} = (\gamma_L + 2\gamma_S)/3$	-2.05 ± 0.01	-2.35	-2.59	-2.41

for vitreous SiO_2 (Table 6.1). Hence the bulk modulus, given to the first order term in pressure P by

$$B(P) = B_0 + P(\partial B/\partial P)_{T,P=0} \tag{6.4}$$

becomes smaller as pressure is increased. When subjected to high pressures, vitreous SiO_2 shows the remarkable property of becoming easier to squeeze.

The negative sign of the hydrostatic pressure derivatives $(\partial C_{IJ}/\partial P)_{T,P=0}$ of the SOEC and $(\partial B/\partial P)_{T,P=0}$ of the bulk modulus B and the positive sign of the TOEC display anomalous effects in the vibrational anharmonicity. The acoustic mode Grüneisen parameters are negative (Table 6.1) so that the mode frequencies, and hence the energies of the long-wavelength acoustic modes, decrease under pressure. Both longitudinal γ_L and shear γ_S mode Grüneisen parameters are negative with $|\gamma_L|$ being much greater than $|\gamma_S|$: the effect on the longitudinal mode is more pronounced than that of shear mode, the results confirm that vitreous SiO_2 displays enhanced acoustic mode softening under pressure, especially for the longitudinal mode.

6.3 THE TEMPERATURE DEPENDENCES OF THE SOEC, AND ITS RELATED PHYSICAL PROPERTIES.

The temperature dependences of the ultrasonic velocities of both longitudinal v_L and shear v_L waves propagated in vitreous SiO_2 have been measured from 293K down to 77K using the pulse superposition technique. The data have been used to investigate the temperature dependences of the SOEC and related elastic moduli for vitreous SiO_2. The elastic stiffnesses $C_{11} = \rho v_L^2$ and $C_{44} = \rho v_S^2$ and elastic moduli are found to decrease approximately linearly with decreasing temperature, as shown in Table 6.2. Below 70K both $C_{11} = \rho v_L^2$ and $C_{44} = \rho v_S^2$ begin to increase drastically with decreasing temperature (Krause 1971, 1973) due to phonon interactions with two-level systems (Phillips 1972, Anderson et al. 1972). This is now a well-known phenomenon associated with the

Table 6.2. The temperature dependences of the longitudinal v_L and shear v_S ultrasonic wave velocities, adiabatic elastic stiffnesses C_{11}^S and C_{44}^S together with the technical elastic moduli: the bulk modulus B^S, Young's modulus E^S and Poisson's ratio σ^S of vitreous SiO_2. The estimated experimental errors are $C_{11}^S \pm 0.1$, $C_{44}^S \pm 0.2$, $B^S \pm 0.4$, $E^S \pm 0.4$ and $\sigma^S \pm 0.002$.

T (K)	v_L (m/s)	v_S (m/s)	C_{11}^S (GPa)	C_{44}^S (GPa)	B_0^S (GPa)	E^S (GPa)	σ^S
77	5893	3620	76.5	28.9	38.0	69.1	0.197
93	5899	3623	76.7	28.9	34.0	69.2	0.198
103	5911	3632	76.7	29.1	37.9	69.5	0.195
113	5902	3641	76.7	29.2	37.8	69.7	0.193
123	5909	3645	76.9	29.3	37.9	69.8	0.193
143	5912	3651	77.0	29.4	37.8	70.0	0.192
173	5927	3665	77.4	29.6	38.0	70.5	0.191
193	5938	3669	77.7	29.7	38.1	70.7	0.191
213	5940	3675	77.7	29.8	38.1	70.8	0.190
233	5947	3681	77.9	29.9	38.1	71.0	0.189
253	5957	3688	78.2	30.0	38.2	71.3	0.189
273	5971	3723	78.5	30.6	37.7	72.3	0.181
293	5974	3733	78.6	30.7	37.7	72.4	0.180

structural relaxation processes which produce the broad peak characteristic of the ultrasonic attenuation in silicate glasses (Anderson and Bömmel 1955, Krause and kurkjian 1968, Krause 1971, Strakna 1961 and Maynell et al. 1973). It contrasts markedly with the behaviour of a pure dielectric crystal for which the velocity of sound decreases with increasing temperature due to the effects of vibrational anharmonicity.

The temperature dependences of the ultrasonic wave attenuation in vitreous SiO_2 have been investigated intensively by many authors (Anderson and Bömmel 1955, Hunklinger and Arnold 1976, Phillips 1990). Figure 6.2 shows the temperature dependence of the ultrasonic attenuation in vitreous SiO_2 and in other glasses. It is dominated by a broad maximum with P_{max} at about 50K whose origin lies in classical, thermally activated structural relaxation processes in double-well asymmetric potentials (Anderson et al. 1972, Phillips 1972, Gilroy and Phillips 1981, Phillips 1990). Although a wide range of low temperature thermodynamical and transport properties of glasses can be understood within the framework of this phenomenological model, the effects of pressure on the two-level systems have yet to be investigated theoretically. The problem has been identified experimentally by Bartell and Hunklinger (1982) and more recently by Tielbürger et al. (1992). Using a Brillouin scattering technique, Tielbürger et al. (1992) have made measurements of the effect of pressure on the acoustic absorption of longitudinal phonons in vitreous silica at temperatures between 50K and 300K and pressures up to 3 GPa. They found that the broad absorption peak rises strongly with pressure at the high temperature side of the absorption peak. At the same time the position of the maximum P_{max} shifts toward higher temperatures. In fact, no peak is observed in the range up to room temperature if a pressure of 2 GPa is applied. Similar shifts of the peak temperature from about 50K at atmospheric pressure to 90K under a pressure of 0.42GPa have been observed previously using ultrasonic measurements (Bartell and Hunklinger 1982). The anomalous positive temperature dependence of the SOEC of vitreous SiO_2 may be also be a consequence of the double-well relaxation

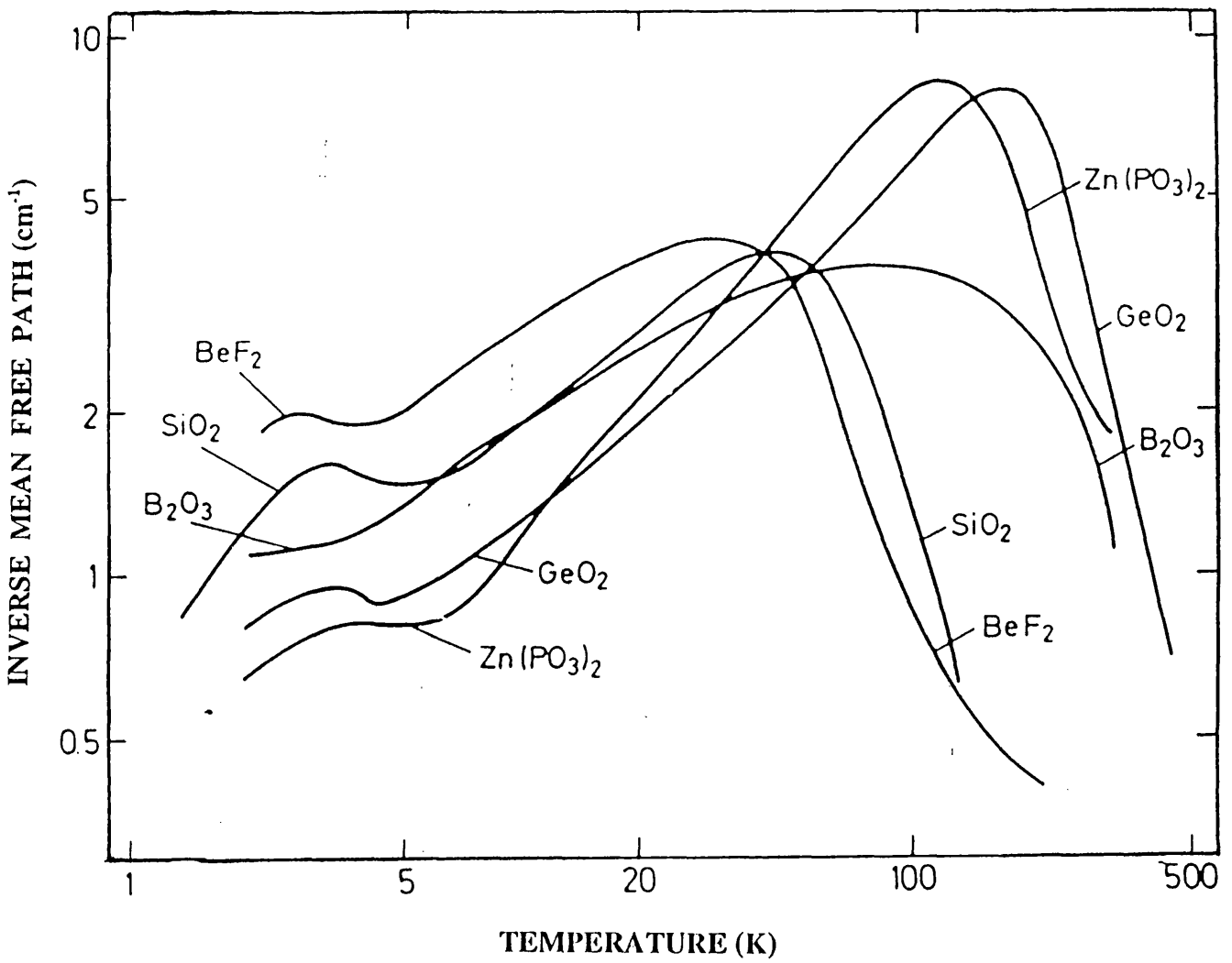

Figure 6.2. Temperature dependence of the 20 MHz, longitudinal Acoustic wave absorption (or inverse mean free path) for vitreous SiO_2 and several other glasses. (Hunklinger and Schickfus 1981).

processes which produce this attenuation peak. Furthermore since this broad attenuation peak extends right up to room temperature under the application of pressure, it is assumed that the thermally activated relaxation processes would seem to remain operative over this temperature regime.

6.4 THE TEMPERATURE DEPENDENCES OF THE TOEC

The central objective of the present work has been to determine the temperature dependences of the TOEC of vitreous SiO_2 from 293K down to 77K. Using the experimental configurations for determination of the TOEC of an isotropic material described in § 3.7 of chapter 3, three independent combinations of the TOEC have been determined and the results used to obtain a complete set of the TOEC of vitreous SiO_2 as a function of temperature (Figure 6.3). It can be seen that the TOEC C_{111}, C_{112} and C_{123} are strongly temperature dependent, increasing to more positive values as the temperature is reduced. Similar but smaller temperature dependences have been observed for C_{144} and C_{155}. The smallest TOEC C_{456} remains negative and almost independent of temperature. The results show that the pressure-induced acoustic mode softening is more pronounced for the longitudinal mode, which is associated with the volume effect, as compared with shear mode; this effect becomes enhanced at lower temperatures. Therefore, vitreous SiO_2 shows anomalous elastic behaviour under pressure, becoming easier to squeeze under pressure and temperature.

Second harmonic generation from the fundamental of longitudinal ultrasonic waves propagated in four different types of vitreous SiO_2 has been used by Cantrell and Breazeale (1978) to determine the nonlinearity parameter

$$\beta = -\frac{(3C_{11} + C_{111})}{3C_{11}} \tag{6.5}$$

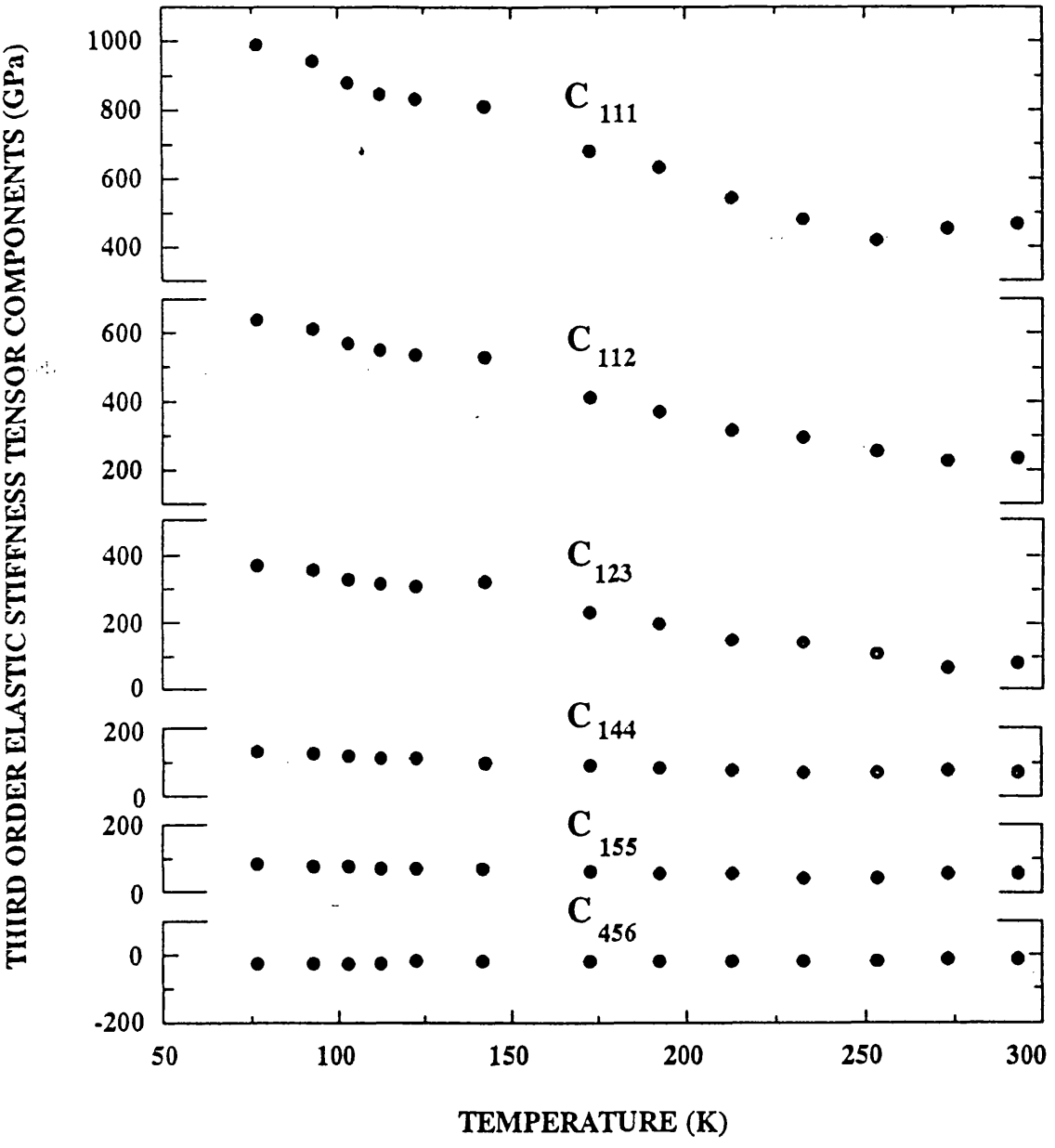

Figure 6.3. The temperature dependences of the third order elastic stiffness tensor components C_{IJK} for vitreous SiO_2.

between 4.2K and 300K. In combination with longitudinal wave velocity v_L measurements which give C_{11} from putting C_{11} equal to ρv_L^2, the adiabatic TOEC C_{111}^S could be determined as a function of temperature. It was found that C_{111}^S showed a small decrease with decreasing temperature for Suprasil W1, W2 and Suprasil 2, but an increase for Suprasil 1. However, the present results show that C_{111} increases with decreasing temperature, as do the other TOEC (with the exception of C_{456}) of vitreous SiO_2 (Figure 6.3).

6.5 THE TEMPERATURE DEPENDENCES OF THE HYDROSTATIC PRESSURE DERIVATIVES OF THE SOEC AND BULK MODULUS.

The elastic behaviour under pressure of the acoustic vibrational properties of vitreous SiO_2 is a remarkable. At room temperature the hydrostatic pressure derivatives $(\partial C_{IJ}^S/\partial P)_{T,P=0}$ of the elastic stiffnesses and $(\partial B^S/\partial P)_{T,P=0}$ of the bulk modulus are large and negative (Table 6.1). With decreasing temperature each pressure derivative $(\partial C_{11}^S/\partial P)_{T,P=0}$, $(\partial C_{44}^S/\partial P)_{T,P=0}$ and $(\partial B^S/\partial P)_{T,P=0}$ gets larger (Figure 6.4): it is interesting that the anomalous behaviour becomes enhanced at lower temperatures.

Central experimental observations are that $|(\partial C_{11}^S/\partial P)_{T,P=0}|$ is much greater than $|(\partial C_{44}^S/\partial P)_{T,P=0}|$ and that C_{111} is positive and the largest TOEC throughout this temperature range. These findings show that the acoustic mode softening induced by pressure is substantially greater for the longitudinal than the shear acoustic modes. The same processes of thermally activated relaxations are probably responsible for the anomalous nonlinear acoustic vibrational behaviour under pressure, namely the positive signs of the TOEC and the negative values found for the $(\partial C_{IJ}^S/\partial P)_{T,P=0}$. The observation that $(\partial C_{11}^S/\partial P)_{T,P=0}$ has a much larger negative value than $(\partial C_{44}^S/\partial P)_{T,P=0}$ throughout this temperature range indicates that the double-well relaxation processes are more effective in softening the longitudinal than the shear acoustic waves.

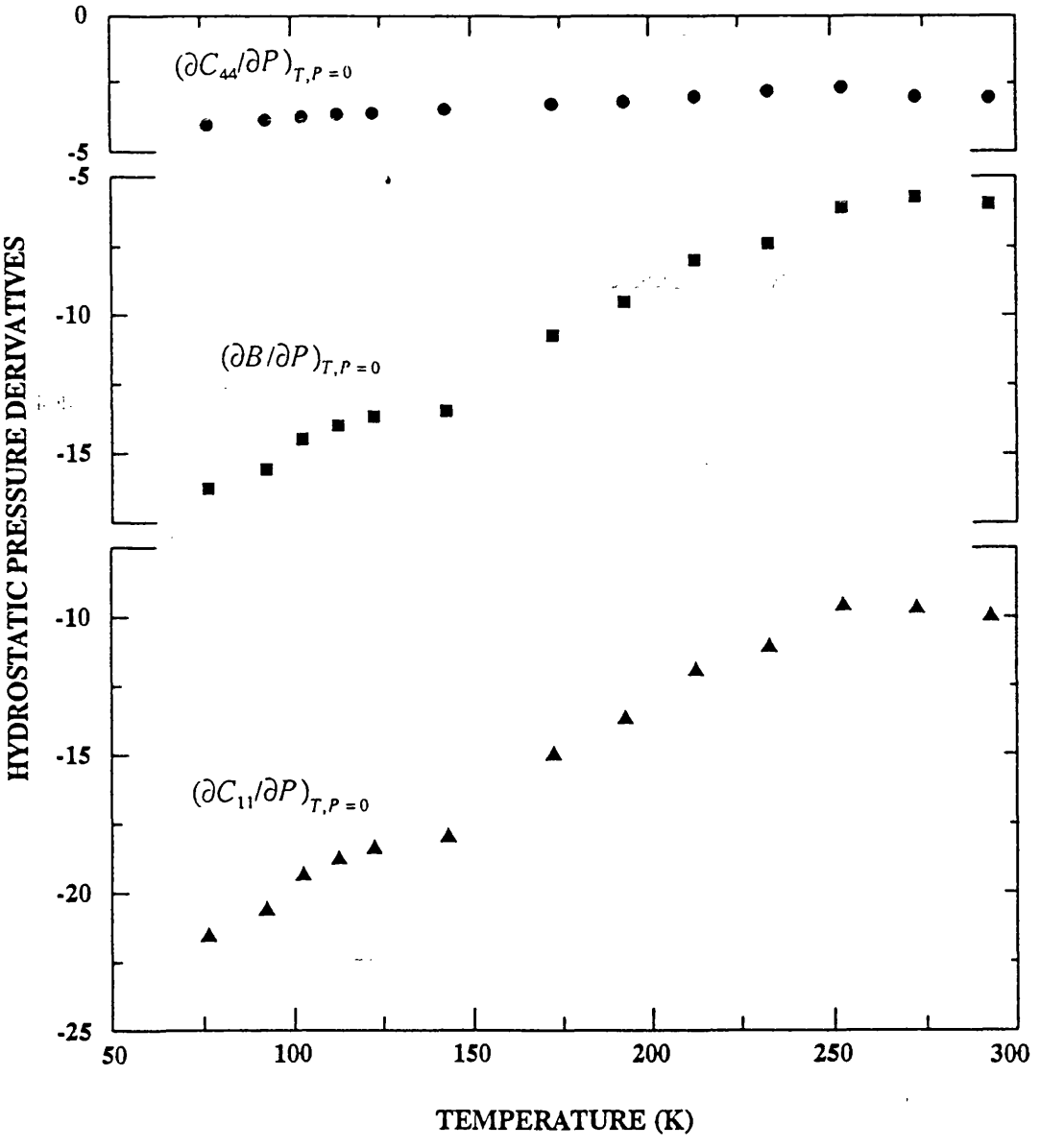

Figure 6.4. The temperature dependences of the hydrostatic pressure derivatives of the second order elastic stiffness tensor components C_{ij} and bulk modulus for vitreous SiO_2.

TOEC data have as yet been obtained only down to 77K (Figure 6.3) still somewhat above the temperature T_{max} at which the maximum relaxation occurs where the effects of the relaxation processes on the vibrational anharmonicity could be much enhanced.

6.6 THE COMPRESSION $V(P)/V_0$ OF VITREOUS SiO_2

The compression of vitreous SiO_2 extrapolated to high pressures by using each of the equations-of-state of Murnaghan (1944), Birch (1952), Anderson (1966), McWhan (1967) is compared with experimental data from Bridgman (1948) in Figure 6.5. Each compression curve has been calculated using the ultrasonic data given in Table 6.1. From the plot, it can be seen that the Birch equation-of-state fails at high pressure. Below 2GPa the Murnaghan equation-of-state, the quadratic polynomial and the cubic polynomial each fit reasonably well the experimental data. However, above 3.5GPa, the computed compression deviates from the experimental data; this is due to the change of the sign of the pressure dependence of the bulk modulus so that higher order pressure derivatives dominate the pressure variation of the bulk modulus. This feature is that expected for a solid material with a negative $(\partial B/\partial P)_{T,P=0}$. Thus, the preferred option for estimation of the compression at high pressures for vitreous SiO_2 with negative $(\partial B/\partial P)_{T,P=0}$ is Anderson's quadratic polynomial.

6.7 THE TEMPERATURE DEPENDENCES OF THE LONG-WAVELENGTH ACOUSTIC MODE GRÜNEISEN PARAMETERS.

The long-wavelength acoustic mode Grüneisen parameters can be determined from measurements of either the hydrostatic pressure derivatives of the SOEC or the TOEC. In addition to being responsible for nonlinear acoustic vibrational properties, vibrational anharmonicity is the source of thermal expansion. Normally, the glasses which show the anomalous elastic behaviour under pressure or with temperature can

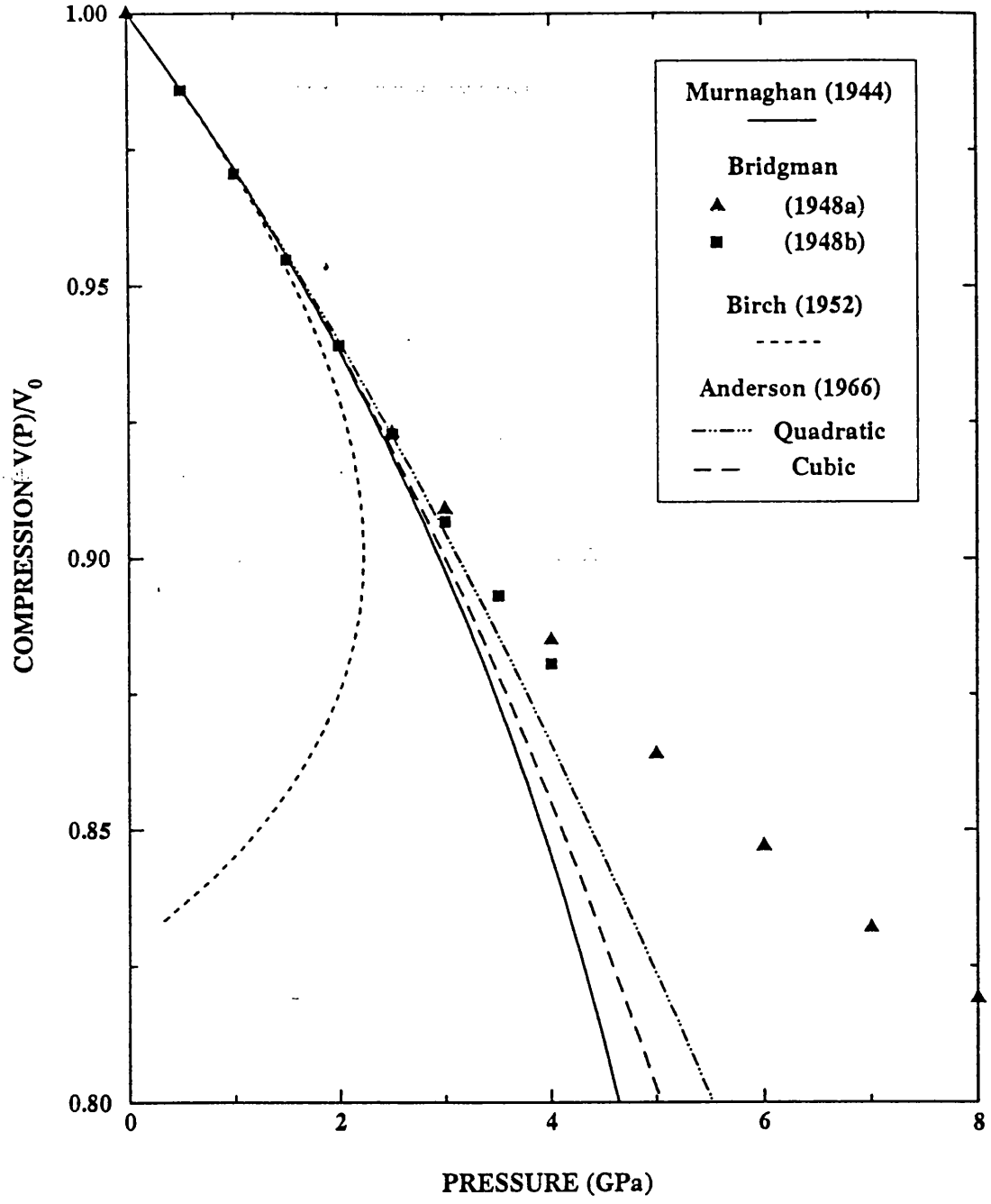

Figure 6.5. The compression $V(V)/V_0$ of vitreous SiO_2 at 293K extrapolated to high pressure by using each of the equations of state given by Murnaghan (1944), Bridgman (1948), Birch (1952) and Anderson (1966).

also exhibit a negative thermal expansion at low temperature where contributions from the long-wavelength, low frequency acoustic vibrational modes play a dominant role (Kurkjian et al. 1972). Therefore knowledge of the acoustic mode Grüneisen parameters is necessary for understanding the thermal expansion at low temperatures.

Negative hydrostatic pressure derivatives $(\partial C_{IJ}/\partial P)_{P=0}$ and positive temperature dependences of the SOEC and positive TOEC (Table 6.1) reveal anomalous effects in the vibrational anharmonicity: the frequencies of the long-wavelength acoustic modes decrease under pressure so that the mode Grüneisen parameters γ_L and γ_S are negative (Table 6.1).

Knowledge of the TOEC below room temperature helps us to clarify further the origins of the anomalous behaviour of the thermal expansion of vitreous SiO_2 because the thermal expansion and nonlinear acoustic vibrational properties both relate to the vibrational anharmonicity. The thermal Grüneisen parameter $\gamma^h = 3\alpha V/KC$ (which can be obtained from data for the linear coefficient of thermal expansion α, the volume V, the compressibility K and the specific heat C) results from the sum of excited modes (see Eqn. 3.50). The second and third order elastic stiffnesses provide a measure, which can be expressed by acoustic mode Grüneisen parameters, of the anharmonicity of the long-wavelength acoustic modes alone.

For an isotropic solid, there are two components: γ_L and γ_S, which refer to the longitudinal and shear elastic waves, respectively. These acoustic mode Grüneisen parameters for vitreous SiO_2, obtained from the experimental SOEC and TOEC data are plotted as a function of temperature in Figure 6.6. Also shown is the mean long-wavelength acoustic mode Grüneisen parameter γ^l. The results that γ_L, γ_S and γ^l are negative and become larger when the temperature is reduced, are consistent with the behaviour of the thermal expansion with temperature. The thermal expansion coefficient of vitreous SiO_2 is over an order of magnitude smaller than that of crystalline

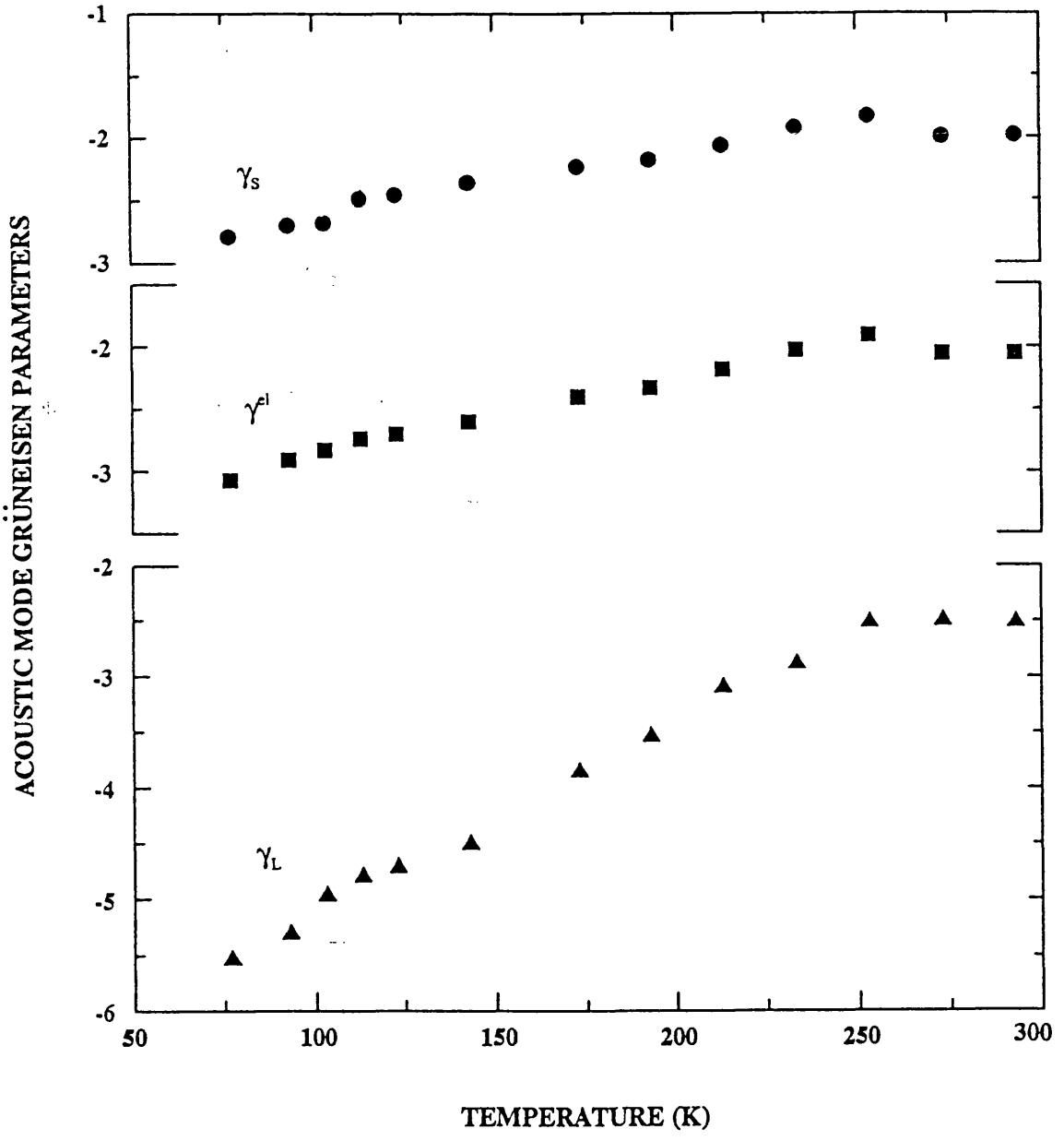

Figure 6.6. The temperature dependences of the Grüneisen parameters γ_L (triangles) and γ_S (circles) of the long-wavelength longitudinal and shear acoustic modes respectively and the mean γ^{el} (squares) for vitreous SiO_2.

quartz (which in turn is comparable to that of many other crystalline solids). The temperature dependence of the thermal expansion coefficient of vitreous SiO_2 has been investigated by Gibbons (1959), White (1964), White and Birch (1965) and White (1975). To summarise, it is small and positive ~ +5 x $10^{-7}K^{-1}$ at room temperature, decreases as the temperature is reduced and changes sign at about 180K, reaches a minimum at about 40-50K and then tends to zero as the temperature tends to 0K. The thermal expansion accrues from the summation over the excited vibrational states including the long-wavelength acoustic modes.

The infrared spectrum of vitreous SiO_2 is dominated by three peaks at about $100cm^{-1}$, $800cm^{-1}$ and $460cm^{-1}$. Each of the vibrational modes responsible for these peaks involves both stretching and bending of the silicon-oxygen bond and in general the higher the frequency the larger the contribution made by stretching (Bell et al. 1968). The mode Grüneisen gammas γ_i for these modes have been determined from the pressure dependences of the peak positions (Ferraro and Manghnani 1972, Chow et al. 1973). While the sign of the γ_i for the $800cm^{-1}$ mode is positive, those for $1100cm^{-1}$ and $470cm^{-1}$ are negative. A physical description of how these signs arise in terms of the stretching and bending of the Si-O bond has been given by Chow et al. (1973). They showed that the vibrational density-of-states calculation by Bell et al. (1968) can be used to obtain a specific heat and thermal expansion which are in reasonable agreement with experiment, indicating that the small value for the thermal expansion of vitreous SiO_2 comes about as a result of summation over the effects of modes with different Grüneisen parameter signs. As the temperature is lowered, the long-wavelength acoustic phonons with negative Grüneisen parameters can be expected to make an increasingly important contribution to the thermal expansion.

At low temperatures, when the excited phonon population includes a high proportion of long-wavelength acoustic modes, the values of the elastic γ_L' and thermal

γ_L^h Grüneisen parameters would be expected to become equal, like the elastic and thermal values of $(C/T^3)_{T->0K}$ (Flubacher et al. 1959, Anderson and Dienes 1960, Antoniou and Morrison 1965). For crystalline dielectric solids, the Debye approximation is reasonably valid at low temperatures; γ_L^h and γ_L^l do tend to become equal. In general, amorphous materials show anomalous thermal properties at low temperatures (see § 2.7-2.10 in chapter 2), thus the Debye model is not valid. The specific heat is dominated by the high density of the soft vibrational energy states (Buchenau et al. 1988) which also contributes to the thermal expansion (Phillips 1981) and to the ultrasonic wave velocities and attenuation (Piche et al. 1974).

Brugger and Fritz (1967) have noted, in the case of vitreous SiO_2, a complete lack of agreement between the estimated low temperature limits of the elastic γ_L^l and thermal γ_L^h Grüneisen parameters. The rapid increase of the negative thermal expansion at low temperatures (White 1964, 1975) demonstrates a large increase in γ^h as the temperature is lowered (Kurkjian et al. 1972, Yost et al. 1973). The magnitude of the discrepancy between γ_L^h and γ_L^l has been examined later by Phillips (1981) using White's (1975) thermal expansion data, and the specific heat measured on the same sample. At 1.5K he found that γ_L^h is -17 while γ_L^l is only -2.2. Thus in the estimation of γ_L^l, Brugger et al. (1967) and Phillips (1981) assumed that the TOEC for vitreous SiO_2 are independent of temperature. However, the present measurements of the TOEC (Figure 6.3) show that this assumption is not strictly valid. The mean long-wavelength acoustic mode Grüneisen parameter γ^l calculated from the present measurements of the TOEC decreases somewhat as the temperature is reduced. The mean acoustic mode Grüneisen parameter γ^l increases to a larger negative value than previously suspected on the basis of the assumption of temperature independent TOEC. So the discrepancy between γ_L^h and γ_L^l may not be as large as previously envisaged. The vibrational anharmonicity of

the acoustic modes plays an important part in causing the thermal expansion of vitreous SiO_2 to be negative at low temperatures.

The hydrostatic pressure derivative $(\partial C_{11}^S/\partial P)_{T,P=0}$ is much larger than $(\partial C_{44}^S/\partial P)_{T,P=0}$ over the whole temperature range: the longitudinal acoustic mode softens more with pressure than the shear mode. This is emphasised by the observation that the acoustic mode Grüneisen parameters are negative with $|\gamma_L| > |\gamma_S|$. As the temperature is reduced, the longitudinal acoustic mode Grüneisen parameter γ_L increases in magnitude considerably.

6.8 THE FOURTH ORDER ELASTIC STIFFNESSES TENSOR COMPONENTS (FOEC)

The higher order elastic stiffness tensor components provide details of the nonlinearity of the atomic forces with respect to atomic displacements. A complete set of the FOEC of an amorphous material was determined in our group for a-As_2S_3 (Brassington et al. 1981a). Using the Eqs. (3.61 - 3.64), previously derived by Brassington et al. (1981a), the FOEC of vitreous SiO_2 have been estimated using the data of the SOEC and TOEC (Table 6.1) and the main physical quantities as summarized in Table 6.3

The estimated values of the FOEC for vitreous SiO_2 at room temperature are given in Table 6.4 and compared with the published data of Shull (1969) and also with an a-As_2S_3 (Brassington et al. 1981a), which displays a normal elastic behaviour under pressure. The absolute values of the FOEC obtained are almost all positive and much larger as compared to that for a-As_2S_3. The present sets of TOEC and FOEC provide data essential to a detailed understanding of the acoustic vibrational anharmonicity and its influence on the physical properties of vitreous SiO_2.

Table 6.3. Values of the main physical quantities of vitreous SiO_2 used for calculation of the FOEC.

N (kg^{-1})	$\left(\frac{\partial^2 C_{11}}{\partial P^2}\right)$ (GPa^{-1})	$\left(\frac{\partial^2 C_{44}}{\partial P^2}\right)$ (GPa^{-1})	$\left(\frac{\partial C_{11}}{\partial T}\right)$ ($MPaK^{-1}$)	$\left(\frac{\partial C_{44}}{\partial T}\right)$ ($MPaK^{-1}$)
3.01×10^{25}	3.32	-0.18	40.9	9.77

Table 6.4. Comparison of FOEC (in units of GPa) of vitreous SiO_2 with the data of Shull (1969) and for amorphous As_2S_3 (Brassington et al. 1981a).

	SiO_2 (present)	SiO_2 Shull (1969)	As_2S_3 Brassington et al. (1981a)
C_{1111}	8909	10918	2700
C_{1112}	5894	6690	900
C_{1144}	-223	-197	-70
C_{1122}	5855	5464	100
C_{1123}	6302	5858	240
C_{1166}	502	705	310
C_{1266}	261	659	350
C_{1244}	-102	208	170
C_{1456}	181	225	90
C_{4444}	362	69	-70
C_{4455}	121	23	-24

6.9 MICROSCOPIC ORIGIN OF THE ANOMALOUS ACOUSTIC VIBRATIONAL PROPERTIES UNDER PRESSURE

Vitreous SiO_2 is built from SiO_4 tetrahedra which have a Si atom at each centre. Each tetrahedron shares the O atom at each corner with another tetrahedron. The linkage at the corner is rather weak and represents the softest spring of the system. It has been proposed that the low-frequency vibrational excitations in vitreous SiO_2 originate from the coupled rotation of these tetrahedra (Buchenau et al. 1986) as seen in the inelastic neutron scattering measurements (Buchenau et al 1988) (see § 2.7-2.10 in chapter 2). It is further assumed that in a regular array of SiO_4 tetrahedra, such rotational motion is harmonic in a first approximation and extends over the whole solid. This vibration is assumed to be spatially localised, although some neighbouring tetrahedra are involved in this motion (Buchenau et al. 1988). In addition, one can imagine that because of the irregularity of the environment of a vibrating tetrahedron, this unit can have two positions of equilibrium, leading to double-well potentials. At very low temperatures, the use of double-well potentials is appropriate since tunnelling can occur only between the lowest states. However, in our present measurements, the lowest temperature reached is 77K. At these high temperatures, tunnelling is not important and the two-level systems can be considered as classical defect states. As such, an alternative explanation on the anomalous elastic behaviour under pressure is needed.

More recently similar relaxation states have been seen to give a quasielastic contribution to Raman (Winterling 1975) and neutron scattering (Buchenau et al. 1988) experiments. The temperature dependence is similar to that seen in quasielastic scattering, indicating a common microscopic origin. Thus, the attenuation, Raman and neutron scattering can be linked and understood in a coherent way by assuming that the essential physics of relaxation is contained in a model which represents each relaxation state by an asymmetric double-well potential (Gilroy and Phillips 1981). In fitting the 50K peak, a distribution $P(V) \propto \exp(-V/V_0)$ has been used. Here, the fitting

50K peak, a distribution $P(V) \propto \exp(-V/V_0)$ has been used. Here, the fitting parameter V_0 is related to the glass transition temperature. As recently shown by Buchenau et al. (1988) and Phillips (1990), the ultrasonic, Raman and neutron data can be explained by a single set of relaxation states. In the case of vitreous SiO_2, the relaxation involves coupled rotation of a SiO_4 tetrahedron in which the oxygen atom moves through about 0.5Å. Therefore the same relaxation nature at low temperatures can be extended further to higher temperature to explain the nature of thermally activated structural relaxation of the two-level systems.

The application of pressure does not change much the shape of the SiO_4 tetrahedra because they are rather rigid units. According to NMR investigation, pressure causes a slight reduction of the average bond angle at the oxygen atom (Devine et al. 1987, Susman et al. 1991). Tielbürger et al. (1992) have argued that with decreasing bond angle, the rotational motion becomes increasingly hindered and the positions of equilibrium are more and more pronounced, resulting in an increase of the average barrier heights. Because the volume effect is more pronounced in vitreous SiO_2 under pressure, the distance between adjacent Si atoms will be reduced proportionately with pressure. The bond length of covalent bonds is practically constant; thus, the angle of rotation necessary for SiO_4 to go from one potential well to the other should increase proportionately with pressure P. Furthermore, the barrier height depends quadratically on the configurational coordinate of two-well potential. Consequently, it seem to be quite natural that the barrier height increases proportional as P^2. At the same time the SiO_4 tetrahedra, having only one well-defined site at zero pressure, are now driven into positions which exhibit more potential minima. In this way new defect states are formed which have small barriers and the distribution function $P(\Delta,\lambda)$ becomes generally wider. However, it is suggested that, even under high pressure, only a small fraction of the existing SiO_4 tetrahedra act as defect states. The model of defect state developed

by Tielbürger et al. (1992) does not account quantitatively for all observations of acoustic vibrational properties of glasses under pressure. The soft-potential model (Karpov et al. 1983) could probably give a more adequate description.

CHAPTER 7

THE VELOCITY AND ATTENUATION OF ULTRASONIC WAVES PROPAGATED IN RARE EARTH PHOSPHATE GLASSES AND THEIR TEMPERATURE DEPENDENCES

7.1 INTRODUCTION

In the work described in the previous chapter, acoustic methods were used to investigate the elastic behaviour as a function of temperature and pressure of vitreous SiO_2. The same methods (described in chapter 5), have been used to measure the ultrasonic wave velocity and attenuation propagated in rare earth phosphate glasses. To my knowledge, the first study of the elastic and anelastic behaviour of phosphate glasses was carried out by Field (1969), on glasses belonging to the V_2O_5-P_2O_5 system. He observed a relaxation maximum that was strongly dependent upon composition. The dependence of elastic stiffness on glass composition of a number of phosphate glasses was first examined using pulse echo ultrasonic methods by Farley and Saunders (1975a). They investigated the elastic properties of semiconducting phosphate glasses containing transition element metals belonging to MoO_3-P_2O_5 and V_2O_5-P_2O_5 systems. In addition, Farley and Saunders (1975a) carried out a systematic study of sound absorption in Fe_2O_3(38%)-P_2O_5(62%) glass system. They found that there was no large relaxation peak in the ultrasound attenuation over the temperature range of 100K to 380K, there being just a steady increase of absorption with increasing temperature. Ultrasonic studies were later continued on transition metal phosphate glasses containing iron (Brassington et al. 1981b), cobalt (Higazy and Bridge 1985) and molybdenum (Comins et al. 1987, Lambson 1988, Bridge and Patel 1986). Measurements of the temperature dependences of the ultrasound absorption and the velocity of sound in ternary $(Rb_2O)_{0.35}(P_2O_5)_{0.35}(Nb_2O_5)_{0.3}$ glasses were carried out by Ilisavskii et al (1988, 1989). They found that the two-well potential model gave a good explanation of the

acoustic absorption results. The observed temperature dependence of the velocity of sound in these glasses was a result of different mechanisms including the two-level systems, thermally activated relaxation and phonon anharmonicity.

There has been extensive work by Hogarth and co-workers on optical, electrical and structural properties of a number of rare earth phosphate glasses (Harani and Hogarth 1986, 1989, Ananthamohan and Hogarth 1990, Hogarth and Khan 1990). Previous ultrasonic measurements concentrated only on phosphate glasses containing samarium or lanthanum ions as network modifiers (Mierzejewski et al. 1988a,b, Sidek et al. 1988, Wang et al. 1990, Carini et al. 1990a,b). The present work has been concerned with a wider range of rare earth phosphate glasses.

To characterise the various phosphate glasses at room temperature, measurements have been made of the velocity of longitudinal and shear ultrasonic wave at 10 MHz. The data have been used to determine the adiabatic SOEC and their related physical properties such as bulk modulus and fractal dimension (Bergman and Kantor 1984). Experimental results on the measurements of velocity and attenuation of both longitudinal and shear ultrasonic waves propagated in binary rare earth phosphate glasses at temperatures ranging from 10K to 300K are also reported. One aim has been to find out whether the broad acoustic loss peak and its thermally activated relaxation could occur at an intermediate temperature and if there are observable low temperature elastic anomalies due to the presence of two-level systems in these glasses.

7.2 THE ELASTIC PROPERTIES AT ROOM TEMPERATURE

The compositions and the densities of the rare earth phosphate glasses studied are listed in Table 7.1. Each of the glasses had a composition close to that of $(R_2O_3)_{0.25}(P_2O_5)_{0.75}$, that is, in the vicinity of 25 mole.% rare earth oxide content. This composition is referred to as the metaphosphate composition $R(PO_3)_x$, where R is the rare earth modifier cation and x is its valence state. Commercial phosphate glasses are

TABLE 7.1. Comparison of the elastic properties of rare earth phosphate glasses with those of other phosphate glasses at room temperature (293K .

Glasses	molar fraction	Density (kg/m^3)	Ultrasonic wave velocity (m/s)		Elastic moduli (GPa)			Fractal dimension
	x	ρ	v_L	v_S	C_{11}	C_{44}	B	$(4C_{44}/B)$
Pure P_2O_5 [5]		2520	4055	2190	41.4	12.1	25.3	1.91
$(La_2O_3)_x$ $(P_2O_5)_{1-x}$	0.222	3346	4428	2491	65.9	20.8	38.2	2.18
	0.263	3413	4451	2599	67.6	23.1	36.9	2.50
$(CeO_2)_x$ $(P_2O_5)_{1-x}$	0.226	3060	4791	2778	70.3	23.6	38.8	2.43
	0.235	3120	4744	2725	70.2	23.2	39.3	2.36
	0.245	3124	4733	2695	70.0	22.7	39.7	2.29
	0.254	3178	4723	2640	70.9	22.1	41.4	2.14
	0.257	3234	4735	2722	72.5	24.0	40.6	2.37
$(Pr_6O_{11})_x$ $(P_2O_5)_{1-x}$	0.216	3094	4686	2605	67.9	23.4	36.7	2.55
	0.254	3315	4680	2699	72.6	24.2	40.3	2.40
	0.256	3338	4718	2699	74.3	24.3	41.9	2.32
$(Nd_2O_3)_x$ $(P_2O_5)_{1-x}$	0.157	2938	4674	2751	64.2	22.2	34.6	2.57
	0.182	3121	4707	2753	69.1	23.6	37.6	2.51
	0.196	3233	4671	2768	70.5	24.8	37.4	2.65
	0.234	3358	4636	2786	72.2	26.1	37.4	2.79
	0.254	3497	4589	2668	73.6	24.9	40.4	2.46
$(Sm_2O_3)_x$ $(P_2O_5)_{1-x}$ [1]	0.190	3217	4755	2825	72.7	25.7	38.5	2.67
	0.195	3263	4642	2739	70.3	24.5	37.7	2.60
	0.212	3326	4356	2656	63.1	23.5	31.8	2.96
	0.224	3280	4500	2684	66.4	23.6	34.9	2.71
	0.248	3514	4421	2516	68.7	22.3	39.1	2.28
$(Eu_2O_3)_x$ $(P_2O_5)_{1-x}$	0.186	3182	4728	2741	71.1	23.9	39.2	2.44
	0.200	3204	4671	2708	69.9	23.5	38.6	2.44
	0.208	3215	4639	2686	69.2	23.2	38.3	2.42
	0.218	3260	4600	2662	69.0	23.1	38.2	2.42
	0.252	3438	4525	2598	70.4	23.2	39.5	2.35
$(Gd_2O_3)_x$ $(P_2O_5)_{1-x}$	0.222	3339	4523	2636	68.4	23.2	37.5	2.48
	0.226	3362	4498	2623	68.0	23.1	37.2	2.48
	0.229	3371	4446	2611	66.6	23.0	36.0	2.56
	0.245	3415	4473	2623	68.3	23.5	37.0	2.54
	0.250	3535	4500	2660	71.6	25.0	38.2	2.62
$(Tb_2O_3)_x$ $(P_2O_5)_{1-x}$	0.226	3435	4637	2653	73.9	24.2	41.6	2.33
	0.247	3501	4622	2695	74.8	25.4	40.9	2.48
	0.263	3578	4616	2680	76.2	25.7	42.0	2.45
	0.271	3666	4621	2628	78.3	25.3	44.5	2.27
$(Dy_2O_3)_x$ $(P_2O_5)_{1-x}$	0.225	3372	4637	2714	72.5	24.8	39.4	2.52

Table 7.1 (continued)

	x	ρ	v_L	v_S	C_{11}	C_{44}	B	$(4C_{44}/B)$
$(Ho_2O_3)_x$ $(P_2O_5)_{1-x}$	0.208	3327	4688	2727	73.1	24.7	40.1	2.46
	0.220	3347	4643	2682	72.2	24.1	40.1	2.40
	0.231	3516	4652	2616	76.1	24.1	44.1	2.19
$(Er_2O_3)_x$ $(P_2O_5)_{1-x}$	0.239	3488	4599	2738	73.8	26.2	38.9	2.69
$(Fe_2O_3)_x$ $(P_2O_5)_{1-x}$ [2]	0.38	3010	5253	3043	83.0	27.9	45.9	2.44
$(CuO)_x$ $(P_2O_5)_{1-x}$ [3]	0.54	3290	4700	2740	72.7	24.7	39.7	2.49
$(V_2O_5)_x$ $(P_2O_5)_{1-x}$ [3]	0.45	2810	4900	2790	67.5	21.8	38.4	2.27
	0.60	2820	4620	2610	60.2	19.2	34.5	2.23
	0.70	2880	4430	2520	56.5	18.3	32.1	2.28
	0.80	2920	4290	2450	53.7	17.5	30.3	2.31
	0.85	2950	4130	2360	50.3	16.4	28.4	2.31
$(MoO_3)_x$ $(P_2O_5)_{1-x}$ [3,4]	0.35	2840	3950	2432	44.3	16.8	21.9	3.07
	0.38	2860	4071	2445	47.4	17.1	24.6	2.78
	0.47	2960	4106	2553	49.9	19.3	24.2	3.19
	0.50	3020	3991	2482	48.1	18.6	23.3	3.19
	0.60	3110	3880	2340	46.8	17.0	24.2	2.81
	0.66	3220	3850	2340	47.7	17.6	24.1	2.92
	0.76	3530	3920	2280	54.2	18.4	29.7	2.48
	0.85	3710	4000	2320	59.4	20.0	32.8	2.44
$(ZnO)_x$ $(P_2O_5)_{1-x}$ [6]	0.140	2715	4240	2360	48.8	15.1	28.7	2.11
	0.243	2793	4331	2459	52.4	16.9	29.9	2.26
	0.335	2834	4373	2511	54.2	17.9	30.3	2.36
	0.430	2852	4329	2503	53.4	17.9	29.5	2.43
	0.535	2915	4081	2333	48.5	15.9	27.3	2.33
	0.607	3010	4125	2340	51.2	16.5	29.2	2.26
	0.653	3052	4150	2370	52.6	17.1	29.8	2.30
	0.701	3111	4372	2418	59.5	18.2	35.2	2.07
	0.750	3199	4874	2683	67.0	23.0	45.3	2.03
Vitreous SiO_2		2203	5974	3732	78.6	30.7	37.7	3.26
$(La_2O_3)_{0.055}(Sm_2O_3)_{0.206}$ $(P_2O_5)_{0.739}$		3505	4582	2608	73.7	23.8	41.9	2.27
$(La_2O_3)_{0.166}(Sm_2O_3)_{0.086}$ $(P_2O_5)_{0.748}$		3569	4630	2631	76.5	24.7	46.6	2.12

[1] Mierzejewski et al. 1988a, [2] Brassington et al. 1981b, [3] Farley and Saunders 1975a, [4] Lambson 1988, [5] Bridge et al. 1983, [6] Higazy et al. 1989.

commonly in this composition range. The density of each glass increases with increasing R_2O_3 content, with glasses containing cerium being the less dense and terbium the most dense (Figure 7.1).

The velocities of longitudinal v_L and shear v_S ultrasonic waves, the adiabatic SOEC, $C_{11} = \rho v_L^2$ and $C_{44} = \rho v_S^2$, the bulk modulus B^S and the fractal dimension at room temperature and atmospheric pressure of the series of the various phosphate glasses studied are presented in Table 7.1. Elastic data of phosphate glasses, which contain other ions than rare earth as network modifiers, have also been compiled (Farley and Saunders 1975a, Brassington et al. 1981b, Bridge et al. 1983, Lambson 1988, Mierzejewski et al. 1988a, Higazy et al. 1989). The elastic data for a pure P_2O_5 glass are also included for comparison (Bridge et al. 1983).

There are no considerable differences in ultrasonic wave velocity from sample to sample, although slight change in the sample density and composition have been observed (Figure 7.1). Generally, the observed longitudinal and shear ultrasonic wave velocities correlate well with those of other phosphate glasses determined previously. The rare earth phosphate glasses studied have higher densities; hence the velocities are greater. This is because the ultrasonic wave velocity in a glass depends primarily on the intermolecular potential which is related to the intermolecular separation and hence to the glass density. As a consequence, the presence of rare earth ions in glass increases the ultrasonic wave velocities as compared to a pure P_2O_5 glass (Table 7.1). This observation suggests that the ultrasonic waves are in part associated with the motion of the mobile rare earth ions which are weakly connected, ionically, to the phosphate skeleton.

The fractal dimension has been calculated using an expression derived by Bergman and Kantor (1984) for an inhomogeneous random mixture of fluid and a solid backbone near the percolation limit. The fractal dimension should be close to unity for a material having a one-dimensional backbone (Bergman and Kantor 1984). Bogue and Sladek (1990) found that the values of fractal dimension ranging from about 3.32 for

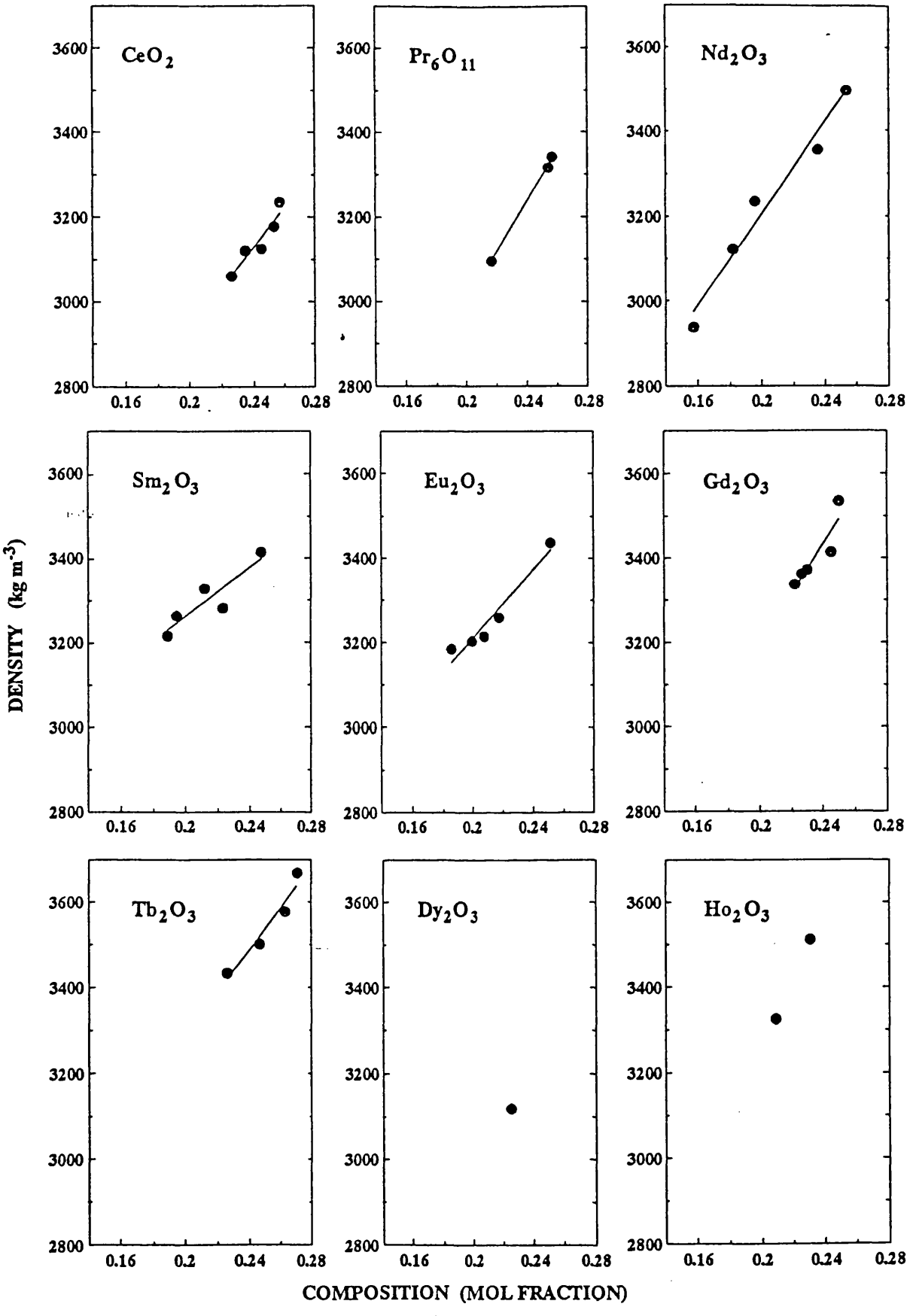

Figure 7.1. The dependence of densities of glasses with their composition.

tetrahedrally coordinated network glasses such as SiO_2 and GeO_2 and decreasing through 2 for quasi-two-dimensional glasses such as a-As (Brassington et al. 1980) and a-As_2S_3 (Brassington et al. 1981a) to about 1.08 for the pure $AgPO_3$ (Bogue and Sladek 1990) and about 0.84 for some polymer glasses (Chan et al. 1978). The closeness of the fractal dimension to one for the pure $AgPO_3$ and polymer glasses suggests weak cross-linking between phosphate chains. Carini et al. (1984) have reported that the fractal dimension is about 1.82 for the borate glasses without AgI, which do not contain long chains. This fractal dimension varies nonmonotonically with increasing AgI concentration, but remains in the range 1.78-1.93.

The fractal dimensions for the rare earth phosphate glasses determined here are in the range of about 2.14 to 2.79 (Table 7.1). This suggests a structure intermediate between a two and a three-dimensional disordered network, indicating cross-links between PO_4 chains. The shear modulus increases as fractal dimension increases, stiffening the phosphate backbone to transverse vibration. This observation is consistent with the infrared spectra of vitreous metaphosphate, which shows that the glass structure consists of a zigzag chain rather than a straight one (Hall et al. 1982, Sun and Risen 1986). A Similar variation of fractal dimension from 2.44 to about 3.19 is seen (Table 7.1) for molybdenum phosphate glasses, whose elastic data are reported by Farley and Saunders (1975a) and Lambson (1988).

In the case of GeO_2 glass, using the data of Soga (1969), the calculated fractal dimension is about 3.03; vitreous SiO_2 has a fractal dimension of about 3.26 (Table 7.1). These fractal dimensionalities indicate that those tetrahedrally coordinated network glasses consist of a three-dimensional network. This is consistent with the glass structure suggested by Bridge et al. (1983): the structures of vitreous SiO_2 and GeO_2 are built up of a three-dimensional network, consisting of Si_6O_6 or Ge_6O_6 rings, respectively.

In the case of pure P_2O_5 glass, using the data of Bridge et al. (1983), the calculated

fractal dimension is about 1.91 (Table 7.1), suggesting that the structure of pure P_2O_5 glass consists of a two-dimensional network. This expectation is consistent with the two-dimensional network structure of molten P_2O_5 proposed by Corima et al. (1963). However, this finding is not convincing. Bridge et al. (1983) argued that pure P_2O_5 glass should consist of P_6O_6 rings; then it should have a three-dimensional network structure; this is consistent with the structure of the pure P_2O_5 glass proposed on the basis of the continuous random network structure of Zachariasen (1932). However, it is possible that, the lower values of the shear wave velocity for pure P_2O_5 glass are a consequence of its hygroscopic nature. The measured value of the shear wave velocity propagated in the pure P_2O_5 glass may be reduced by the motion of the mobile H_2O molecules present in this glass. This situation was highlighted by Bridge et al (1983) when calculating the Young's modulus of pure P_2O_5 glass. The Young's modulus obtained by Bridge et al. (1983) is only 31.3GPa (with H_2O content <0.7 mol.%) as compared with that of 50.1GPa for a glass free from H_2O molecules (Tarasov 1963).

The Debye temperature is relevant to the understanding of the lattice vibrational properties of glasses when describing the specific heat. The Debye temperature has been calculated from room temperature ultrasound velocities and densities. The Debye mean sound velocity $\bar{v}_D$ has been calculated using the expression

$$\bar{v}_D = \left[\frac{1/v_L^3 + 2/v_S^3}{3} \right]^{-\frac{1}{3}} \tag{7.1}$$

and the Debye temperature Θ_D obtained from

$$\Theta_D = \frac{h}{k} \left(\frac{3\rho A n}{4\pi M} \right)^{\frac{1}{3}} \bar{v}_D \tag{7.2}$$

where A is the Avogadro's number, n is the number of atoms in unit formula and M is the molecular weight.

In Table 7.2 are given Debye temperatures calculated using Eq. 7.2 from the room

TABLE 7.2. The main physical quantities of phosphate glasses. Here x is the mole fraction, M the molecular weight in units of g/mole, n the number of atoms per molecular formula, V the molar volume in units of cm^3/mole, N/V the number of atoms per unit volume in units of 10^{28} atoms/m^3, $\bar{v}_D$ the mean Debye sound velocity in unit of ms^{-1} and Θ_D the Debye temperature in K.

	x	n	M	V	N/V	$\bar{v}_D$	Θ_D
Pure P_2O_5 [5]		7	141.94	56.3	7.48	2444	307
$(La_2O_3)_x$ $(P_2O_5)_{1-x}$	0.222	6.61	182.8	54.6	7.23	2771	344
	0.263	6.47	190.3	55.8	6.99	2882	354
$(CeO_2)_x$ $(P_2O_5)_{1-x}$	0.226	6.10	148.8	48.6	7.55	3083	388
	0.235	6.06	149.0	47.8	7.04	3026	383
	0.245	6.02	149.3	47.8	7.58	2995	378
	0.254	5.98	149.6	47.1	7.66	2939	372
	0.257	5.97	149.7	46.3	7.77	3023	384
$(Pr_6O_{11})_x$ $(P_2O_5)_{1-x}$	0.216	9.16	331.9	107	5.14	2901	322
	0.254	9.54	365.3	110	5.21	2996	334
	0.256	9.56	367.1	110	5.23	2999	334
$(Nd_2O_3)_x$ $(P_2O_5)_{1-x}$	0.157	6.69	172.5	58.7	6.81	3049	372
	0.182	6.63	177.4	56.8	7.03	3053	376
	0.196	6.60	180.1	55.7	7.15	3065	379
	0.234	6.53	187.5	55.8	7.05	3081	379
	0.254	6.49	191.4	54.7	7.15	2960	366
$(Sm_2O_3)_x$ $(P_2O_5)_{1-x}$ [1]	0.190	6.62	181.2	56.3	7.08	3128	386
	0.195	6.61	182.3	55.9	7.13	3035	375
	0.212	6.58	185.8	55.9	7.09	2933	362
	0.224	6.55	188.3	57.4	6.88	2971	363
	0.248	6.50	193.2	55.0	7.12	2796	345
$(Eu_2O_3)_x$ $(P_2O_5)_{1-x}$	0.186	6.63	181.0	56.9	7.02	3042	374
	0.200	6.60	183.9	57.4	6.92	3005	368
	0.208	6.58	185.6	57.7	6.87	2981	364
	0.218	6.56	187.7	57.6	6.87	2954	361
	0.252	6.49	194.9	56.7	6.90	2885	353
$(Gd_2O_3)_x$ $(P_2O_5)_{1-x}$	0.222	6.56	190.9	57.2	6.91	2924	358
	0.226	6.55	191.8	57.0	6.91	2909	356
	0.229	6.54	192.5	57.1	6.90	2894	354
	0.245	6.51	196.0	57.4	6.83	2908	354
	0.250	6.50	197.1	55.8	7.02	2947	362
$(Tb_2O_3)_x$ $(P_2O_5)_{1-x}$	0.226	6.55	192.6	56.1	7.04	2947	363
	0.247	6.51	197.3	56.3	6.95	2989	366
	0.263	6.47	200.8	56.1	6.95	2974	364
	0.271	6.45	202.6	55.3	7.04	2921	359
$(Dy_2O_3)_x$ $(P_2O_5)_{1-x}$	0.225	6.55	193.9	57.5	6.86	3009	367

Table 7.2 (continued)

	x	n	M	V	N/V	$\bar{v}_D$	Θ_D
$(Ho_2O_3)_x$ $(P_2O_5)_{1-x}$	0.208 0.220 0.231	6.58 6.85 6.54	191.0 159.6 194.4	57.4 47.7 55.9	6.94 8.65 7.05	3025 2977 2911	370 392 358
$(Er_2O_3)_x$ $(P_2O_5)_{1-x}$	0.239	6.80	166.0	47.6	8.60	3031	399
$(Fe_2O_3)_x$ $(P_2O_5)_{1-x}$ [2]	0.38	6.24	148.7	49.4	7.61	3377	426
$(CuO)_x$ $(P_2O_5)_{1-x}$ [3]	0.54	4.30	108.3	32.9	7.87	3039	388
$(V_2O_5)_x$ $(P_2O_5)_{1-x}$ [3]	0.45 0.60 0.70 0.80 0.85	7 7 7 7 7	159.9 165.9 169.9 173.9 175.9	56.9 58.8 59.0 59.6 59.6	7.41 7.17 7.15 7.08 7.07	3101 2903 2801 2722 2622	381 359 346 336 323
$(MoO_3)_x$ $(P_2O_5)_{1-x}$ [3,4]	0.35 0.38 0.47 0.50 0.60 0.66 0.76 0.85	5.95 5.86 5.59 5.50 5.20 5.02 4.72 4.45	142.6 142.7 142.9 142.9 143.1 143.3 143.5 143.6	50.2 49.9 48.3 47.3 46.0 44.5 40.6 38.7	7.13 7.07 6.97 7.00 6.80 6.79 6.99 6.92	2683 2704 2814 2735 2587 2585 2529 2574	332 333 345 336 315 314 311 315
$(ZnO)_x$ $(P_2O_5)_{1-x}$ [6]	0.140 0.243 0.335 0.430 0.535 0.607 0.653 0.701 0.750	6.30 5.79 5.33 4.85 4.33 3.96 3.74 3.49 3.25	133.5 127.2 121.7 115.9 109.5 105.2 102.4 99.5 96.5	49.2 45.6 42.9 40.6 37.6 34.9 33.6 32.0 30.2	7.72 7.65 7.47 7.19 6.93 6.83 6.70 6.58 6.49	2628 2734 2789 2778 2592 2602 2633 2694 2990	333 346 350 344 317 317 319 324 358
Vitreous SiO_2		3	60.0	27.3	6.62	4111	496
$(La_2O_3)_{0.055}(Sm_2O_3)_{0.206}$ $(P_2O_5)_{0.739}$		6.48	194.7	55.5	7.02	2899	356
$(La_2O_3)_{0.166}(Sm_2O_3)_{0.086}$ $(P_2O_5)_{0.748}$		6.50	190.3	53.3	7.34	2925	365

[1] Mierzejewski et al. 1988a, [2] Brassington et al. 1981b, [3] Farley and Saunders 1975a, [4] Lambson 1988, [5] Bridge et al. 1983, [6] Higazy et al. 1989.

temperature densities and ultrasonic wave velocities. The calculated values between about 300K and 500K are similar to those found for other glasses. The values obtained are considerably larger than those for the weakly bound chalcogenide glasses (≈140K) (Farley and Saunders 1975b) or amorphous chalcogenide alloys (≈102K) (Avogadro et al. 1987). However, the Debye temperatures of phosphate glasses are quite close to that of $Ag_2O.2B_2O_3$ (Θ_D= 334K) and larger than those for superionic glasses (Avogadro et al. 1986, Carini et al. 1994b).

7.3 ULTRASONIC WAVE VELOCITIES AND THEIR TEMPERATURE DEPENDENCES.

An important part of the work is to measure the temperature dependences of the ultrasonic wave velocities propagated in rare earth phosphate glasses. The measurements of the longitudinal v_L and shear v_S mode 10 MHz ultrasonic wave velocities have mostly been carried out from 10K-300K, but for europium and terbium phosphate glasses between 10K and 400K. In some samples of rare earth phosphate glasses, the measurements of the ultrasonic wave velocities have been made at 50 and 60 MHz.

The temperature dependences of the velocities of longitudinal and shear ultrasonic waves propagated in phosphate glasses, which contain different rare earth ions as network modifiers, are shown in Figures 7.2-7.10. Measurements of ultrasonic wave velocity in phosphate glasses within this wide temperature range clearly show an anomalous temperature dependence: the temperature dependences of the ultrasonic wave velocities of these glasses do not follow the behaviour expected from vibrational anharmonicity, namely a linear increase with decreasing temperature and a zero slope at 0K.

In the case of vitreous SiO_2, the ultrasonic wave velocities decrease with decreasing temperature, pass through a minimum in the low temperature region (T_{min}~60K) and then increase drastically with decreasing temperature (see Figure 6.1

in Chapter 6). Even though phosphate glasses are built up from a high percentage of tetrahedrally coordinate structure, similar to that of vitreous SiO_2, such a minimum barely occurs. Indeed, in some of the phosphate glasses, there is no minimum in the variation of ultrasonic wave velocities with temperature; the velocities steadily decrease with increasing temperature. Thus in the temperature range under investigation, two somewhat different types of temperature dependences of ultrasonic wave velocities are founds:

1. For the case of cerium (Figure 7.2), praseodymium (Figure 7.3), neodymium (Figure 7.4) and gadolinium (Figure 7.7) glasses, both longitudinal v_L and shear v_S ultrasonic wave velocities increase approximately linearly with decreasing temperature down to about 100K, the usual behaviour associated with phonon vibrational anharmonicity.

2. Phosphate glasses containing europium (Figure 7.5), samarium (Figure 7.6), terbium (Figure 7.8), holmium (Figure 7.9) and erbium (Figure 7.10) display slightly different temperature dependences in their longitudinal ultrasonic wave velocity. The shear wave velocity increases approximately linearly with decreasing temperature down to about 100K. However, the longitudinal wave velocity has an anomalous temperature dependence; for the $(Eu_2O_3)_{0.186}(P_2O_5)_{0.814}$ (Figure 7.5) and $(Ho_2O_3)_{0.220}(P_2O_5)_{0.780}$ (Figure 7.9), v_L actually decreases with temperature to reach a minimum value at about 180K and 60K, respectively. The $(Ho_2O_3)_{0.231}(P_2O_5)_{0.769}$ glass (Figure 7.9) displays a clear phonon mode softening in the temperature region of about 110K to 150K. For other phosphate glasses studied, such as $(Eu_2O_3)_{0.20}(P_2O_5)_{0.80}$ (Figure 7.5) and $(Tb_2O_3)_{0.247}(P_2O_5)_{0.753}$ (Figure 7.8) glasses, v_L remains almost independent of temperature from 400K down to about 160K. For $(Er_2O_3)_{0.239}(P_2O_5)_{0.761}$ glass (Figure 7.10), v_L remains almost independent of temperature from 300K down to even lower temperature, that is, at about 100K. Similar but more pronounced longitudinal and shear phonon softening effects have been observed in vitreous SiO_2 (Figure 6.1).

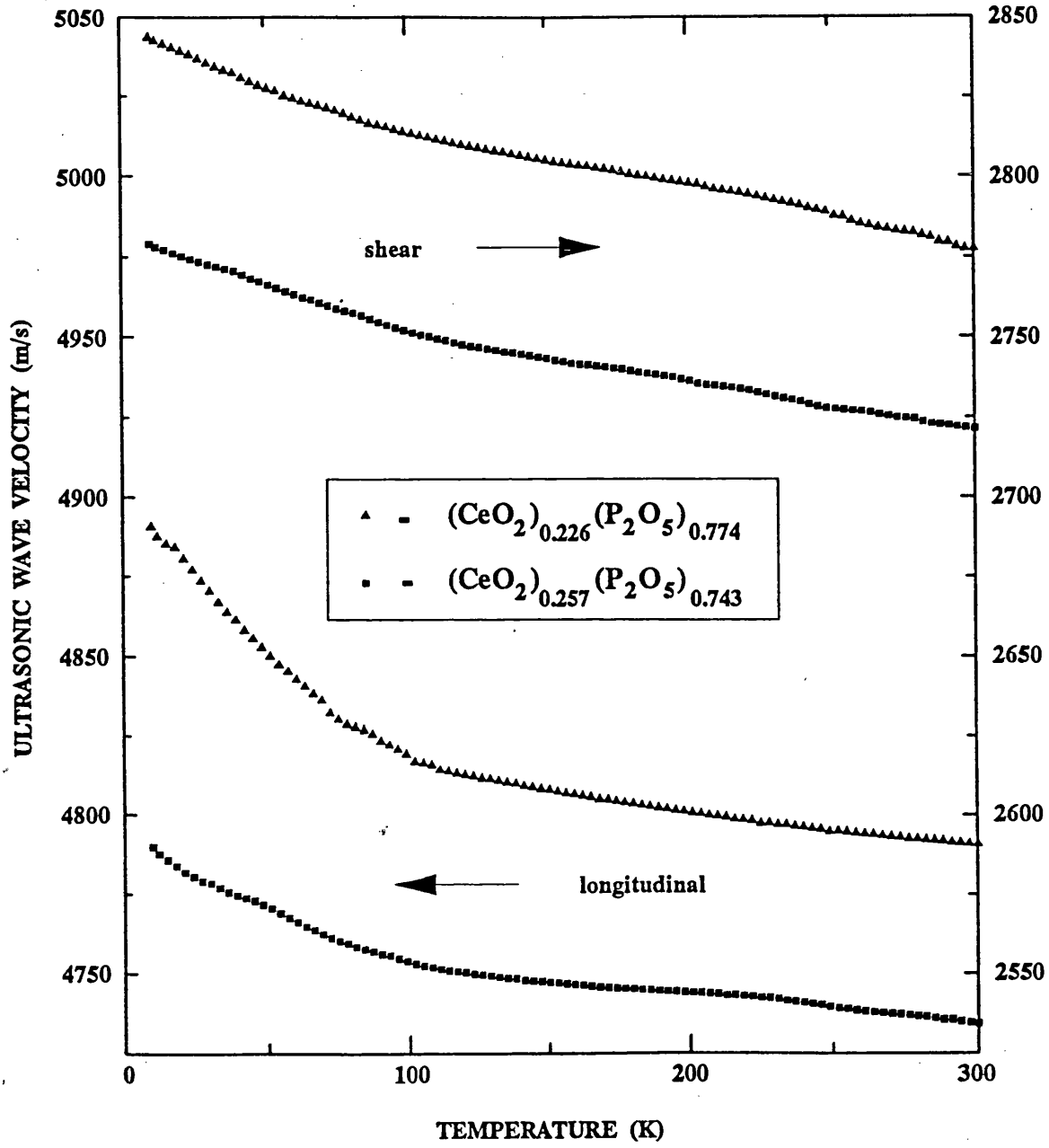

Figure 7.2. The temperature dependences of the velocities of 10MHz longitudinal and shear ultrasonic waves propagated in cerium phosphate glasses.

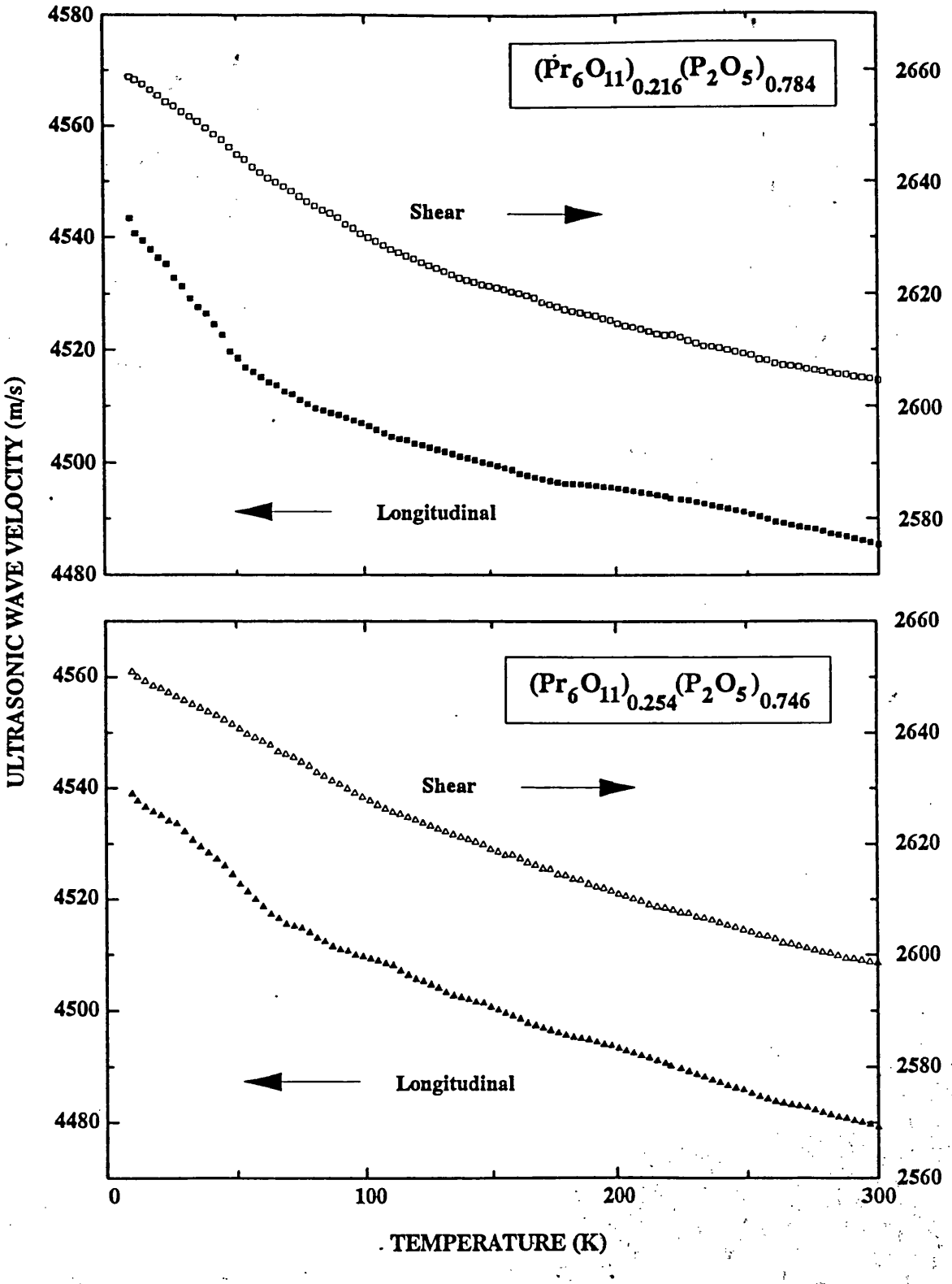

Figure 7.3. The temperature dependences of the velocities of 10MHz longitudinal and shear ultrasonic waves propagated in praseodymium phosphate glasses.

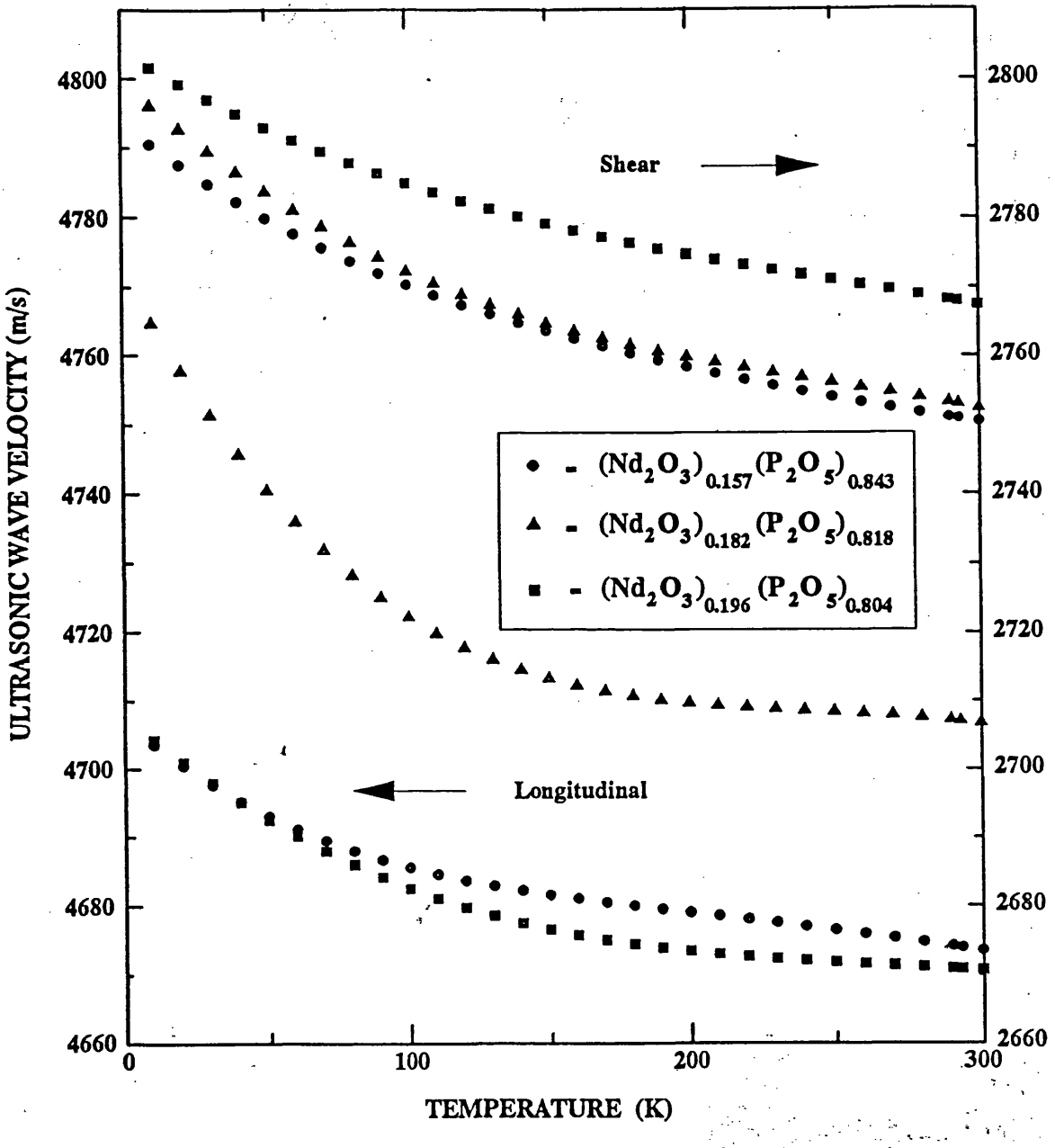

Figure 7.4. The temperature dependences of the velocities of 10MHz longitudinal and shear ultrasonic waves propagated in neodymium phosphate glasses.

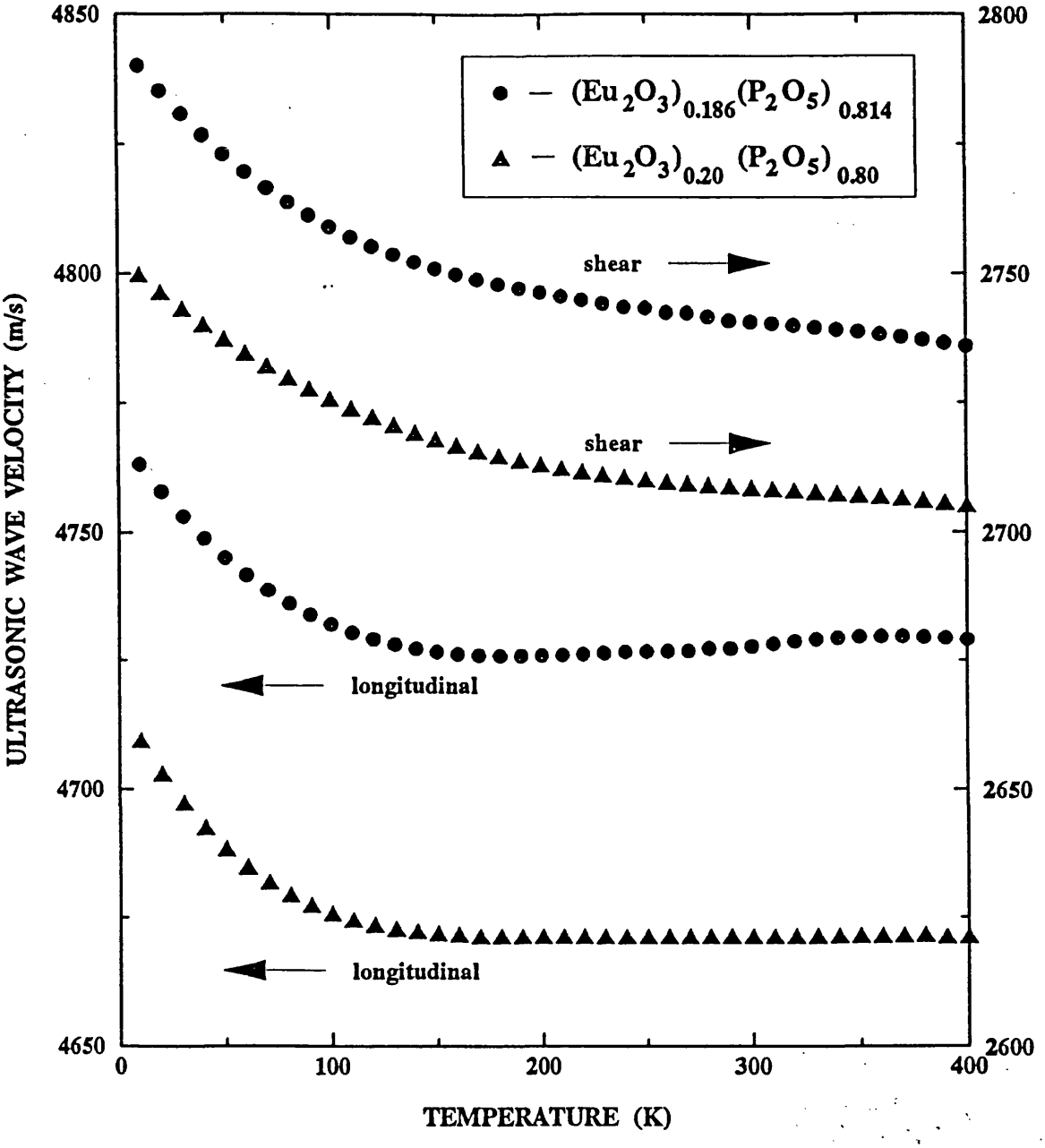

Figure 7.5. The temperature dependences of the velocities of 10MHz longitudinal and shear ultrasonic waves propagated in europium phosphate glasses.

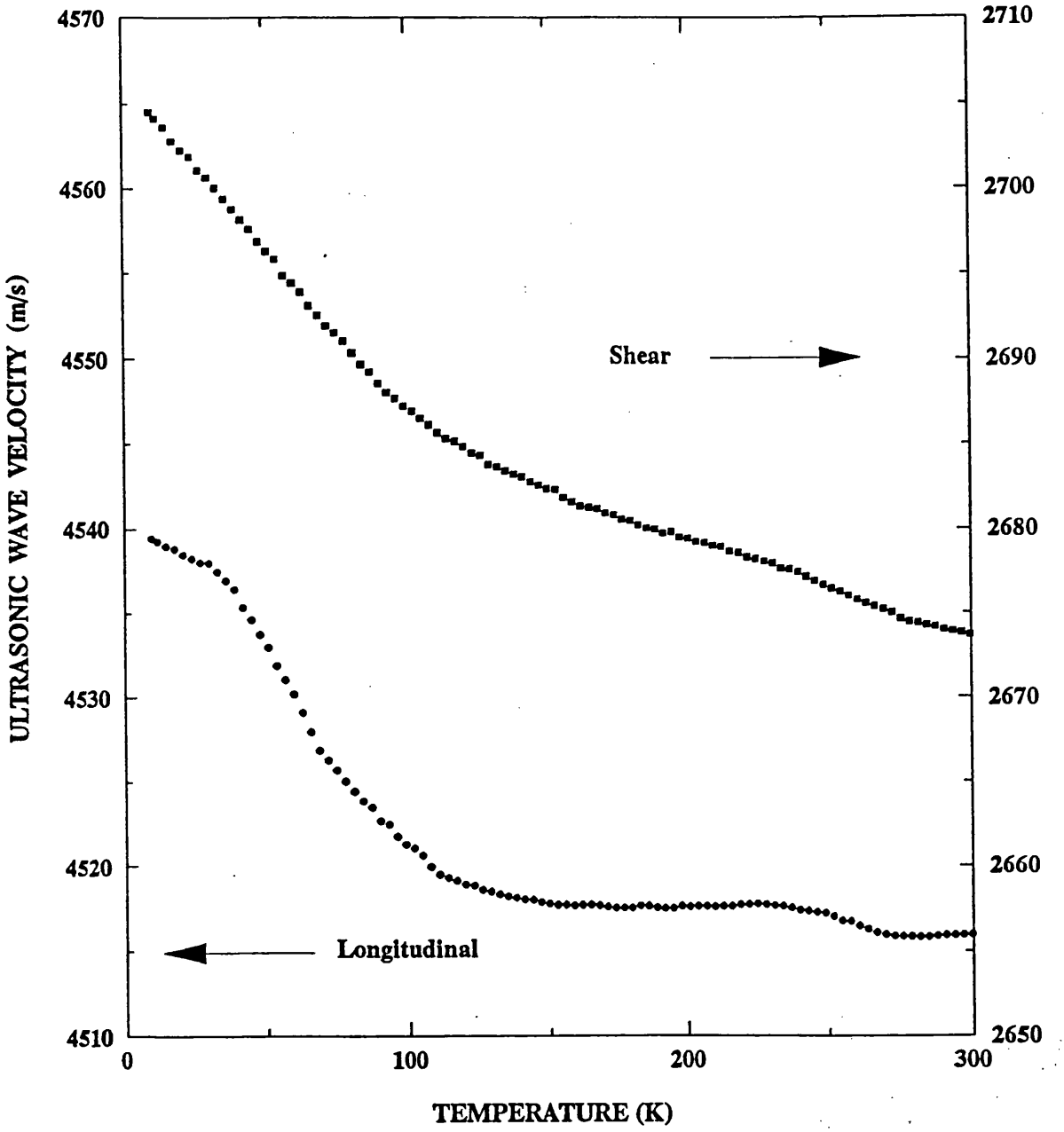

Figure 7.6. The temperature dependences of the velocities of 10MHz longitudinal and shear ultrasonic waves propagated in $(Sm_2O_3)_{0.212}(P_2O_5)_{0.788}$ glass.

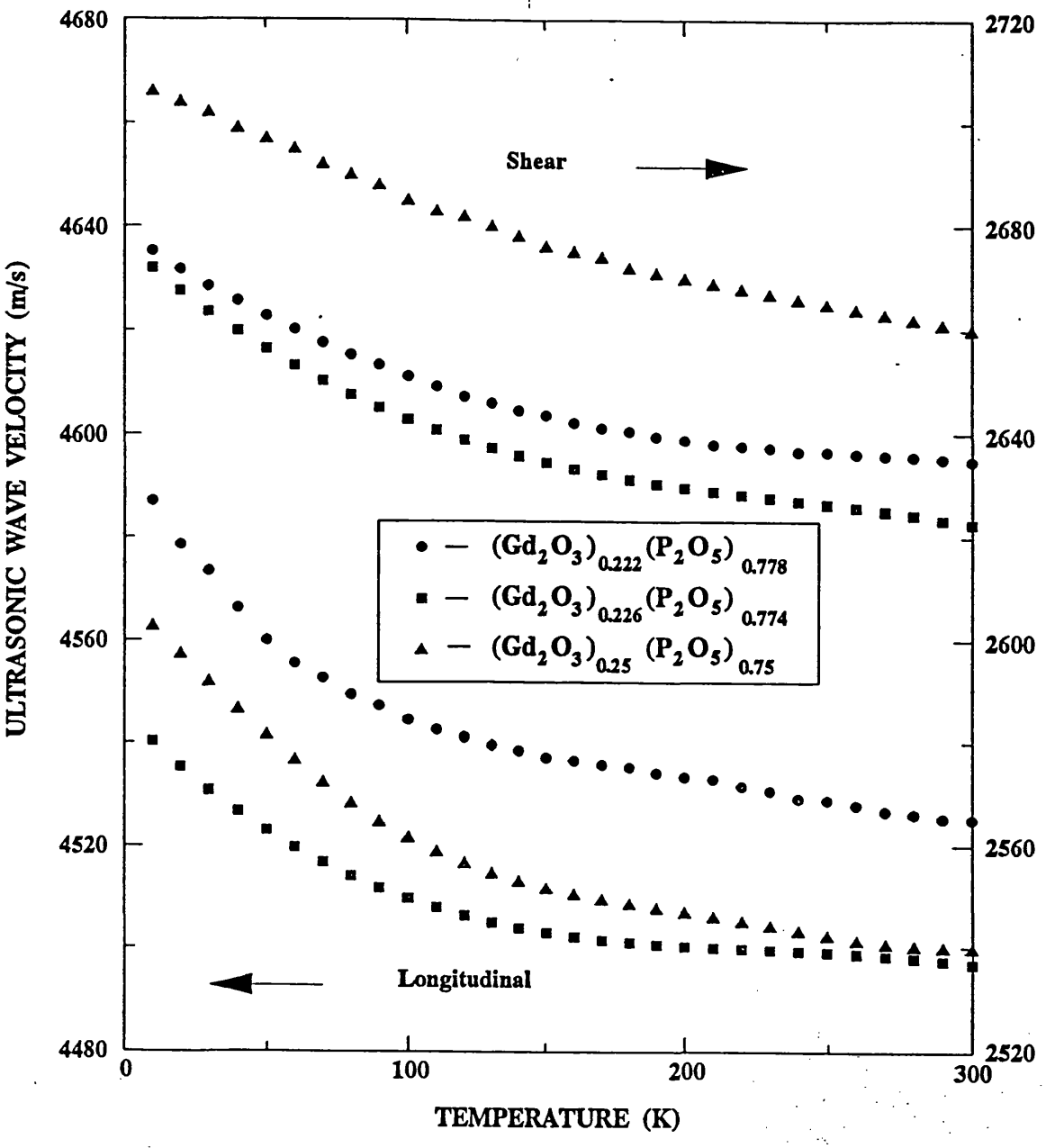

Figure 7.7. The temperature dependences of the velocities of 10MHz longitudinal and shear ultrasonic waves propagated in gadolinium phosphate glasses.

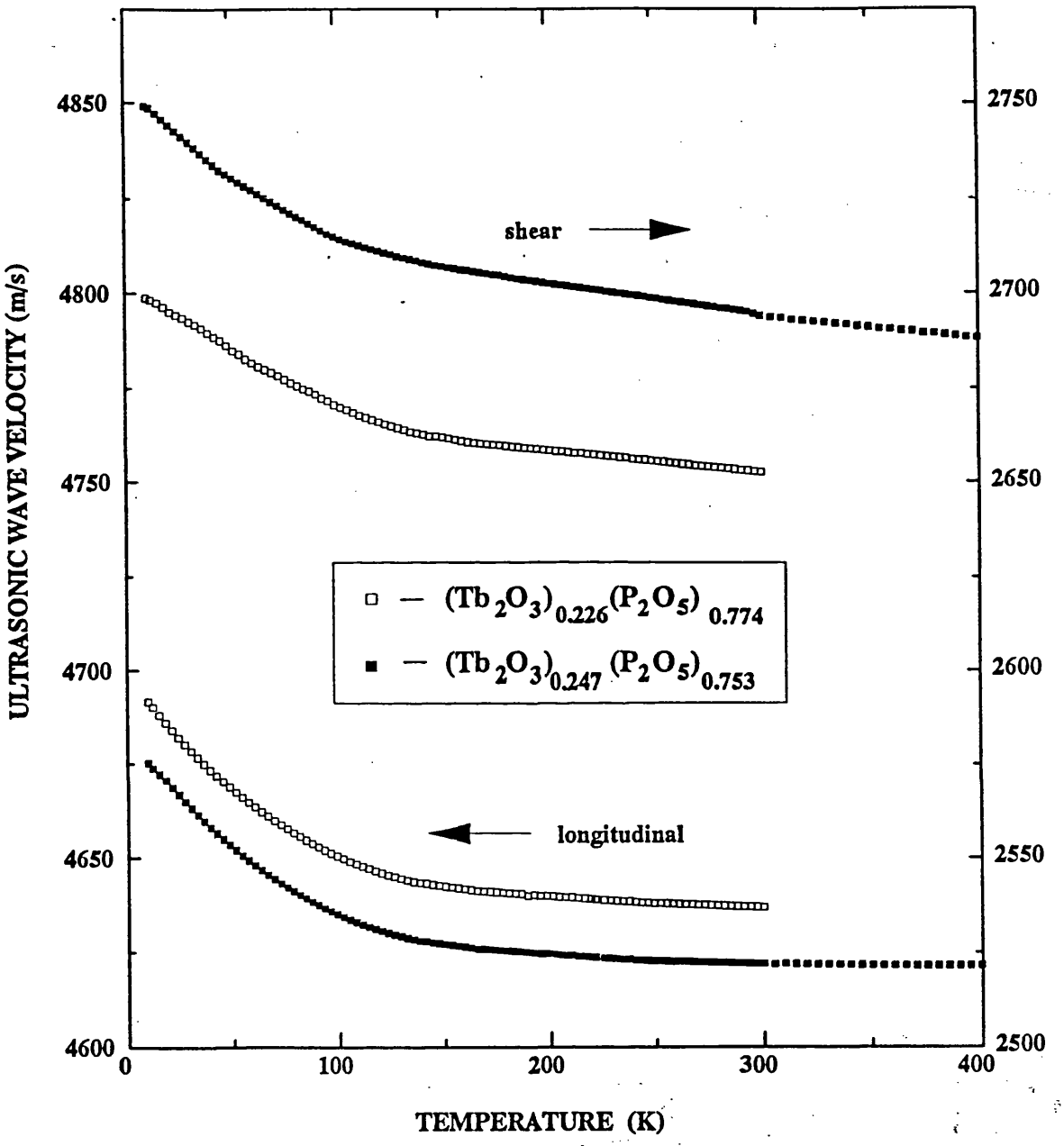

Figure 7.8. The temperature dependences of the velocities of 10MHz longitudinal and shear ultrasonic waves propagated in terbium phosphate glasses.

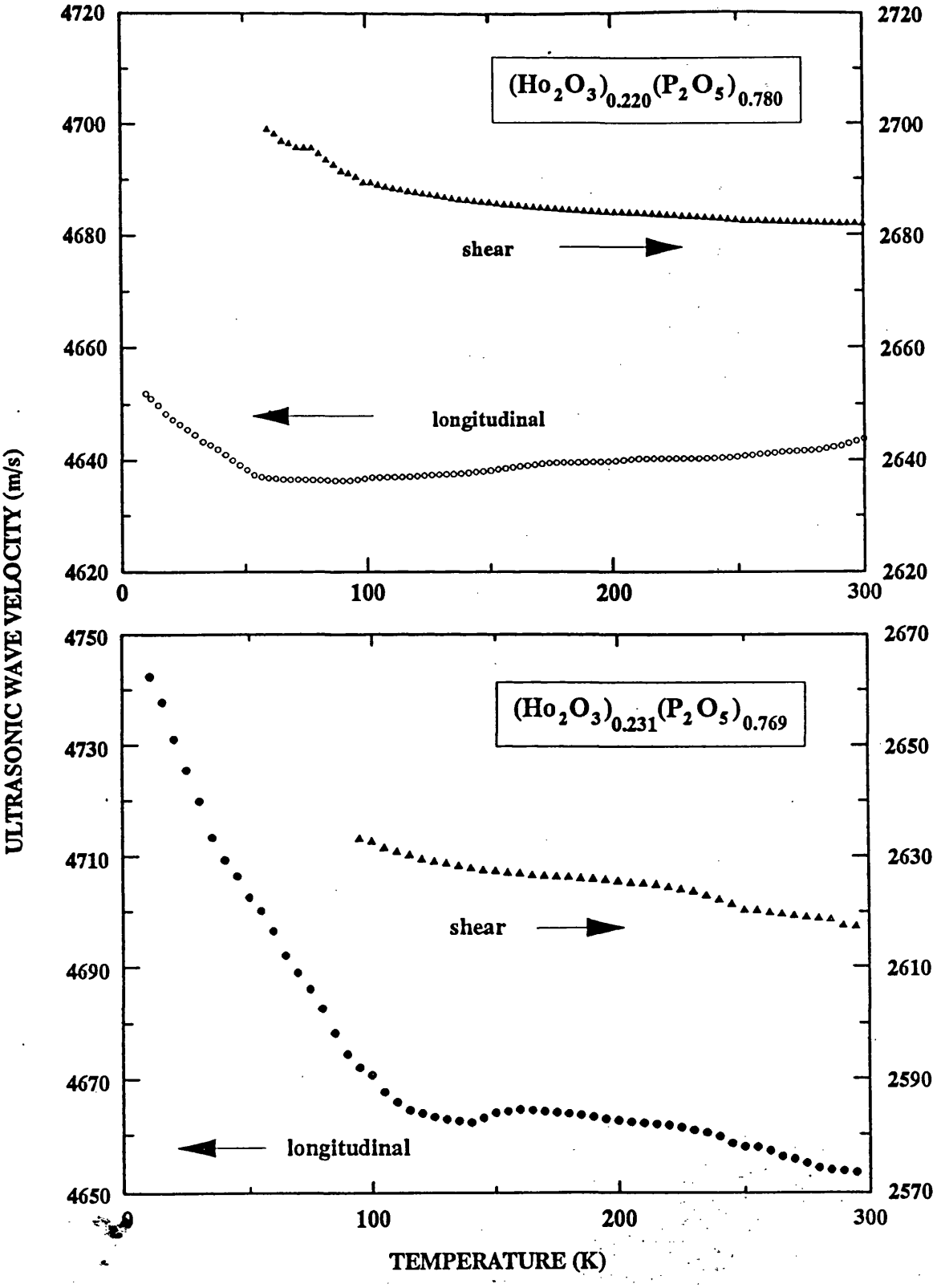

Figure 7.9. The temperature dependences of the velocities of 10MHz longitudinal and shear ultrasonic waves propagated in holmium phosphate glasses.

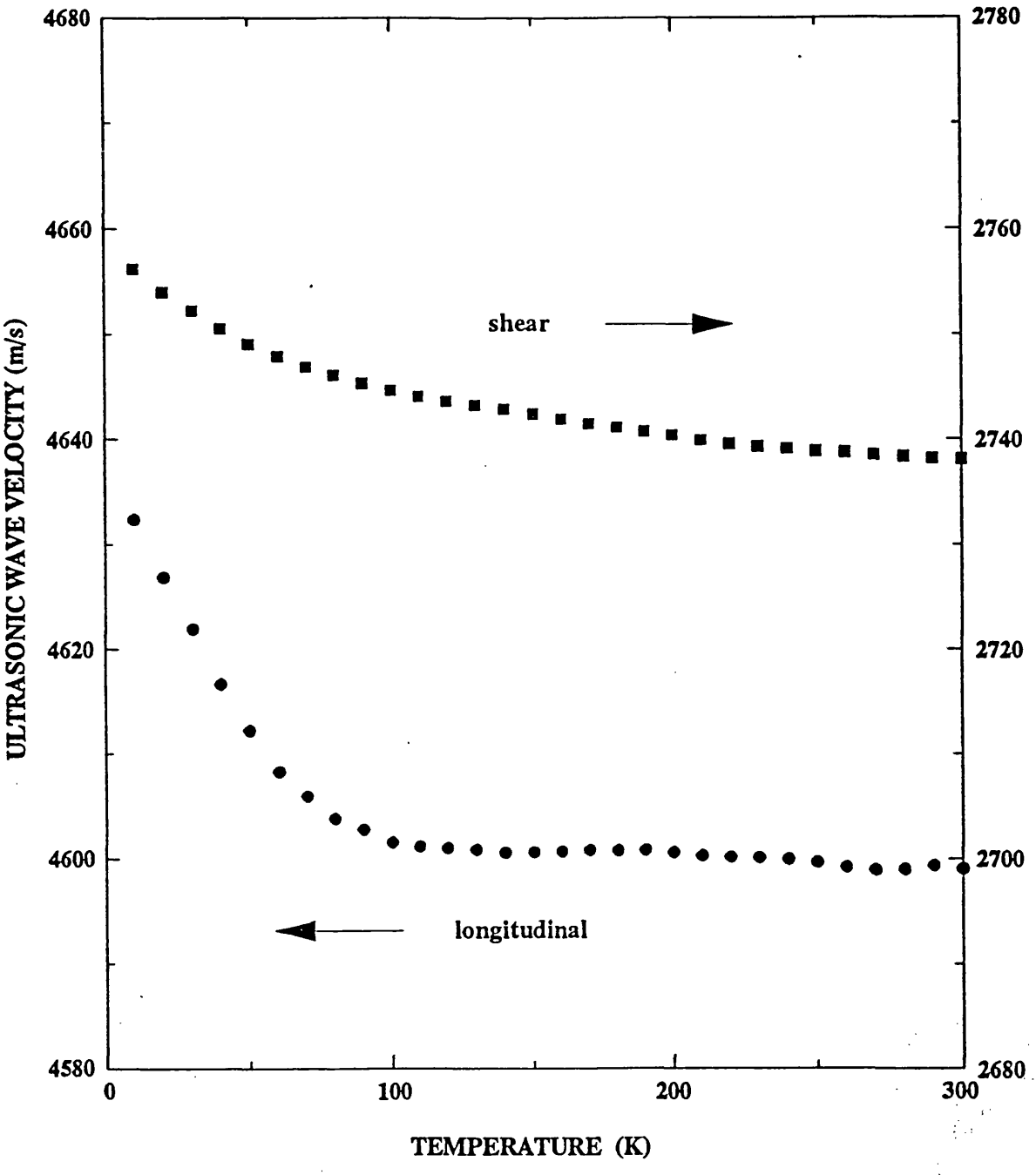

Figure 7.10. The temperature dependences of the velocities of 10MHz longitudinal and shear ultrasonic waves propagated in erbium $(Er_2O_3)_{0.239}(P_2O_5)_{0.761}$ glass.

Below the temperature of about 120K, the ultrasonic wave velocities propagated in rare earth phosphate glasses increase more rapidly and this continues until the lowest temperatures are reached. However, in the case of $(Ho_2O_3)_{0.220}(P_2O_5)_{0.780}$ the increase begins at about 60K (a temperature that is rather similar to that found for vitreous SiO_2). The steepening rise of the ultrasonic wave velocities as temperature is lowered below 120K bears some resemblance to the behaviour observed in the temperature dependence of the velocities of ultrasonic waves propagated in vitreous SiO_2, GeO_2 (Piché et al. 1974, Hunklinger 1982, Raychaudhuri and Hunklinger 1984) and TeO_2 (Benbattouche et al. 1989), although it commences at a rather higher temperature in these rare earth phosphate glasses.

It is suggested that, at temperature below 120K, the anomalous temperature dependences of the ultrasonic wave velocities in the rare earth phosphate glasses are consistent with there being a substantial contribution from relaxation interactions with two-level systems (Anderson et al. 1972, Phillips 1972). Such behaviour is due to the interaction of the ultrasonic waves with two-level systems (Jäckle 1972) through a thermally activated, structural relaxation process first proposed by Anderson and Bömmel (1955). This process is visualised as a particle moving in a double well potential corresponding to two equilibrium configurations which arises out of the defect structure in the amorphous network (see section §2.7).

To assess the magnitude of the excess contribution to the ultrasonic wave velocities, the more usual anharmonic effects have first been extracted on the basis of the Debye model coupled with an anharmonic oscillator. The temperature dependence of each elastic stiffness has been approximated by the conventional model for vibrational anharmonicity, Eq. (3-21) in chapter 3. In the case of $(Sm_2O_3)_{0.212}(P_2O_5)_{0.788}$ glass, the relative difference in velocity $\Delta v/v$ between the measured values (Figure 7.6) and that after the anharmonic contribution has been extracted is shown in Figure 7.11. This additional contribution to each mode velocity is of similar magnitude to that found

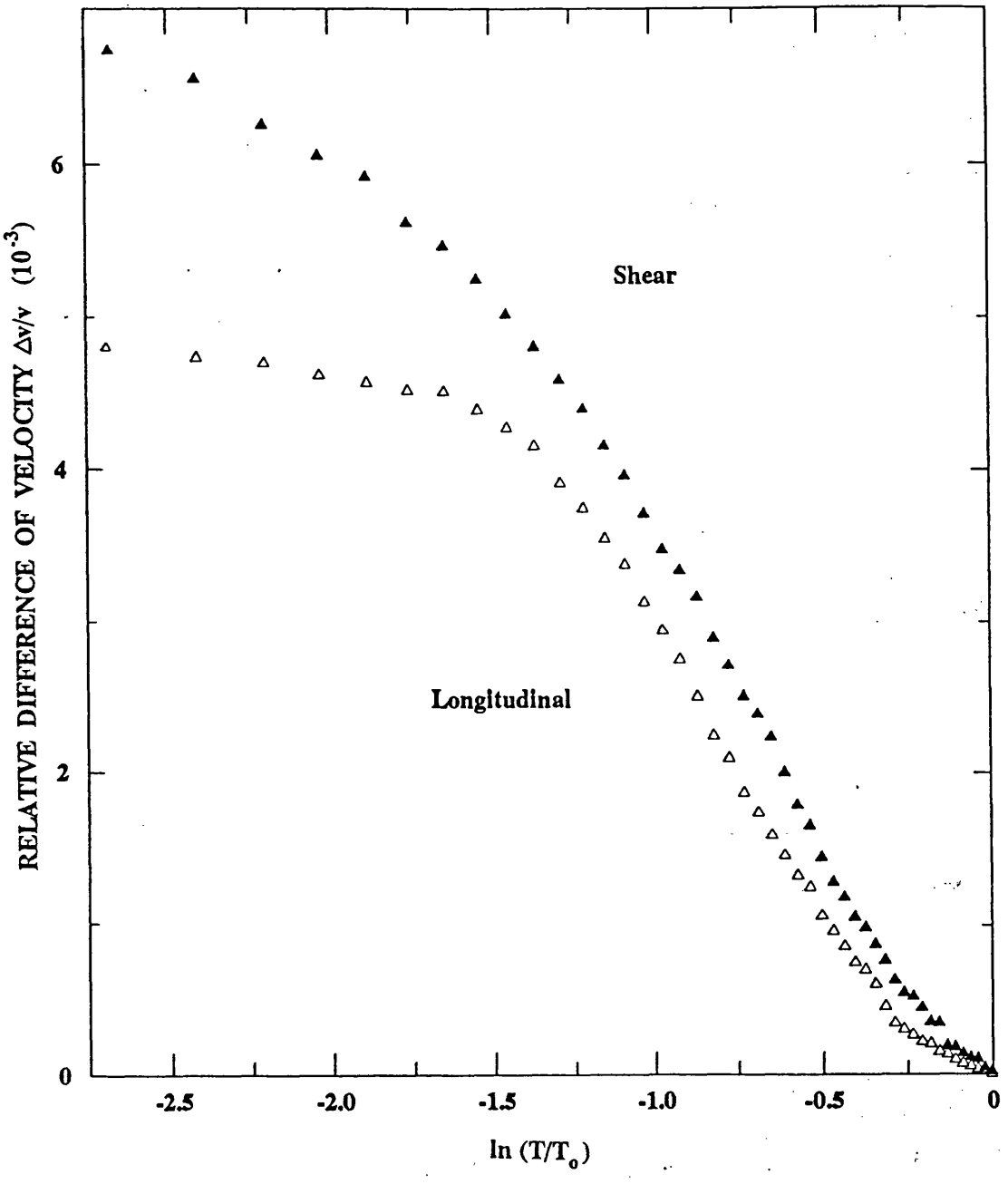

Figure 7.11. The relative difference in velocity $\Delta v/v$ (between the measured values (Figure 7.6) and that after the anharmonic contribution has been removed) for $(Sm_2O_3)_{0.212}(P_2O_5)_{0.788}$ glass.

for vitreous TeO_2 (Benbattouche et al. 1989). However, this excess contribution does not in itself provide a quantitative description of the phonons interaction with the two-level systems; a more satisfactory treatment has been given recently on samarium and lanthanum phosphate glasses (Carini et al. 1994a) using a soft-potential model (Parshin 1993); this will be presented in Chapter 9.

7.4 THE TEMPERATURE DEPENDENCES OF THE ULTRASONIC WAVE ATTENUATION

The ultrasonic wave attenuation of rare earth phosphate glasses is characterized by large and broad attenuation peaks with the loss for shear wave being greater than that of the longitudinal wave (Figures 7.12-7.15). The heights and positions of these peaks are frequency dependent. For vitreous SiO_2 the ultrasonic velocity reaches a maximum at a temperature T_m below which it decreases as a result of a resonant interaction (see inset in Figure 6.1). Above T_m there is a relaxation effect arising from the energy splitting of the two-level systems in the ultrasonic strain field. At the temperatures at which measurements have been made, the phosphate glasses should be well above T_m and correspond to the relaxation interaction regime. Thus, these characteristics can be associated with thermally activated relaxations of the two-level systems. Similar evidence for this is provided by the ultrasonic attenuation of samarium phosphate glasses between 10K and about 250K, which is characterised by a broad peak typical of a spectrum of thermally activated relaxations (Carini et al. 1990b). This feature is common to many glasses, including vitreous SiO_2 (Hunklinger 1982, Raychaudhuri and Hunklinger 1984) and TeO_2 (Benbattouche et al. 1989). The ultrasonic wave disturbs the equilibrium and produces a relative energy shift between the minimum of the two wells by an amount $\Delta E = De$ in a strain field of magnitude e, where D is the deformation potential expressing the energy shift of the relaxing states in a strain field of unit strength. Thus, the ultrasonic waves generate thermal

inequilibrium and a relaxation process occurs to restore the equilibrium. Excitations arising from thermally activated motion of relaxing "particles" over potential barriers are believed to be the cause of this broad acoustic attenuation peak.

In the case of vitreous SiO_2, the ultrasonic velocity and attenuation data can be explained by a single set of relaxation states (Buchenau et al. 1988, Phillips 1990); they have a common microscopic origin. The same relaxation state at low temperatures can be extended further to higher temperature to explain the nature of thermally activated structural relaxation of the two-level systems. The relaxation comprises of the rotation of coupled SiO_4 tetrahedra involved in low-frequency harmonic vibrations (Buchenau et al. 1986, 1988). Thus, it is plausible that the same relaxation nature could be applied to vitreous rare earth phosphates. The similar nature of coupled rotations of PO_4 tetrahedra could be used to explain the nature of thermally activated local motions of the two-level systems in phosphate glasses.

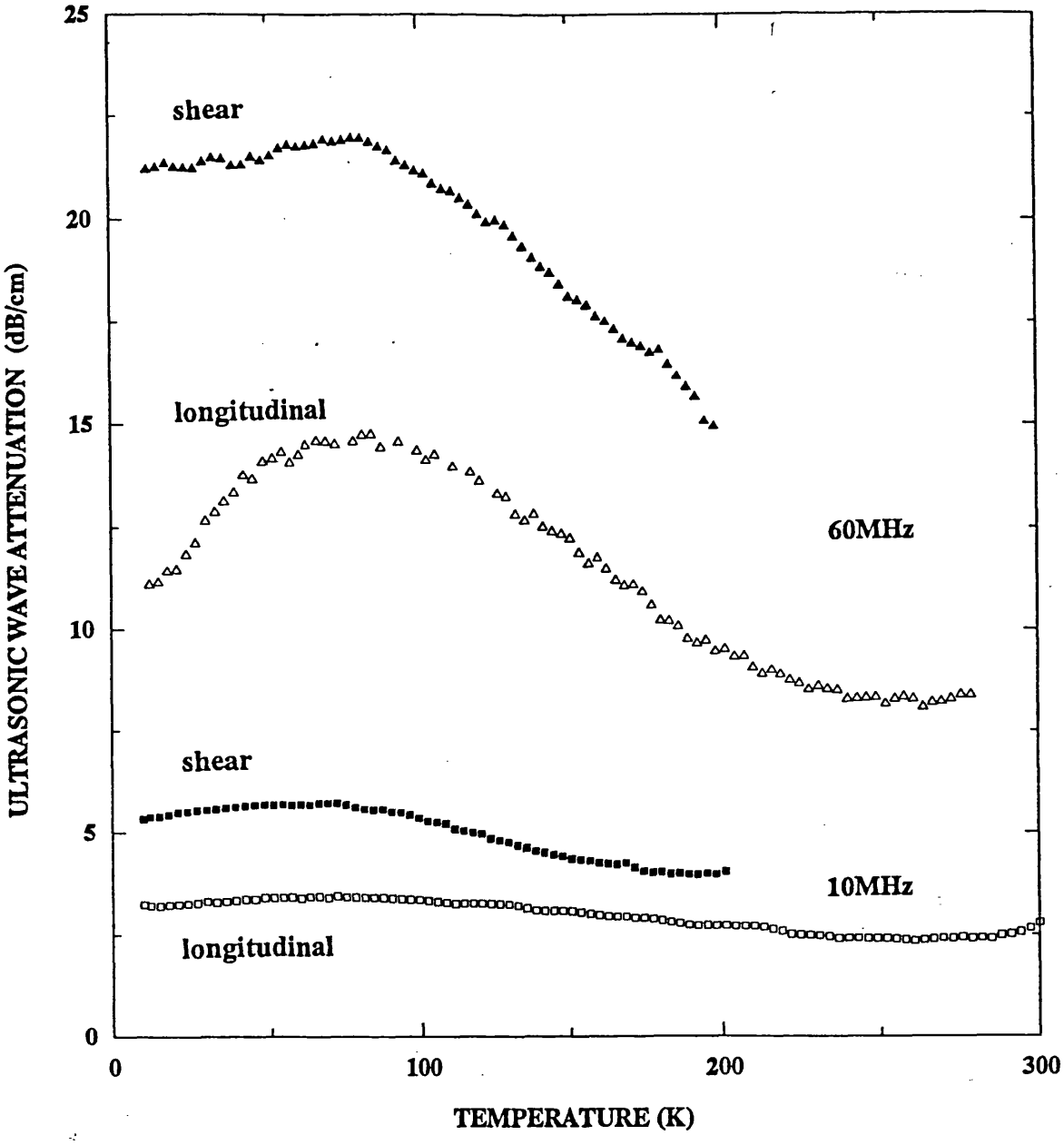

Figure 7.12. The temperature dependences of the attenuation of 10MHz and 60MHz of longitudinal and shear ultrasonic waves propagated in $(Pr_6O_{11})_{0.216}(P_2O_5)_{0.784}$ glass.

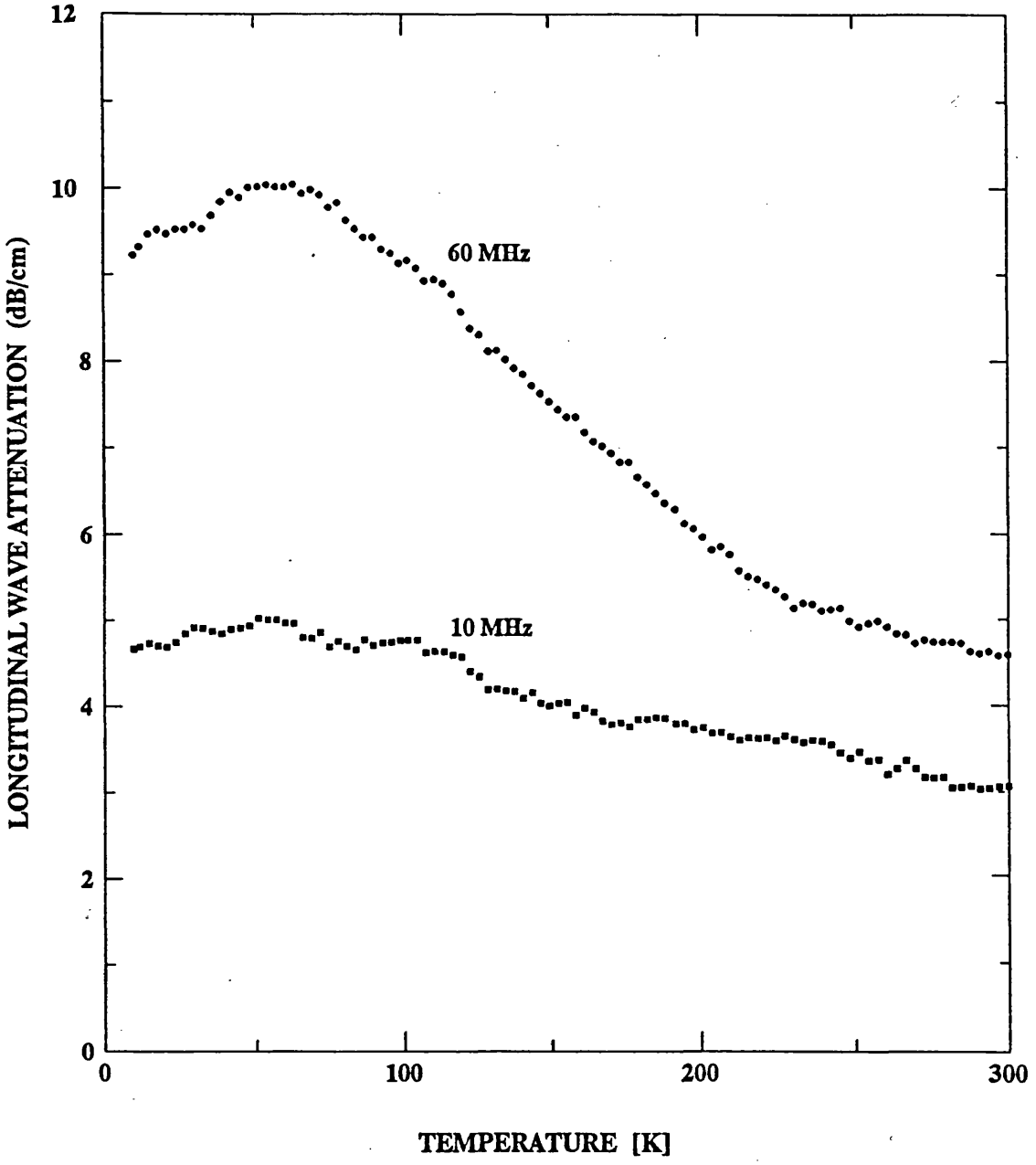

Figure 7.13. The temperature dependence of the attenuation of 10MHz and 60MHz of longitudinal ultrasonic wave propagated in $(Eu_2O_3)_{0.20}(P_2O_5)_{0.80}$ glass.

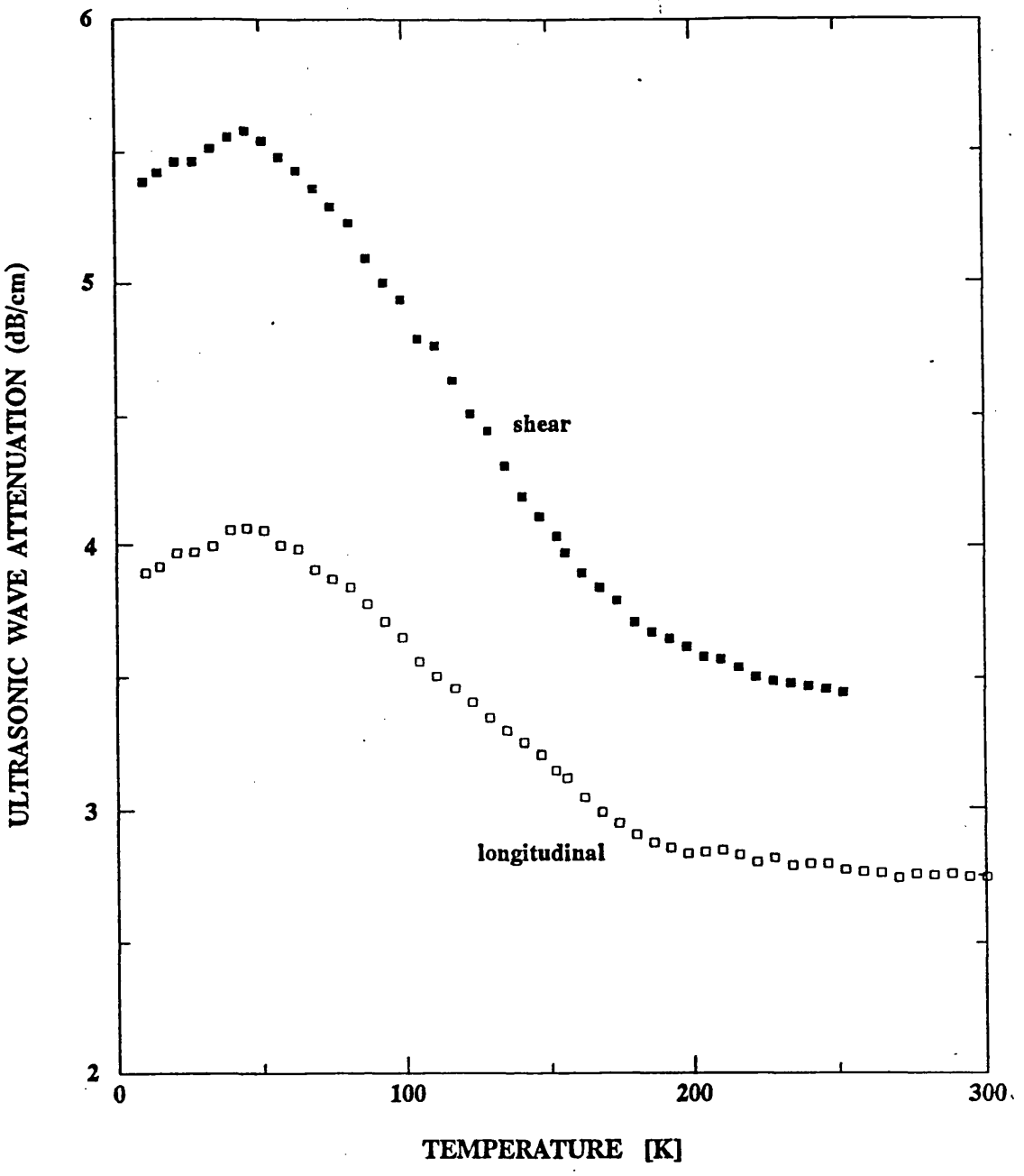

Figure 7.14. The temperature dependences of the attenuation of 10MHz of longitudinal and shear ultrasonic waves propagated in $(Gd_2O_3)_{0.222}(P_2O_5)_{0.778}$ glass.

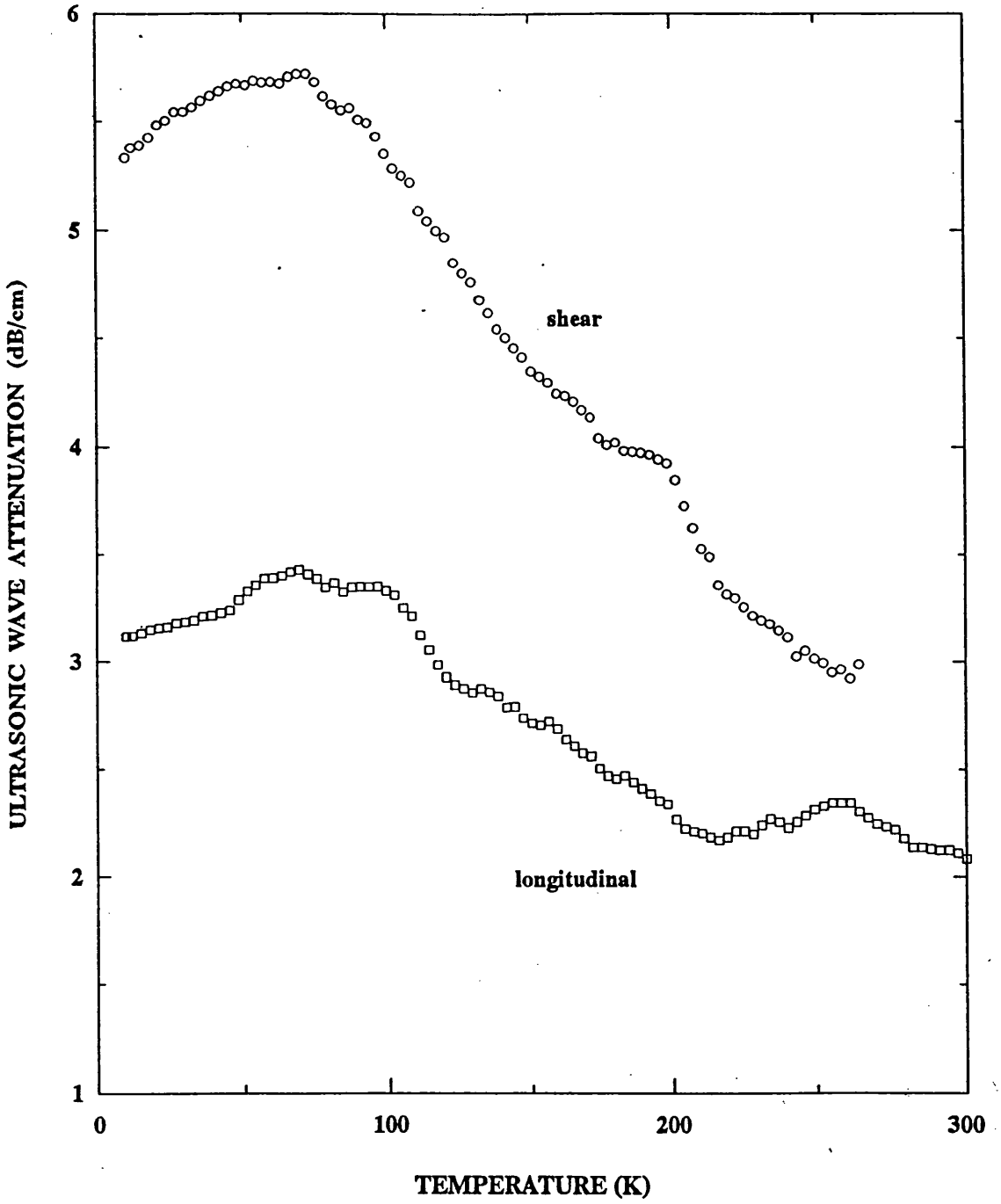

Figure 7.15. The temperature dependences of the attenuation of 10MHz of longitudinal and shear ultrasonic waves propagated in $(Tb_2O_3)_{0.226}(P_2O_5)_{0.774}$ glass.

CHAPTER 8

THE TOEC, HYDROSTATIC PRESSURE DERIVATIVES AND ACOUSTIC MODE GRÜNEISEN PARAMETERS OF RARE EARTH PHOSPHATE GLASSES AND THEIR TEMPERATURE DEPENDENCES.

8.1 INTRODUCTION

The experimental results on the velocities and attenuation of ultrasonic wave propagated in rare earth phosphate glasses as a function of temperature have been described in the previous chapter. In the present chapter, measurements of the effects of hydrostatic pressure and uniaxial stress on the velocity of ultrasonic waves propagating through these same phosphate glasses will be presented. The data provide the hydrostatic pressure derivatives of the SOEC and the TOEC.

The previous ultrasonic studies on binary lanthanum and samarium phosphate glasses have been concentrated on measurement of the hydrostatic pressure derivatives of the elastic stiffness tensor components which define only partially the elastic effects to third order in strain (Mierzejewski et al. 1988a,b, Sidek et al. 1988, Wang et al. 1990). The hydrostatic pressure derivatives of the SOEC give quantitative information of the vibrational mode dependences upon volume. A complete description of the nonlinear acoustic vibrational properties of these glasses demands knowledge of the three independent third order elastic stiffness tensor components (TOEC), which comprise the coefficients of the cubic terms in the strain free energy and quantify the primary contributions to the vibrational anharmonicity of the acoustic modes. By using the recently derived approach of measuring only uniaxial strain dependences of ultrasonic wave velocities (§ 5.3 in Chapter 5), complete sets of TOEC have now been determined for several rare earth phosphate glasses as a function of temperature. This has enabled an investigation of the vibrational anharmonicity of the long-wavelength acoustic modes down to much lower temperatures than reached before. The aim of the work in

this chapter is to present the measured TOEC, hydrostatic pressure derivatives of the SOEC and the bulk modulus, and the acoustic mode Grüneisen parameters as a function of temperature of binary phosphate glasses containing Sm^{3+}, Eu^{3+}, Gd^{3+} or Tb^{3+} as network modifier. The data of the TOEC and the related nonlinear acoustic vibrational properties of these and other rare earth phosphate glasses at room temperature (293K) will be given first. The data are compared with those of other glasses studied previously.

8.2 THE TOEC, HYDROSTATIC PRESSURE DERIVATIVES AND GRÜNEISEN PARAMETERS AT ROOM TEMPERATURE

All the TOEC measured at room temperature have been obtained for the various phosphate glasses and are compared in Table 8.1 with the other complete sets reported previously for other types of vitreous materials. Mixed adiabatic-isothermal TOEC are obtained by the techniques used here. The differences between the mixed C_{IJK} and adiabatic C^S_{IJK} are small compared to the experimental error (Saunders et al. 1993): the results given in Table 8.1 can be used as adiabatic TOEC. These values are in good agreement within experimental error with the published data for other amorphous materials studied previously.

The TOEC, which define the nonlinear acoustic vibrational properties to third order in strain, tend to be negative for $(La_2O_3)_{0.222}(P_2O_5)_{0.778}$ and $(Nd_2O_3)_{0.235}(P_2O_5)_{0.765}$ glasses. Thus, these glasses display a normal elastic behaviour under pressure, similar in kind to those shown by other glasses such as a semiconducting iron phosphate glass (Brassington et al. 1981b), a-As (Brassington et al. 1980), a-As_2S_3 (Brassington et al. 1981a) and a-TeO_2 (Benbattouche et al. 1989) (Table 8.1). In marked contrast, the $(Eu_2O_3)_{0.186}(P_2O_5)_{0.814}$, $(Eu_2O_3)_{0.20}(P_2O_5)_{0.80}$, $(Sm_2O_3)_{0.212}(P_2O_5)_{0.788}$, $(Sm_2O_3)_{0.248}(P_2O_5)_{0.752}$, the TOEC are mostly positive. For these phosphate glasses, negative values of the hydrostatic pressure derivatives $(\partial C^S_{IJ}/\partial P)_{T,P=0}$ of the adiabatic SOEC C^S_{IJ} (the sign of a tensile stress is defined as being positive) have been found

TABLE 8.1. Comparison of the TOEC of phosphate glasses with those of other amorphous materials at room temperature (293K):

	mole fraction	TOEC (GPa)					
	x	C_{111}	C_{112}	C_{123}	C_{144}	C_{155}	C_{456}
$(La_2O_3)_x$ $(P_2O_5)_{1-x}$	0.222	-328 ± 7	-50 ± 4	-33 ± 4	-8 ± 0.8	-70 ± 5	-31 ± 3
$(Nd_2O_3)_x$ $(P_2O_5)_{1-x}$	0.235	-339 ± 8	-24 ± 2	-32 ± 4	4 ± 0.2	-79 ± 5	-41 ± 4
$(Sm_2O_3)_x$ $(P_2O_5)_{1-x}$	0.212 0.248	-105 ± 2 -176 ± 4	37 ± 3 21 ± 2	10 ± 1 20 ± 2	13 ± 0.5 0.6 ± 0.02	36 ± 2 -50 ± 3	-25 ± 2 -25 ± 2
$(Eu_2O_3)_x$ $(P_2O_5)_{1-x}$	0.186 0.200	8 ± 0.2 48 ± 1	74 ± 5 55 ± 4	41 ± 5 7 ± 0.8	17 ± 0.7 24 ± 0.9	-17 ± 1 -2 ± 0.1	-17 ± 2 -13 ± 1
$(Gd_2O_3)_x$ $(P_2O_5)_{1-x}$	0.229	-267 ± 6	79 ± 6	-128 ± 15	104 ± 4	-87 ± 5	-95 ± 7
$(Tb_2O_3)_x$ $(P_2O_5)_{1-x}$	0.247	-128 ± 3	61 ± 4	2 ± 0.2	29 ± 1	-47 ± 3	-38 ± 3
SiO_2		467	233	85	74	59	-8
$(Fe_2O_3)_x$ $(P_2O_5)_{1-x}$ [1]	0.38	-450	-200	-160	-18	-62	-22
As [2]		-465	-33	-162	64	-108	-86
As_2S_3 [3]		-267	-78	-26	-67	-47	-11
TeO_2 [4]		-740	-117	-185	34	-156	-95

[1] Brassington et al. (1981b), [2] Brassington et al. (1980), [3] Brassington et al. (1981a), [4] Benbattouche et al. (1989)

(Table 8.2). The positive values of the TOEC of these glasses (Table 8.1) are in accord with this. Therefore, these glasses show anomalous elastic behaviour: the longitudinal and shear ultrasonic wave velocities decrease under pressure; behaviour which can be referred to as acoustic mode softening. Similar anomalous elastic behaviour under pressure has been shown by vitreous SiO_2 (discussed earlier in Chapter 6). The $(Gd_2O_3)_{0.229}(P_2O_5)_{0.7718}$ and $(Tb_2O_3)_{0.247}(P_2O_5)_{0.753}$ glasses displays an intermediate behaviour; the TOEC are either positive or negative.

A qualitative physical reason can be given for the negative sign of the TOEC of the phosphate glasses studied. At the low pressure involved in measurement of the TOEC, both attractive $-B/\mathbf{r}^n$ and repulsive $A/\mathbf{r}^m$ components of the interatomic potential $\Phi(\mathbf{r})$, which can be represented schematically by

$$\Phi(\mathbf{r}) = \frac{A}{\mathbf{r}^m} - \frac{B}{\mathbf{r}^n} \tag{8.1}$$

contribute to the elastic stiffnesses. For a glass, which does not have a regular atomic arrangement, $\mathbf{r}$ is the mean interatomic distance. The relative contributions depend on the order of the modulus. An adiabatic elastic stiffness tensor component $C_{ijklpq....}$ of order a is the a^{th} derivative

$$(\partial^a \Phi(\mathbf{r})/\partial\eta_{ij}\partial\eta_{kl}\partial\eta_{pq}....)_{S,\underline{\eta}=0}$$

of the interatomic potential $\Phi(\mathbf{r})$ with respect to Lagrangian strain η_{ij}. For stability the exponent m must be larger than n and so the higher the order a, the more the influence of the repulsive term $A/\mathbf{r}^m$ on the stiffness tensor component $C_{ijklpq....}$ (Benbattouche et al. 1989). When a material is subjected to pressure, contraction is resisted by the interatomic repulsive forces, which have a shorter range than the attractive forces and tend to dominate the third order elastic stiffness tensor components. Hence the shorter range and larger exponent m of the repulsive term requires predominantly negative of the TOEC, especially $C_{111}(=\partial^3\Phi(\mathbf{r})/\partial\eta_{11}^3)$, which is dominated by nearest neighbour repulsive forces and does not have a shear contribution and so should be large and

TABLE 8.2. The hydrostatic pressure derivatives and acoustic mode Grüneisen parameters of rare earth phosphate glasses at room temperature (293K).

	mole fraction	Pressure derivative			Grüneisen parameters		
	x	$\left(\frac{\partial C_{11}}{\partial P}\right)_{P=0}$	$\left(\frac{\partial C_{44}}{\partial P}\right)_{P=0}$	$\left(\frac{\partial B}{\partial P}\right)_{P=0}$	γ_L	γ_S	γ'
$(CeO_2)_x (P_2O_5)_{1-x}$	0.226	0.75	-0.30	1.15	-0.04	-0.41	-0.26
	0.235	0.89	-0.30	1.30	0.08	-0.42	-0.26
	0.245	1.04	-0.03	0.99	0.13	-0.14	-0.05
	0.254	1.41	-0.18	1.65	0.24	-0.33	-0.14
	0.257	1.49	-0.31	1.91	0.25	-0.43	-0.21
$(Pr_2O_3)_x (P_2O_5)_{1-x}$	0.216	0.84	-0.37	1.33	0.06	-0.46	-0.28
	0.254	2.93	-0.03	2.97	0.65	-0.19	0.09
	0.256	2.52	0.64	1.67	0.54	0.38	0.43
$(Nd_2O_3)_x (P_2O_5)_{1-x}$	0.194	3.87	-1.39	5.72	0.89	-1.28	-0.55
	0.196	2.60	-1.30	4.33	0.52	-1.15	-0.59
	0.235	1.81	0.14	1.63	0.30	-0.07	0.05
	0.254	2.30	-0.05	2.36	0.46	-0.21	0.02
$(Sm_2O_3)_x (P_2O_5)_{1-x}$	0.212	-1.31	-0.67	-0.41	-0.51	-0.68	-0.67
	0.224	-1.09	-0.72	-0.13	-0.45	-0.70	-0.62
	0.248	-0.46	-0.36	0.02	-0.29	-0.46	-0.45
$(Eu_2O_3)_x (P_2O_5)_{1-x}$	0.186	-2.94	-1.06	-1.53	-0.98	-1.04	-1.02
	0.200	-2.97	-1.39	-1.12	-0.99	-1.31	-1.20
	0.208	-3.21	-1.51	-1.20	-1.05	-1.41	-1.29
	0.218	-3.35	-1.56	-1.27	-1.09	-1.46	-1.34
	0.252	-2.05	-0.99	-0.73	-0.74	-1.01	-0.92
$(Gd_2O_3)_x (P_2O_5)_{1-x}$	0.222	0.73	-0.37	1.22	0.03	-0.46	-0.30
	0.226	-0.18	-0.54	0.53	-0.22	-0.60	-0.47
	0.229	-0.61	-0.57	0.15	-0.33	-0.61	-0.52
	0.245	-0.47	-0.60	0.33	-0.29	-0.64	-0.52
	0.250	0.21	-0.62	0.85	-0.16	-0.64	-0.48
$(Tb_2O_3)_x (P_2O_5)_{1-x}$	0.226	-1.57	-0.74	-0.58	-0.61	-0.81	-0.74
	0.247	-1.58	-0.68	-0.67	-0.60	-0.71	-0.68
	0.263	-0.54	-0.82	0.56	-0.32	-0.84	-0.66
	0.271	0.60	-0.49	1.25	0.01	-0.59	-0.39
$(Dy_2O_3)_x (P_2O_5)_{1-x}$	0.225	-0.92	-1.30	0.75	-0.39	-1.00	-0.80
$(Ho_2O_3)_x (P_2O_5)_{1-x}$	0.208	-0.82	-0.50	-0.15	-0.39	-0.58	-0.51
	0.220	-0.55	-0.24	-0.24	-0.32	-0.36	-0.35
	0.231	-0.36	-0.16	-0.14	-0.27	-0.32	-0.30
$(Er_2O_3)_x (P_2O_5)_{1-x}$	0.239	-1.30	-1.08	0.14	-0.51	-0.97	-0.82

negative, which it does for $(La_2O_3)_{0.222}(P_2O_5)_{0.778}$ and $(Nd_2O_3)_{0.235}(P_2O_5)_{0.765}$ glasses (Table 8.1). The hydrostatic pressure derivatives $(\partial C_{IJ}^S/\partial P)_{T,P=0}$ of the elastic stiffness tensor components should be positive in a material which shows this normal response to an applied stress. In a glass the interatomic forces are functions of bond angle as well as atomic separation both of which change under the influence of an applied hydrostatic pressure or uniaxial stress. A complicating feature is that two-well systems are present in the amorphous state as a result of the spreads in bond angles and lengths, and the application of pressure perturbs these systems.

The hydrostatic pressure derivatives of the SOEC and of the bulk modulus in zero pressure limit and measured at room temperature for rare earth phosphate glasses are given in Table 8.2. The hydrostatic pressure derivatives of the $(La_2O_3)_{0.222}(P_2O_5)_{0.778}$ and $(Nd_2O_3)_{0.235}(P_2O_5)_{0.765}$, $(Eu_2O_3)_{0.186}(P_2O_5)_{0.814}$, $(Eu_2O_3)_{0.20}(P_2O_5)_{0.80}$, $(Sm_2O_3)_{0.212}(P_2O_5)_{0.788}$, $(Sm_2O_3)_{0.248}(P_2O_5)_{0.752}$, $(Gd_2O_3)_{0.229}(P_2O_5)_{0.7718}$ glass and $(Tb_2O_3)_{0.247}(P_2O_5)_{0.753}$ glasses have been calculated using the TOEC data in which the measurements have been carried out using the uniaxial stress, while for the other phosphate glasses, the data were obtained directly from hydrostatic pressure measurements alone. The internal consistency of data obtained from uniaxial stress and those of from hydrostatic pressure has been tested and good agreement is found (Brassington et al. 1981a,b, Wang et al. 1992, Senin et al. 1993). The results show that the biggest negative value of $(\partial C_{11}^S/\partial P)_{T,P=0}$ is found for $(Eu_2O_3)_x(P_2O_5)_{1-x}$ glasses, while the $(Nd_2O_3)_x(P_2O_5)_{1-x}$ glasses display the largest positive values amongst these rare earth glasses.

The hydrostatic pressure derivatives $(\partial C_{11}^S/\partial P)_{T,P=0}$ of the elastic stiffness C_{11}^S and $(\partial B^S/\partial P)_{T,P=0}$ of the bulk modulus of the rare earth phosphate glasses studied are small either positive or negative. But, the hydrostatic pressure derivative $(\partial C_{44}^S/\partial P)_{T,P=0}$ of the elastic stiffness C_{44}^S is always negative.

In the case of cerium, praseodymium and neodymium phosphate glasses, while

the hydrostatic pressure derivatives $(\partial C_{11}^S/\partial P)_{T,P=0}$ and $(\partial B^S/\partial P)_{T,P=0}$ are positive, $(\partial C_{44}^S/\partial P)_{T,P=0}$ is just negative. This indicates that the longitudinal acoustic modes stiffen while the shear acoustic modes soften slightly. The elastic behaviour under pressure of these glasses is similar in kind to that of the soda-lime silica glass (Sato and Anderson 1980) and that for iron phosphate glass (Brassington et al. 1981b); as these workers point out, the presence of metal cations in the interstices of the glass network inhibits the soft transverse vibrations. A similar situation may occur in cerium, praseodymium and neodymium phosphate glasses: the transverse vibrations are inhibited by the presence of a network modifier. The small but negative value found for $(\partial C_{44}^S/\partial P)_{T,P=0}$ implies that for these glasses the structure is open enough to allow a degree of bond-bending vibrations, but less so than in vitreous SiO_2.

In the case of europium, terbium and holmium phosphate glasses, the hydrostatic pressure derivatives $(\partial C_{11}^S/\partial P)_{T,P=0}$ and $(\partial C_{44}^S/\partial P)_{T,P=0}$ are negative. Both longitudinal and shear modes soften under pressure, the remarkable property of acoustic mode softening. As a consequence, the hydrostatic pressure derivative $(\partial B^S/\partial P)_{T,P=0}$ of the adiabatic bulk modulus is negative for europium, terbium and holmium phosphate glasses (Table 8.2) similar to that shown by samarium phosphate glasses (Mierzejewski et al. 1988a,b). Hence the bulk modulus, given to the first order term in pressure P by

$$B^S(P) = B_0^S + P(\partial B^S/\partial P)$$

becomes smaller as pressure is increased, confirming that the Sm^{3+}, Eu^{3+}, Tb^{3+} and also Ho^{3+} phosphate glasses become easier to squeeze under pressure.

For other phosphate glasses, such as those containing gadolinium, dysprosium and erbium, the hydrostatic pressure derivatives $(\partial C_{11}^S/\partial P)_{T,P=0}$ and $(\partial C_{44}^S/\partial P)_{T,P=0}$ are small and negative and their $(\partial B^S/\partial P)_{T,P=0}$ is also small but positive. It seems that these glasses display intermediate elastic behaviour under pressure between those of other phosphate glasses described above.

Further physical insight into the vibrational properties of these glasses can be

gained by investigating the anharmonicity of their long-wavelength acoustic modes. The longitudinal γ_L and shear γ_S acoustic mode Grüneisen parameters, which measure the shift $-(\partial \ln \omega/\partial \ln V)$ of the long-wavelength acoustic mode frequency ω with volume V, have been calculated at room temperature from the ultrasonic data (Table 8.2).

For each of the glasses containing cerium, praseodymium and neodymium, the longitudinal γ_L is mainly small and positive while the shear γ_S is small and negative; this confirms that, at room temperature longitudinal modes stiffen but shear modes soften with applied hydrostatic pressure. A negative shear acoustic mode Grüneisen parameter for these phosphate glasses is an indication of a slight bond bending vibrations and a small force constant for the corresponding long-wavelength shear acoustic waves.

In marked contrast, other phosphate glasses such as those containing Sm^{3+}, Eu^{3+}, Gd^{3+}, Tb^{3+}, Dy^{3+}, Ho^{3+} or Er^{3+} as network modifiers, both the longitudinal γ_L and shear γ_S mode Grüneisen parameters, have negative values at room temperature (Table 8.2): application of pressure leads to a decrease in the mode frequencies, and hence in their vibrational energy. As a result the mean long-wavelength acoustic mode Grüneisen parameter γ^l is also negative confirming that these glasses are easier to squeeze under high pressures.

In general so far as the effects of pressure on their elastic behaviour of glasses fall into two distinct categories. Many glasses including the covalently bound amorphous element arsenic (Brassington et al. 1980), amorphous As_2S_3 (Brassington et al. 1981a), fluorozirconate glass (Brassington et al. 1981c) and vitreous TeO_2 (Benbattouche et al. 1989) behave normally in that the longitudinal, shear and bulk moduli increase under hydrostatic pressure and their TOEC are negative (Table 8.1) - a feature consistent with the positive signs of the hydrostatic pressure derivatives $(\partial C_{11}^S/\partial P)_{T,P=0}$, $(\partial C_{44}^S/\partial P)_{T,P=0}$ and $(\partial B^S/\partial P)_{T,P=0}$ (Table 8.2). Phosphate glasses containing the transition elements metals, iron (Brassington et al. 1981b) and molybdenum (Comins et al. 1987), as network modifiers also show the normal positive values of the pressure derivatives

$(\partial C_{11}^S/\partial P)_{T,P=0}$ and $(\partial B^S/\partial P)_{T,P=0}$. And so do phosphate glasses containing lanthanum (Sidek et al. 1988), cerium, praseodymium and neodymium (Table 8.2).

The other category includes glasses, such as those based on silica (Thurston and Brugger 1964, Bogardus 1965, Shull 1969, Brassington et al. 1981c) and BeF_2 (Bogardus 1965), whose nonlinear elastic properties are quite different in kind from the majority of materials in that the hydrostatic pressure derivatives $(\partial C_{11}^S/\partial P)_{T,P=0}$, $(\partial C_{44}^S/\partial P)_{T,P=0}$ and $(\partial B^S/\partial P)_{T,P=0}$ are strongly negative and the TOEC are large and positive. The europium and samarium phosphate glasses come into this second category (Tables 8.1 and 8.2). Application of pressure induces a decrease in the elastic stiffnesses of these phosphate glasses similar to that observed for the vitreous SiO_2. The TOEC of europium and samarium are mostly positive (Table 8.1). The long-wavelength acoustic modes soften under pressure. The phosphate glasses containing gadolinium, terbium, dysprosium, holmium and erbium are found to show elastic behaviour under pressure intermediate between these two types of glasses.

8.3 THE TEMPERATURE DEPENDENCES OF THE TOEC

An important part of the project has been to determine the temperature dependences of the TOEC for rare earth phosphate glasses. The calculated TOEC of $(Sm_2O_3)_{0.212}(P_2O_5)_{0.788}$, $(Sm_2O_3)_{0.248}(P_2O_5)_{0.752}$, $(Eu_2O_3)_{0.186}(P_2O_5)_{0.814}$, $(Eu_2O_3)_{0.20}(P_2O_5)_{0.80}$, $(Gd_2O_3)_{0.229}(P_2O_5)_{0.771}$ and $(Tb_2O_3)_{0.247}(P_2O_5)_{0.753}$ glasses as a function of temperature are given in Tables 8.3-8.8. Their plots are shown in Figures 8.1-8.4. In general, the values of the largest TOEC C_{111} and C_{112} become more positive with decreasing temperature. For the $(Sm_2O_3)_{0.212}(P_2O_5)_{0.788}$, $(Sm_2O_3)_{0.248}(P_2O_5)_{0.752}$, $(Eu_2O_3)_{0.186}(P_2O_5)_{0.814}$, $(Eu_2O_3)_{0.20}(P_2O_5)_{0.80}$ and $(Tb_2O_3)_{0.247}(P_2O_5)_{0.753}$ glasses, at low temperatures C_{111}, C_{112}, C_{123} and C_{144} are anomalously positive, while the smaller TOEC C_{155} and C_{456} retain the more usual negative values. The results imply longitudinal acoustic mode softening, which becomes increasingly more pronounced as the tem-

Table 8.3. The TOEC of $(Sm_2O_3)_{0.212}(P_2O_5)_{0.788}$ glass in the temperature range betwen 77K and 293K.

T (K)	C_{111} (GPa)	C_{112} (GPa)	C_{123} (GPa)	C_{144} (GPa)	C_{155} (GPa)	C_{456} (GPa)
77	165 ± 4	211 ± 16	122 ± 14	45 ± 2	-12 ± 1	-28 ± 3
103	119 ± 3	186 ± 14	111 ± 13	38 ± 2	-17 ± 1	-27 ± 3
113	95 ± 2	175 ± 14	108 ± 12	33 ± 1	-20 ± 1	-27 ± 2
123	72 ± 2	156 ± 12	91 ± 10	32 ± 1	-21 ± 1	-27 ± 2
143	65 ± 1	149 ± 11	86 ± 9	32 ± 1	-21 ± 1	-26 ± 2
153	50 ± 1	139 ± 11	82 ± 9	28 ± 1	-22 ± 1	-25 ± 2
163	40 ± 0.9	133 ± 10	78 ± 9	27 ± 1	-23 ± 2	-25 ± 2
173	36 ± 0.8	132 ± 10	79 ± 9	27 ± 1	-24 ± 2	-25 ± 2
183	34 ± 0.7	128 ± 10	75 ± 9	27 ± 1	-24 ± 2	-25 ± 2
193	24 ± 0.5	124 ± 10	73 ± 8	26 ± 1	-25 ± 2	-25 ± 2
213	17 ± 0.4	120 ± 9	71 ± 8	25 ± 1	-26 ± 2	-25 ± 2
223	10 ± 0.2	116 ± 9	67 ± 8	24 ± 0.9	-26 ± 2	-25 ± 2
233	-3 ± 0.06	109 ± 8	63 ± 7	23 ± 0.9	-28 ± 2	-25 ± 2
243	-20 ± 0.4	98 ± 8	56 ± 6	21 ± 0.9	-30 ± 2	-26 ± 2
253	-39 ± 0.8	81 ± 7	39 ± 5	21 ± 0.8	-30 ± 2	-26 ± 2
263	-45 ± 1	79 ± 6	39 ± 5	20 ± 0.8	-31 ± 2	-25 ± 2
273	-56 ± 1	74 ± 6	40 ± 5	17 ± 0.7	-32 ± 2	-25 ± 2
283	-83 ± 2	57 ± 4	29 ± 3	14 ± 0.5	-35 ± 2	-25 ± 2
293	-105 ± 2	37 ± 3	10 ± 1	13 ± 0.5	-36 ± 2	-25 ± 2

Table 8.4. The TOEC of $(Sm_2O_3)_{0.248}(P_2O_5)_{0.752}$ glass in the temperature range between 83K and 293K.

T (K)	C_{111} (GPa)	C_{112} (GPa)	C_{123} (GPa)	C_{144} (GPa)	C_{155} (GPa)	C_{456} (GPa)
83	299 ± 7	321 ± 25	185 ± 21	68 ± 2	-5 ± 0.02	-37 ±3
93	146 ± 3	203 ± 16	108 ± 12	48 ± 2	-14 ± 2	-31 ±3
103	47 ± 1	124 ± 10	46 ± 5	39 ± 2	-19 ± 2	-29 ±3
153	-86 ± 2	66 ± 5	24 ± 3	21 ± 2	-38 ± 2	-30 ±3
173	-118 ± 3	42 ± 3	16 ± 2	13 ± 2	-40 ± 2	-27 ±2
193	-160 ± 4	15 ± 1	2 ± 0.2	7 ± 0.02	-44 ± 2	-25 ±2
213	-166 ± 4	15 ± 1	4 ± 0.5	6 ± 0.02	-45 ± 2	-25 ±2
233	-175 ± 4	12 ± 1	3 ± 0.3	4 ± 0.02	-47 ± 2	-26 ±2
253	-177 ± 4	24 ± 2	26 ± 3	-1 ± 0.02	-50 ± 2	-25 ±2
273	-158 ± 4	32 ± 2	26 ± 3	3 ± 0.02	-47 ± 2	-25 ±2
293	-176 ± 4	21 ± 2	20 ± 2	0.6 ± 0.02	-50 ± 2	-25 ±2

Table 8.5. The TOEC of $(Eu_2O_3)_{0.186}(P_2O_5)_{0.814}$ glass as a function of temperature.

T (K)	C_{111} (GPa)	C_{112} (GPa)	C_{123} (GPa)	C_{144} (GPa)	C_{155} (GPa)	C_{456} (GPa)
77	313 ± 7	343 ± 15	290 ± 33	26 ± 1	-7 ± 1	-17 ± 2
80	307 ± 7	339 ± 15	288 ± 33	26 ± 1	-8 ± 1	-17 ± 2
90	289 ± 6	322 ± 15	270 ± 31	26 ± 1	-8 ± 1	-17 ± 2
100	282 ± 6	316 ± 15	265 ± 31	25 ± 1	-8 ± 1	-17 ± 2
110	256 ± 6	291 ± 15	241 ± 28	25 ± 1	-9 ± 1	-17 ± 2
120	238 ± 5	274 ± 15	224 ± 26	25 ± 1	-9 ± 1	-17 ± 2
130	227 ± 5	263 ± 14	214 ± 25	25 ± 1	-9 ± 1	-17 ± 2
140	206 ± 4	244 ± 13	196 ± 23	24 ± 1	-10 ± 1	-17 ± 2
150	181 ± 4	220 ± 11	172 ± 20	24 ± 1	-10 ± 1	-17 ± 2
160	163 ± 4	204 ± 10	157 ± 18	24 ± 1	-10 ± 1	-17 ± 2
170	149 ± 3	191 ± 8	145 ± 17	23 ± 1	-11 ± 1	-17 ± 2
180	133 ± 3	178 ± 8	133 ± 15	23 ± 1	-11 ± 1	-17 ± 2
190	119 ± 3	165 ± 8	121 ± 14	22 ± 1	-12 ± 1	-17 ± 2
200	106 ± 3	154 ± 8	111 ± 13	22 ± 1	-12 ± 1	-17 ± 2
210	90 ± 2	138 ± 8	96 ± 11	21 ± 1	-12 ± 1	-17 ± 2
220	81 ± 2	132 ± 7	92 ± 11	21 ± 1	-13 ± 1	-17 ± 2
230	68 ± 1	122 ± 7	83 ± 10	20 ± 1	-14 ± 1	-17 ± 2
240	58 ± 1	115 ± 7	76 ± 9	19 ± 1	-14 ± 1	-17 ± 2
250	47 ± 1	106 ± 6	69 ± 8	19 ± 1	-15 ± 1	-17 ± 2
260	39 ± 0.8	98 ± 5	62 ± 7	18 ± 1	-15 ± 1	-17 ± 2
270	31 ± 0.7	93 ± 5	57 ± 7	18 ± 1	-15 ± 1	-17 ± 2
280	20 ± 0.4	84 ± 4	51 ± 6	17 ± 1	-16 ± 1	-16 ± 2
290	10 ± 0.2	76 ± 3	44 ± 5	17 ± 1	-17 ± 1	-17 ± 2
293	8.3 ± 0.2	74 ± 3	42 ± 5	17 ± 1	-17 ± 1	-17 ± 2
300	8.6 ± 0.2	74 ± 3	41 ± 5	17 ± 1	-17 ± 1	-17 ± 2
310	8.8 ± 0.2	75 ± 3	42 ± 5	17 ± 1	-16 ± 1	-17 ± 2
320	9.1 ± 0.2	75 ± 3	42 ± 5	17 ± 1	-16 ± 1	-17 ± 2
330	9.2 ± 0.2	75 ± 3	42 ± 5	17 ± 1	-16 ± 1	-17 ± 2
340	9.6 ± 0.2	75 ± 3	42 ± 5	17 ± 1	-16 ± 1	-17 ± 2
350	9.5 ± 0.2	75 ± 3	41 ± 5	17 ± 1	-16 ± 1	-17 ± 2
360	9.4 ± 0.2	75 ± 3	41 ± 5	17 ± 1	-16 ± 1	-17 ± 2
370	9.1 ± 0.2	74 ± 3	40 ± 5	17 ± 1	-16 ± 1	-17 ± 2
380	8.6 ± 0.2	74 ± 3	39 ± 4	17 ± 1	-16 ± 1	-17 ± 2
390	7.6 ± 0.2	72 ± 3	38 ± 4	17 ± 1	-16 ± 1	-17 ± 2
400	6.5 ± 0.1	71 ± 3	37 ± 4	17 ± 1	-16 ± 1	-17 ± 2

Table 8.6. The TOEC of $(Eu_2O_3)_{0.20}(P_2O_5)_{0.80}$ glass as a function of temperature.

T (K)	C_{111} (GPa)	C_{112} (GPa)	C_{123} (GPa)	C_{144} (GPa)	C_{155} (GPa)	C_{456} (GPa)
77	344 ± 8	315 ± 25	247 ± 28	34 ± 2	7.2 ±0.4	-13 ± 1
80	338 ± 7	311 ± 25	245 ± 28	33 ± 2	6.7 ±0.4	-13 ± 1
90	320 ± 7	294 ± 25	228 ± 28	33 ± 2	6.4 ±0.4	-13 ± 1
100	313 ± 7	289 ± 25	223 ± 25	33 ± 2	6.1 ±0.4	-13 ± 1
110	288 ± 6	264 ± 25	200 ± 25	32 ± 2	5.9 ±0.4	-13 ± 1
120	270 ± 6	248 ± 25	183 ± 18	32 ± 2	5.7 ±0.4	-13 ± 1
130	260 ± 6	238 ± 25	174 ± 18	32 ± 2	5.4 ±0.3	-13 ± 1
140	240 ± 5	219 ± 25	156 ± 18	32 ± 2	5.0 ±0.3	-13 ± 1
150	215 ± 5	196 ± 25	133 ± 15	32 ± 2	4.7 ±0.3	-13 ± 1
160	198 ± 4	181 ± 23	118 ± 15	31 ± 2	4.3 ±0.3	-14 ± 1
170	184 ± 4	168 ± 20	107 ± 15	31 ± 2	4.0 ±0.3	-14 ± 1
180	169 ± 4	155 ± 20	95 ± 12	30 ± 2	3.4 ±0.3	-13 ± 1
190	155 ± 3	143 ± 20	84 ± 12	30 ± 2	2.9 ±0.2	-13 ± 1
200	142 ± 3	132 ± 20	74 ± 10	29 ± 1	2.6 ±0.2	-13 ± 1
210	126 ± 3	117 ± 20	60 ± 8	29 ± 1	2.3 ±0.1	-13 ± 1
220	117 ± 3	112 ± 15	55 ± 8	28 ± 1	1.6 ±0.1	-13 ± 1
230	106 ± 2	102 ± 15	47 ± 8	27 ± 0.8	0.5 ± 0.03	-13 ± 1
240	96 ± 2	94 ± 12	40 ± 5	27 ± 0.8	0.01 ± 0.001	-13 ± 1
250	86 ± 2	85 ± 12	33 ± 3	26 ± 0.8	-0.2 ± 0.01	-13 ± 1
260	78 ± 2	78 ± 9	27 ± 1	26 ± 0.8	-0.8 ± 0.05	-13 ± 1
270	70 ± 2	73 ± 9	22 ± 0.9	25 ± 0.8	-1.4 ± 0.1	-13 ± 1
280	59 ± 1	65 ± 9	16 ± 0.8	24 ± 0.8	-1.9 ± 0.1	-13 ± 1
290	50 ± 1	57 ± 9	9 ± 0.5	24 ± 0.8	-1.8 ± 0.1	-13 ± 1
293	48 ± 1	55 ± 9	7 ± 0.5	24 ± 0.8	-1.8 ± 0.1	-13 ± 1
300	48 ± 1	55 ± 9	6 ± 0.5	24 ± 0.8	-1.8 ± 0.1	-13 ± 1
310	48 ± 1	55 ± 9	7 ± 0.5	24 ± 0.8	-1.8 ± 0.1	-13 ± 1
320	48 ± 1	55 ± 9	7 ± 0.5	24 ± 0.8	-1.8 ± 0.1	-13 ± 1
330	48 ± 1	55 ± 9	7 ± 0.5	24 ± 0.8	-1.7 ± 0.1	-13 ± 1
340	48 ± 1	55 ± 9	7 ± 0.5	24 ± 0.8	-1.7 ± 0.1	-13 ± 1
350	48 ± 1	55 ± 9	6 ± 0.5	25 ± 0.8	-1.7 ± 0.1	-13 ± 1
360	48 ± 1	55 ± 9	6 ± 0.4	25 ± 0.8	-1.6 ± 0.1	-13 ± 1
370	48 ± 1	54 ± 8	5 ± 0.3	25 ± 0.8	-1.6 ± 0.1	-13 ± 1
380	47 ± 1	54 ± 8	5 ± 0.3	25 ± 0.8	-1.6 ± 0.1	-13 ± 1
390	46 ± 1	53 ± 8	3 ± 0.2	25 ± 0.8	-1.6 ± 0.1	-13 ± 1
400	45 ± 1	52 ± 8	2 ± 0.1	25 ± 0.8	-1.6 ± 0.1	-13 ± 1

Table 8.7. The TOEC of $(Gd_2O_3)_{0.229}(P_2O_5)_{0.771}$ glass in the temperature range between 77K and 293K.

T (K)	C_{111} (GPa)	C_{112} (GPa)	C_{123} (GPa)	C_{144} (GPa)	C_{155} (GPa)	C_{456} (GPa)
77	-80 ± 2	216 ± 12	-33 ± 2	124 ± 5	-74 ± 5	-99 ± 9
80	-91 ± 2	212 ± 12	-35 ± 2	123 ± 5	-76 ± 5	-100 ± 9
90	-102 ± 2	206 ± 12	-38 ± 2	121 ± 5	-77 ± 5	-100 ± 9
100	-108 ± 2	202 ± 12	-39 ± 2	120 ± 5	-78 ± 5	-99 ± 9
110	-115 ± 3	197 ± 12	-43 ± 2	119 ± 5	-78 ± 5	-99 ± 9
120	-121 ± 3	192 ± 12	-45 ± 2	118 ± 5	-78 ± 5	-99 ± 9
130	-126 ± 3	189 ± 12	-47 ± 2	117 ± 5	-79 ± 5	-98 ± 9
140	-133 ± 3	183 ± 12	-50 ± 2	116 ± 5	-79 ± 5	-98 ± 9
150	-148 ± 3	170 ± 11	-62 ± 2	115 ± 5	-79 ± 5	-98 ± 9
160	-157 ± 4	162 ± 11	-68 ± 2	114 ± 5	-80 ± 5	-97 ± 9
170	-166 ± 4	156 ± 11	-73 ± 2	114 ± 5	-80 ± 5	-97 ± 9
180	-175 ± 4	148 ± 11	-79 ± 2	113 ± 5	-81 ± 5	-97 ± 9
190	-182 ± 4	142 ± 11	-82 ± 2	112 ± 5	-81 ± 5	-97 ± 9
200	-193 ± 4	135 ± 11	-88 ± 2	111 ± 5	-82 ± 5	-97 ± 9
210	-193 ± 4	133 ± 11	-89 ± 2	111 ± 5	-82 ± 5	-96 ± 9
220	-215 ± 5	123 ± 11	-96 ± 2	109 ± 5	-84 ± 5	-97 ± 9
230	-218 ± 5	118 ± 11	-100 ± 5	108 ± 5	-84 ± 5	-96 ± 9
240	-219 ± 5	114 ± 11	-103 ± 5	109 ± 5	-83 ± 5	-96 ± 9
250	-222 ± 5	108 ± 11	-109 ± 5	108 ± 5	-83 ± 5	-96 ± 9
260	-240 ± 5	98 ± 5	-116 ± 5	107 ± 5	-85 ± 5	-96 ± 9
270	-246 ± 6	91 ± 5	-122 ± 5	107 ± 5	-84 ± 5	-95 ± 9
280	-254 ± 6	86 ± 5	-126 ± 5	106 ± 5	-85 ± 5	-95 ± 9
290	-260 ± 6	82 ± 5	-128 ± 5	105 ± 5	-86 ± 5	-95 ± 9
293	-267 ± 6	79 ± 5	-128 ± 5	104 ± 5	-87 ± 5	-95 ± 9

Table 8.8. The TOEC of $(Tb_2O_3)_{0.247}(P_2O_5)_{0.753}$ glass in the temperature range between 77K and 293K.

T (K)	C_{111} (GPa)	C_{112} (GPa)	C_{123} (GPa)	C_{144} (GPa)	C_{155} (GPa)	C_{456} (GPa)
77	132 ± 3	280 ± 8	196 ± 6	42 ± 2	-36 ± 3	-39 ± 4
80	123 ± 3	273 ± 8	191 ± 6	41 ± 2	-38 ± 3	-39 ± 4
90	114 ± 3	265 ± 8	184 ± 6	41 ± 2	-38 ± 3	-39 ± 4
100	111 ± 3	262 ± 8	182 ± 6	40 ± 2	-38 ± 3	-39 ± 4
110	106 ± 2	258 ± 8	178 ± 6	40 ± 2	-38 ± 3	-39 ± 4
120	104 ± 2	256 ± 8	177 ± 6	40 ± 2	-38 ± 3	-39 ± 4
130	94 ± 2	247 ± 8	169 ± 6	39 ± 2	-38 ± 3	-39 ± 4
140	87 ± 2	241 ± 8	163 ± 6	39 ± 2	-38 ± 3	-39 ± 4
150	77 ± 2	232 ± 8	156 ± 6	38 ± 2	-39 ± 3	-38 ± 3
160	71 ± 2	227 ± 8	151 ± 6	38 ± 2	-39 ± 3	-38 ± 3
170	62 ± 1	219 ± 8	145 ± 6	37 ± 2	-39 ± 3	-38 ± 3
180	49 ± 1	210 ± 8	137 ± 5	37 ± 2	-40 ± 3	-38 ± 3
190	32 ± 0.7	194 ± 7	123 ± 4	36 ± 2	-41 ± 3	-38 ± 3
200	7 ± 0.1	172 ± 6	102 ± 4	35 ± 2	-41 ± 3	-38 ± 3
210	-8 ± 0.1	159 ± 6	89 ± 4	35 ± 2	-42 ± 3	-38 ± 3
220	-33 ± 0.7	138 ± 6	70 ± 4	34 ± 2	-43 ± 3	-38 ± 3
230	-46 ± 1	127 ± 5	60 ± 4	33 ± 2	-43 ± 3	-38 ± 3
240	-62 ± 1	114 ± 5	49 ± 3	33 ± 2	-44 ± 3	-38 ± 3
250	-80 ± 2	98 ± 5	35 ± 2	32 ± 2	-45 ± 3	-38 ± 3
260	-94 ± 2	87 ± 4	24 ± 1	31 ± 2	-45 ± 3	-38 ± 3
270	-103 ± 2	80 ± 3	18 ± 1	31 ± 2	-46 ± 3	-38 ± 3
280	-120 ± 3	69 ± 2	9 ± 0.5	30 ± 2	-47 ± 3	-38 ± 3
290	-125 ± 3	63 ± 2	5 ± 0.1	29 ± 2	-47 ± 3	-38 ± 3
293	-128 ± 3	61 ± 2	2 ± 0.1	29 ± 2	-47 ± 3	-38 ± 3
300	-131 ± 3	58 ± 2	-0.5 ± 0.01	30 ± 2	-47 ± 3	-38 ± 3
310	-136 ± 3	54 ± 2	-7 ± 0.2	31 ± 2	-48 ± 3	-39 ± 4
320	-142 ± 3	51 ± 2	-14 ± 0.5	33 ± 2	-48 ± 3	-40 ± 4
330	-144 ± 3	49 ± 2	-19 ± 1	34 ± 2	-48 ± 3	-41 ± 4
340	-145 ± 3	48 ± 2	-19 ± 1	33 ± 2	-48 ± 3	-41 ± 4
350	-146 ± 3	45 ± 2	-17 ± 1	31 ± 2	-48 ± 3	-39 ± 4
360	-149 ± 3	43 ± 2	-20 ± 1	31 ± 2	-48 ± 3	-40 ± 4
370	-151 ± 3	41 ± 2	-20 ± 1	30 ± 2	-48 ± 3	-39 ± 4
380	-151 ± 3	38 ± 2	-18 ± 1	28 ± 2	-47 ± 3	-38 ± 3
390	-152 ± 3	36 ± 2	-18 ± 1	27 ± 2	-47 ± 3	-37 ± 3
400	-151 ± 3	33 ± 2	-16 ± 1	25 ± 1	-46 ± 3	-35 ± 3

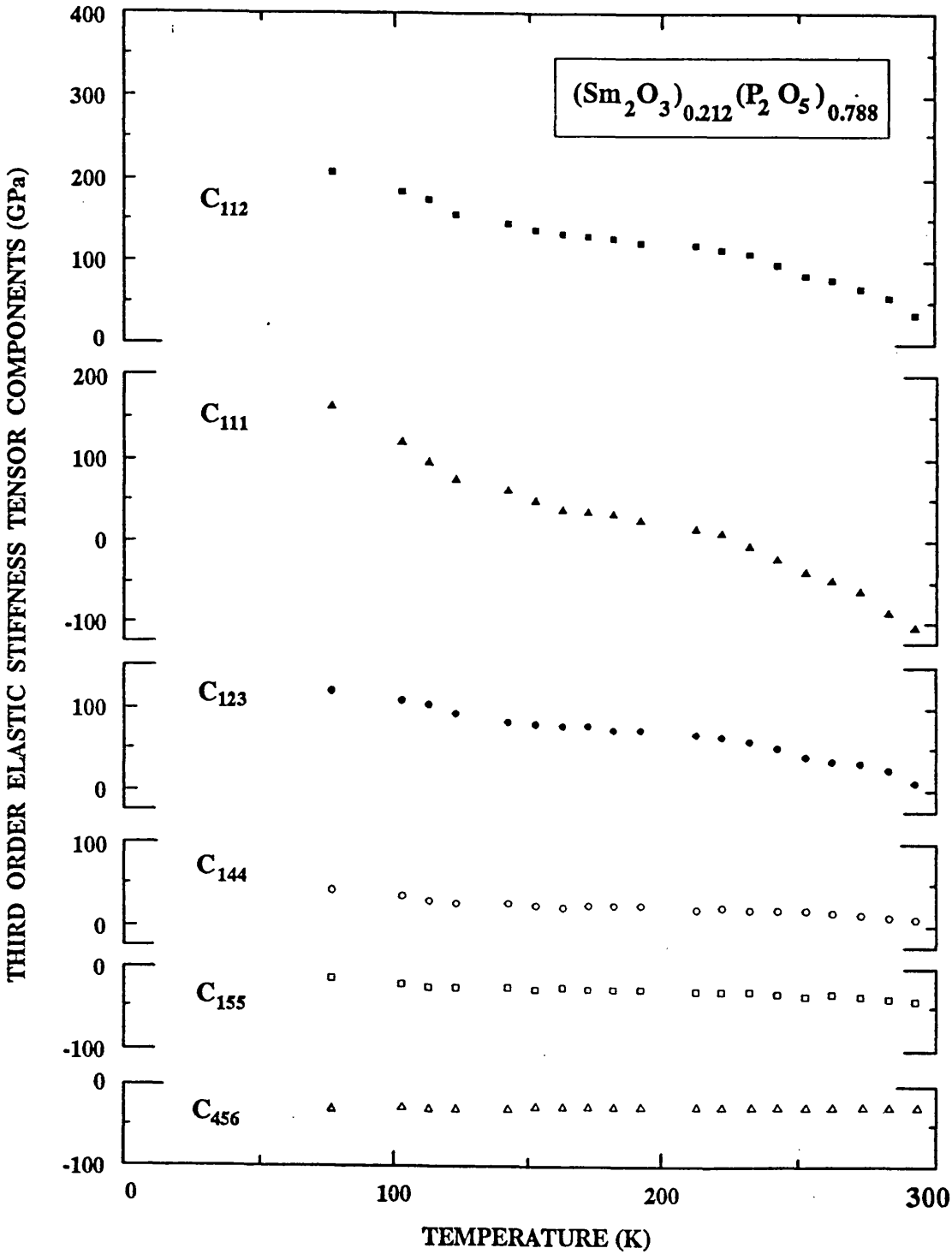

Figure 8.1(a). The temperature dependences of the TOEC for $(Sm_2O_3)_{0.212}(P_2O_5)_{0.788}$ glass.

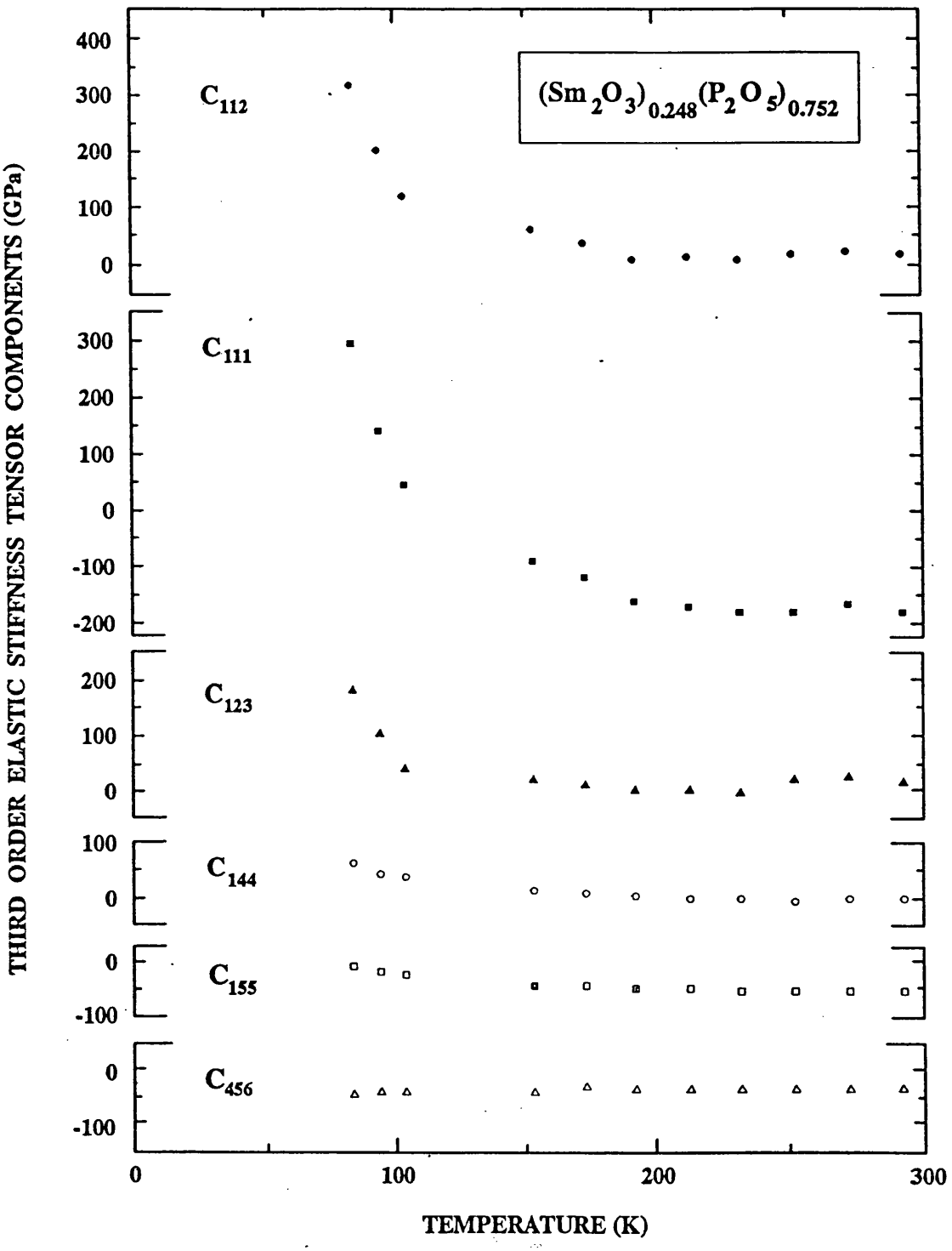

Figure 8.1(b). The temperature dependences of the TOEC for $(Sm_2O_3)_{0.248}(P_2O_5)_{0.752}$ glass.

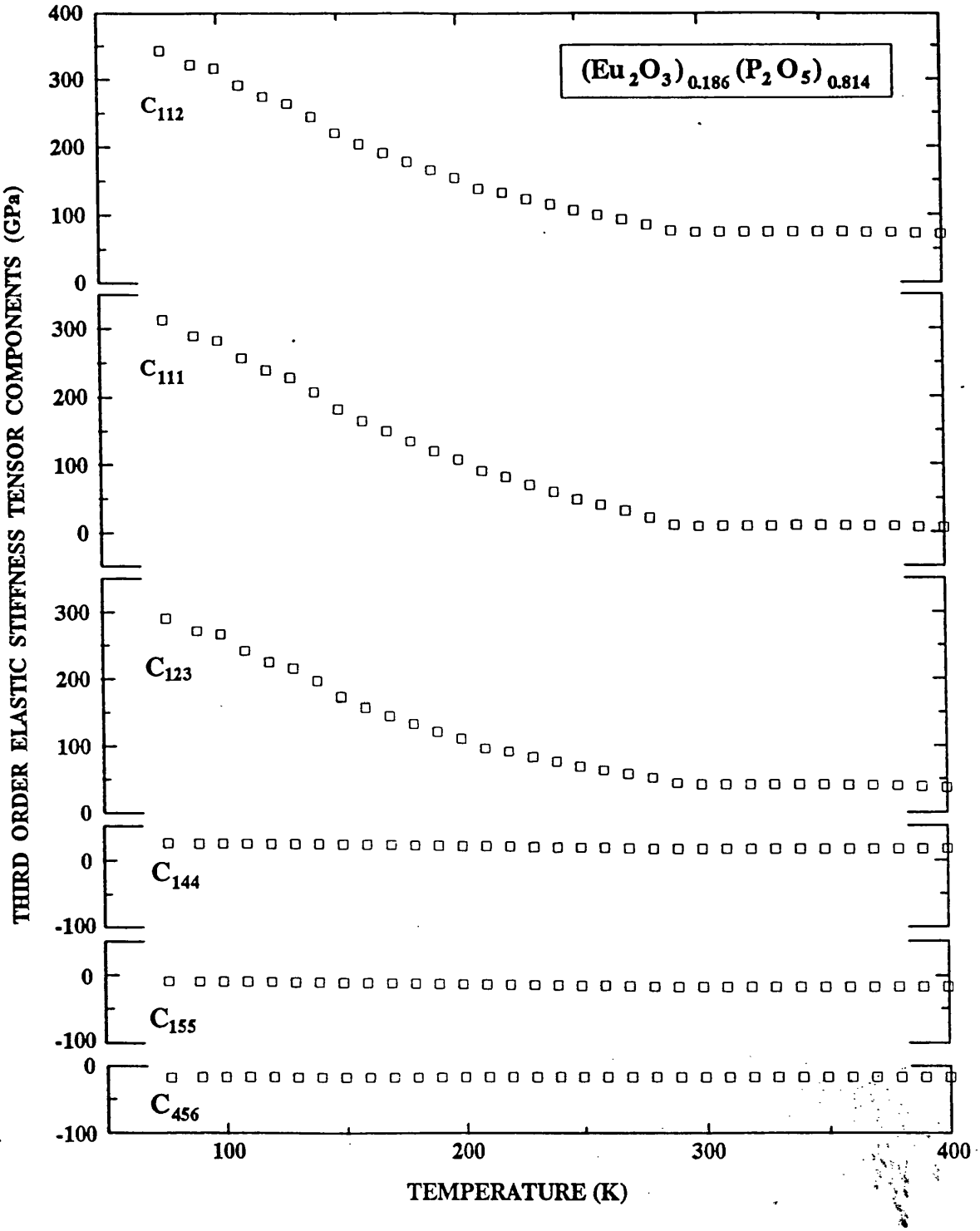

Figure 8.2(a). The temperature dependences of the TOEC for $(Eu_2O_3)_{0.186}(P_2O_5)_{0.814}$ glass.

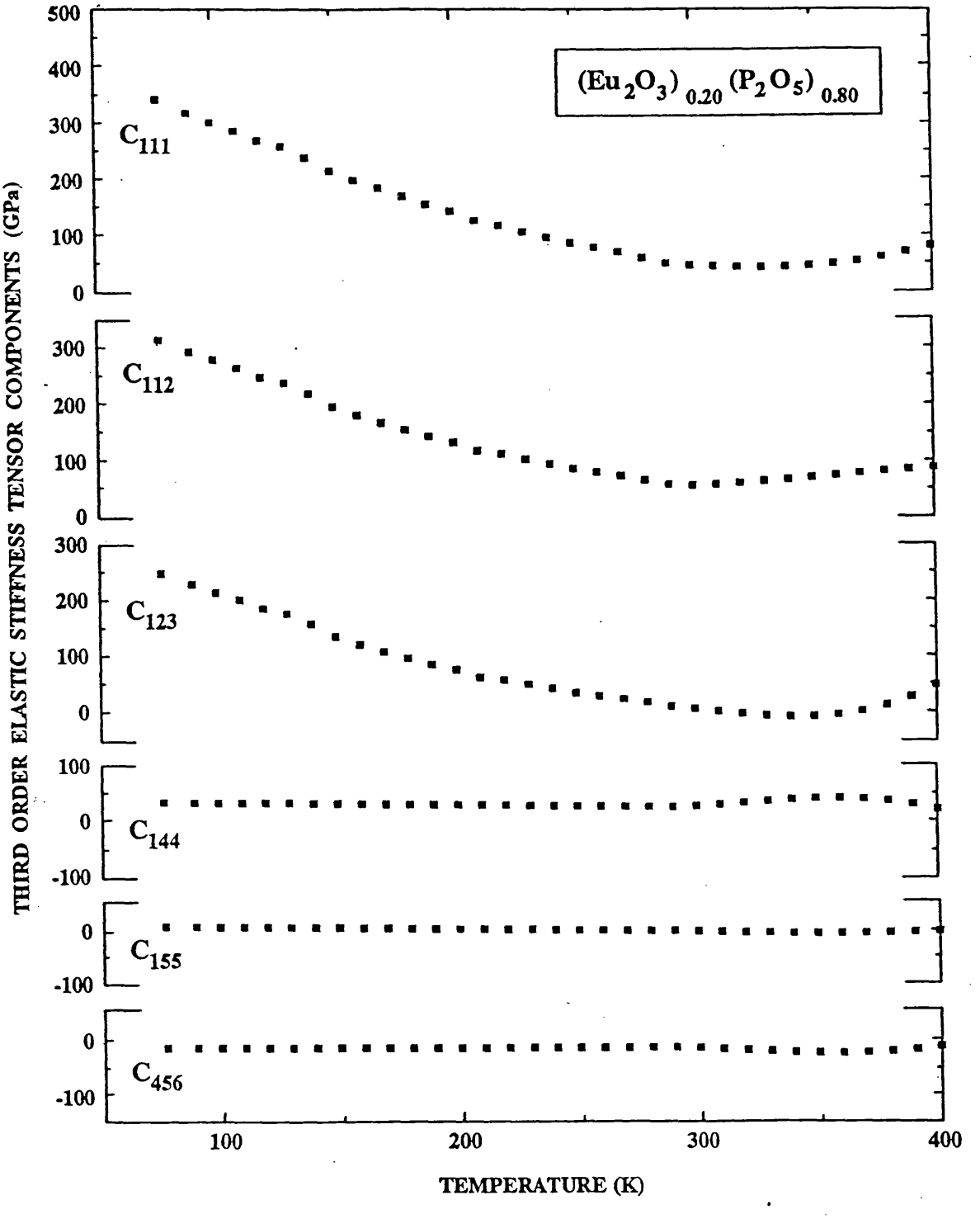

Figure 8.2(b). The temperature dependences of the TOEC for $(Eu_2O_3)_{0.20}(P_2O_5)_{0.80}$ glass.

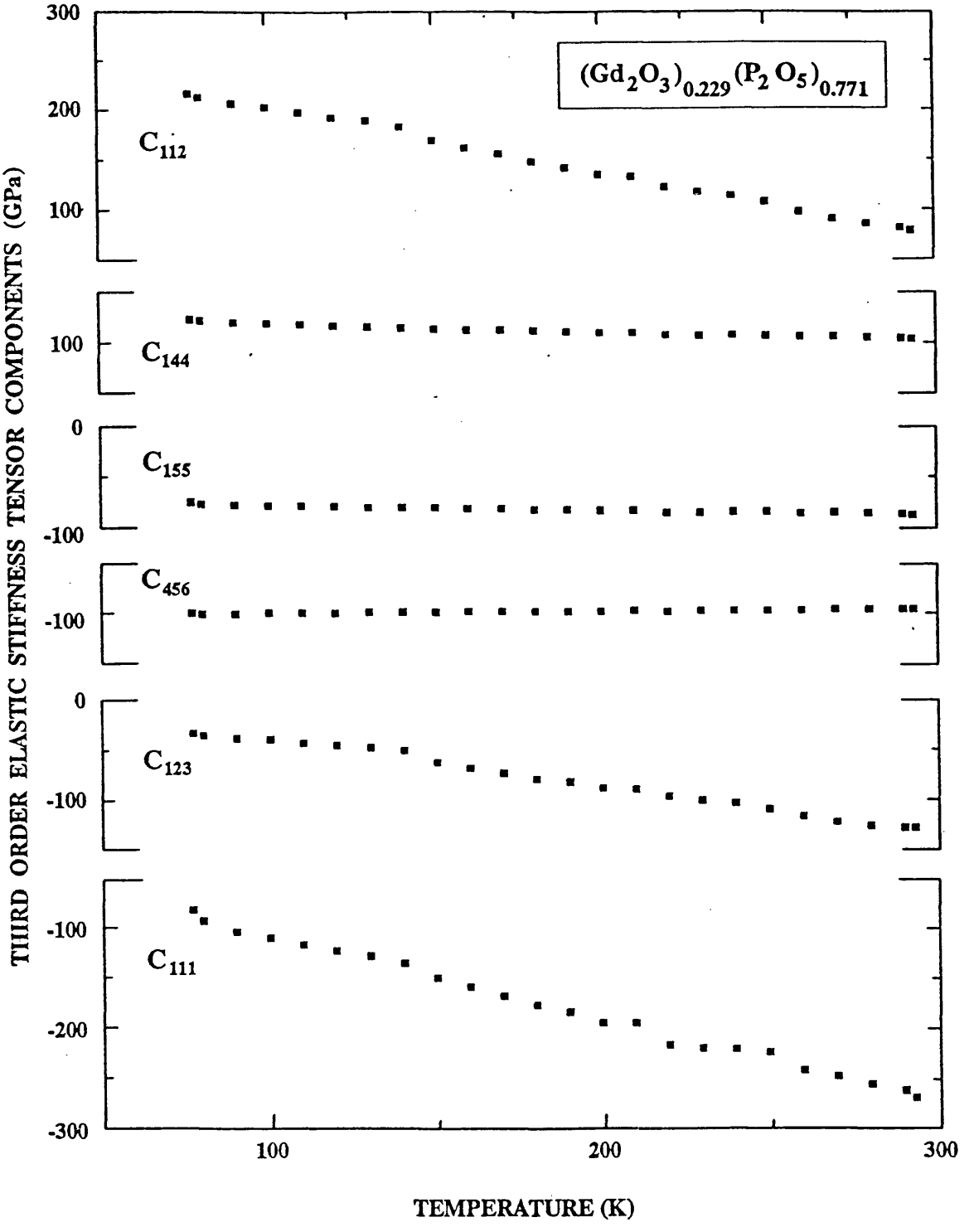

Figure 8.3. The temperature dependences of the TOEC for $(Gd_2O_3)_{0.229}(P_2O_5)_{0.771}$ glass.

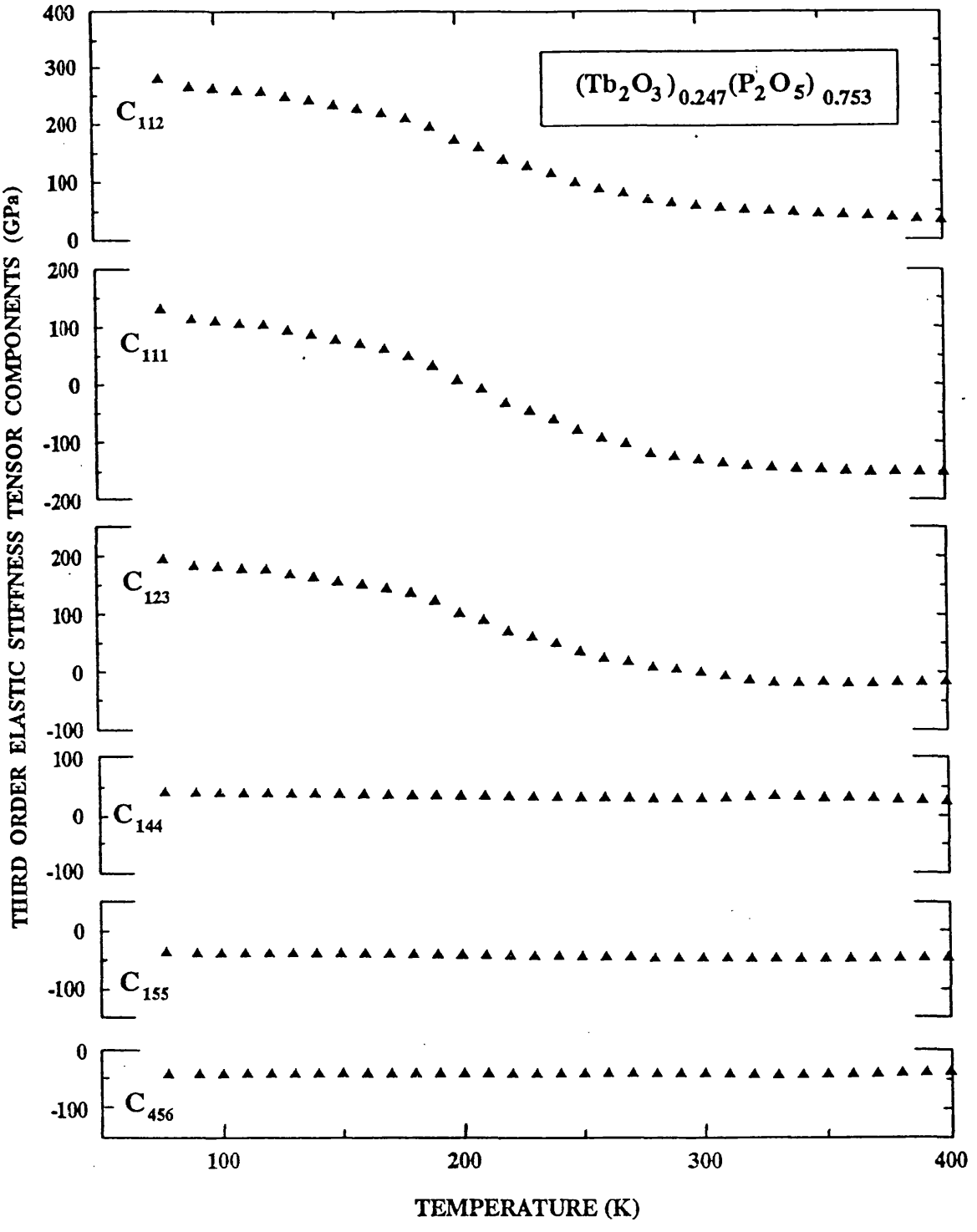

Figure 8.4. The temperature dependences of the TOEC of $(Tb_2O_3)_{0.247}(P_2O_5)_{0.753}$ glass.

perature is reduced, and a similar but somewhat smaller effect for shear modes. Nevertheless, for the $(Gd_2O_3)_{0.229}(P_2O_5)_{0.771}$ glass, only C_{112} and C_{144} are positive and the rest of the TOEC are still negative at low temperatures. The mode softening effect does not display pronounced effect for this glass. Above room temperature the TOEC are almost independent of temperature for the $(Eu_2O_3)_{0.186}(P_2O_5)_{0.814}$, the $(Eu_2O_3)_{0.20}(P_2O_5)_{0.80}$ and the $(Tb_2O_3)_{0.247}(P_2O_5)_{0.753}$ glasses (Figures 8.2 and 8.4): the acoustic mode softening does not change much at higher temperatures.

8.4 THE TEMPERATURE DEPENDENCES OF THE HYDROSTATIC PRESSURE DERIVATIVES OF THE SOEC AND BULK MODULUS

The hydrostatic pressure derivatives, which are rather more accessible to physical understanding, have been calculated below room temperature from the TOEC data. The temperature dependences of the hydrostatic pressure derivatives of the SOEC and bulk modulus of the $(Eu_2O_3)_{0.186}(P_2O_5)_{0.814}$, $(Eu_2O_3)_{0.20}(P_2O_5)_{0.80}$, $(Sm_2O_3)_{0.212}(P_2O_5)_{0.788}$, $(Sm_2O_3)_{0.248}(P_2O_5)_{0.752}$, $(Gd_2O_3)_{0.229}(P_2O_5)_{0.752}$ and $(Tb_2O_3)_{0.247}(P_2O_5)_{0.753}$ glasses are shown in Figures 8.5-8.8.

In the previous ultrasonic studies on phosphate glasses containing samarium as network modifier (Mierzejewski et al. 1988a,b), the hydrostatic pressure derivatives $(\partial C_{11}^S/\partial P)_{T,P=0}$ and $(\partial C_{44}^S/\partial P)_{T,P=0}$ of the elastic stiffnesses and $(\partial B^S/\partial P)_{T,P=0}$ of the bulk modulus were measured, in the case of the $(Sm_2O_3)_{0.212}(P_2O_5)_{0.788}$ glass as a function of temperature between 250K and 450K (Wang et al. 1990). They found that in the temperature range between 450K and 300K $(\partial C_{11}^S/\partial P)_{T,P=0}$ had a value of about -1 but, as the temperature was lowered to 250K, this anomalously negative value became progressively larger. The present work extends knowledge of $(\partial C_{11}^S/\partial P)_{T,P=0}$, $(\partial C_{44}^S/\partial P)_{T,P=0}$ and $(\partial B^S/\partial P)_{T,P=0}$ down to 77K. Taking their results and our present data, the temperature dependences of the hydrostatic pressure derivatives of $(Sm_2O_3)_{0.212}(P_2O_5)_{0.788}$ glass in the temperature range between 77K to 450K is shown in

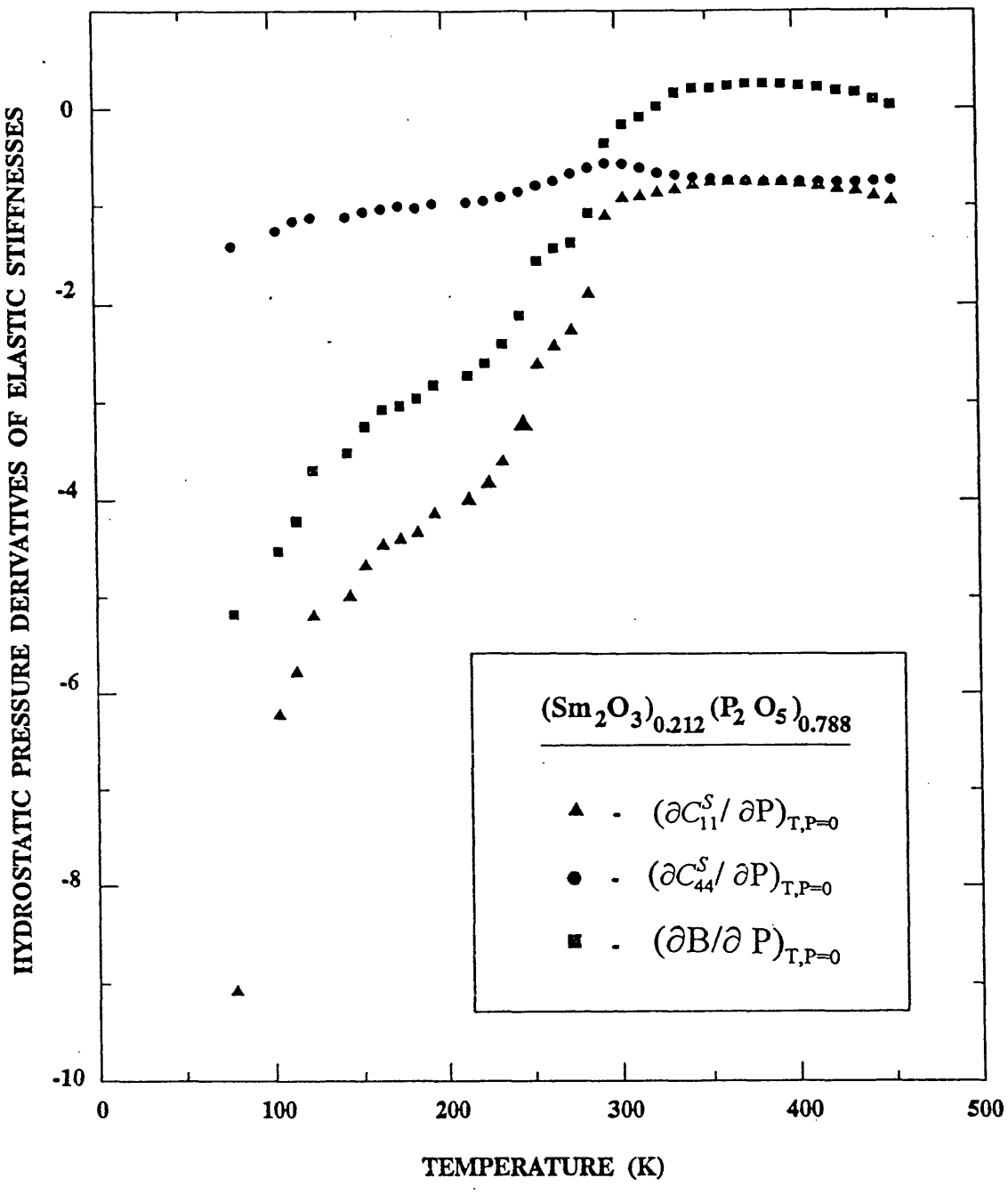

Figure 8.5a. The temperature dependences of hydrostatic pressure derivatives of the SOEC and bulk modulus for $(Sm_2O_3)_{0.212}(P_2O_5)_{0.788}$ glass.

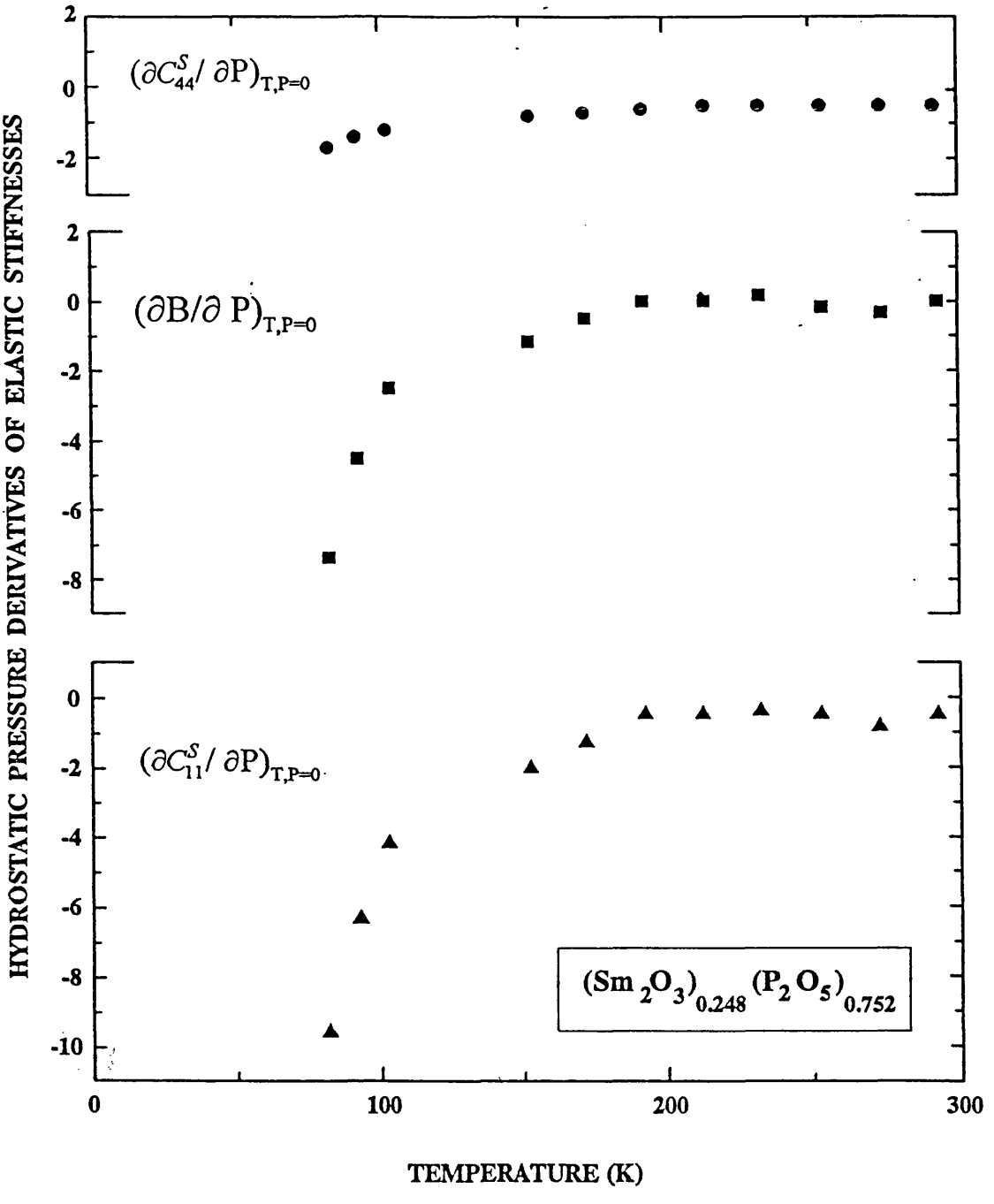

Figure 8.5b. The temperature dependences of hydrostatic pressure derivatives of the SOEC and bulk modulus for $(Sm_2O_3)_{0.248}(P_2O_5)_{0.752}$ glass.

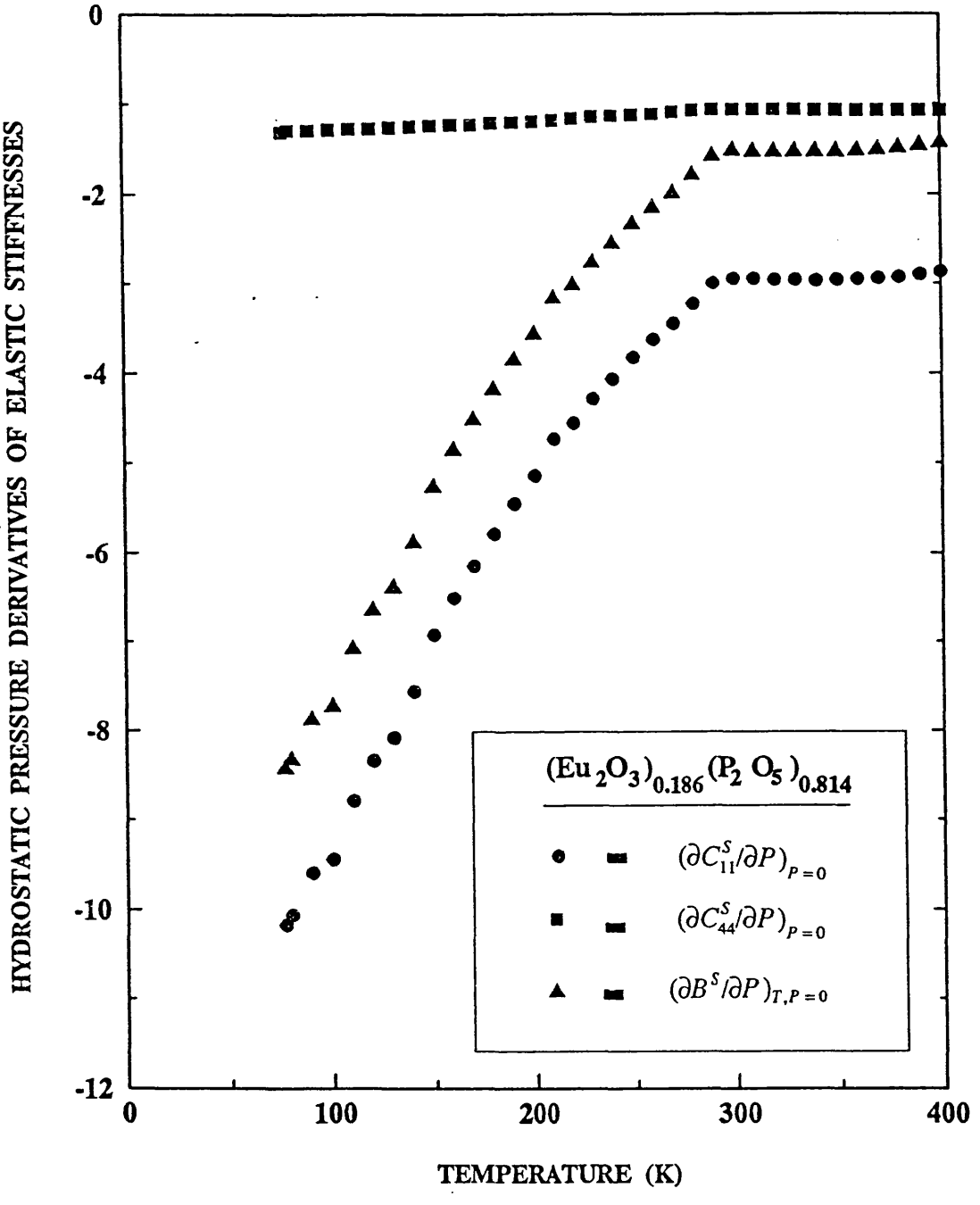

Figure 8.6(a). The temperature dependences of hydrostatic pressure derivatives of the SOEC and bulk modulus for $(Eu_2O_3)_{0.186}(P_2O_5)_{0.814}$ glass.

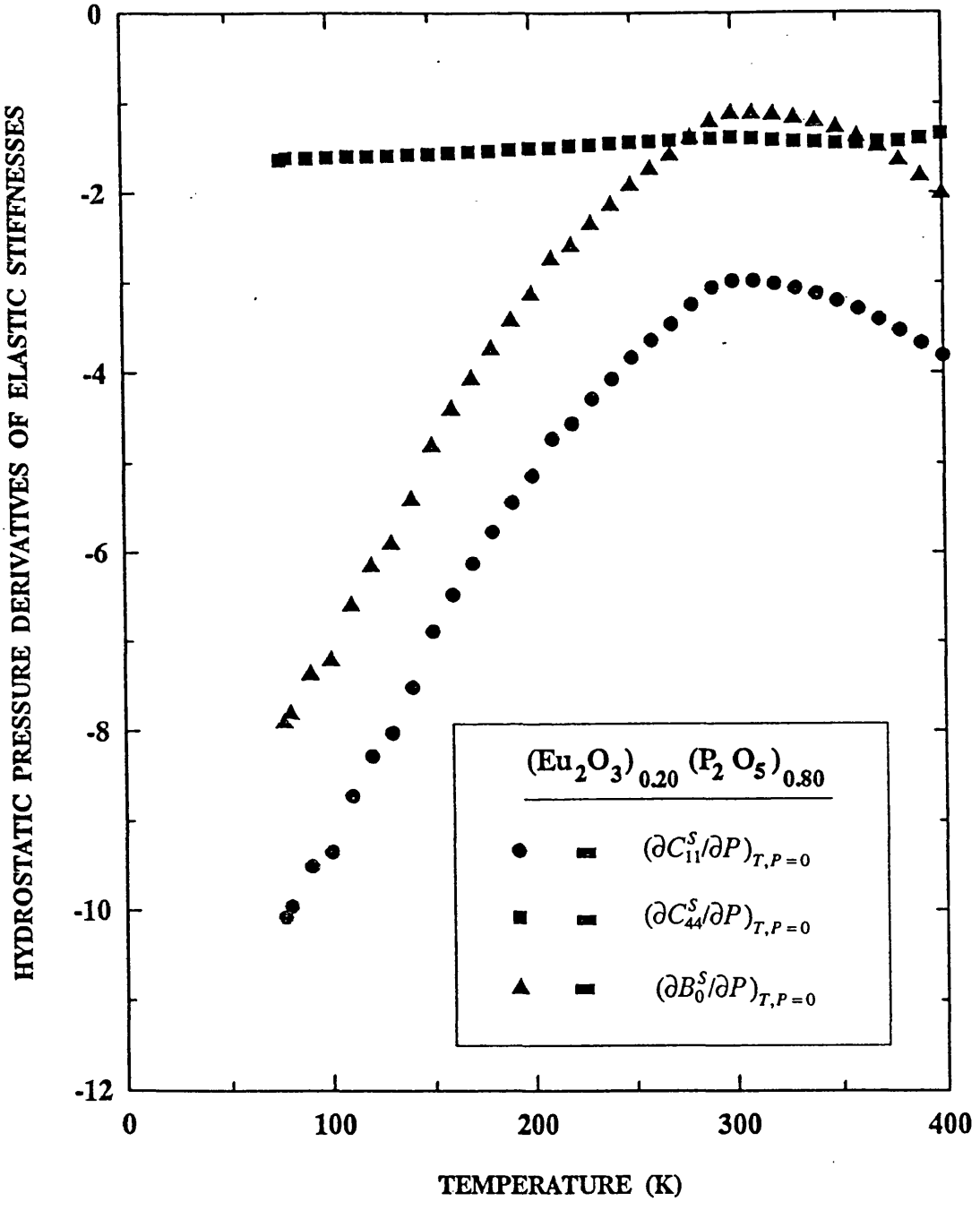

Figure 8.6(b). The temperature dependences of hydrostatic pressure derivatives of the SOEC and bulk modulus for $(Eu_2O_3)_{0.20}(P_2O_5)_{0.80}$ glass.

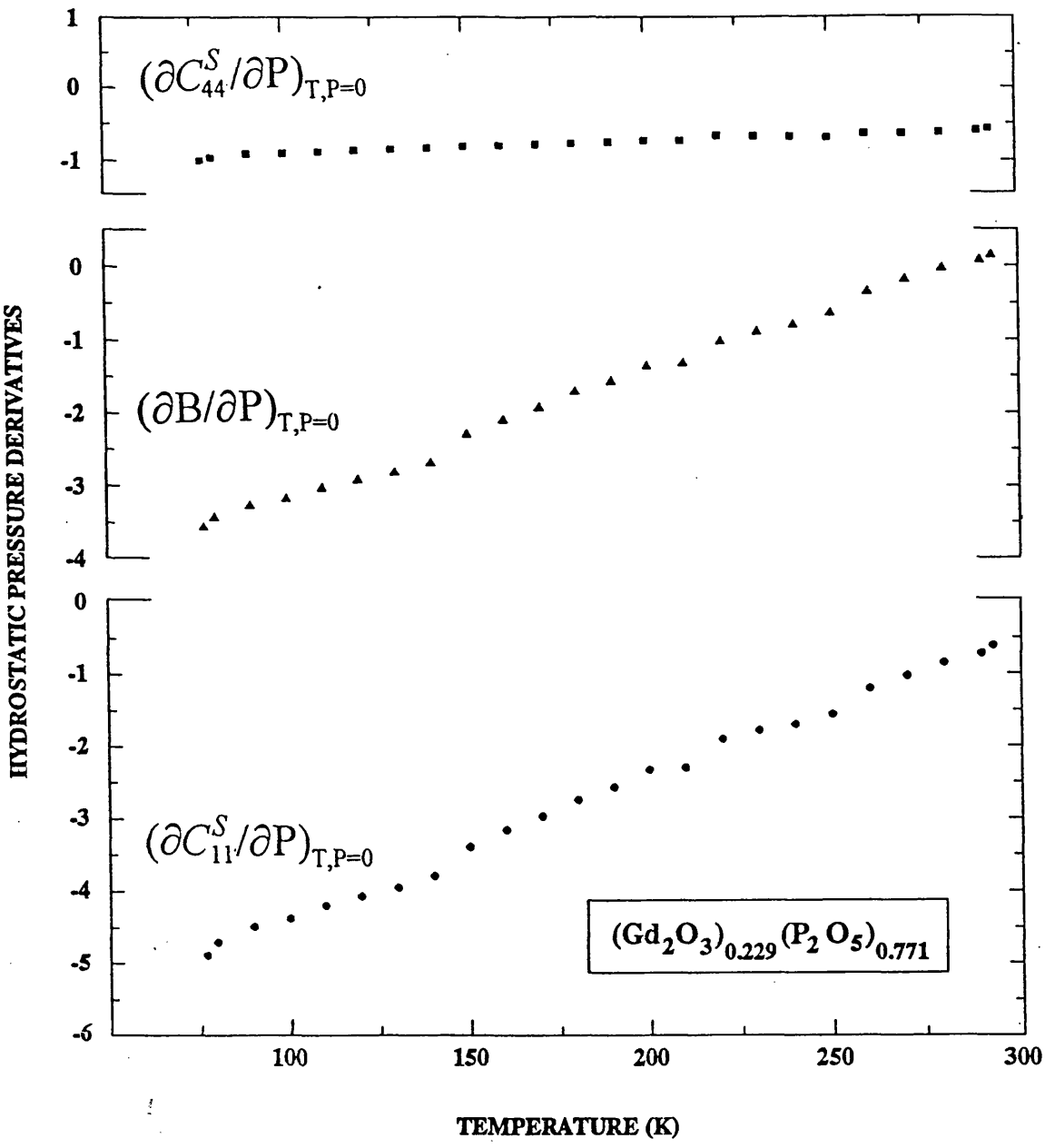

Figure 8.7. The temperature dependences of hydrostatic pressure derivatives of the SOEC and bulk modulus for $(Gd_2O_3)_{0.229}(P_2O_5)_{0.771}$ glass.

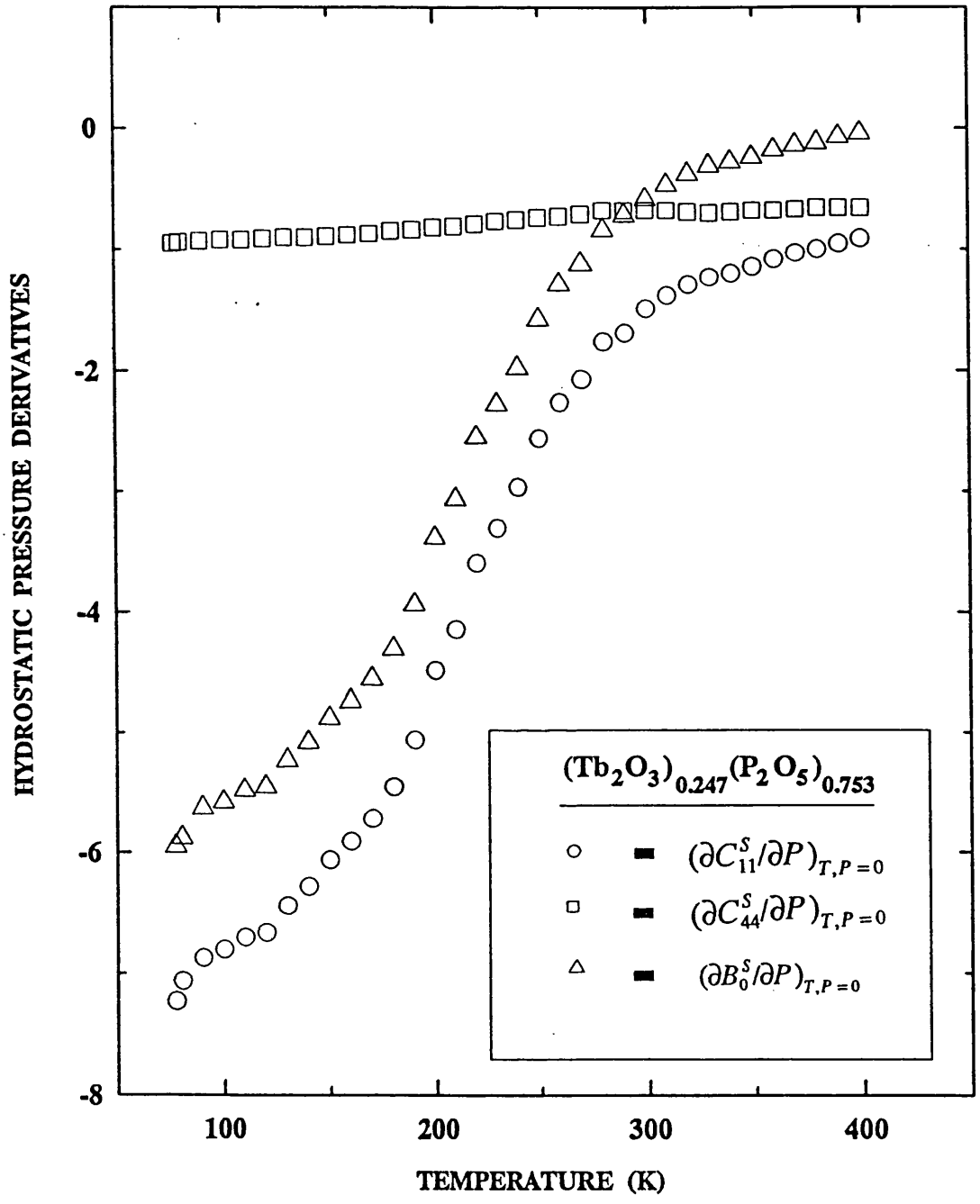

Figure 8.8. The temperature dependences of hydrostatic pressure derivatives of the SOEC and bulk modulus for $(Tb_2O_3)_{0.247}(P_2O_5)_{0.753}$ glass.

Figure 8.5a. The values obtained here over the temperature range between 250K and 293K are in agreement within experimental error with those obtained previously by Wang et al. (1990). The negative value of $(\partial C_{11}^S/\partial P)_{T,P=0}$ becomes larger as the temperature is reduced down to 77K. The same trend with temperature for $(\partial C_{11}^S/\partial P)_{T,P=0}$ also occurs for the $(Sm_2O_3)_{0.248}(P_2O_5)_{0.788}$ (Figure 8.5b), $(Eu_2O_3)_{0.186}(P_2O_5)_{0.714}$ (Figure 8.6a), $(Eu_2O_3)_{0.20}(P_2O_5)_{0.80}$ (Figure 8.6b), $(Gd_2O_3)_{0.229}(P_2O_5)_{0.771}$ (Figure 8.7) and $(Tb_2O_3)_{0.247}(P_2O_5)_{0.753}$ glasses (Figure 8.8). The negative value of $(\partial B^S/\partial P)_{T,P=0}$ becoming larger for these glasses as the temperature is reduced down to 77K. These results show that the extraordinary acoustic mode softening effect becomes enhanced as the temperature is reduced. The values of $(\partial C_{44}^S/\partial P)_{T,P=0}$ also follow the same trend though to a rather smaller extent than those of $(\partial C_{11}^S/\partial P)_{T,P=0}$ but are also negative and increase in magnitude as the temperature is lowered.

8.5 THE COMPRESSION V(P)/V_0 INDUCED BY APPLICATION OF PRESSURE

The compression V(P)/V_0 of various rare earth phosphate glasses estimated at room temperature are shown in Figures 8.9(a-i). The comparison of the compression on selective phosphate glasses to those of vitreous SiO_2 at 293K and 77K are shown in Figures 8.10(a,b). These compressions have been computed from the ultrasonic wave velocity and the pressure dependence data using Anderson's equation-of-state for those glasses with negative $(\partial B^S/\partial P)_{T,P=0}$, while the Murnaghan's equation-of-state has been used for those glasses with positive $(\partial B^S/\partial P)_{T,P=0}$. Data used in the calculations and the value of P_m obtained from the linear approximation to the bulk modulus as a function of pressure for those glasses with a negative $(\partial B^S/\partial P)_{T,P=0}$ are listed in Table 8.9. The behaviour of the compression at comparatively low pressures is similar for each glass. When pressure is increased, the compressions V(V)/V_0 of the glasses with negative

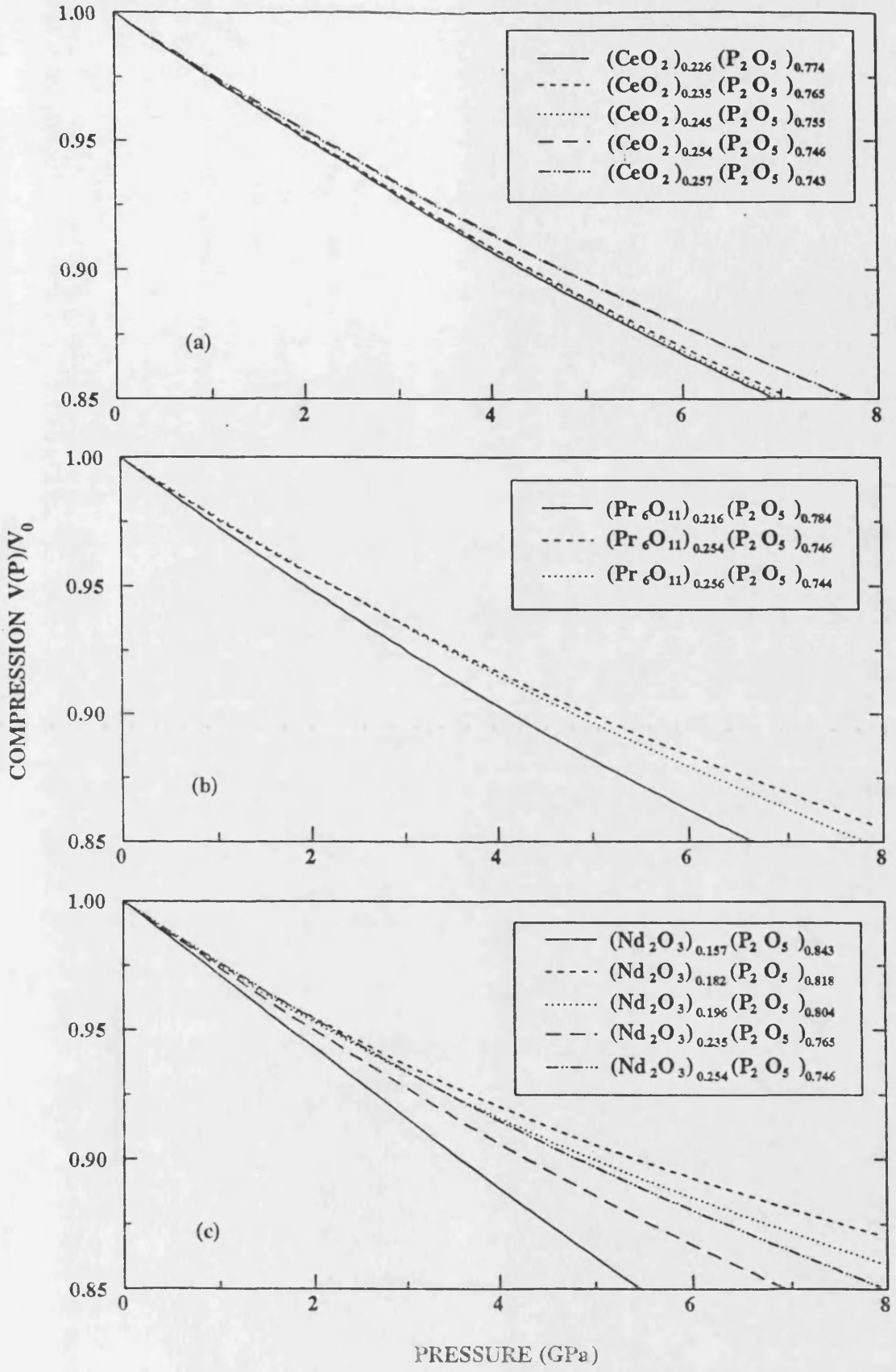

Figure 8.9. The compression $V(P)/V_o$ of phosphate glasses at 293K extrapolated to high pressure using equations-of-states.

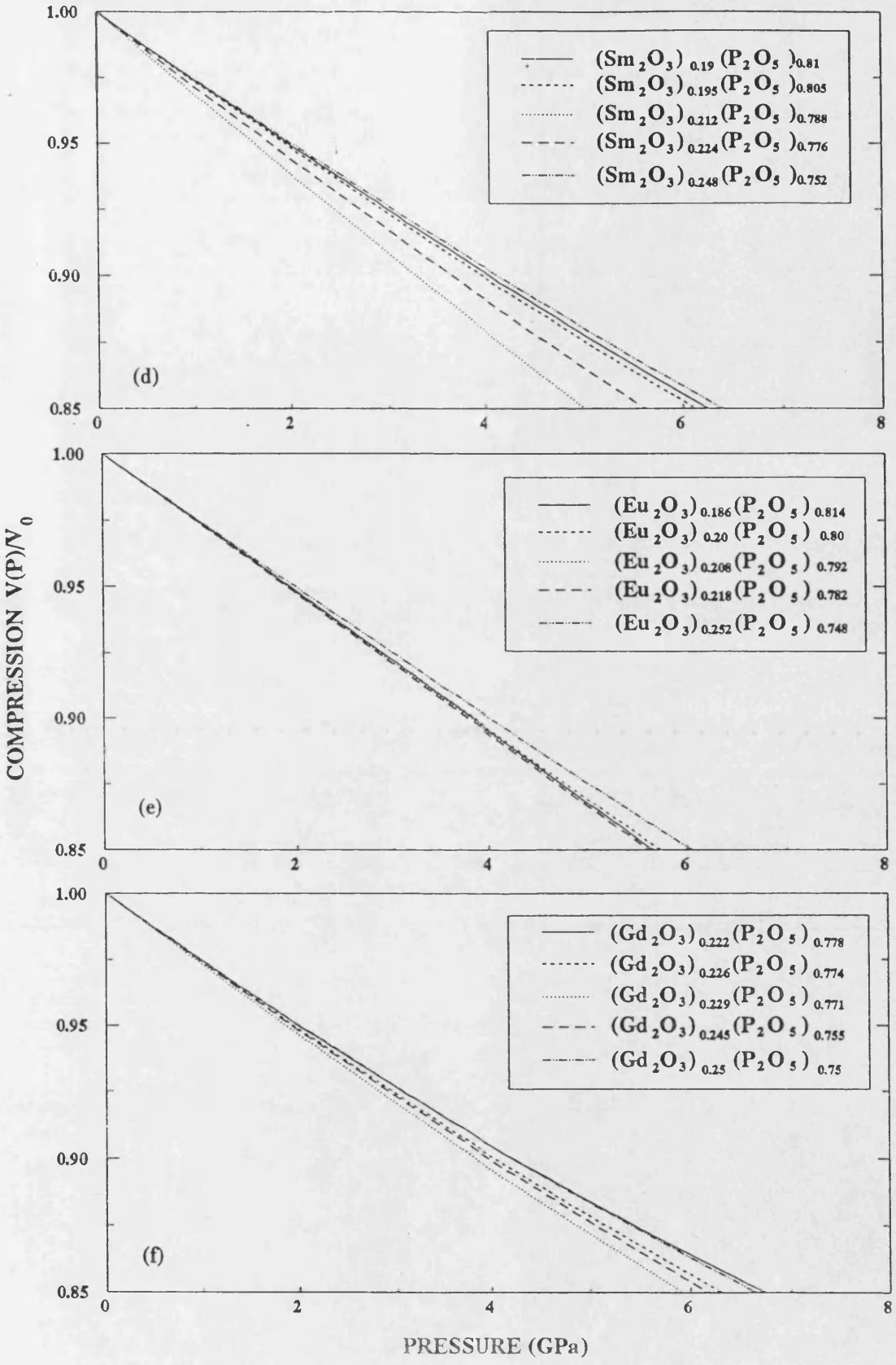

Figure 8.9. The compression $V(P)/V_o$ of phosphate glasses at 293K extrapolated to high pressure using equations-of-states.

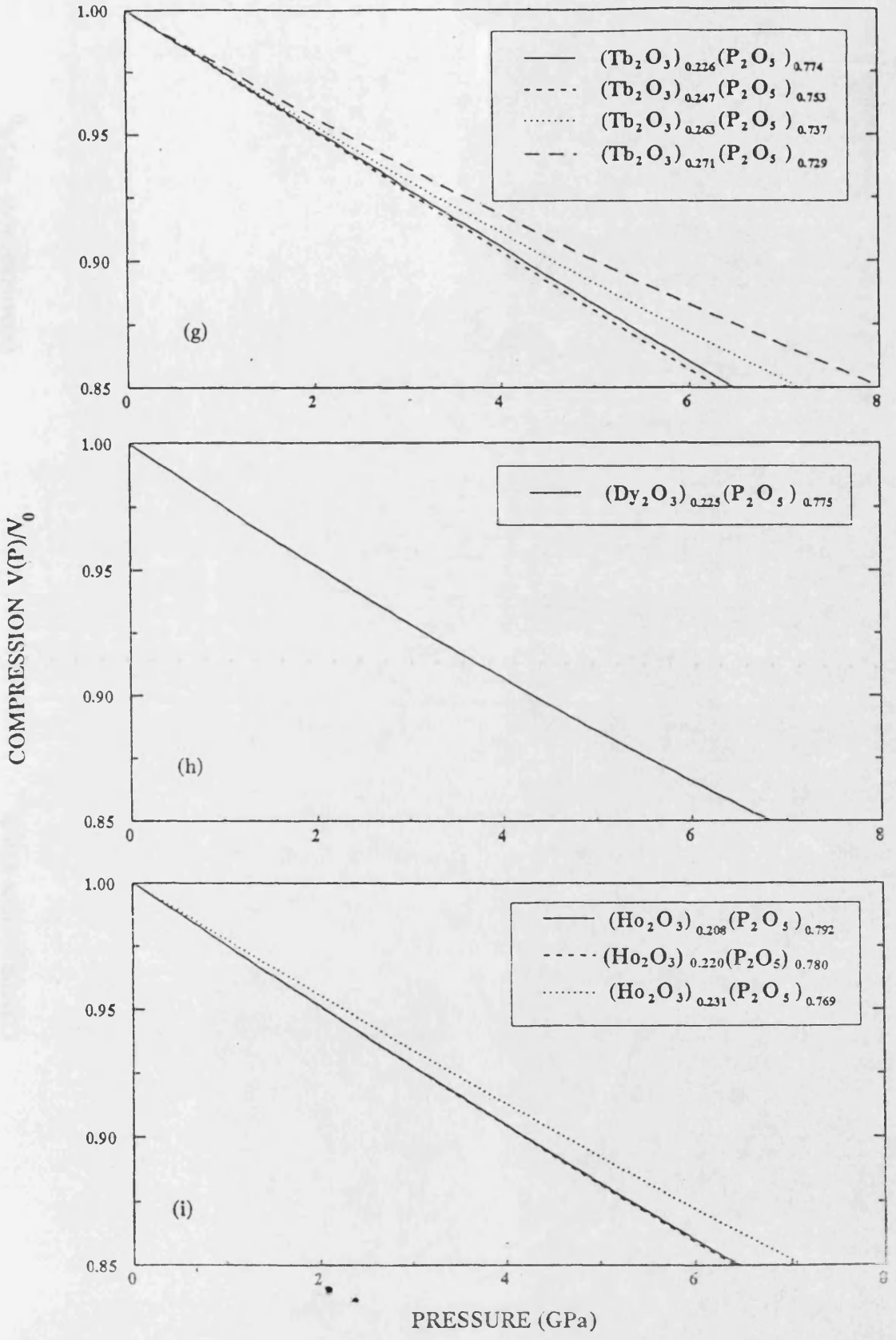

Figure 8.9. The compression $V(P)/V_o$ of phosphate glasses at 293K extrapolated to high pressure using equations-of-states.

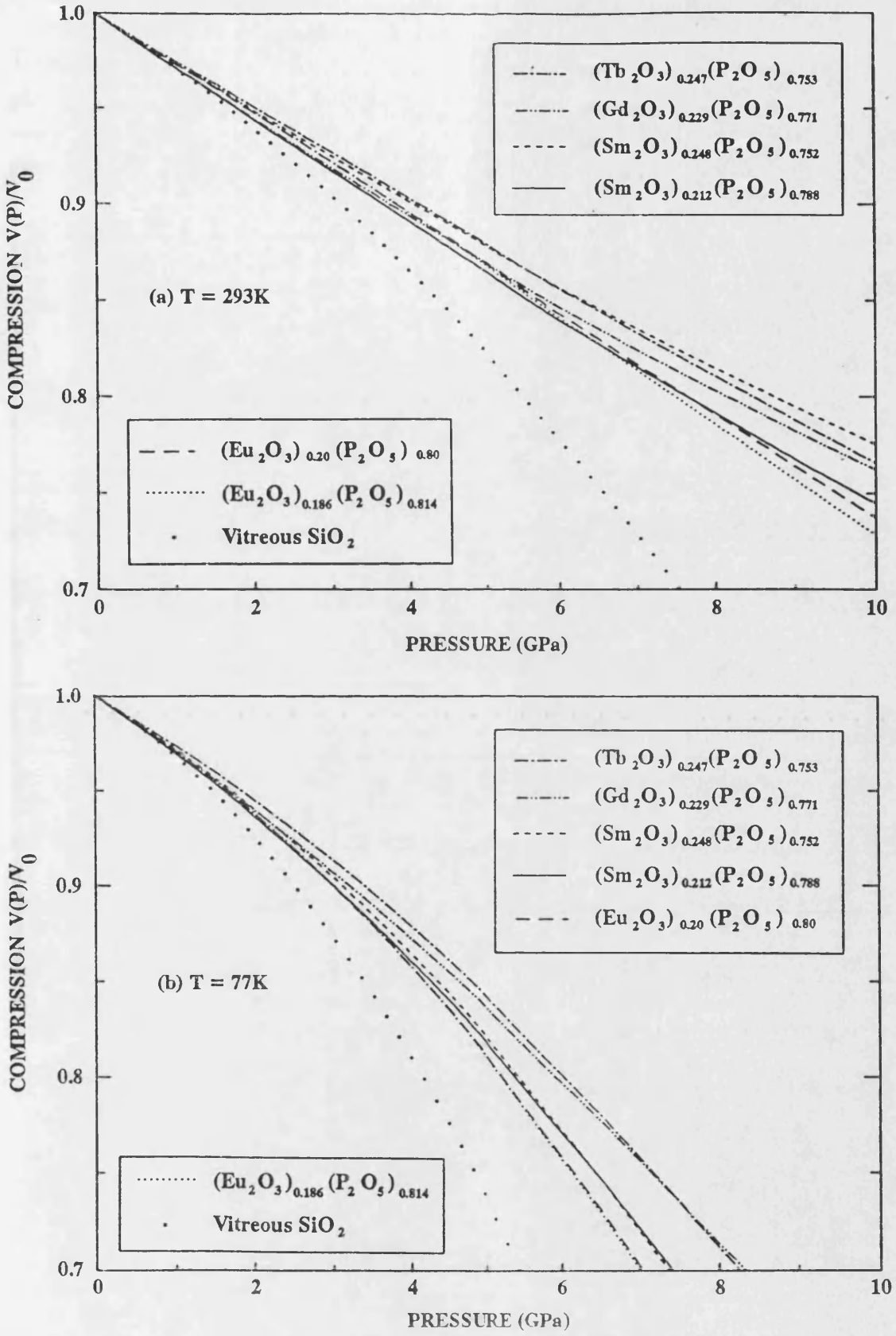

Figure 8.10. The compression $V(P)/V_o$ of phosphate glasses and vitreous SiO_2 at 77K and 293K extrapolated to high pressure using equations-of-states.

Table 8.9. The data used for computing the compression $V(P)/V_0$ and P_m of rare earth phosphate glasses and vitreous SiO_2.

Glasses	T (K)	B^S (GPa)	$(\partial B^S/\partial P)_{T,P=0}$	P_m (GPa)
$(La_2O_3)_{0.263}(P_2O_5)_{0.737}$	293	36.9	3.39	
$(Sm_2O_3)_{0.212}(P_2O_5)_{0.788}$	293	35.9	-0.41	87.6
	77	35.5	-5.19	6.84
$(Sm_2O_3)_{0.248}(P_2O_5)_{0.752}$	293	39.1	0.02	
	83	39.2	-7.37	5.31
$(Eu_2O_3)_{0.186}(P_2O_5)_{0.814}$	293	39.2	-1.53	25.6
	77	38.9	-8.43	5.31
$(Eu_2O_3)_{0.20}(P_2O_5)_{0.804}$	293	38.6	-1.12	34.5
	77	38.3	-7.91	4.84
$(Gd_2O_3)_{0.229}(P_2O_5)_{0.771}$	293	36.0	0.15	
	77	35.9	-3.56	10.1
$(Tb_2O_3)_{0.247}(P_2O_5)_{0.753}$	293	40.9	-0.67	61.0
	77	41.1	-5.95	6.91
Vitreous SiO_2	293	37.7	-5.99	6.30
	77	38.0	-16.3	2.33

$(\partial B^S/\partial P)_{T,P=0}$ such as europium and samarium phosphate glasses display a stronger volume effect under compression as compared to the other phosphate glasses (Figures 8.9d,e). Their compression curves increase faster than those of the glasses with positive $(\partial B^S/\partial P)_{T,P=0}$, and as the temperature is reduced to 77K, this effect is enhanced as expected (Figure 8.10b). As pressure increases, the volume compression shows more curvature (Figure 8.10b). In contrast, for phosphate glasses with positive $(\partial B^S/\partial P)_{T,P=0}$ such as cerium, praseodymium and neodymium phosphate glasses (Figures 8.9a,b,c), the compression curves show a normal dependence on pressure.

On the microscopic scale a volume compression under pressure in vitreous SiO_2 can occur in three different ways. These are: (i) rigid rotation of the linked tetrahedra, (ii) a slight distortion of the tetrahedra arising from the bond-angles changes within the tetrahedra with bond lengths remaining constant, (iii) a hardly decrease in bond length (Susman et al. 1991, Tielbürger 1992). Since phosphate glasses are built from PO_4 tetrahedra, a similar situation could prevail under pressure. Thus, when subjected to applied pressure or a temperature change, the structural change of phosphate glasses or vitreous SiO_2 may include a combination of tetrahedral distortion or tilting.

8.6 TEMPERATURE DEPENDENCES OF THE ACOUSTIC MODE GRÜNEISEN PARAMETERS AND VIBRATIONAL ANHARMONICITY

The elastic behaviour of the rare earth phosphate glasses under pressure can be investigated further by investigating the vibrational anharmonicity of the long-wavelength acoustic mode Grüneisen parameters. The measurements made down to 77K of the TOEC of the $(Eu_2O_3)_{0.186}(P_2O_5)_{0.814}$, $(Eu_2O_3)_{0.20}(P_2O_5)_{0.80}$, $(Sm_2O_3)_{0.212}(P_2O_5)_{0.788}$, $(Sm_2O_3)_{0.248}(P_2O_5)_{0.752}$, $(Gd_2O_3)_{0.229}(P_2O_5)_{0.771}$ and $(Tb_2O_3)_{0.247}(P_2O_5)_{0.753}$ glasses (Tables 8.3-8.8, Figures 8.1-8.4), enable determination of the temperature dependences of the longitudinal γ_L and shear γ_S acoustic mode Grüneisen parameters of these glasses (Figure 8.11-8.14). These are particularly instructive. They show that application of pressure

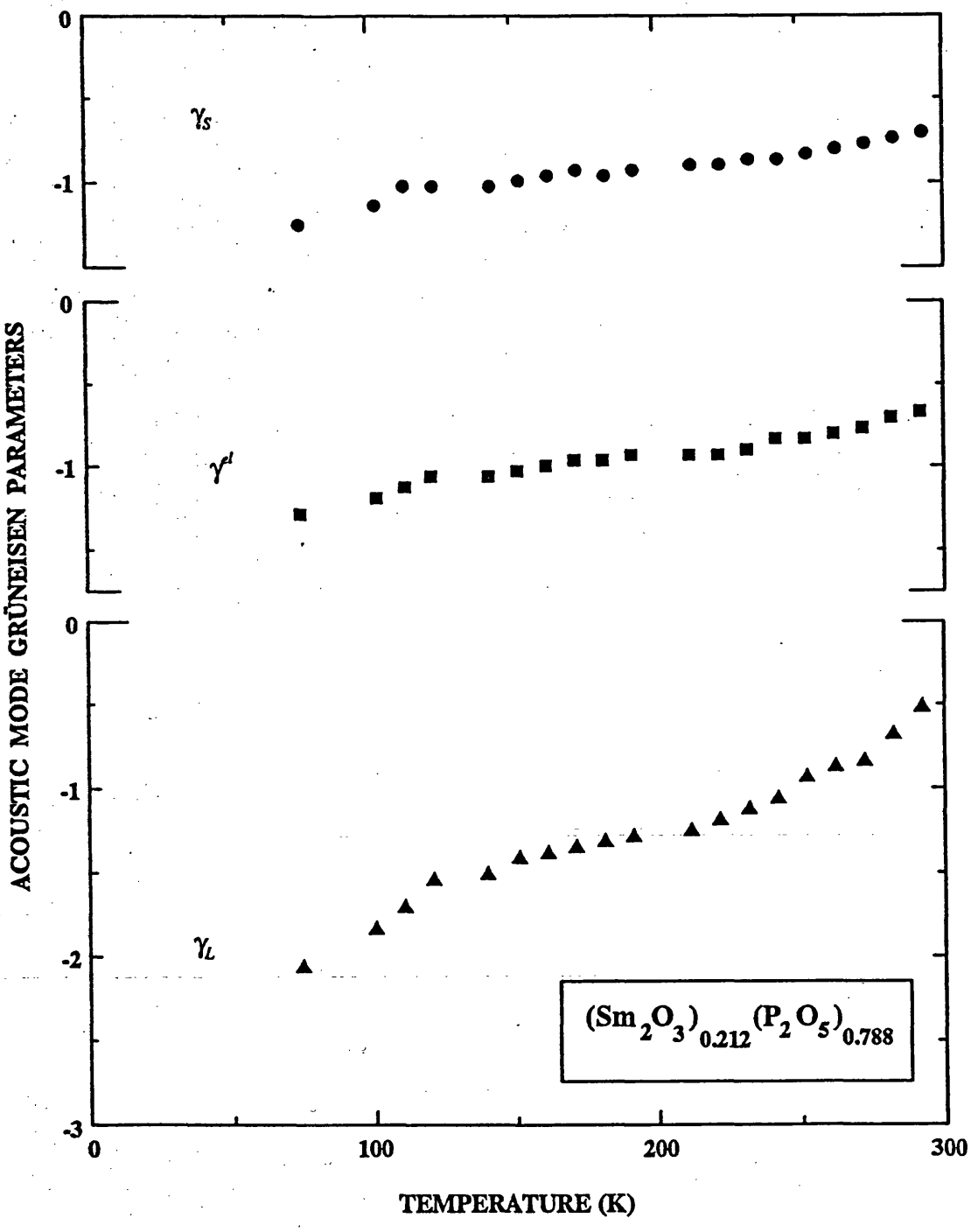

Figure 8.11(a). The temperature dependences of the acoustic mode Grüneisen parameters for $(Sm_2O_3)_{0.212}(P_2O_5)_{0.788}$ glass.

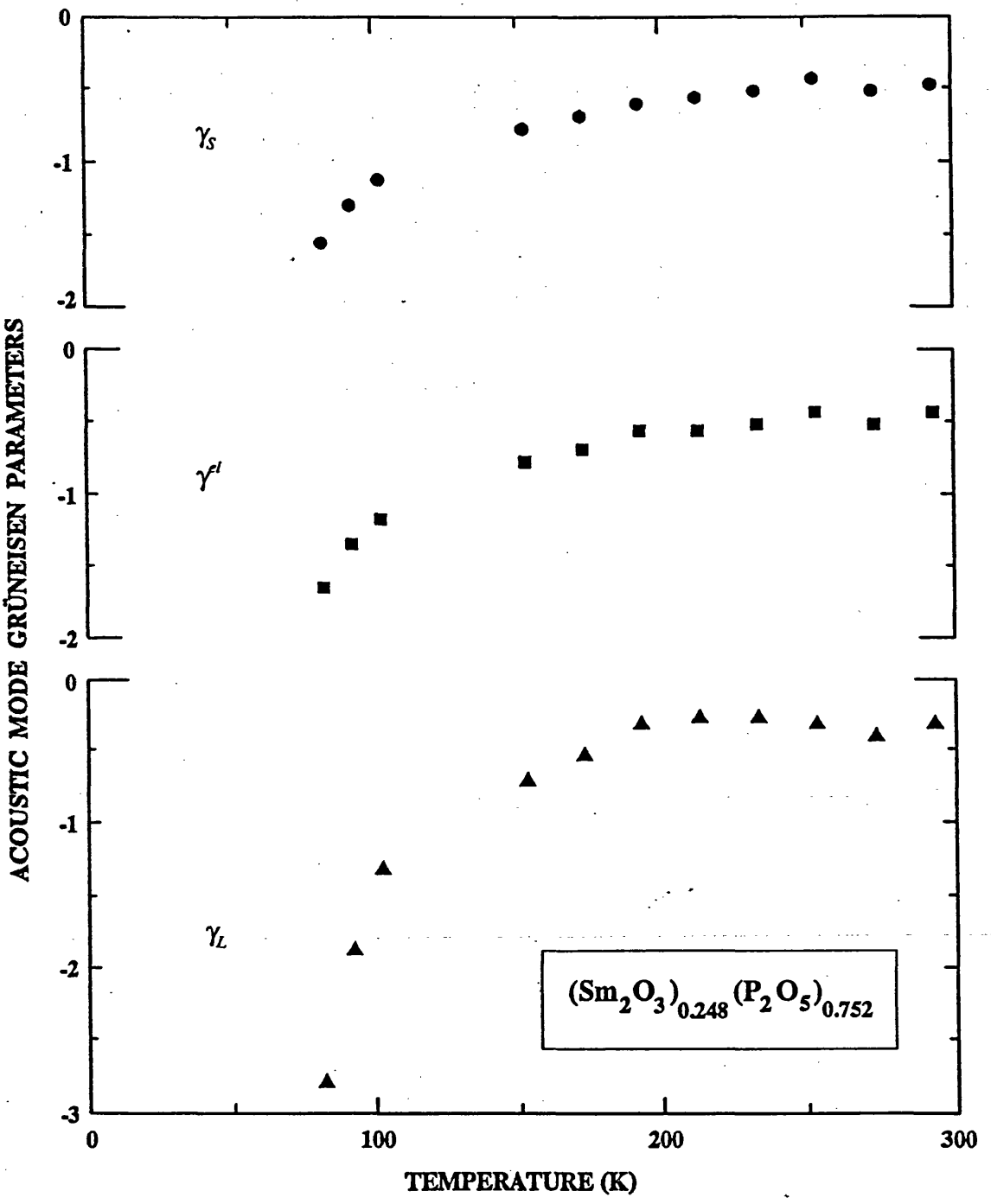

Figure 8.11(b). The temperature dependences of the acoustic mode Grüneisen parameters for $(Sm_2O_3)_{0.248}(P_2O_5)_{0.752}$ glass.

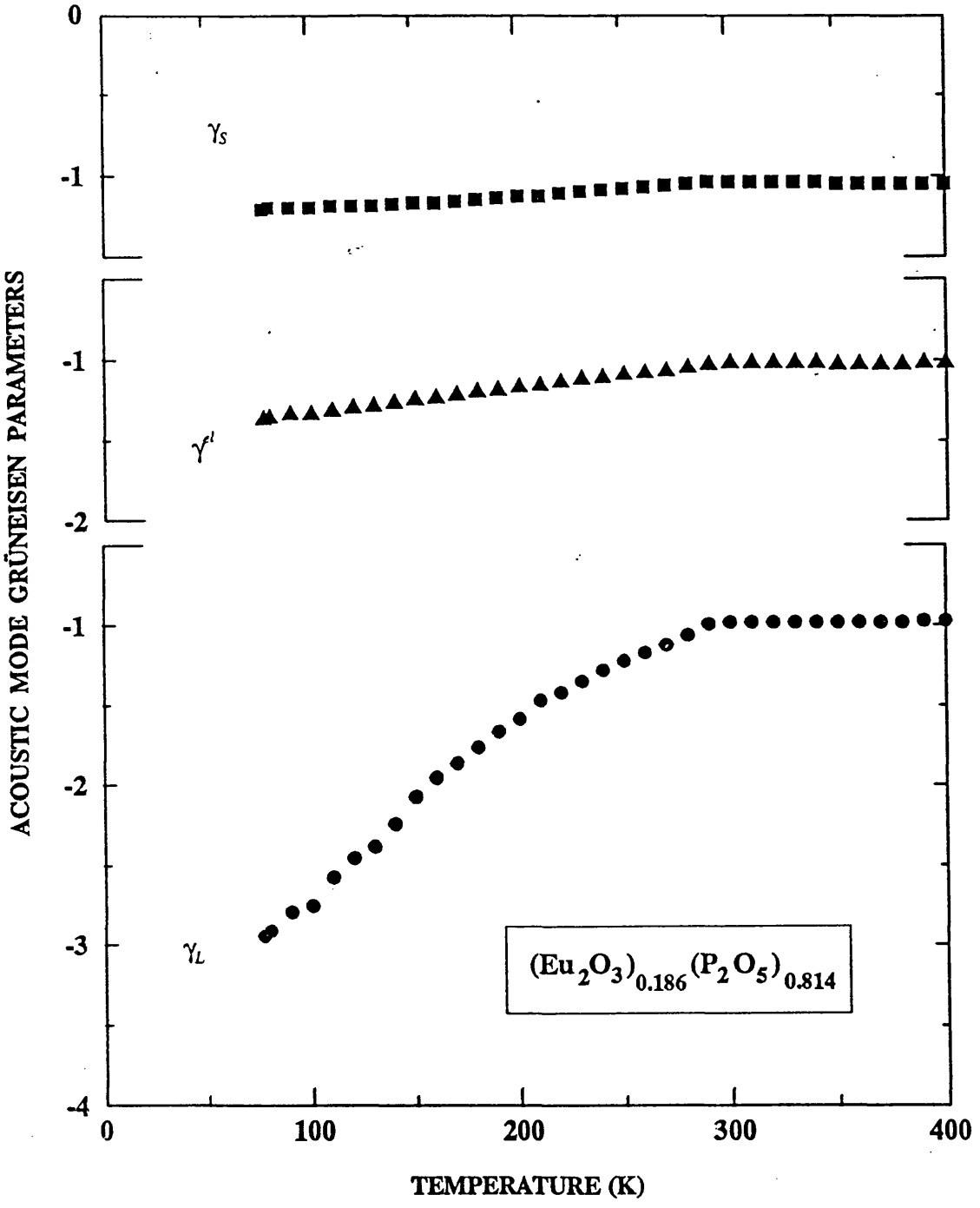

Figure 8.12(a). The temperature dependences of the acoustic mode Grüneisen parameters for $(Eu_2O_3)_{0.186}(P_2O_5)_{0.814}$ glass.

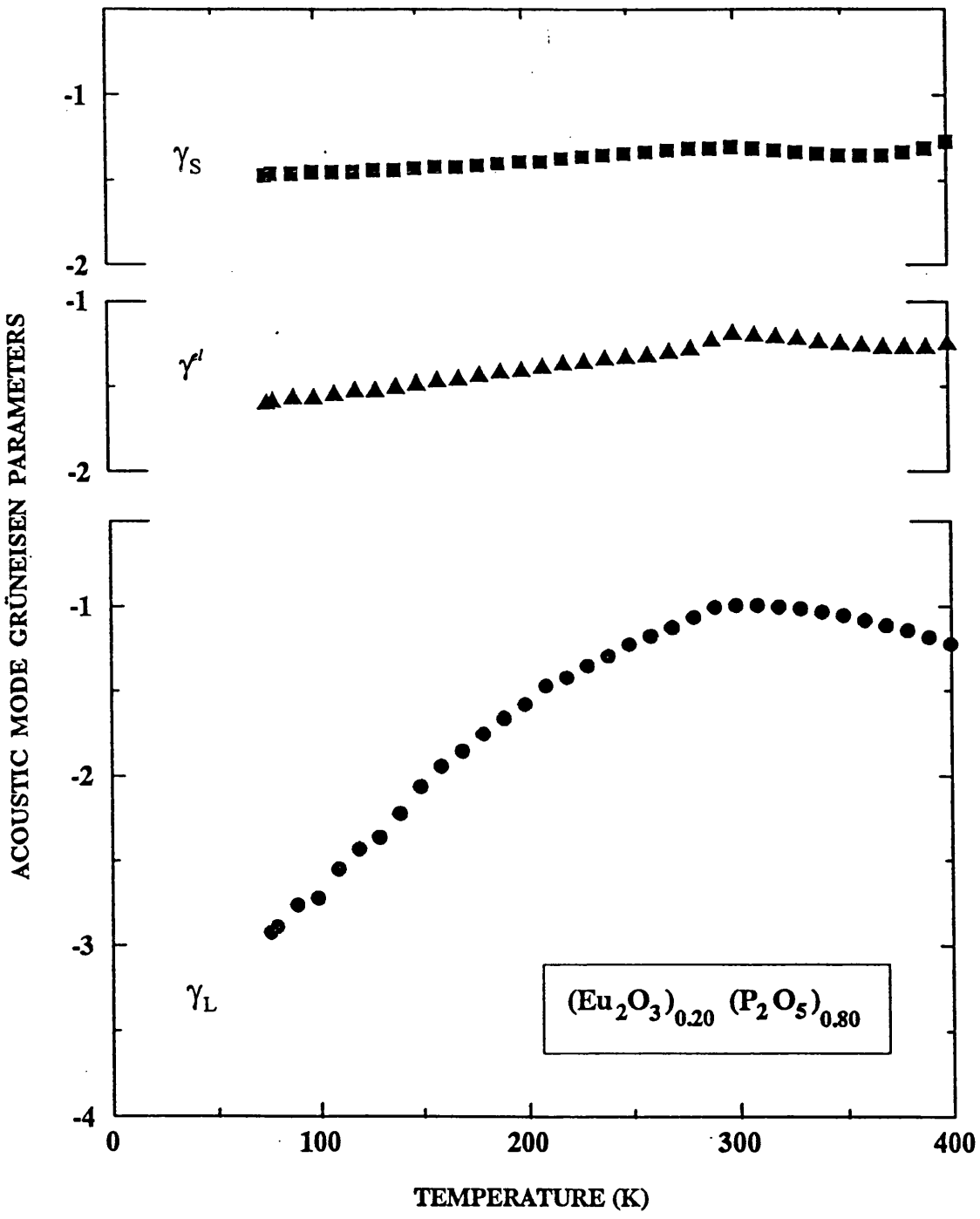

Figure 8.12(b). The temperature dependences of the acoustic mode Grüneisen parameters for $(Eu_2O_3)_{0.20}(P_2O_5)_{0.80}$ glass.

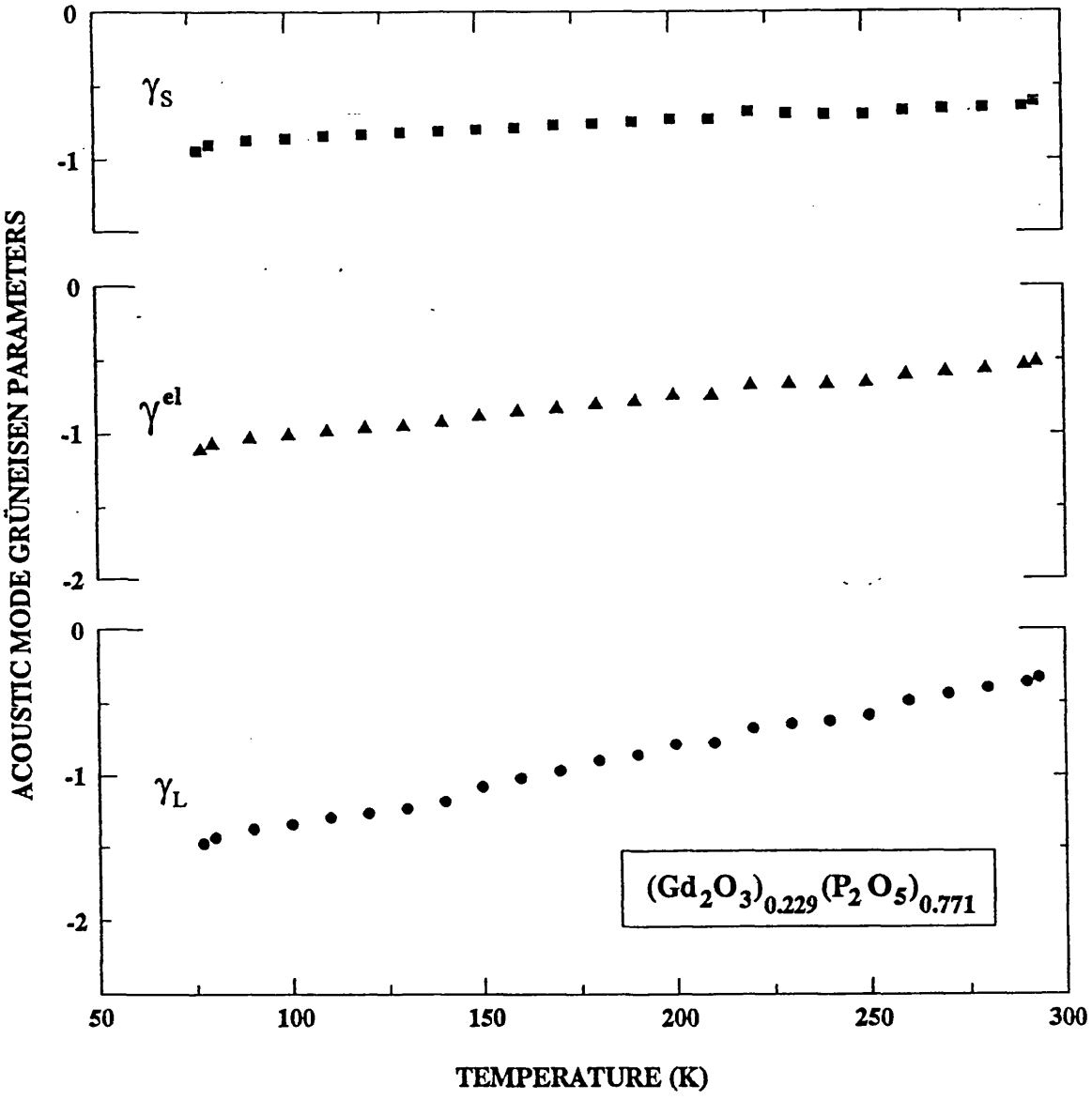

Figure 8.13. The temperature dependences of the acoustic mode Grüneisen parameters for $(Gd_2O_3)_{0.229}(P_2O_5)_{0.771}$ glass.

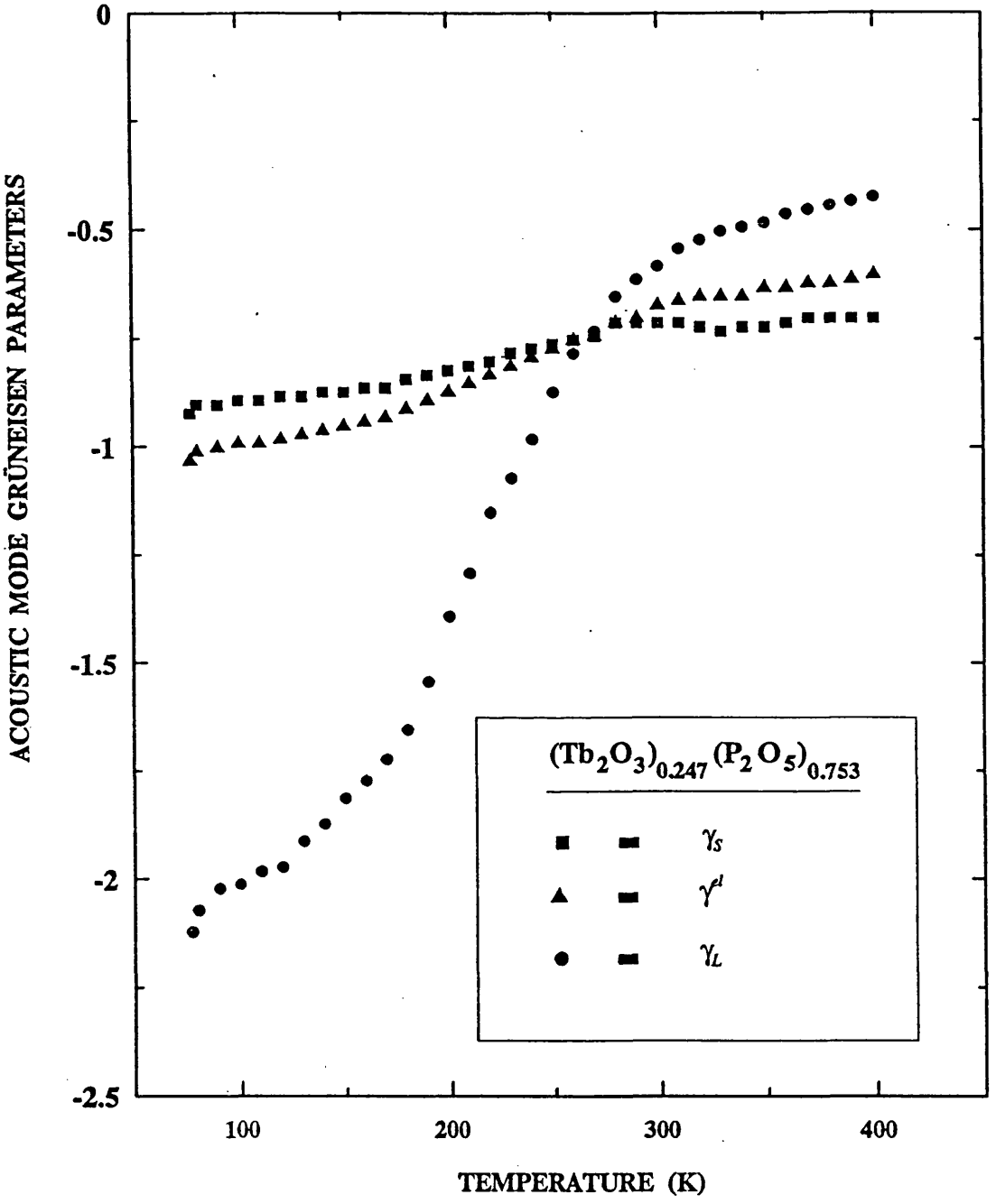

Figure 8.14. The temperature dependences of the acoustic mode Grüneisen parameters for $(Tb_2O_3)_{0.247}(P_2O_5)_{0.753}$ glass.

leads to a decrease in the frequencies, and hence vibrational energy, of the long-wavelength acoustic modes. Both types of modes soften under pressure; γ_L is substantially larger than γ_S: the longitudinal acoustic mode softening is much more pronounced than that of the shear modes. As the temperature is reduced the magnitude of γ_L gets much greater: the longitudinal acoustic mode softening becomes more enhanced at low temperatures. The shear mode γ_S does get bigger but not to the same extent. Similar behaviour has been found for vitreous SiO_2, as the temperature is reduced from 293K to 77K, and negative acoustic mode Grüneisen parameters γ_L and γ_S, the former being the larger, both increasing as the temperature decreases (see §6.7 in Chapter 6). However, this unusual vibrational anharmonicity of the long-wavelength acoustic modes is not a general characteristic of amorphous materials: vitreous TeO_2, the only glass with more normal elastic properties whose nonlinear elastic properties have as yet been studied as a function of temperature, has negative TOEC and its γ_L and γ_S are positive and do not vary much with temperature (Benbattouche et al. 1989). Above room temperature the acoustic mode gammas are almost independent of temperature for the $(Eu_2O_3)_{0.186}(P_2O_5)_{0.814}$, the $(Eu_2O_3)_{0.20}(P_2O_5)_{0.80}$ and the $(Tb_2O_3)_{0.20}(P_2O_5)_{0.80}$ glasses (Figures 8.12 and 8.14): the acoustic mode vibrational anharmonicities do not change much at higher temperatures.

The thermal expansion is also related to vibrational anharmonicity. The thermal Grüneisen parameter γ^h is related to the linear coefficient of thermal expansion, compressibility and also the specific heat. All excited modes contribute to the thermal expansion, γ^h resulting from summation over the excited vibrational states including the long-wavelength acoustic modes. At low temperatures, both the γ_L and γ_S mode Grüneisen parameters are negative for each of the glasses studied: application of pressure leads to a decrease in the mode frequencies, and hence in their vibrational energy. As a result the mean long-wavelength acoustic mode Grüneisen parameter γ^l is also negative intimating that the net contribution from the long-wavelength acoustic

phonon modes to the thermal expansion should be negative. This property has been investigated by Wang et al. (1990) for $(Sm_2O_3)_{0.212}(P_2O_5)_{0.788}$ glass but remains unexplored for the rest of these vitreous rare earth phosphates.

The thermal expansion coefficient of $(Sm_2O_3)_{0.212}(P_2O_5)_{0.788}$ glass is quite small and positive ($\sim +4.3 \times 10^{-6} K^{-1}$) at room temperature, decreases rapidly as the temperature is reduced and changes sign at about 120K (Wang et al. (1990). The finding that γ_L, γ_S and γ' are negative and become larger when the temperature is reduced, is consistent with the behaviour of the thermal expansion with temperature. Plausibly the small value for the thermal expansion comes about as a result of summation over the effects of modes with different Grüneisen parameter signs. As the temperature is lowered the low-energy, long-wavelength acoustic phonons with negative Grüneisen parameters provide an increasingly greater proportion of the phonon population and a progressively larger contribution to the thermal expansion so that it becomes negative at low temperature.

Glasses appear to include three groups of excess excitations in addition to sound waves: (i) harmonic modes in the range 200GHz to 1THz, (ii) a relaxation contribution to the excitation spectrum, (iii) tunnelling or two-level states (Buchenau et al. 1988). There is evidence to support (Buchenau et al. 1988) a common interpretation (Ignatiev et al. 1983) of these low-frequency excitations in vitreous SiO_2 in terms of thermally activated relaxation processes. In the case of Sm^{3+} phosphate glasses the ultrasonic attenuation as a function of temperature shows a broad peak in the range above 20K (Carini et al. 1990a), characteristic of many vitreous materials, including those of phosphate glasses studied here. Excitations arising from thermally activated motions of relaxing "particles" over potential barriers are believed to be the cause of this acoustic attenuation peak. These samarium phosphate glasses also show an excess of quasi-elastic contribution to the Raman scattering, which is superimposed on the low frequency part of the disordered induced one-phonon scattering (Carini et al. 1993).

This general effect has been attributed by Jäckle (1981) to the structural relaxation of a population of defects with different polarisability, which are usually represented in terms of symmetric double-well potentials. The rare earth phosphate glasses show this acoustic attenuation peak above 20K (see § 7.3 in chapter 7).

Application of pressure induces decreases in the elastic stiffnesses of vitreous SiO_2 (Bogardus 1965, Shull 1969) similar to those observed for the Sm^{3+}, Eu^{3+}, Gd^{3+} and Tb^{3+} phosphate glasses (Figures 8.5-8.8). Furthermore the TOEC of vitreous SiO_2 are positive and increase strongly as the temperature is decreased (Wang et al. 1992) in a similar way to the TOEC of these Sm^{3+}, Eu^{3+}, Gd^{3+} and Tb^{3+} phosphate glasses (Figures 8.1-8.4). As a consequence both types of glass have negative long-wavelength acoustic phonon Grüneisen parameters. Although common to vitreous silicates and rare earth phosphates, this unusual behaviour of the vibrational anharmonicity of the long-wavelength acoustic modes is not a general characteristic of amorphous materials: other glasses, including vitreous arsenic (Brassington et al. 1980), As_2S_3 (Brassington et al. 1981a) and TeO_2 (Benbattouche et al. 1989) show positive $(\partial C_{11}^S/\partial P)_{T,P=0}$ and, correspondingly, negative TOEC and positive γ_L and γ_S.

In the case of vitreous SiO_2 the pressure-induced, acoustic mode softening effects have been attributed to nonlinear acoustic contributions from bending vibrations of the bridging oxygen atoms which correspond to transverse motion against small force constants and are allowed in the open structure based on SiO_4 tetrahedra (Sato and Anderson 1980, Lambson et al. 1984); another possible source is rotations of coupled SiO_4 tetrahedra involved in low-frequency harmonic vibrations (Buchenau et al. 1988, Guttmann and Rahman 1986). It is possible that similar nonlinear effects in vibrational modes associated with the linked PO_4 tetrahedra could be responsible for the elastic anomalies of Sm^{3+}, Eu^{3+}, Gd^{3+}, Tb^{3+}, Dy^{3+}, Ho^{3+} and also Er^{3+} phosphate glasses. Thus either bending vibrations of the bridging oxygen ions or rotations of coupled PO_4 tetrahedra could be the origin of the acoustic mode softening under pressure.

The structure of binary metaphosphates is based on linked PO_4 tetrahedra (Sales et al. 1986, Martin 1991). Metaphosphate glasses, containing ions such as sodium, seem to form chains of PO_4 tetrahedra, which are connected at two corners and have two non-bridging oxygen atoms (see § 2.6 in Chapter 2). The rare earth ions present in phosphate glasses are strictly trivalent as recently shown by Prof. B. Rainford (private communication), with exception of praseodymium and cerium phosphate glasses that may contain tetravalent metal cation. Bending vibrations of the bridging oxygen ions or rotations of coupled PO_4 tetrahedra could be the origin of the acoustic mode softening under pressure. However if this explanation were correct, then other phosphate glasses should also show negative values for the hydrostatic pressure derivatives $(\partial C_{11}^S/\partial P)_{T,P=0}$ and $(\partial C_{44}^S/\partial P)_{T,P=0}$ of the elastic stiffnesses and $(\partial B^S/\partial P)_{T,P=0}$ of the bulk modulus. By no means all do: the pressure derivatives $(\partial C_{11}^S/\partial P)_{T,P=0}$ and $(\partial B^S/\partial P)_{T,P=0}$ of phosphate glasses containing lanthanum (Sidek et al. 1988), cerium, praseodymium, neodymium, iron (Brassington et al. 1981b) and molybdenum (Comins et al. 1987) have the normal positive values. These glasses could have unrecognised subtle structural features different from those of rare earth phosphate glasses.

The TOEC data yield negative ultrasonic mode Grüneisen parameters confirming that application of pressure induces a decrease in the long-wavelength acoustic phonon mode frequencies. As the temperature is reduced the pressure-induced mode softening becomes enhanced. The hydrostatic pressure derivative $(\partial C_{11}^S/\partial P)_{T,P=0}$ is larger than $(\partial C_{44}^S/\partial P)_{T,P=0}$ over the whole temperature range, and the longitudinal acoustic mode Grüneisen parameter $|\gamma_L|$ is larger than that $|\gamma_S|$ of the shear wave: the longitudinal mode softens more with pressure than the shear mode. The vibrational anharmonicity of the acoustic modes plays an important part in causing the thermal expansion of $(Sm_2O_3)_{0.212}(P_2O_5)_{0.788}$ glass to be negative below 120K (Wang et al. 1990). This behaviour is in marked contrast to that of lanthanum phosphate glasses which show normal elastic response to pressure (Sidek et al. 1988). Yet the Raman spectra of both

La^{3+}, Sm^{3+} (Mierzejewski et al. 1988b) and Eu^{3+} (Farok et al. 1994) phosphate glasses are similar, indicating that their structures are practically the same: the differences between their elastic behaviour under pressure and as a function of temperature are not likely to be due to gross structural dissimilarities.

The physical origin of the anomalous negative values obtained for the hydrostatic pressure derivatives $(\partial C_{11}^S/\partial P)_{T,P=0}$ and $(\partial C_{44}^S/\partial P)_{T,P=0}$ of the elastic stiffnesses and $(\partial B^S/\partial P)_{T,P=0}$ of the bulk modulus and the positive values for the corresponding TOEC combinations and the negative acoustic mode Grüneisen parameters γ_L and γ_S of the rare earth phosphate glasses and vitreous SiO_2 remains uncertain. Both the rare earth elements europium and samarium, and probably terbium, can show pressure varying, volume sensitive, mixed valence - a possible explanation (Mierzejewski et al. 1988a,b, Senin et al. 1993). However, the recent laser-induced fluorescence studies of europium phosphate (Farok et al. 1994) were unable to establish the presence of divalent europium ion in sufficient quantities to produce the observed large elastic anomalies. This is also the case in the samarium phosphate glasses (Farok et al. 1992). Mixed valence is not the cause of the anomalous acoustic vibrational anharmonicity.

It is plausible that the anomalous elastic behaviour under pressure of the vitreous europium and samarium phosphates could result from previously unrecognised subtle structural features different from those of the other phosphate glasses, which have been studied to date. The fluorescence of the europium phosphate glasses is consistent with presence of two distinct sites close in energy for the Eu^{3+} ions (Farok et al. 1994). These sites could comprise the double-well system required to explain the elastic and nonlinear acoustic vibrational properties of these glasses. Resolution of the problem of whether the origin of these effects is associated with a structural feature must await the results of structural studies of rare earth phosphate glasses.

CHAPTER 9

THE EFFECTS OF SAMARIUM AND LANTHANUM MODIFIERS ON THE ACOUSTIC AND THERMAL PROPERTIES OF PHOSPHATE GLASSES

9.1 INTRODUCTION

The purpose of this chapter is to discuss the effect of samarium and lanthanum ions in phosphate glasses on the elastic behaviour under pressure and the influence of low-energy vibrational states to the acoustic and thermal properties of these glasses at much lower temperatures.

The elastic and nonlinear acoustic properties of phosphate glasses which have been intensively investigated were presented in Chapter 7 and 8. The most remarkable result of these investigations was the discovery of differences in the elastic behaviour under pressure. The lanthanum, praseodymium, cerium and neodymium phosphate glasses show normal elastic behaviour. The applications of hydrostatic pressure and uniaxial stress increase the ultrasonic wave velocities, the TOEC are mostly negative - the usual elastic response to pressure. By contrast, samarium, europium and terbium phosphate glasses show anomalous elastic behaviour under pressure. The TOEC are mostly positive; as a consequence, the hydrostatic pressure derivatives $(\partial C_{11}^S/\partial P)_{T,P=0}$ and $(\partial C_{44}^S/\partial P)_{T,P=0}$ and the long-wavelength acoustic mode Grüneisen parameters γ_L and γ_S are negative. Thus, the long-wavelength acoustic phonons soften under pressure. As a result, these phosphate glasses have a negative hydrostatic pressure derivative $(\partial B^S/\partial P)_{T,P=0}$ of the adiabatic bulk modulus B^S: when subjected to high pressures, they have the remarkable property of becoming easier to squeeze.

Lanthanum and samarium phosphate glasses display pronounced dissimilarity in the nonlinear acoustic properties and are the most studied rare earth phosphate glasses up until now (Mierzejewski et al. 1988a,b, Sidek et al. 1988, Wang et al. 1990, Carini

et al. 1990a,b). Therefore binary and ternary glasses containing samarium and lanthanum as network modifiers have been selected for a comparative study of their elastic behaviour under pressure.

A comparative study of the elastic behaviour of ternary $(La_2O_3)_x(Sm_2O_3)_y(P_2O_5)_{1-x-y}$ glasses and those of the binary $(La_2O_3)_x(P_2O_5)_{1-x}$ and $(Sm_2O_3)_x(P_2O_5)_{1-x}$ glasses has been made. The objective has been to find out whether the elastic properties under pressure change systematically when lanthanum replaces samarium. To achieve this, measurements at room temperature have been made on the effect of hydrostatic pressure up to 0.15GPa on the velocity of ultrasonic waves propagated in binary La_2O_3-P_2O_5 and Sm_2O_3-P_2O_5 and ternary La_2O_3-Sm_2O_3-P_2O_5 glasses. The experimental results provide details of the hydrostatic pressure derivatives of the elastic stiffnesses and bulk modulus. The SOEC and their hydrostatic pressure derivatives at room temperature have been used to determine the long-wavelength acoustic mode Grüneisen parameters. The results provide a quantitative description of the vibrational anharmonicity of the long-wavelength acoustic phonons of these binary and ternary lanthanum-samarium phosphate glasses.

Further acoustic and thermal investigations at much lower temperatures have been made to study the nature of the low-energy vibrational states in rare earth phosphate glasses. Measurements have been made of the attenuation and velocity of ultrasonic waves propagated in La_2O_3-P_2O_5 and Sm_2O_3-P_2O_5 glasses with different lanthanide concentrations as a function of temperature between 1.5K and 400K (Carini et al. 1994a). In the case of the ternary La_2O_3-Sm_2O_3-P_2O_5 system, the velocity of ultrasonic waves propagated has been measured from 10K to 350K. Specific heat measurements have been performed for Sm_2O_3-P_2O_5 glasses in the temperature range 1.5K to 30K. The ultrasonic wave attenuation has been interpreted by Carini et al. (1994a) using the thermally activated structural relaxation model of Jäckle (1972) (see §7.3 in Chapter 7). The recent soft-potential model (SPM) which postulates that the low-temperature

anomalies of glasses arise as a result of two-level systems (TLS) and soft harmonic oscillators (HO) (Parshin 1993) (see §2.9 in Chapter 2) has been used to interpret (Carini et al. 1994a) the ultrasonic wave velocity below 100K. The results obtained are in accord with the hypothesis of a common origin for distinct attenuation anomalies found in the low and high temperature regions. Moreover, the same mechanisms appear to regulate both the acoustic attenuation and the ultrasound wave velocity at temperature below 50K as predicted by SPM. A large contribution to the specific heat, well above what be expected from acoustic phonons (in the Debye approximation), has been discussed (Carini et al. 1990b) in terms of the theoretical predictions of a phonon-fracton cross-over approach (Orbach 1986). The phonon-fracton density of states used to fit the excess specific heat gives rise to model parameters having the same magnitudes as those found previously for a wide range of glasses.

9.2 EXPERIMENTAL DETAILS

The measurements of the ultrasonic wave attenuation and velocities of $(Sm_2O_3)_x(P_2O_5)_{1-x}$ and $(La_2O_3)_x(P_2O_5)_{1-x}$ between 1.5K and 400K and the specific heat of $(Sm_2O_3)_x(P_2O_5)_{1-x}$ glasses between 1.5K and 30K have been carried out at the University of Messina, Italy (Prof. G. Carini and Prof. G.A. Saunders - private communication) and the details have been given in Carini et al. (1994a, 1994b). Measurements of ultrasonic wave velocity over the temperature range of 10 to 300K and under the effect of hydrostatic pressure at room temperature have been carried out here at the University of Bath, using the techniques described in Chapter 5.

9.3 THE ELASTIC BEHAVIOUR UNDER PRESSURE AT ROOM TEMPERATURE

A comparison of the nonlinear acoustic vibrational properties of binary and ternary lanthanum and samarium phosphate glasses measured at room temperature is presented

in Table 9.1. The data show that the ternary glasses display intermediate pressure dependences to those of the binary lanthanum and samarium phosphate glasses.

Table 9.1. A comparison of the nonlinear acoustic properties at room temperature (293K) of the ternary La^{3+}-Sm^{3+} glasses with those of the binary La^{3+} and Sm^{3+} phosphate glasses.

Glass	$(La_2O_3)_x$ $(P_2O_5)_{1-x}$ [1]	$(La_2O_3)_x(Sm_2O_3)_y(P_2O_5)_{1-x}$		$(Sm_2O_3)_x(P_2O_5)_{1-x}$ [2]	
Mole fraction x	x=0.263	x=0.055 y=0.206	x=0.166 y=0.086	x=0.190	x=0.248
Pressure derivatives					
$(\partial C_{11}^S/\partial P)_{P=0}$	3.56	0.08	1.50	-0.75	-0.46
$(\partial C_{44}^S/\partial P)_{P=0}$	0.13	0.02	0.06	-0.52	-0.36
$(\partial B_0^S/\partial P)_{P=0}$	3.39	0.05	1.43	-0.06	0.02
Long-wavelength acoustic mode Grüneisen parameters					
γ_L	0.80	-0.14	0.26	-0.36	-0.29
γ_S	-0.06	-0.15	-0.12	-0.55	-0.46
γ^{el}	0.23	-0.15	0.01	-0.49	-0.45

[1] Sidek et al. (1988), [2] Mierzejewski et al. (1988a).

An instructive result is that in ternary $(La_2O_3)_{0.055}(Sm_2O_3)_{0.206}(P_2O_5)_{0.739}$ and $(La_2O_3)_{0.166}(Sm_2O_3)_{0.086}(P_2O_5)_{0.748}$ glasses the hydrostatic pressure derivatives $(\partial C_{IJ}^S/\partial P)_{T,P=0}$ and $(\partial B^S/\partial P)_{T,P=0}$ have positive values. Thus, unlike the binary samarium

phosphate glasses, the ternary lanthanum-samarium phosphate glasses stiffen in the normal manner under pressure: the bulk modulus $\dot{B}(P)$ becomes larger as the pressure is increased. The ternary $(La_2O_3)_x(Sm_2O_3)_y(P_2O_5)_{1-x-y}$ glasses, like the $(La_2O_3)_x(P_2O_5)_{1-x}$ glasses but in sharp distinction from the $(Sm_2O_3)_x(P_2O_5)_{1-x}$ glasses, become harder to squeeze under pressure in the more usual way.

The long-wavelength acoustic mode Grüneisen parameters of the ternary $(La_2O_3)_x(Sm_2O_3)_y(P_2O_5)_{1-x-y}$ glasses also display an intermediate situation between those of the binary glasses. The longitudinal γ_L and shear γ_S acoustic mode Grüneisen parameters are shifted in the positive direction. Application of pressure causes the long-wavelength acoustic mode frequencies and energies associated with these mode to increase slightly. Thus, in the ternary lanthanum-samarium phosphate glasses replacement of samarium by lanthanum cancels the mode softening effect.

9.4 THE TEMPERATURE DEPENDENCES OF ULTRASONIC WAVE ATTENUATION

The work described in this section was carried out at the University of Messina, Italy by a group headed by Prof. G. Carini assisted by Prof. G.A. Saunders. It was carried out on the glasses prepared and analysed by the present author. It has been submitted for publication in a paper entitled 'The Effects of Lanthanide ion Modifiers on the Local Motion of Relaxing Particles in Phosphate Glasses' by 'G. Carini, G. D'Angelo G, M. Federico, G. Tripodo, G.A. Saunders and H.B. Senin'. As this work extends the knowledge of the ultrasonic and vibrational properties of the rare earth phosphate glasses studied to much lower temperature, it forms a natural addition to the experimental work described in the thesis and so is included here.

The temperature dependence from 1.5K to 400K of the ultrasonic attenuation of the $(La_2O_3)_{0.263}(P_2O_5)_{0.737}$ glass at selected frequencies is shown in Figure 9.1. As the temperature is increased from 1.5K, the attenuation rises until it reaches a plateau which

extends up to about 10K. Above this region the attenuation increases up towards a broad peak, typical of oxide glasses, whose maximum shifts to higher temperatures as the ultrasonic driving frequency is increased. To illustrate the effects of lanthanide ion concentration, the temperature dependence of the attenuation of 70MHz ultrasonic waves for the $(Sm_2O_3)_{0.190}(P_2O_5)_{0.810}$ and $(Sm_2O_3)_{0.248}(P_2O_5)_{0.752}$ glasses are compared in Figure 9.2. It can be seen that the low-temperature attenuation, up to and including the plateau, and that across the temperature range spanned by the broad peak are decreased with increasing concentration of the Sm^{3+} ion.

A particularly interesting feature of the results is that the differences in attenuation between the $(Sm_2O_3)_{0.190}(P_2O_5)_{0.810}$ and $(Sm_2O_3)_{0.248}(P_2O_5)_{0.752}$ glasses are similar for the low-temperature tunnelling plateau and the higher temperature relaxation peak (Figure 9.2). This implies that the same centres are responsible for both the tunnelling and high temperature classical relaxation effects. The view has been cogently expressed by Phillips (1990) who gave a theoretical construct of the temperature dependence of the acoustic loss, linking both the one phonon-assisted tunnelling and classical relaxation rates. The forms of the experimental curves obtained for the temperature dependences of the attenuation of both the La^{3+} (Figure 9.1) and Sm^{3+} (Figure 9.2) phosphate glasses exhibit a marked resemblance to the theoretical curves given by Phillips (1990) as shown in Figure 9.4.

Attenuation measurements have also been made for both longitudinal and shear ultrasonic waves. This was done to find out if the attenuation mechanism was different for the two mode polarisations. To make the comparison, the attenuation has been transformed into the internal friction Q^{-1} ($= \alpha\lambda/\pi$). The results obtained at a frequency of 30MHz are plotted in Figure 9.3. Within the experimental error, the internal friction for both the longitudinal and shear modes is the same.

The ultrasonic attenuation as a function of temperature of these glasses shows the two distinct regions that are characteristic of many oxide glasses.

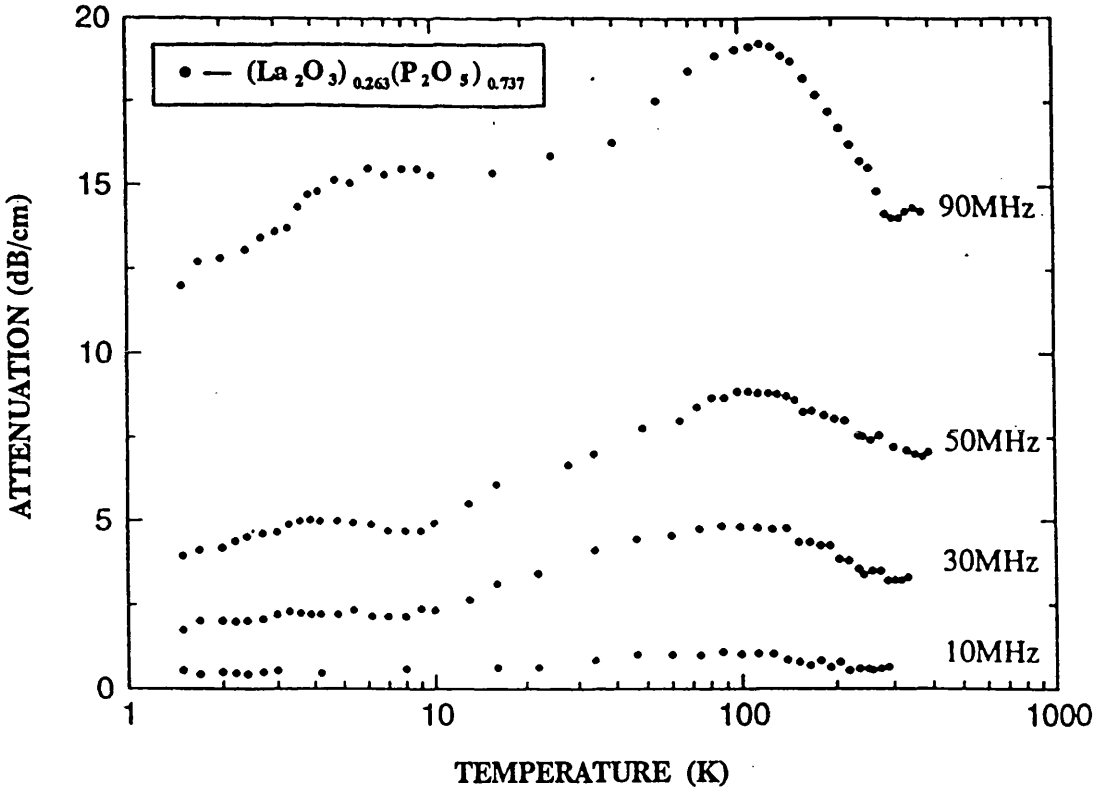

Figure 9.1. The temperature dependence of the ultrasonic attenuation at selected driving frequencies in the $(La_2O_3)_{0.263}(P_2O_5)_{0.737}$ glass (after Carini et al. 1994a).

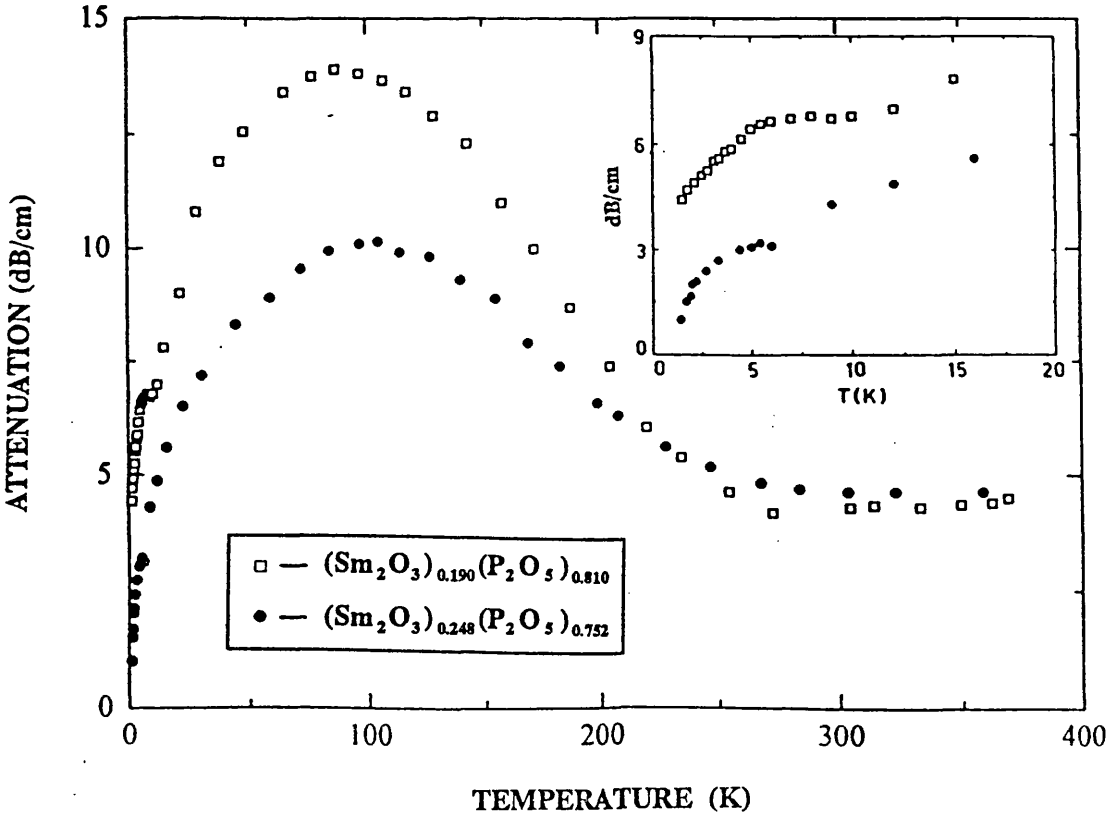

Figure 9.2. The effect of samarium ion concentration on the temperature dependence of the ultrasonic attenuation shown by Sm^{3+} phosphate glasses (after Carini et al. 1994a).

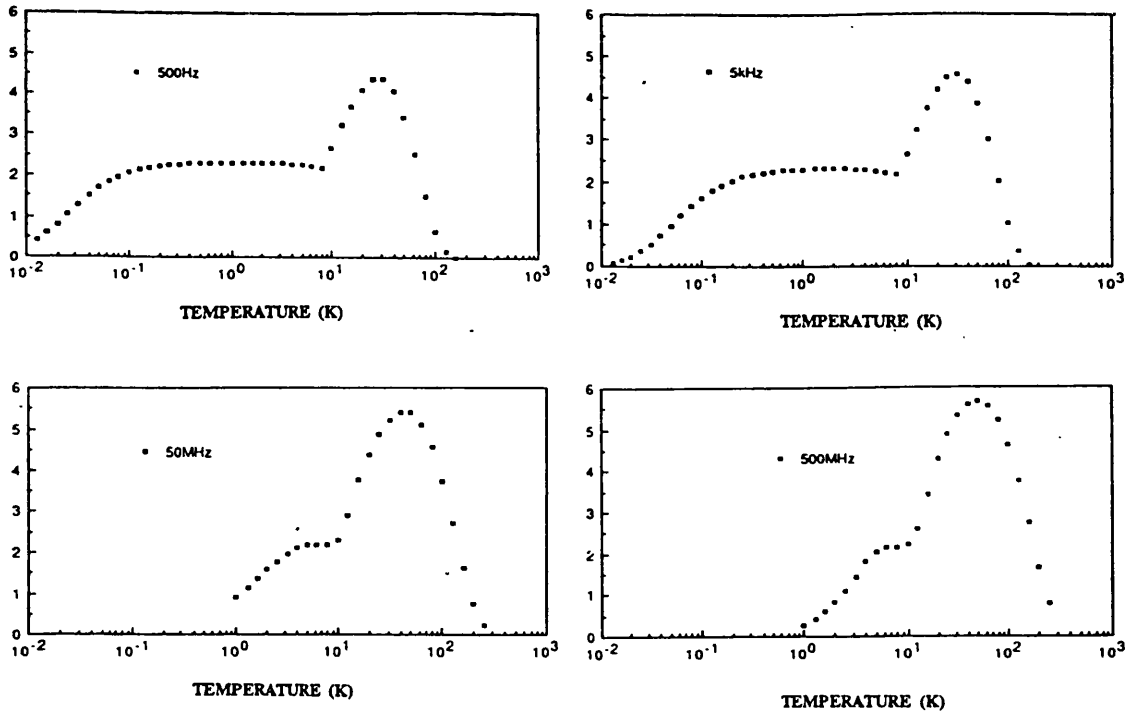

Figure 9.3. Calculated values of the acoustic loss in vitreous SiO_2 at 500Hz, 5kHz, 50MHz and 500MHz (after Phillips 1990).

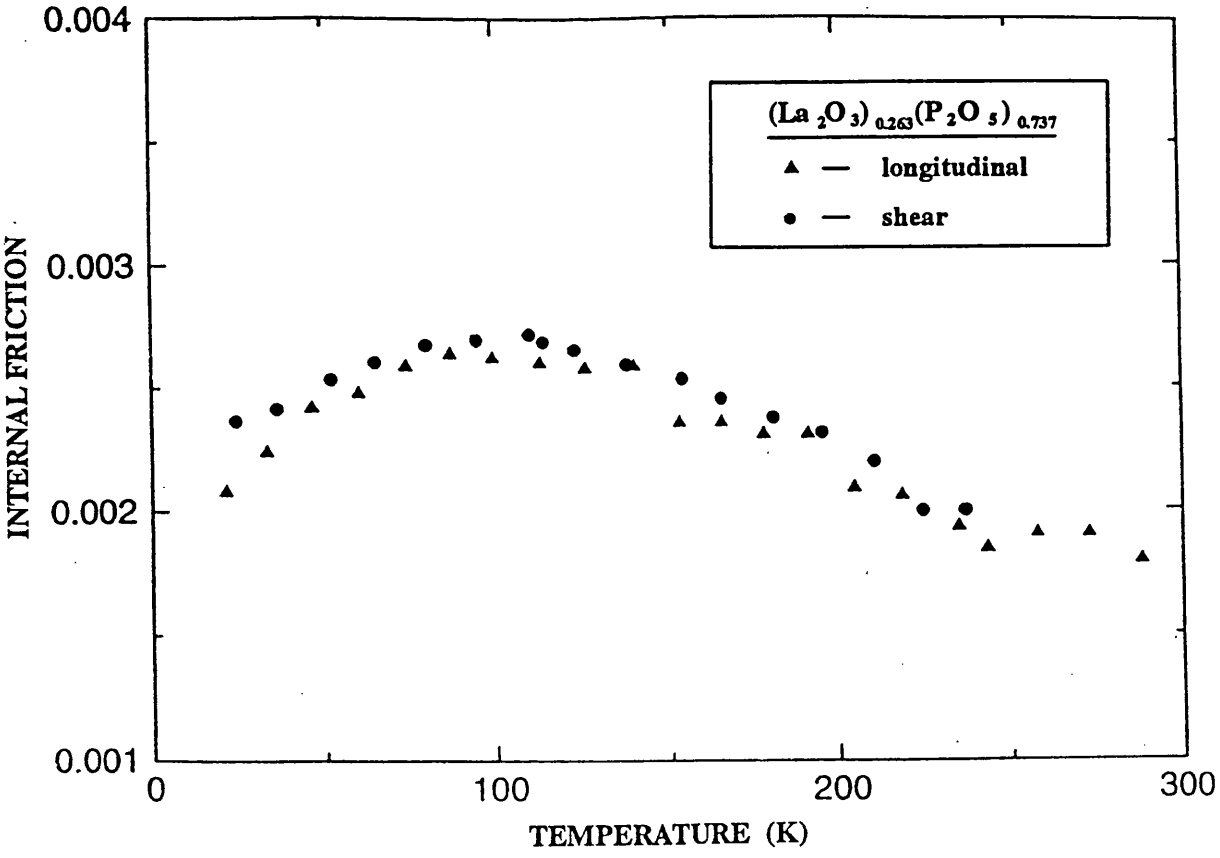

Figure 9.4. Comparison between the internal friction for longitudinal and shear 30MHz ultrasonic waves in the $(La_2O_3)_{0.263}(P_2O_5)_{0.737}$ glass (after Carini et al. 1994a).

(i) At temperatures below about 15K, the temperature dependence of the attenuations of both the La^{3+} (Figure 9.1) and Sm^{3+} (Figure 9.2) phosphate glasses are defined by a plateau. The existence of such a plateau was predicted by Jäckle (1972) from his theoretical study of the phonon-assisted tunnelling in two-level systems. The mechanism involves the interaction of the acoustic wave with the two-level systems and modifies their thermal equilibrium population so that a new equilibrium distribution is attained by the cooperation of thermal phonons in a characteristic relaxation time T_1. In fact, due to the structural randomness of a glass, there is a distribution of relaxation times. In the high temperature limit, when $\omega T_1^{min} \ll 1$ (T_1^{min} being the minimum value of the relaxation time), the attenuation for both longitudinal and shear ultrasonic wave of frequency ω is given by (Jäckle 1972)

$$\alpha = \pi \left[\frac{\overline{P}\gamma^2}{2\rho v^3} \right] \omega = \frac{\pi}{2v} C\omega \qquad (9.1)$$

Here v is the ultrasound velocity, γ the deformation potential, $\overline{P}$ the two-level system density of states and ρ the sample density. The plateau position shifts to higher temperatures with increasing ultrasonic driving frequency (Figure 9.1); this is consistent with the linear frequency dependence predicted by this tunnelling mechanism, although for a plateau it is not possible to make a quantitative test of the frequency-temperature dependence. The influence of other interactions, which could lead to ultrasonic attenuation in this range of temperature, has been examined using the procedures described in detail by Carini et al. (1988). The values of $\overline{P}\gamma^2$, determined using the techniques detailed by those workers, are of the same order of magnitude for both the samarium and lanthanum glasses and decrease with increasing concentration of lanthanide ion (Table 9.2.)

(ii) The high temperature acoustic attenuation has been analysed using (Jäckle 1972):

$$\alpha = \frac{B^2}{4\rho v^3 kT} \int P(E) \frac{\omega^2 \tau(E)}{1 + \omega^2 \tau^2(E)} dE \qquad (9.2)$$

where B is an average deformation potential that expresses the coupling between the ultrasonic stress and the system, $P(E)$ the activation energy E distribution function, T the absolute temperature, ω the ultrasonic angular frequency and τ the relaxation time which is connected to E for the thermally activated relaxation process of an Arrhenius type law: $\tau = \tau_0 \exp(E/kT)$.

Due to the inherent randomness of the glassy network, it is quite reasonable to assume a Gaussian distribution for $P(E)$:

$$P(E) = \frac{N}{(2\pi)^{1/2} E_0} \exp\left[-\frac{(E - E_m)^2}{2E_0^2} \right] \qquad (9.3)$$

Here N is the total number of relaxing particles per unit volume, E_m and E_0 are the most probable of the width of the distribution. From the data analysis, the values of E_m, E_0, NB^2 and τ were obtained by least-square fits of the results using a Minuit minimum search program (Carini et al. 1994a) (Table 9.2).

Typical fits of the relaxation loss are shown by a continuous line in Figure 9.5. The good fit to the shape of the experimental results, and the finding that the theoretical parameters obtained from the fits to the experimental data at various frequencies are the same within a few percent, illustrate the validity of using this theoretical approach. The relaxation parameters, resulting from this analysis, are also given in Table 9.2. The mean activation energy E_m is independent of both the type and concentration of the lanthanide ion. This finding strongly suggests that the local arrangement of the relaxing particles is not greatly influenced by the addition of the network modifier ions. The other striking feature of the results is that the product NB^2, involving the density N of the relaxing particles and the deformation potential B, decreases markedly as the samarium ion concentration is increased. Taken together, these two observations involving E_m and NB^2 suggest that the relaxing particles are sited in the phosphate

skeleton. First, if the relaxations do occur in the skeleton: the activation energy should not be greatly affected by alteration of the number of modifier ions as found. Secondly, the deformation potential B, which describes the coupling between ultrasonic stress and the two-well systems, should be dependent upon the elastic stiffness of the glass material (Hunklinger and Raychaudhury 1986). However the elastic stiffness tensor components of these glasses do not change markedly with rare earth concentration (Mierzejewski et al. 1988a), implying that neither does the deformation potential. Consequently, the quantity in NB^2 which decreases with increasing rare earth modifier content must be the density N of relaxing particles.

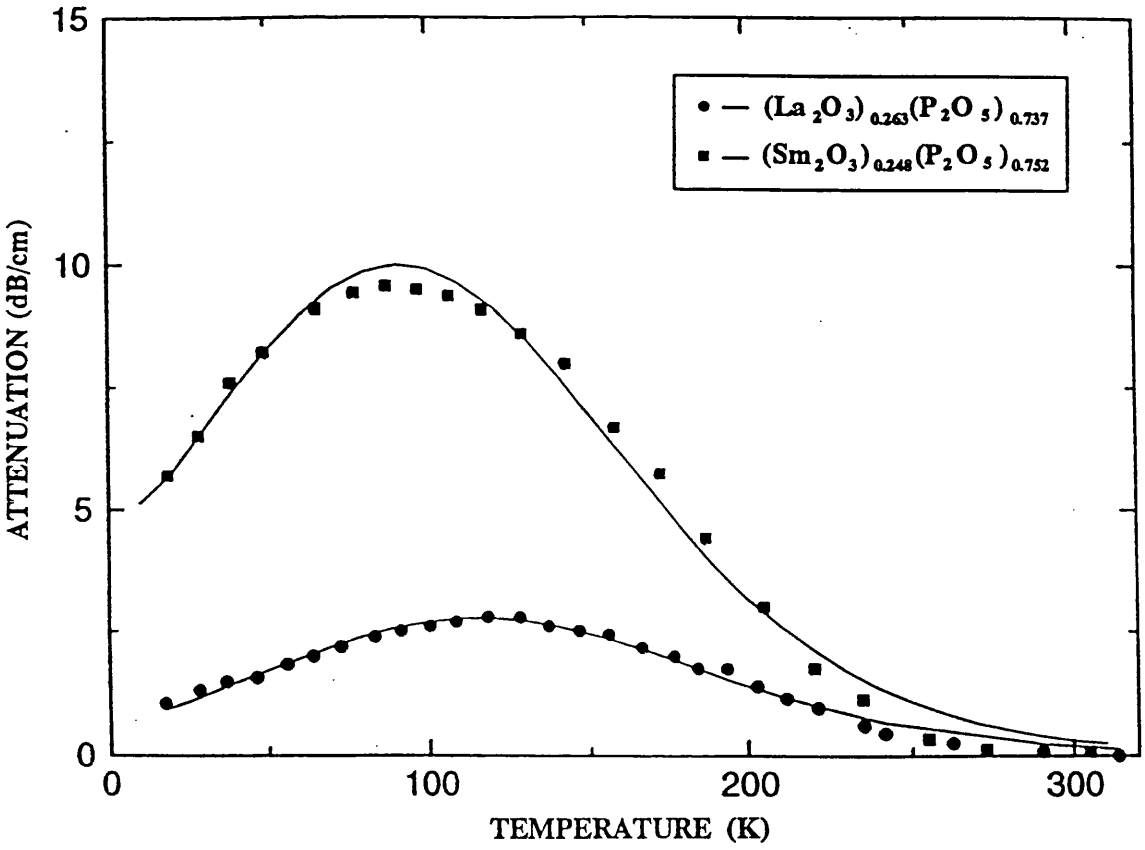

Figure 9.5. Comparison between experimental data for the ultrasonic attenuation across the broad relaxation peak and the fit with the distribution of activation energies (continuous line) for La^{3+} and Sm^{3+} phosphate glasses (after Carini et al. 1994a).

Although a number of different models have been proposed, there is broad consensus that the structural relaxations of vitreous SiO_2 and silicate glasses are associated with structural glass network. To cite briefly, in one type of model, the two-well systems have been taken to involve different configurations of the oxygen atoms which bridge neighbouring tetrahedra (Anderson and Bömmel 1955, Strakna and Savage 1964, Vuckevich 1972). More recently, it has been demonstrated that a model of harmonic libration of the coupled SiO_4 tetrahedra provides a coherent explanation of all the relaxation phenomena observed experimentally in vitreous SiO_2 (Buchenau et al. 1988). Since the skeleton of the vitreous phosphate is also constructed from corner bonded tetrahedra PO_4, it is plausible that the relaxation mechanism is similar to that operating in the silicates. Addition of modifier reduces the number of PO_4 tetrahedra which are bonded at three corners. It would also lead to a reduction in the number of degrees of freedom in the librational model. So the reduction of the number N of relaxing centres cannot in itself be used to distinguish between the two types of models depicting the relaxation mechanism.

It can be argued similarly that in the low-temperature tunnelling region below about 15K, the major effect on $\overline{P}\gamma^2$ due to the changes in the concentration of rare earth modifier ions should be on the spectral density $\overline{P}$ of the relaxation centres rather than on the deformation potential γ. Thus, the decrease in $\overline{P}\gamma^2$ with increasing concentration in the glass of both samarium and lanthanum ions (Table 9.2) may be ascribed to a reduction in this density $\overline{P}$.

Table 9.2. Values of parameters related to the thermal relaxation (E_m, E_0, τ_0 and NB^2) and to tunnelling effects (C and $\overline{P}\gamma^2$) in Sm^{3+} and La^{3+} phosphate glasses. Here γ and B are deformation potentials and $\overline{P}$ and N are TLS density of states. The density ρ and the velocity of longitudinal ultrasound v_l are those measured at room temperature (Carini et al. 1994a).

	ρ	v_l	E_m	E_0	NB^2	τ_0	C	$\overline{P}\gamma^2$
	kg/cm^3	m/s	meV	meV	$10^{20}eV^2/cm^3$	$10^{-14}s$	10^{-4}	$10^8 erg/cm^3$
$(Sm_2O_3)_x(P_2O_5)_{1-x}$								
x = 0.190	3271	4755	95	68	3.21	1.7	2.9	2.12
x = 0.248	3515	4421	99	53	1.22	4.5	2.4	1.63
$(La_2O_3)_x(P_2O_5)_{1-x}$								
x = 0.263	3413	4463	107	60	0.61	5.8	2.8	1.88

9.5 THE TEMPERATURE DEPENDENCES OF ULTRASOUND WAVE VELOCITIES

Some of the work described in this section was carried out at the University of Messina, Italy by a group headed by Prof. G. Carini assisted by Prof. G.A. Saunders. It was carried out on the glasses prepared and analysed by the present author. The results for the ternary samarium-lanthanum phosphate glasses discussed here were obtained by the present author. The interpretation of the temperature dependences of ultrasound velocities presented in this section has been submitted for publication in a paper entitled 'The Effects of Lanthanide ion Modifiers on the Local Motion of Relaxing Particles in Phosphate Glasses' by 'G. Carini, G. D'Angelo G, M. Federico, G. Tripodo, G.A. Saunders and H.B. Senin'. As that part of the work carried out at the University of Messina, Italy further extends the knowledge of the ultrasonic and vibrational properties of the rare earth phosphate glasses studied to much lower temperature, it forms a natural addition to the experimental work described in the thesis and so is included here.

The velocity of the 10 MHz longitudinal ultrasound waves decreases with increasing temperature from 1.5K to 300K in $(La_2O_3)_{0.263}(P_2O_5)_{0.737}$ and $(Sm_2O_3)_{0.248}(P_2O_5)_{0.752}$ glasses, and from 10K to 300K in $(La_2O_3)_x(Sm_2O_3)_y(P_2O_5)_{(1-x-y)}$ glasses (Figure 9.6); for these glasses, there is a continuously changing slope for temperatures below 100K and nearly linear trend for higher temperature. The decrease at low temperatures, as the temperature is increased, is greater in the glass containing lanthanum, than that with samarium. Ternary phosphate glasses display less temperature dependence.

The temperature dependences of the ultrasound velocities in these lanthanide glasses differ markedly from the expected vibrational anharmonicity which would be a nearly linear behaviour with a negative slope at high temperatures becoming flat when the temperature is lowered down to 0K. Similar behaviour has been described for the other phosphate glasses studied (see § 7.2 in Chapter 7). a-As_2S_3 and a-As_2Se_3 are a

classical example of glasses in which the sound velocity is governed by the anharmonicity only in the 40K-300K range (Claytor and Sladek 1978). In contrast, tetrahedrally bonded glasses, such as SiO_2, BeF_2 and GeO_2, show a minimum in the sound velocity over the same temperature range (see Figure 6.1 in chapter 6), which has been interpreted by several models but without a satisfactory and conclusive explanation (Hunklinger and Schickfus 1981). The present curves are similar to those obtained in pure boron dioxide (Krause 1964) and sodium borate glasses (Krause and Kurkjian 1972), which show a negative temperature coefficient in the whole range investigated, but with the interesting increasing slope at low temperatures. A quantitative explanation was not given in those cases and the experimental behaviour was interpreted as being governed by anharmonic effects at high temperatures (T>100K) and by thermally activated relaxations of structural defects (which cause peaks in the acoustic attenuation at about 60K) at low temperatures (see Figure 6.2 in Chapter 6). The existence of broad peaks between 20K and 300K in the acoustic attenuation of various phosphate glasses (see Figure 7-12-7.15 in Chapter 7) suggests that a similar interpretation can also be applied to phosphate glasses studied here.

Estimation of the magnitude of the excess contribution to the sound velocity is first needed before any insight can be gained into the microscopic mechanisms which cause the increasing slope below 100K. Anharmonic contributions have been extracted by using an extension of the quasiharmonic continuum model of Garber and Granato (1975) to isotropic materials (Claytor and Sladek 1978). The temperature dependence of the longitudinal sound velocity is

$$v_l = v_{l0}\left(\frac{L}{L_0}\right)^{\frac{3}{2}}\left[1 - T_l F\left(\frac{T}{\Theta}\right)^4\right]^{\frac{1}{2}} \qquad (9.4)$$

with

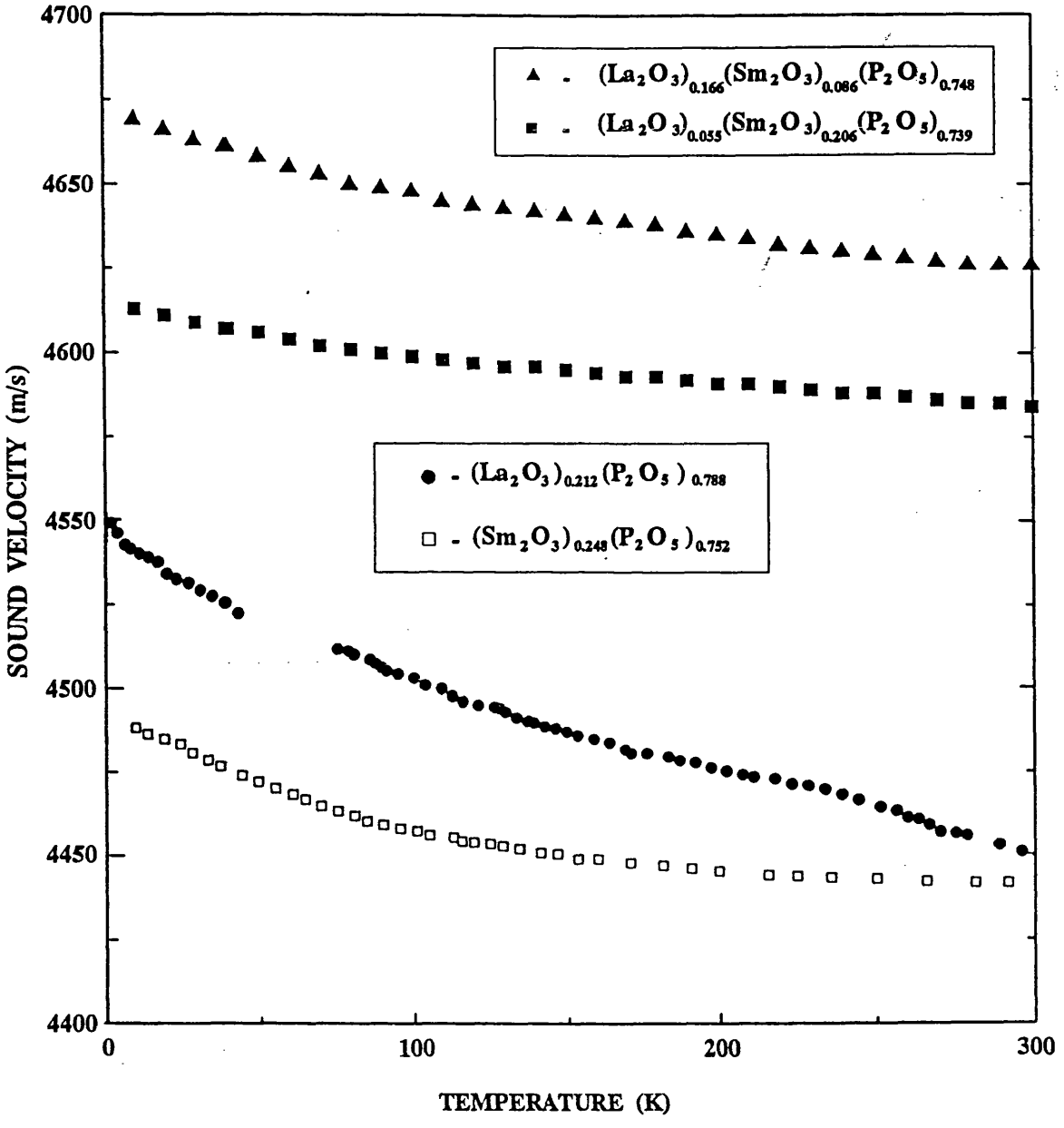

Figure 9.6. Temperature dependence of the velocity of 10MHz longitudinal sound waves in binary La^{3+}, Sm^{3+} phosphate glasses (after Carini et al. 1994a) and ternary La^{3+}- Sm^{3+} phosphate glasses.

$$F\left(\frac{T}{\Theta_D}\right)=\left[3\left(\frac{T}{\Theta_D}\right)^4\int_0^{\frac{\Theta_D}{T}}\frac{x^3dx}{e^x-1}\right] \qquad (9.5)$$

Here v_0 is the sound velocity at T equal to 0K, L is the length of the sample, Θ_D is the Debye temperature and T_l is a coefficient which depends on the Grüneisen coefficient, among other things. The constant T_l has been chosen to fit the data at high temperature where the influence of the relaxation is expected to be negligible. The length of the sample has been assumed as constant since the linear thermal expansion coefficient (~10^{-6} K^{-1} or less) is small over the whole temperature range (Wang et al. 1990). The relative difference in velocity $\Delta v/v_0$ due to anharmonic effects has been calculated for the $(La_2O_3)_{0.263}(P_2O_5)_{0.737}$ glass and is shown in Figure 9.7.

The dispersion arising from the thermally activated relaxations of the structural defects, which cause the peak of acoustic attenuation, can be expressed by (Hunklinger and Schickfus 1981):

$$\left[\frac{\Delta v}{v_0}\right]_{rel}=-\frac{B^2}{8\rho v^2 kT}\int P(E)\frac{1}{1+\omega^2\tau(E)}dE \qquad (9.6)$$

By inserting in Eq. (9.6), the values of the parameters in Table 9.2, obtained by Carini et al. (1994a) from the fit of the relaxation loss. It has been possible to access the dispersive contribution in both the lanthanum and samarium glasses. The curve in Figure 9.7 corresponds to the lanthanum glass. The summed anharmonic (Anh) and relaxation (Rel) contributions underestimate the experimental effects, emphasizing the presence of an excess term in $\Delta v/v_0$ arising from mechanisms of distinct microscopic nature (Figure 9.7). The differences obtained between the experimental values and those calculated by Eqs. (9.5) and (9.6), are given in Figure 9.8. They follow a linear trend with increasing temperature and with a slope which is larger for the lanthanum glass. Similar linear temperature dependence of the sound velocity has been observed in the a-As_2S_3, a-As_2Se_3 and a-Se, which has been attributed to the soft harmonic oscillators

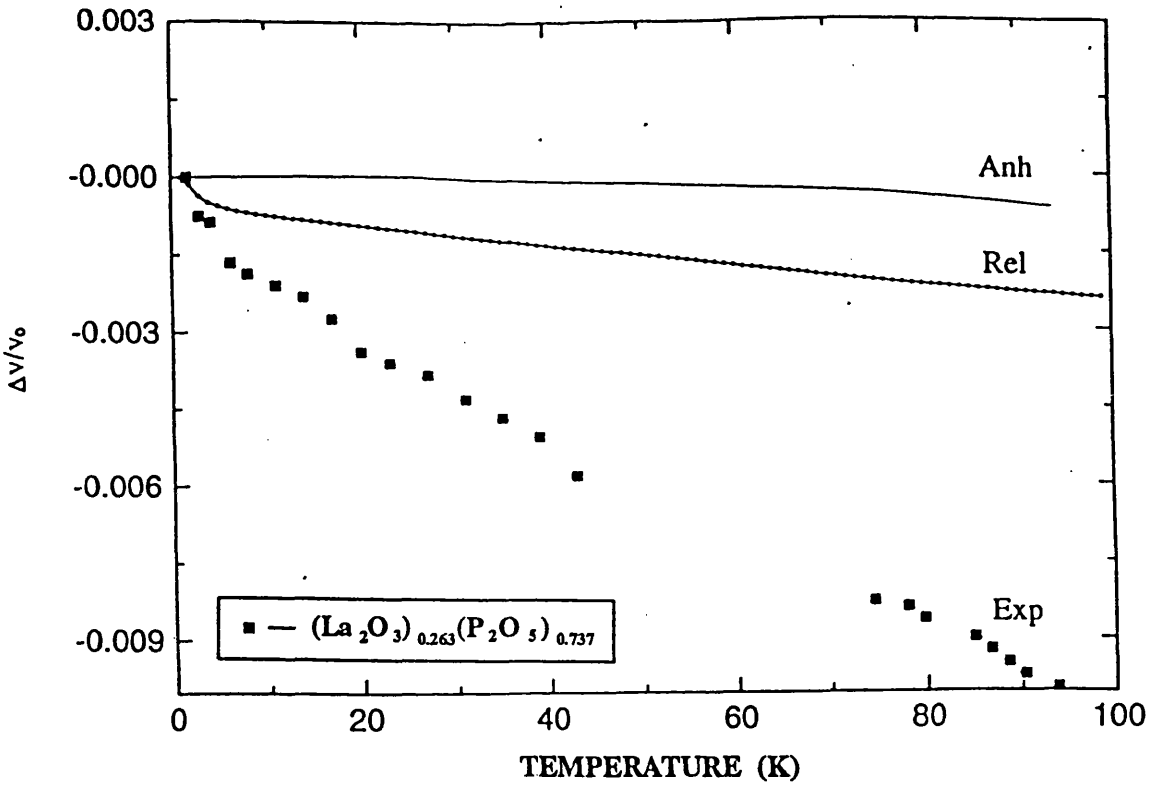

Figure 9.7. The temperature dependences of the fractional sound velocity of 10MHz ultrasounds in $(La_2O_3)_{0.263}(P_2O_5)_{0.737}$ glass. The anharmonic and relaxation contributions to $\Delta v/v_0$, calculated using Eqs. (9.5) and (9.6) respectively, are inserted to show the presence of an excess contribution to the sound velocity in this temperature region (after Carini et al. 1994a).

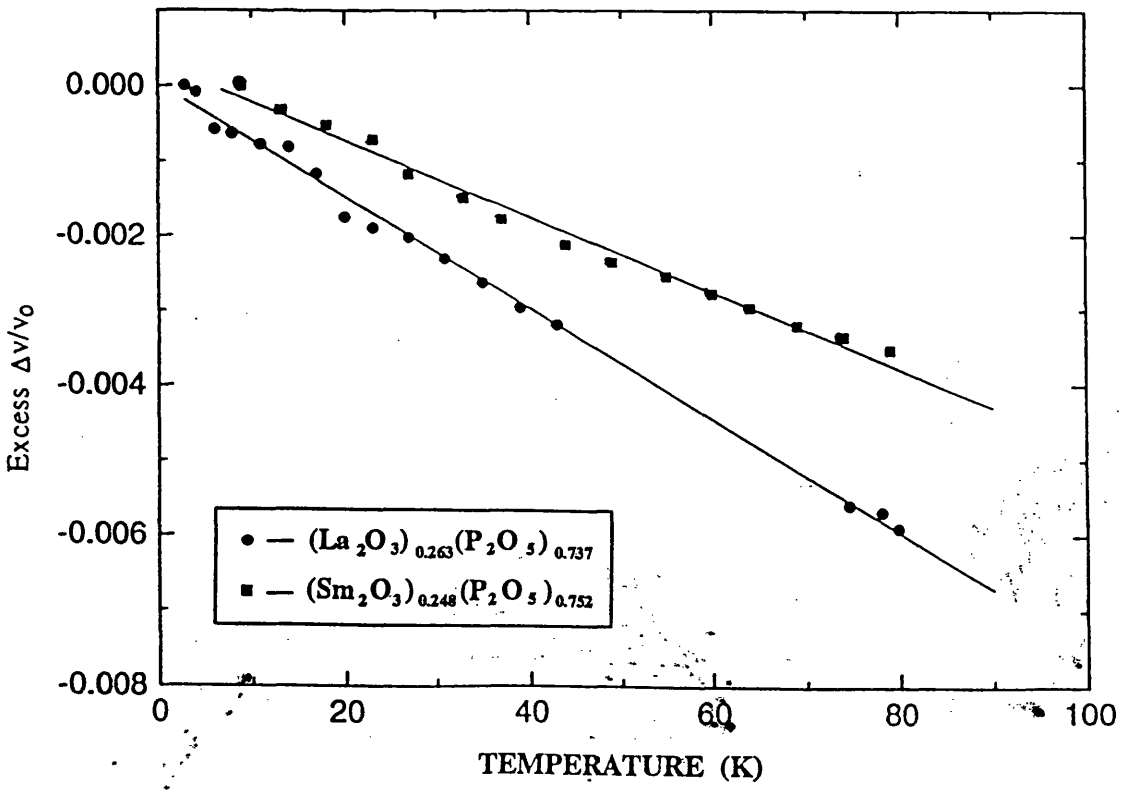

Figure 9.8. Excess contribution to the sound velocity over that provided by the addition of the anharmonic and relaxation terms for La^{3+} and Sm^{3+} phosphate glasses. The continuous lines represent the best linear fit (after Carini et al. 1994a).

contribution only (Parshin 1993).

The physical mechanisms which could contribute to the velocity in this temperature range, include TLS resonance and the same TLS phonon-assisted relaxation which is considered to cause the plateau in the acoustic attenuation for T>3K. In the $\omega T_1^{min} \ll 1$ region, the temperature dependence of $\Delta v/v_0$ due to the overlap of the two contributions, can be written as (Hunklinger and Schickfus 1981)

$$\left(\frac{\Delta v}{v_0}\right) = -nC\ln\left(\frac{T}{T_0}\right) \tag{9.7}$$

The parameters n is equal to 1/2 in the case of a direct or one-phonon process and to 5/2 in the case of a first-order Raman or two-phonon process (Dossineau et al. 1980).

The results shown in Figure 9.7 demonstrate that the excess contribution does not follow the logarithmic temperature dependence predicted by Eq. (9.7). The SPM approach, which suggests that the low-temperature anomalies in the physical properties of glasses result from a distribution of anharmonic soft potentials (Buchenau et al. 1991, Parshin 1993), provides an alternative explanation. The description of the tunnelling states and soft harmonic oscillator characterizing a glassy network originate from such potentials. The SPM predicts that, in the temperature region explored, the TLS's contribution to the sound velocity arises from phonon-assisted tunnelling ($\omega T_1^{min} \ll 1$) and from thermally activated hopping over the barrier separating the two wells, when the temperature is higher than a cross-over temperature (Galperin et al. 1989)

$$T_c \approx \frac{0.27W\ln^{1/3}(1/\omega\tau_0)}{k} .$$

Here W represents a characteristic energy in the soft anharmonic potential

$$V(x) = \varepsilon_0\left[\eta\left(\frac{x}{a}\right)^2 + \zeta\left(\frac{x}{a}\right)^3 + \left(\frac{x}{a}\right)^4\right] \tag{9.8}$$

for $\eta = \zeta = 0$; x is the generalized coordinate of the soft mode and a a characteristic length of the order of the interatomic spacing. The energy W can be evaluated from the position of the minimum ($W \approx 2kT_{min}$) in the temperature dependence of $C(T)/T^3$ (Figure

9.10). The value of T_{min} for all the glasses studied is ≈2.5K, so that T_c turns out to be ≈3K for an ultrasonic frequency of 10 MHz and $\tau_0 \sim 10^{-14}$s.

The TLS phonon-assisted relaxation gives rise to a temperature dependence of $\Delta v/v_0$ equal to that given by Eq. (9.7), while the TLS thermal relaxation produces the following contribution to the sound velocity (Karpov et al. 1983, Parshin 1993):

$$\left[\frac{\Delta v}{v_0}\right]_{rel} = -\frac{4C}{3}\left(\frac{kT}{W}\right)^{3/4} \ln^{3/4}\frac{1}{\omega\tau_0} \tag{9.9}$$

A further mechanism contributing to the sound velocity is the relaxation of HO and is due to the modulation of interlevel spacing by the sound wave. In the ultrasonic frequency range, this process causes a negligible attenuation and the following behaviour for the sound velocity (Parshin 1993):

$$\left[\frac{\Delta v}{v_0}\right]_{HO} = -\frac{28\sqrt{2}}{9}\frac{Ck}{E_0}(T - T_0) \tag{9.10}$$

In Eqs. (9.9) and (9.10), C is the same parameter as defined in Eqs. (9.1) and (9.7); $E_0 \equiv 3W$ sets the cross-over between the TLS and HO description.

Both the Eqs. (9.9) and (9.10) predict similar temperature dependence for $\Delta v/v_0$, even though the coefficient of $T^{3/4}$ in Eq. (9.9) has been evaluated as $\equiv 2.68C$, while that of $(T - T_0)$ in Eq. (9.10) $\equiv 0.29C$. This difference in magnitude enables an evaluation of the relative influences of the two mechanisms on the observed behaviour. The full lines in Figure 9.8 are a linear fit, as expressed by Eq. (9.10), to the experimental data; the slopes give a value for C of $2.62 \cdot 10^{-4}$ for the $(La_2O_3)_{0.263}(P_2O_5)_{0.737}$ glass and of $1.91 \cdot 10^{-4}$ for the $(Sm_2O_3)_{0.248}(P_2O_5)_{0.752}$ glass, respectively. Eq. (9.9) also gives a good fit to the excess $\Delta v/v_0$ providing values of C equal to $0.90 \cdot 10^{-4}$ for the $(La_2O_3)_{0.263}(P_2O_5)_{0.737}$ glass and $0.64 \cdot 10^{-4}$ for the $(Sm_2O_3)_{0.248}(P_2O_5)_{0.752}$ glass. It is found that both the values of C obtained by Eq. (9.10) are very close to those obtained by the analysis of the plateau of acoustic attenuation (Table 9.2); this provides evidence that

that the HO relaxation of the SPM is the dominant process in determining the excess contribution to the sound velocity in the temperature region below 100K.

9.6 SPECIFIC HEAT STUDY OF LOW-ENERGY VIBRATIONAL STATES

The work described in this section was also carried out at the University of Messina, Italy by the group headed by Prof. G. Carini assisted by Prof. G.A. Saunders. It was carried out on the glasses prepared and analysed by the present author. It is to be submitted for publication in a paper entitled 'Specific Heat and Low Energy Excitations of Samarium Phosphate Glasses' by 'Carini G, D'Angelo G, Tripodo G and Saunders'. As the phonon-fracton cross-over model extends the knowledge of the nature of the low-energy vibrational states of the rare earth phosphate glasses studied here, it forms a natural addition to the experimental work described in the thesis and so is included here.

The experimental results obtained for the specific heat C_p of $(Sm_2O_3)_{0.190}(P_2O_5)_{0.810}$ and $(Sm_2O_3)_{0.248}(P_2O_5)_{0.752}$ glasses between 1.5K and 30K are shown in Figure 9.9. At low temperatures the difference between C_p and C_v is negligible (Bachmann et al. 1972), especially for these glasses in which the thermal expansion is very small (Wang et al. 1990). These specific heat results, when plotted as $C(T)/T^3$, show behaviour very different from the Debye prediction (Figure 9.10). The anomalies appear in the same temperature region that the thermal conductivity should display a plateau; however this property has not yet been examined for these glasses. As the temperature is reduced below 2K, there is a steep rise; this is due to the paramagnetic contribution to the specific heat (Prof. G. A. Saunders, private communication). The present concern is mainly the peak centred at about 11K. Such feature has been observed in many glasses, including vitreous SiO_2 (Zeller and Pohl 1971), As (Jones et al. 1978) Se and AgI-Ag_2O-B_2O_3 glasses (Avogadro et al. 1987) and has been analysed in terms of the phonon-fracton

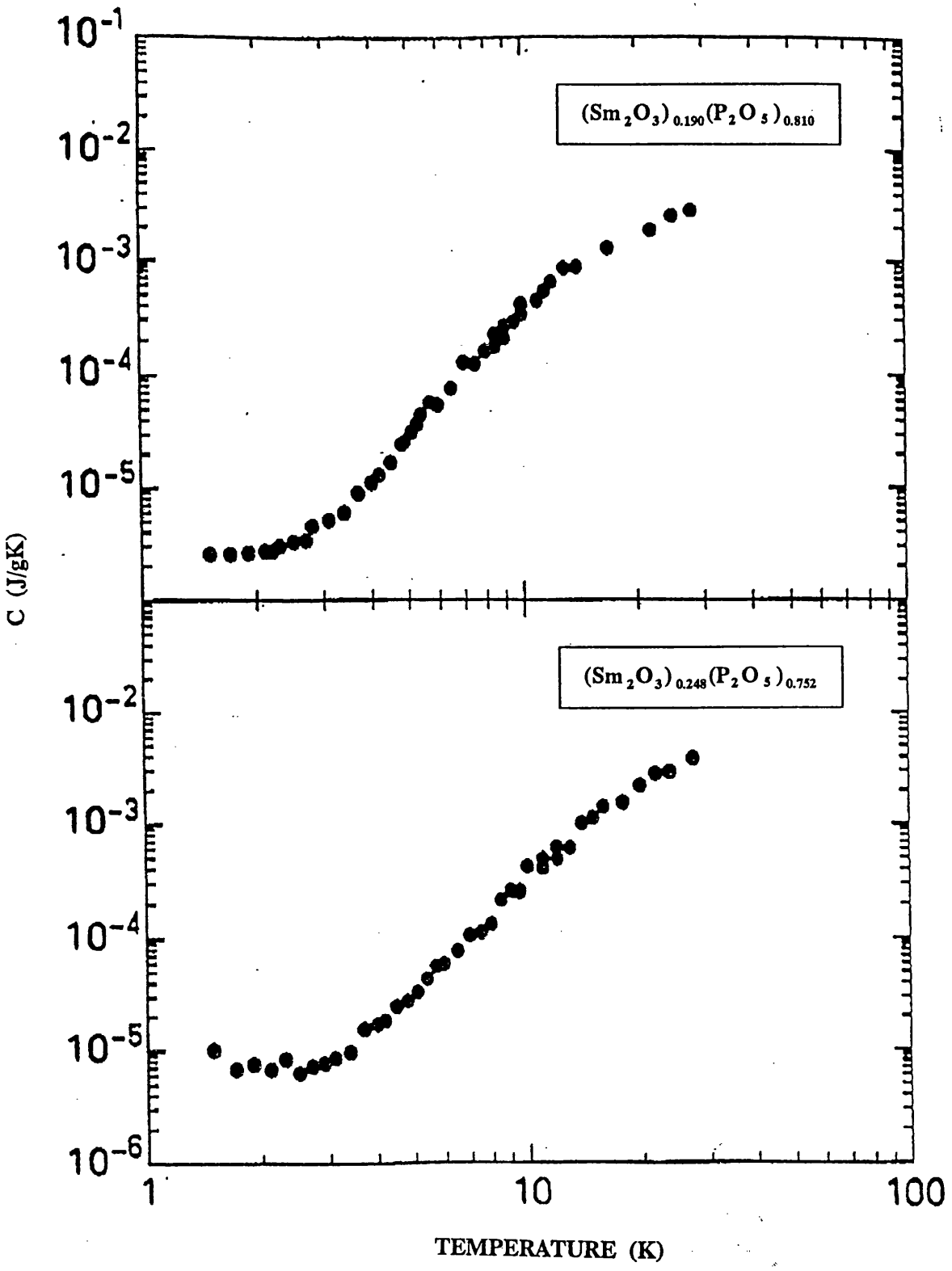

Figure 9.9. The specific heat C_p for Sm^{3+} phosphate glasses measured between 1.5K and 30K (after Carini et al. 1994b).

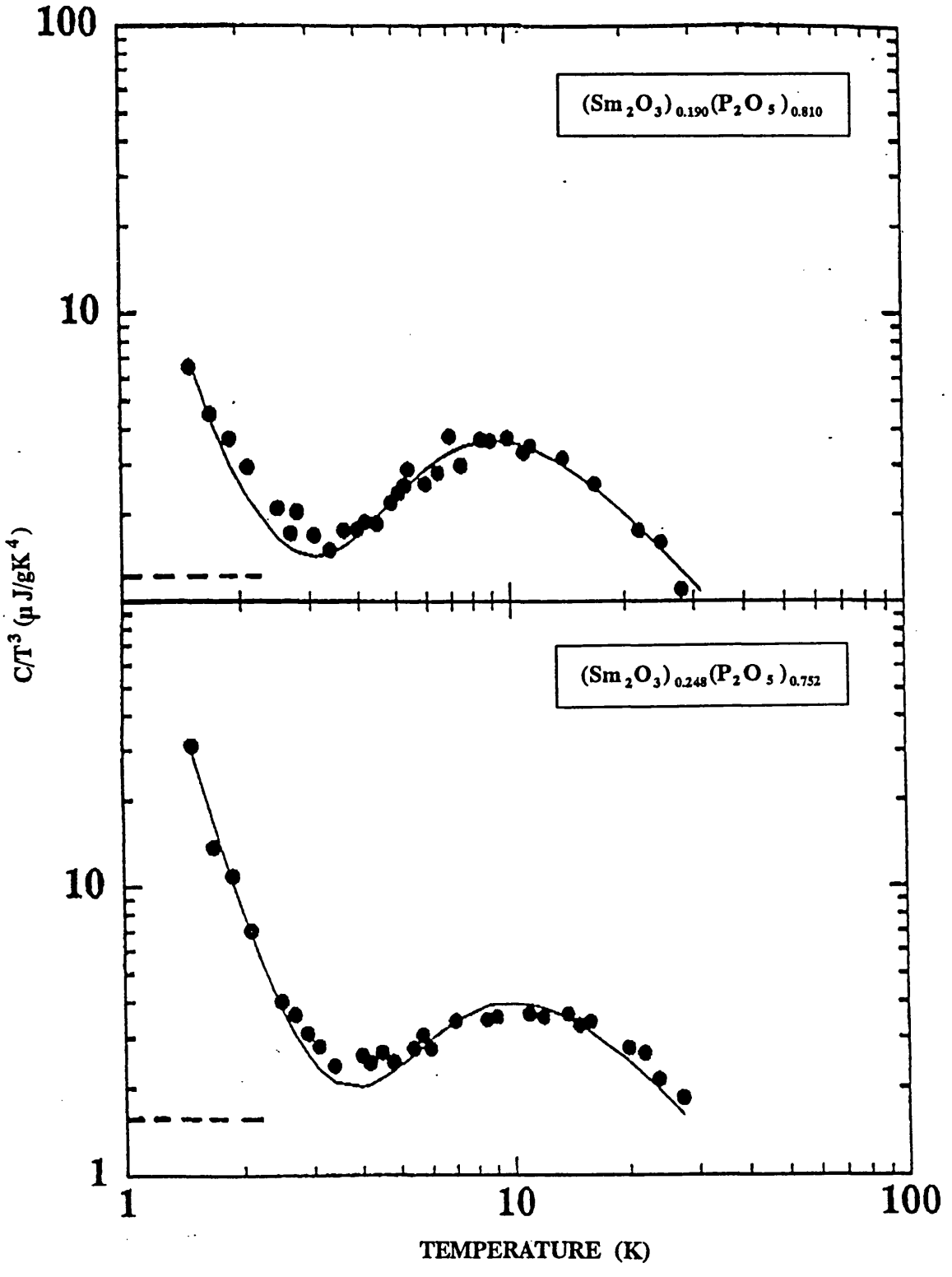

Figure 9.10. The temperature dependence of C_v/T^3 for Sm^{3+} phosphate glasses. The dotted line corresponds to the Debye elastic contribution calculated from ultrasonic wave velocities. The solid line is the best fit of the magnetic and phonon-fracton contributions to the excess specific heat (after Carini et al. 1994b).

cross-over model (Alexander et al. 1983, Orbach 1986), which predicts (Avogadro et al. 1986)

$$\frac{C}{kA} = 9n\left(\frac{T}{\Theta_D}\right)^3 \int_0^{\Theta_D/T} \frac{x^4 \exp(x)}{[\exp(x)-1]^2} dx + 9n\left(\frac{T}{\Theta_D}\right) Q \int_{\Theta_{CO}/T}^{\Theta_M/T} \frac{x^2 \exp(x)}{[\exp(x)-1]^2} dx \quad (9.11)$$

where Θ_D is the Debye temperature (Eq. (7.2) in Chapter 7), $\Theta_{CO} = \hbar\omega_{CO}/k$, $\Theta_M = \hbar\omega_M/k$ and a dimensionless constant

$$Q = \frac{D_{fr}(\omega) k \Theta_D}{9An}$$

The high frequency cut-off of the spectrum, ω_M, is determined by the normalisation condition (Avogadro et al. 1986)

$$\int_0^{\omega_M} D(\omega) d\omega = 3An \quad (9.12)$$

According to phonon-fracton cross-over model (Orbach 1986), the density of states increases as ω^2 up to a cross-over frequency ω_{CO} (Figure 2.21 in Chapter 2), corresponding to a wavelength for the Debye-type elastic modes comparable to the characteristic size of structural units in the disordered system. For frequency higher than ω_{CO}, the density of fracton states $D_{fr}(\omega)$ has a frequency dependence ω^{p-1}, p<3, with a sudden increase at ω_{CO} (Orbach 1986). In the present theoretical fit (Carini et al. 1994a), it has been assumed that p=1, so that $D_{fr}(\omega)$ is frequency-independent:

$$D_{fr}(\omega) = \frac{9AnQ}{k\Theta_D} \quad (9.13)$$

The best fit to the experimental data obtained by considering the addition of the magnetic and phonon-fracton contributions to the specific heat of the $(Sm_2O_3)_x(P_2O_5)_{1-x}$ glasses is shown by the continuous line in Figure 9.10 (Carini et al. 1994a). It can be seen that the shape of the experimental peak as a function of temperature is closely defined by the theory.

Table 9.3 summarises the parameters calculated by Carini et al. (1994a) used to fit the experimental data according to Eq. (9.11). The value of the characteristic length L in Table 9.3 has been obtained from the relationship

$$L = \left(\frac{\Theta_D}{\Theta_{CO}} \right) a \tag{9.14}$$

predicted by the phonon-fracton cross-over model (Orbach 1986), where a is an atomic distance which sets the shortest length scale in the model, and is approximated here by the average interatomic distance. The cross-over temperature Θ_{CO}, corresponding to the cross-over frequency ω_{CO}, is higher for the $(Sm_2O_3)_{0.248}(P_2O_5)_{0.752}$ glass, and in consequence the characteristic length L is shorter than found for the $(Sm_2O_3)_{0.190}(P_2O_5)_{0.810}$ glass. This is consistent with the structure of phosphate glasses discussed in Chapter 2 (§ 2.5). The $(Sm_2O_3)_{0.190}(P_2O_5)_{0.810}$ glass should have a higher degree of three-dimensional network connectivity, in consequence having a larger network coherence and longer characteristic length L than that with the metaphosphate composition.

There is a strong correlation between the temperature T_{max}, which defines the maximum in the peak in the excess specific heat and the Debye temperature Θ_D for a wide range of glasses (Figure 9.11). This can be seen as a consequence of the link between T_{max} and Θ_{CO} (Eq. 9.14), implying that the characteristic length L should be similar for all oxide glasses. In Table 9.3 the model parameters Θ_{CO}, Θ_M, L and Q determined for the samarium phosphate glasses are compared with data of glasses in other systems, such as the covalent network glass $(Ag_2O.B_2O_3)$, the superionic glasses $(AgI)_x(Ag_2O.B_2O_3)_{1-x}$ (Avogadro et al. 1986), the amorphous chalcogenide alloys $Se_{1-x}Te_x$ (Avogadro et al. 1987) and the polymeric Se types (Avogadro et al. 1987). The close similarity between the model parameters shows that this model fits the peak in the excess specific heat of the samarium phosphate in the same way as it does for the other glasses. It is also possible to make an estimate of the cross-over temperature Θ_{CO} from phonon to fracton behaviour from the low-frequency region of the Raman

scattering where the light scattering is determined by the acoustic vibrational modes.

Recently low-frequency Raman-scattering measurements have been made from 8K to room temperature on the samples of samarium phosphate glasses used for the present study (Carini et al. 1993). It was found that there is a reduction in slope of the reduced Raman intensity $I\omega/[n(\omega,T)+1]$ as a function of frequency shift at ~30 cm^{-1} (Figure 9.12). Below this frequency the slope is 3.8 which corresponds to the value expected from Debye-like density of states where the reduced Raman intensity is given by $C(\omega)g(\omega)$ with both the coupling constant $C(\omega)$ and the phonon density of states being proportional to ω^2. Above this frequency the slope is markedly lower corresponding to a possible cross-over into the fracton regime (Carini et al. 1993). A cross-over frequency of 30 cm^{-1} is equivalent to a characteristic temperature of 43K quite close to that of Θ_{CO} determined from the fit to the peak in the normalised specific heat (Table 9.3). This provides additional confirmation that these glasses show an excitation spectrum which can be explained in terms of a long-wavelength (low-frequency) phonons at low temperature and of short-wavelength localised vibrations (fracton) at higher temperature. In general the thermal and ultrasonic properties of the rare earth phosphate glasses comply with the universal observation now widely recognized for the vibrational properties of glasses.

Table 9.3. Values of the main physical quantities used in the fit of the excess of specific heat by Eq. 9-11 (Carini et al. 1994b). The results for the samarium phosphate glasses are compared with data of glasses in other systems by reference to the work of Avogadro et al. (1986, 1987)

Glasses	$\Theta_D(K)$	$\Theta_{CO}(K)$	Q	L(Å)	$Q_M(K)$	a(Å)
$(Sm_2O_3)_{0.190}(P_2O_5)_{0.810}$	387	33.8	0.065	27.7	890	2.42
$(Sm_2O_3)_{0.248}(P_2O_5)_{0.752}$	345	37.3	0.082	22.5	1050	2.44
Se	99.7	16.0	0.08	24.2	411	3.82
$Se_{0.933}Te_{0.067}$	101.4	20.6	0.14	19.2	246	3.90
$Se_{0.866}Te_{0.134}$	103.5	23.5	0.18	17.3	206	3.91
$Se_{0.79}Te_{0.21}$	105.1	24.6	0.19	16.7	200	3.92
$Ag_2O.2B_2O_3$	334	27.3	0.11	28	1035	2.27
$(AgI)_{0.2}(Ag_2O.2B_2O_3)_{0.8}$	313	23.1	0.10	31	993	2.39
$(AgI)_{0.5}(Ag_2O.2B_2O_3)_{0.5}$	255	20.1	0.12	31	722	2.41
$(AgI)_{0.65}(Ag_2O.2B_2O_3)_{0.35}$	207	17.5	0.11	30	613	2.53

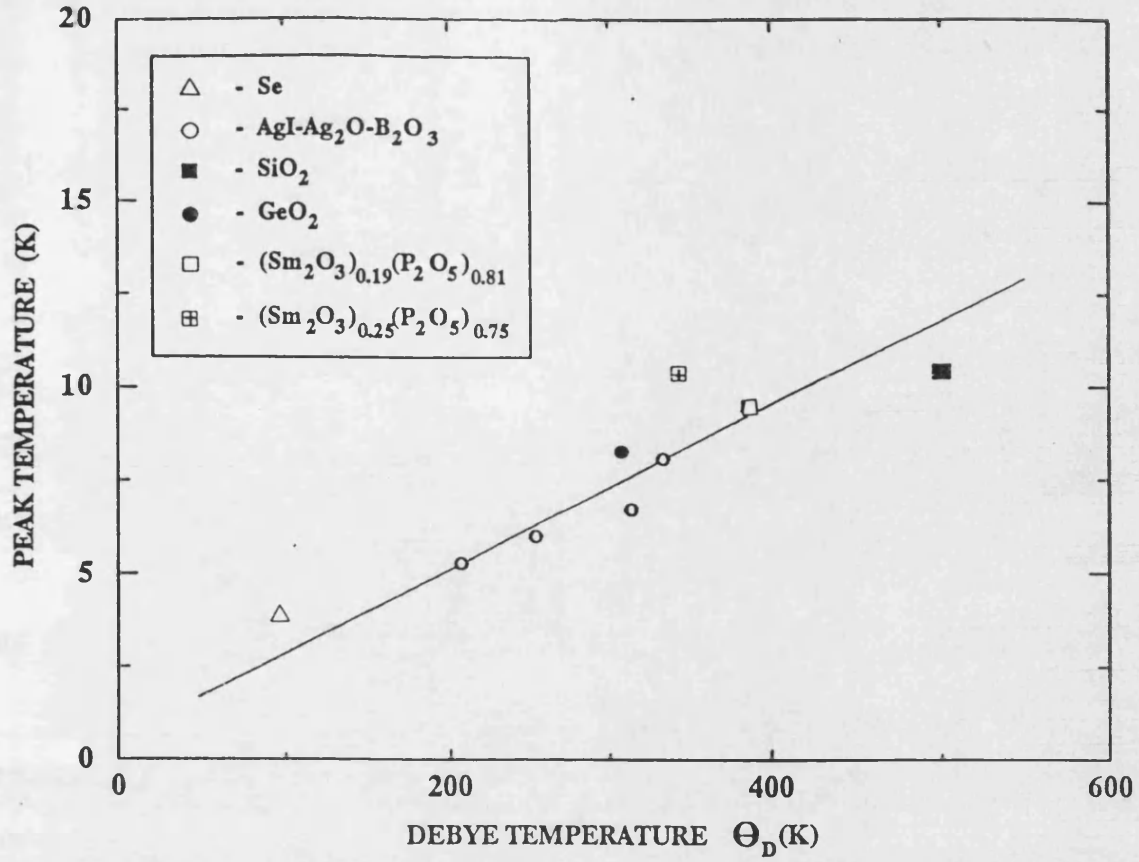

Figure 9.11. A plot of the temperature at which the maximum in C_v/T^3 occurs as a function of the Debye temperature Θ_D for a range of glasses (after Carini et al. 1994b).

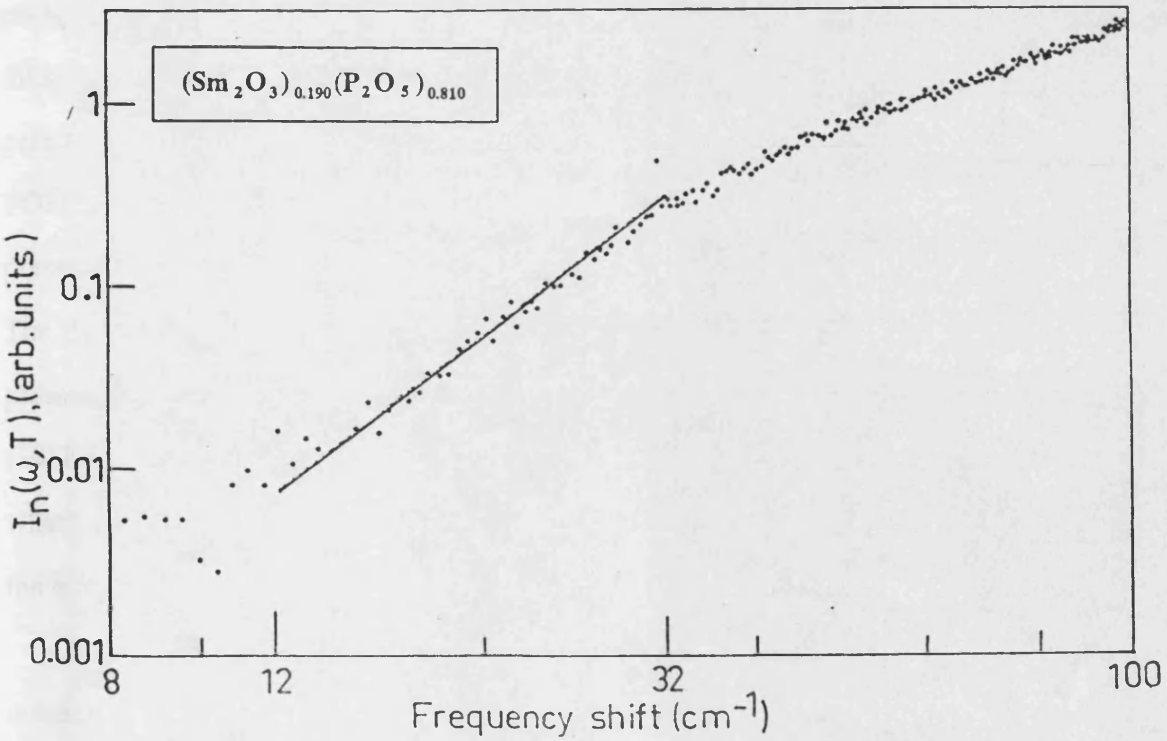

Figure 9.12. Log-log plot of reduced Raman intensity $I\omega/[n(\omega,T)+1]$, denoted as $I_n(\omega,T)$, for $(Sm_2O_3)_{0.190}(P_2O_5)_{0.810}$ glass at 8K. The slope of the straight line is 3.8 (after Carini et al. 1993).

CHAPTER 10

CONCLUSIONS AND OTHER EXPERIMENTAL INVESTIGATIONS CURRENTLY IN PROGRESS

The aim of this chapter is to present the conclusions associated with significant findings of the present work. This is followed by a list of the other experimental investigations that are presently in progress and also future work which needs to be carried out for the rare earth phosphate glasses.

10.1 SUMMARY OF THE EXPERIMENTAL RESULTS

The velocity and attenuation of 10MHz longitudinal and shear ultrasonic waves propagated in vitreous SiO_2 and rare earth phosphate glasses have been measured as a function of temperature and pressure. The hydrostatic pressure derivatives $(\partial C_{IJ}^S/\partial P)_{T,P=0}$ of the SOEC and $(\partial B^S/\partial P)_{T,P=0}$ of the bulk modulus and the long-wavelength acoustic mode Grüneisen parameters have been obtained for several rare earth phosphate glasses at room temperature. The TOEC have been calculated for vitreous SiO_2 and rare earth phosphate glasses at room temperature, and as a function of temperature from 77K to 293K, and, up to 400K for some of the phosphate glasses. The TOEC data have been used to calculate the temperature dependences of the hydrostatic pressure derivatives $(\partial C_{IJ}^S/\partial P)_{T,P=0}$ of the SOEC and $(\partial B^S/\partial P)_{T,P=0}$ of the bulk modulus. The hydrostatic pressure derivatives data have then been used to estimate the compression extrapolated to high pressures for these glasses at 77K and room temperature (293K). To gain further understanding of the thermal expansion at low temperatures, which is related to vibrational anharmonicity of the long-wavelength acoustic modes, the temperature dependences of the Grüneisen parameters have been examined.

Included, as an addition, are the experimental results and discussions of the measurements on the ultrasonic wave velocity and attenuation and also the specific heat,

for glasses manufactured and analysed here at the University of Bath, which have been recently carried out at the University of Messina, İtaly (Prof. G.A. Saunders, private communication).

10.2 CONCLUSIONS

The linear and nonlinear acoustic vibrational properties of vitreous SiO_2 and rare earth phosphate glasses found in the present study can be summarised as follows:

(A) Vitreous SiO_2

1. The velocities of both longitudinal and shear ultrasonic waves propagated in vitreous SiO_2 increase approximately linearly with increasing temperature in the temperature range between 77 and 293K. This is a well-known phenomena associated with the classical thermally activated relaxation processes which produce the broad attenuation peak characteristic of the ultrasonic wave attenuation in silicate glasses (Anderson and Bömmel 1955).

2. Vitreous SiO_2 has positive TOEC (except for the smallest and negative C_{456}) at room temperature. This being positive is consistent with the negative values found for the hydrostatic pressure derivatives $(\partial C_{IJ}^S/\partial P)_{T,P=0}$ and $(\partial B^S/\partial P)_{T,P=0}$. The TOEC increase markedly as the temperature is reduced from 293K to 77K (with the exception of C_{456}). Each of the hydrostatic pressure derivatives $(\partial C_{11}^S/\partial P)_{T,P=0}$, $(\partial C_{44}^S/\partial P)_{T,P=0}$ and $(\partial B^S/\partial P)_{T,P=0}$ become larger with decreasing temperatures; the extraordinary behaviour becomes enhanced at lower temperatures. The fact that $(\partial C_{11}^S/\partial P)_{T,P=0}$ is much greater than $(\partial C_{44}^S/\partial P)_{T,P=0}$ and C_{111} is much the largest TOEC, and is positive, showing that the pressure-induced acoustic mode softening is substantially greater for the longitudinal than for the shear acoustic modes: it is a volume effect rather than a transverse effect.

3. The long-wavelength acoustic mode Grüneisen parameters are negative throughout the whole temperature range, $|\gamma_L|$ for the longitudinal mode being numerically larger than $|\gamma_S|$ for the shear mode. As the temperature is reduced $|\gamma_L|$ increases considerably, reaching -5.5 at 77K. This confirms that these acoustic modes are softened under pressure and that the softening is enhanced at low temperatures. The mean acoustic mode Grüneisen parameters, γ^l, increases to a larger negative value (-3.1 at 77K) than previously suspected on the basis of the assumption of temperature independence TOEC: the discrepancy between the low temperature limits of the thermal, γ^h, and mean, γ^l, Grüneisen parameters is not quite so large as had been thought.

4. The anomalous elastic behaviour under pressure or with temperature of vitreous SiO_2 is consistent with a negative thermal expansion at low temperatures, where contributions from the long-wavelength, low-frequency acoustic modes play a dominant role. The pressure-induced, acoustic mode softening effects have been attributed to nonlinear acoustic contributions from bending vibrations of the bridging oxygen atoms which correspond to transverse motion against small force constants and are allowed in the open structure based on SiO_4 tetrahedra (Sato and Anderson 1980, Lambson et al. 1984). Another possible source are rotations of coupled SiO_4 tetrahedra involved in low-frequency harmonic vibrations (Buchenau et al. 1988, Guttmann and Rahman 1986).

(B) Rare earth phosphate glasses

1. The calculated values of the fractal dimension of rare earth phosphate glasses are consistent with a network intermediate between two and three dimensional connectivity.

2. At low temperatures, ultrasonic wave velocities propagated in rare earth phosphate glasses increase drastically with decreasing temperature and the ultrasonic

wave attenuation shows a broad peak. The anomalous temperature dependences of the ultrasonic wave velocities in phosphate glasses are consistent with substantial interaction of the acoustic phonons with the two-level systems through the thermally activated relaxation processes.

3. The acoustic attenuation and the sound velocity propagated in rare earth phosphate glasses show behaviour mainly determined by mechanisms having localized motions of atom groups as their microscopic origin (Carini et al. 1994a). Relaxation peaks at high temperatures and a plateau at low temperatures (below 10K) characterise the acoustic loss and exhibit similar dependences upon the modifier concentration, suggesting a common microscopic origin. The main parameters regulating both the low and high temperature anomalies can be accounted for by considering that the relaxing centres are within the phosphate skeleton of these glasses, which are built on linked PO_4 tetrahedra.

4. The temperature dependence below 100K of the ultrasound velocity propagated in rare earth phosphate glasses shows an excess contribution (over that expected from the vibrational anharmonicity and the thermally activated relaxation), which has a linear temperature dependence. This observation for binary lanthanum and samarium phosphate glasses has been interpreted (Carini et al. 1994a) using the recent soft-potential model. A comparison between the parameters obtained from modelling the plateau of acoustic attenuation and the excess contribution to the sound velocity indicates that the dominant relaxation mechanism involved has been attributed to the soft harmonic oscillators contribution only.

5. The lanthanum, cerium, praseodymium and neodymium phosphate glasses display normal elastic behaviour under pressure at room temperature. The TOEC of $(Nd_2O_3)_{0.235}(P_2O_5)_{0.765}$ and $(La_2O_3)_{0.222}(P_2O_5)_{0.778}$ are mainly negative. In marked contrast,

the TOEC of $(Eu_2O_3)_{0.186}(P_2O_5)_{0.814}$, $(Eu_2O_3)_{0.20}(P_2O_5)_{0.80}$, $(Sm_2O_3)_{0.212}(P_2O_5)_{0.788}$, $(Sm_2O_3)_{0.248}(P_2O_5)_{0.752}$ and $(Tb_2O_3)_{0.247}(P_2O_5)_{0.753}$ glasses are mainly positive. As a consequence, the hydrostatic pressure derivatives $(\partial C_{11}^S/\partial P)_{T,P=0}$ and $(\partial C_{44}^S/\partial P)_{T,P=0}$ and that of the bulk modulus $(\partial B^S/\partial P)_{T,P=0}$ of these glasses at room temperature are negative. The samarium, europium and terbium phosphate glasses display an extraordinary property of becoming easier to squeeze under pressure. Furthermore, the long-wavelength acoustic modes Grüneisen parameters are negative. These results confirm that the long-wavelength acoustic modes soften under high pressures. Similar behaviour of acoustic mode softening, but to a lesser extent, has been shown by phosphate glasses containing dysprosium, holmium and erbium.

6. The TOEC for samarium and europium glasses become more positive with decreasing temperature. The pronounced increase of the TOEC as the temperature is reduced shows that the pressure-induced acoustic mode softening becomes enhanced at lower temperatures. The hydrostatic pressure derivative $(\partial C_{11}^S/\partial P)_{T,P=0}$ is much larger than $(\partial C_{44}^S/\partial P)_{T,P=0}$ over the whole temperature range: the longitudinal mode softens more with pressure than the shear mode: this is a volume rather than a transverse effect. Furthermore, as the temperature is reduced, the magnitude of $|\gamma_L|$ gets much greater: the longitudinal acoustic mode softening becomes more enhanced at low temperatures. The shear mode $|\gamma_S|$ does get bigger but not to the same extent. As a result the mean long-wavelength acoustic mode Grüneisen parameter γ^l is also negative intimating that the net contribution from the long-wavelength acoustic phonon modes to the thermal expansion should be negative; consistent with a negative thermal expansion of $(Sm_2O_3)_{0.212}(P_2O_5)_{0.788}$ glass at low temperatures. The $(Gd_2O_3)_{0.229}(P_2O_5)_{0.771}$ and $(Tb_2O_3)_{0.247}(P_2O_5)_{0.753}$ glasses also display similar temperature dependence but rather a smaller effect than those found for $(Sm_2O_3)_x(P_2O_5)_{1-x}$ and $(Eu_2O_3)_x(P_2O_5)_{1-x}$ glasses.

Above room temperature the acoustic mode gammas are almost independent of temperature for $(Eu_2O_3)_{0.186}(P_2O_5)_{0.814}$, $(Eu_2O_3)_{0.20}(P_2O_5)_{0.80}$ and $(Tb_2O_3)_{0.247}(P_2O_5)_{0.753}$ glasses: the vibrational anharmonicities do not change much at higher temperatures.

7. The values of compression of the rare earth phosphate glasses (and also vitreous SiO_2) extrapolated to high pressure have been estimated at 77K and 293K from the ultrasonic velocity and the pressure dependence data using Anderson's equation-of-state for those glasses with negative $(\partial B^S/\partial P)_{T,P=0}$, while the Murnaghan's equation-of-state has been used for those glasses with positive $(\partial B^S/\partial P)_{T,P=0}$. The compression curves of the glasses with negative $(\partial B^S/\partial P)_{T,P=0}$ increase much faster under pressure than those with positive $(\partial B^S/\partial P)_{T,P=0}$ and display more curvature at low temperatures.

8. The hydrostatic pressure derivatives of the SOEC $(\partial C_{11}^S/\partial P)_{T,P=0}$ and $(\partial C_{44}^S/\partial P)_{T,P=0}$ and that of the bulk modulus $(\partial B^S/\partial P)_{T,P=0}$ of the ternary $(La_2O_3)_{0.055}(Sm_2O_3)_{0.206}(P_2O_5)_{0.739}$ and $(La_2O_3)_{0.166}(Sm_2O_3)_{0.086}(P_2O_5)_{0.748}$ glasses at room temperature are positive. These ternary glasses stiffen under pressure in the normal way like the binary $(La_2O_3)_x(P_2O_5)_{1-x}$ glasses. The replacement of samarium by lanthanum in the ternary glasses cancels the acoustic mode softening effect of samarium.

9. Plausibly the source of the nonlinear acoustic vibrational effects in the phosphate glasses is somewhat similar to that found for vitreous SiO_2. The acoustic vibrational modes associated with the corner linked PO_4 tetrahedra, which constitute the structure, could be responsible for the elastic anomalies of the phosphate glasses and are not due to valence instability (particularly for the case of Sm^{3+} and Eu^{3+} phosphate glasses) as previously suggested. It is suggested that either the bending vibrations of the bridging oxygens or rotations of coupled PO_4 tetrahedra could be the origin of the acoustic mode softening under pressure of the rare earth phosphate glasses.

10. An additional specific heat of samarium phosphate glasses over the prediction of the Debye theory has been interpreted (Carini et al. 1994b) in terms of phonon-fracton cross-over model. The fracton model provides a self-consistent interpretation of the thermal properties of these glasses. The calculated model parameters are found to be of the same magnitude as those found previously for a wide range of glasses. The samarium phosphate glasses comply with the universality now widely recognized for the vibrational properties of glasses.

10.3 PRESENT AND FUTURE INVESTIGATION OF RARE EARTH PHOSPHATE GLASSES

Experimental investigations on a number of properties of the rare earth phosphate glasses produced and analysed here at the University of Bath are at present in progress at other laboratories:

1. A group at Department of Physics, University of Messina, Italy, headed by Prof. G. Carini has carried out significant investigations on different properties of glasses at very low temperatures. Recently, the attenuation and velocity of ultrasonic waves over the frequency range of 10MHz to 90MHz have been measured in binary lanthanum and samarium phosphate glasses between 1.5K to 400K. To study the low energy vibrational states, specific heat measurements have been made in samarium phosphate glasses from 1.5K to 30K. The interpretation of these experimental results obtained so far in that study have been included in this thesis (with permission of Prof. G.A. Saunders).

2. Preliminary NMR measurements have been made over a wide range of temperature for rare earth phosphate glasses, in particular for the neodymium and gadolinium phosphate glasses. These measurements are being carried out at the Department of Physics, University of Witwatersrand, South Africa, by a group including Prof. M.J.R. Hoch, Dr. J.M. Keartland and Mr. I.P. Goudemond. At present, an investigation of the

crystal field interaction effect in the neodymium phosphate glasses is in progress.

3. A group at Southampton University, headed by Prof. B. Rainford, of the Department of Physics, is carrying out an investigation of the optical and magnetic properties and also structural studies using X-ray and neutron diffraction techniques. Preliminary results indicate that the rare earth ions present in these glasses are in a trivalent state with the possible exception of cerium and praseodymium metal cations which might be present as tetravalent ions. Recent preliminary results of the magnetic susceptibility measurements using 'SQUID - superconducting quantum interference device' for Gd^{3+}, Dy^{3+}, Ho^{3+} and Nd^{3+} phosphate glasses are consistent with the prediction of the Curie's law, as would have been expected, except for the praseodymium phosphate glasses. Further detailed investigations are in progress.

4. Recently an interesting and remarkable property of changing colour with the type of illumination - a phenomena known as the 'alexandrite effect' (Farrell and Newnham 1965, White et al. 1967) has been found for holmium phosphate glasses (Prof. G. A. Saunders, private communication). These glasses are yellow in daylight and dark salmon pink under a fluorescent lamp. The 'alexandrite effect' is defined as the property of a solid to change its apparent colour when viewed under different light sources (Burns 1993). Similar colour changes have also been detected in other materials containing samarium and yttrium (Schmetzer et al. 1980) and Nd^{3+}-bearing monazite (Bernstein 1982). Further investigation of this property is in progress.

REFERENCES

Aharony A, Alexander S, Entin-Wohlman O & Orbach R 1985. *Scattering of Fractons, the Ioffe-Regel Criterion, and the $\frac{4}{3}$ Conjecture.* Phys. Rev. Lett. **58** 132-135.

Ahmad N & Hutt K W 1991. *A Single-coupling-constant Bond Model for Low-frequency Raman Scattering and Infrared Absorption in Glasses.* Philos. Mag. B. **63** 1009-1013.

Alexander S & Orbach R 1982. *Density of States on fractal : <<fracton>>.* J. Phys. Lett. (Paris) **43** L625-631.

Alexander S, Laermans C, Orbach R & Rosenberg H M 1983. *Fracton interpretation of Vibrational Properties of Cross-Linked Polymers, Glasses and Irradiated Quartz.* Phys. Rev. B **28** 4615-4619.

Alexander S, Entin-Wohlman O & Orbach R 1986. *Phonon-Fracton anharmonic Interactions: The Thermal Conductivity of Amorphous Materials.* Phys. Rev. B **34** 2726-2734.

Ananthamohan C & Hogarth C A 1990. *The Effects of the Incorporation of Lutetium Oxide on the Density and Optical Properties of Copper Phosphate Glasses.* J. Mat. Sci. **25** 2115-2117.

Anderson A C 1981. *Thermal Conductivity.* Amorphous Solids Low-Temperatures Properties, Topics in Current Physics, Vol. **24** Ed. W.A. Phillips (Springer-Verlag, Berlin) p. 65.

Anderson O L 1966. *The Use of Ultrasonic Measurements Under Modest Pressure to Estimate Compression at High Pressure.* J. Phys. Chem. Solids **27** 547-565.

Anderson O L & Bömmel H E 1955. *Ultrasonic Absorption in Fused Silica at Low Temperatures and High Frequencies.* J. Am. Cer. Soc. **38** 125-131.

Anderson O L & Dienes G J 1960. *Non-Crystalline Solids.* Ed. Frechette V D (John Wiley, N.Y.) p. 449.

Anderson P W, Halperin B I & Varma C M 1972. *Anomalous Low-temperature Thermal Properties of Glasses and Spin Glasses.* Philos. Mag. **25** 1-9.

Antoniou A A & Morrison J A 1965. *Low-temperature Heat Capacity of Vitreous Germania.* J. Appl. Phys. **36** 1873-1877.

Arzeian J M & Hogarth C A 1991. *Some Structural, Electrical and Optical Properties of Copper Phosphate Glasses Containing the Rare Earth Europium.* J. Mat. Sci. **26** 5353-5366.

Aschroft N W & Mermin N D 1976. *Solid State Physics* (Saunders College, New York).

Avogadro A, Aldrovandi S & Borsa F 1986. *Specific-heat Study of the Phonon-fracton Cross-over in Glassy Ionic Conductors.* Phys. Rev. B **33**, 5637-5641.

Avogadro A, Aldrovandi S, Borsa F & Carini G 1987. *Specific-heat Study of Low-energy Excitations in Glasses.* Philos. Mag. B **56**, 227-236.

Bachmann R, DiSalvo F J, Geballe T H, Greene R L, Howard R E, King C N, Kirsch H C, Lee K N, Schwall R E, Thomas H U & Zubeck R B 1972. *Rev. Sci. Instr.* **43** 205.

Bamford C R 1977. *Coloured Generation and Control in Glasses* (Elsevier).

Bartell U & Hunklinger S 1982. *Pressure-dependence of the Low Temperature Acoustic Anomalies in Vitreous Silica.* J. Phys. (Paris) **43** 489-492.

Bateman P C 1966. *Some materials for Ultrasonic Transducer Bonding at Cryogenic Temperatures.* Acoust. Soc. Am. **41** 1011-1014.

Bell R J, Bird N F & Dean P 1968. *The vibrational spectra of Vitreous Silica, Germania and Berillium Fluoride.* J. Phys. C: Sol. Stat. Phys. **1** 299-303.

Bell R J & Dean P 1972. *The Structure of Vitreous Silica: Validity of the Random Network Theory.* Philos. Mag. **25** 1381-1398.

Benbattouche N, Saunders G A & Sidek H A A 1989. *Anharmonicity of Acoustic Modes in Vitreous* TeO_2. Philos. Mag. B **60** 643-657.

Bergman D J & Kantor Y 1984. *Critical Properties of an Elastic Fractal.* Phys. Rev. Lett. **53** 511-514.

Bernstein L W 1982. *Monazite from North Carolina having the alexandrite effect.* Amer. Mineral. **67** 356-359.

Birch F 1952. *Elasticity and Constitution of the Earth's Interior.* J. Geophys. Res. **57** 227-286.

Biscoe J, Pincus A G, Smith C S & Warren B E 1941. *J. Am. Ceram. Soc.* **24** 116.

Bobovich Y S 1962. *An investigation of the Structure of Glassy Phosphates Using Raman Spectra.* Opt. Spectry. **13** 274-277.

Bogardus E H 1965. *Third-Order Elastic Constants of Ge, MgO, and Fused* SiO_2. J. Appl. Phys. **36** 2504-2513.

Bogue R & Sladek R J 1990. *Elasticity and Thermal Expansivity of* $(AgI)_x(AgPO_3)_{1-x}$ *glasses.* Phys. Rev. **42** 5280-5288.

Bradley C C 1969. *High Pressure Methods in Solid State Research* (Butterworths, London).

Brady G W 1958. *Structure of Sodium Metaphosphate Glass.* J. Chem. Phys. **28** 48-50.

Brand O & Löhneysen H v 1991. *Rigidity Percolation and Low-Energy Excitations in Amorphous* As_xSe_{1-x}. Eur. Phys. Lett. **16** 455-460.

Brassington M P, Lambson W A, Miller A J, Saunders G A & Yogurtcu Y K 1980. *The Second- and Third-Order Elastic Constants of Amorphous Arsenic.* Philos. Mag. B **42** 127-148.

Brassington M P, Miller A J & Saunders G A 1981a. *Higher Order Elasticity of Amorphous* As_2S_3. Philos. Mag. B **43** 1049-1063.

Brassington M P, Miller A J, Pelzl J & Saunders G A 1981b. *Third Order Elastic Constants and Vibrational Anharmonicity of a Semiconducting Iron Phosphate Glasses.* J. Non-cryst. Solids **44** 157-169.

Brassington M P, Tu Hailing, Miller A J & Saunders G A 1981c. *Elastic Constants of a Fluorozirconate Glass.* Mat. Res. Bull. **16** 613-621.

Brassington M P 1982. *Vibrational Anharmonicity and the Elastic Phase Transition of Indium-Thallium Alloys.* PhD thesis. University of Bath.

Brassington M P & Saunders G A 1982. *Vibrational Anharmonicity and the Elastic Phase Transition of Indium-Thallium Alloys.* Proc. R. Soc. Lond. **A387** 289-310.

Bridge B, Patel N D & Waters D N 1983. *On the Elastic Constants and Structure of the Pure Inorganic Oxide Glasses.* Phys. Stat. Sol. A **77** 655-668.

Bridge B & Patel N D 1986. *Correlation between Low-temperature Ultrasonic Relaxation Parameters and Other Physical Properties for the Oxide Glasses.* J. Mat. Sci. Lett. **5** 1255-1257.

Bridgman P W 1948. *Proc. Am. Acad. Arts Sci.* **76** 55; **76** 71.

Bridgman P W 1958. *The Physics of High Pressure* (G Bell & Sons, London).

Brüesch P 1982. *Phonons: Theory and Experiments I (Lattice Dynamics and Methods of Interatomic Forces)* (Springer-Verlag, Berlin).

Brugger K 1964. *Thermodynamic Definition of Higher Order Elastic Coefficients.* Phys. Rev. **133** A1611-A1612.

Brugger K 1965. *Determination of Third-Order Elastic Coefficients in Crystals.* J. Appl. Phys. **36** 768-773.

Brugger K & Fritz T C 1967. *Grüneisen Gamma from Elastic Data.* Phys. Rev. **157** 524-531.

Buchenau U, Prager M, Nücker N, Dianoux A J, Ahmad N & Phillips W A 1986. *Low-Frequency Modes in Vitreous Silica.* Phys. Rev. B **34** 5665-5673.

Buchenau U 1987. *Low Lying Excitations in Silica.* Phys. Scripta. **19** 350-353.

Buchenau U, Zhou H M, Nucker N, Gilroy K S & Phillips W A 1988. *Structural Relaxation in Vitreous Silica.* Phys. Rev. Lett. **60**, 1318-1321.

Buchenau U, Galperin Yu. M, Gurevich V L & Schober H R 1991. *Anharmonic Potentials and Vibrational Localization in Glasses.* Phys. Rev. B **43** 5039-5045.

Buchenau U, Galperin Yu. M, Gurevich V L, Parshin D A, Ramos M A & Schober H R 1992. *Interaction of Soft Modes and Sound Waves in Glasses.* Phys. Rev. B **46** 2798-2808.

Buchenau U 1993. *Soft Modes in Undercooled liquids.* Eur. Phys. News **24** 77-80.

Burn R G 1993. *Mineralogical Applications of Crystal Field Theory* (University Press, Cambridge).

Cantrell J H & Breazeale M A 1978. *Ultrasonic Investigations of the nonlinearity of Fused Silica for different hydroxyl-ion contents and homogeneities between 300K and 3K.* Phys. Rev. B **17** 4864-4870.

Carini G, Cutroni M, Fontana A, Mariotto G & Rocca F 1984. *Inelastic Light Scattering in Superionic Glasses* $(AgI)_x(Ag_2O.Nb_2O3)_{1-x}$. Phys. Rev. B **29** 3567-3572.

Carini G, Cutroni M, Federico M & Tripodo G 1988. *Microscopic Origin of Low-energy Excitations in Superionic Glasses.* Phys. Rev. B **37** 7021-7026.

Carini G, Cutroni M, D'Angelo G, Federico M, Galli G, Saunders G A & Tripodo G 1990a. *Anelastic Relaxations in Rare Earth Phosphate Glasses.* Phonons 90. Ed. Hunklinger S, Ludwig W & Weiss G (World Scientific, Singapore) p. 519.

Carini G, Cutroni M, D'Angelo G, Federico M, Galli G, Tripodo G, Saunders G A & Wang Qingxian 1990b. *Elastic and Anelastic Properties of Rare Earth Phosphate Glasses.* J. Non-Cryst. Solids **121** 288-293.

Carini G, Federico M, Fontana A & Saunders G A 1993. *Low-Frequency Light Scattering and Structural Defects in Samarium Phosphate Glasses.* Phys. Rev. B **47** 3005-3010.

Carini G, D'Angelo G, Federico M, Tripodo G. Saunders G A & Senin H B 1994a. *The Effects of Lanthanide ion Modifiers on the Local Motion of Relaxing Particles in Phosphate Glasses.* Submitted to publication.

Carini G, D'Angelo G, Tripodo G and Saunders G A 1994b. *Specific Heat and Low Energy Excitations of Samarium Phosphate Glasses.* To be submitted for publication.

Chan O K, Chen F C, Choy C L &Ward I M 1978. *The Elastic Constants of Extruded Polypropylene and Polyethylene Terephthalate.* J. Phys. D **11** 617-629.

Chang Fanggao 1992. *Ultrasonic Studies on Polyethylene, Polymethylmethacrylate and Filled Ethylene Propylene Hexadiene Terpolimer.* M. Phil. Thesis. University of Bath.

Chow K, Phillips W A & Bienenstock A I 1973. *Phase transitions.* Ed. Henisch H K & Roy R (Pergamon Press, New York) p. 333

Claytor T N & Sladek R J 1978. *Ultrasonic Velocities in Amorphous As_2S_3 and As_2S_3 between 1.5 and 296K.* Phys. Rev. B 18 5842-5850.

Codden G, Vacher R, Woignier T, Pelous J & Courtens E 1989. *A Neutron Scattering Study of the Vibrational-States of Fractal Silica Aerogels.* J. Phys. (Paris) **50** 7384-7387.

Comins J D, Macdonald J E, Lambson E F, Saunders G A, Rowell A J & Bridge B 1987. *The Elastic Behaviour and Vibrational Anharmonicity of Molybdenum Phosphate Glasses.* J. Mat. Sci. **22** 2113-2118.

Corbridge D E C 1974. *The Structure Chemistry of Phosphorus.* (Elsevier, New York).

Corima R L, Mackenzie J D and Turnbull D 1963. *Viscous Flow and Melt Allotropy of Phosphorus Pentoxide.* J Appl. Phys. **34** 2245-2248.

deDecker H C J & MacGillavry C H 1941. *Rec. Trav. Chim.* **60** 153.

Devine R A B, Dupree R, Farnan I & Capponi J J 1987. *Pressure-Induced Bond-Angle Variation in Amorphous SiO_2.* Phys. Rev. B **35** 2560-2562.

Doremus R H 1973. *Glass Science* (Wiley, New York).

Doussineau P, Frenois Ch, Leisure R Levelut A & Prieur J Y 1980. J. Phys. (Paris) **41** 1193.

Dunham R W & Huntington H B 1970. *Ultrasonic Beam Mixing as a Measure of the Nonlinear Parameters of Fused Silica and Single Crystal NaCl.* Phys. Rev. B **2** 1098-1107.

Elliott S R 1990. *Physics of Amorphous Materials* (Longman, England).

Emsley J & Hall D 1976. *The Chemistry of Phosphorus* (Harper and Row, London).

Eros S & Reitz J R 1958. *Elastic Constants by the Ultrasonic Pulse Echo Method.* J Appl. Phys. **29** 683-686.

Exarhos G J, Miller P J & Risen W M Jr 1974. *Inter-ionic Vibrations and Glass Transitions in Ionic Oxide Metaphosphate Glasses.* J. Chem. Phys. **60** 4145-4155.

Farley J M 1973. *Ultrasonic Study of the Elastic Properties of Calcium Tungstate and Other Scheelites.* PhD thesis. University of Durham.

Farley J M & Saunders G A 1975a. *Elastic Properties of Semiconducting Phosphate Glasses.* Phys. Stat. Sol. A **28** 199-203.

Farley J M & Saunders G A 1975b. *Ultrasonic Wave Velocities and Attenuation in IVb-Vb-VIb Chalcogenide Glasses: 2-300K.* J Non-Cryst. Solids **18** 417-427.

Farok H M, Saunders G A, Poon W & Vass H 1992. *Low Temperature Fluorescence, Valence State and Elastic Anomalies of Samarium Phosphate Glasses.* J. Non-Cryst. Solids **142** 175-180.

Farok H M, Senin H B, Saunders G A, Poon W & Vass H 1994. *Optical and Ultrasonic Properties of Europium Phosphate Glasses.* Accepted for publication.

Farrell E F & Newham R E 1965. *Crystal-Field Spectra of Chrysoberyl, Alexandrite, Peridot, and Sinhalite.* Amer. Mineral. **50** 1972-1981.

Federle G & Hunklinger S 1982. *Ultrasonic Studies of Some Polymers at Low Temperatures.* J. Phys. (Paris) **43** 505-508.

Ferraro J R & Manghnani M H 1972. *Infrared Spectra of Several Glasses at High Pressure.* Phys. Chem. Glasses **13** 116-121.

Field M B 1969. *Elastic and Anelastic Behaviour of V_2O_5-P_2O_5 Glasses.* J. Appl. Phys. **40** 2628-2632.

Fine M E, Van Duyne H & Kenney N T 1954. *Low-Temperature Internal Friction and Elasticity Effects in Vitreous Silica.* J. Appl. Phys. **25** 402-405.

Flubacher P, Leadbetter A J, Morrison J A & Stoicheff B P 1959. *J. Phys. Chem. Solids* **12** 53

Freeman J J & Anderson A C 1986. *Thermal Conductivity of Amorphous Solids.* Phys. Rev. B **34** 5684-5690.

Galeener F L & Lucovsky G 1976. *Longitudinal Optical Vibrations in Glasses: GeO_2 and SiO_2.* Phys. Rev. Lett. **37** 1474-1478.

Galeener F L & Mikkelsen Jr J C 1979. *Raman Spectra and Structure of Pure Vitreous P_2O_5.* Sol. Stat. Comm. **30** 505-510.

Galperin Yu M, Karpov V G & Kozub V I 1989. *Localized States in Glasses.* Adv. Phys. **38** 669-737.

Fuxi G 1992. *Optical and Spectroscopic Properties of Glass* (Springer-Verlag, Berlin).

Garber J A & Granato A V 1975. *Theory of the Temperature Dependence of Second-Order Elastic Constants in Cubic Materials.* Phys. Rev. B **11** 3990-3997.

Gibbons D F 1959. *On the Thermal Expansion and Grüneisen Factor of Vitreous Silica.* Phys. Chem. Sol. **11** 246-248.

Gil L, Ramos M A, Bringer A & Buchenau U 1993. *Low-Temperature Specific Heat and Thermal Conductivity of Glasses.* Phys. Rev. Lett. **70** 182-185.

Gilroy K S & Phillips W A 1981. *An Asymmetric Double-Well Potential Model for Structural Relaxation Processes in Amorphous Materials.* Philos. Mag. B **43** 735-746.

Grace J M & Anderson A C 1989. *Low-temperature Specific-heat and Thermal-conductivity of a Glassy Polymer under Applied Pressure.* Phys. Rev. B **40** 1901-1917.

Graebner J E, Golding B & Allen L C 1986. *Phonon Localization in Glasses.* Phys. Rev. **B 34,** 5696-5701.

Greaves G N, Elliott S R & Davis E A 1979. *Amorphous Arsenic.* Adv. Phys. **28** 49-141.

Greaves G N, Fontaine A, Lagarde P, Raoux D & Gurman S J 1981. *Local Structure of Silicate Glasses.* Nature **293** 611-616.

Greaves G N 1985. *EXAFS and Structure of Glass.* J. Non. Cryst. Solids **71** 203-217.

Greaves G N, Gurman S J, Gladden L F, Spence C A, Cox P, Sales B C, Boatner L A & Jenkins R N 1988. *A Structural Basis for the Corrosion Resistance of Lead-Iron-Phosphate Glasses: An X-ray Absorption Spectroscopy Study.* Philos. Mag. B **58** 271-283.

Guttmann L & Rahman S H 1986. *Modeling a "Tunneling" State in Amorphous Silicon Dioxide.* Phys. Rev. B **33** 1506-1508.

Hall D W, Brawer S A & Weber M J 1982. *Vibronic Spectra of Gd^{3+} in Metaphosphate Glasses - Comparison with Raman and Infrared Spectra.* Phys. Rev. **25** 2828-2837.

Harani R & Hogarth C A 1986. *Electrical Conductivity of Praseodymium Phosphate Glasses.* J. Mat. Sci. Lett. **5** 492-494.

Harani R & Hogarth C A 1989. *Excitonic Absorption in Cerium Phosphate Glasses.* J. Mat. Sci. Lett. **8** 150-152.

Hart S 1983. *The Elastic Moduli of Tellurite Glasses.* J. Mat. Sci. **18** 1264-1266.

Higazy A A & Bridge B 1985. *Elastic Constants and Structure of the Vitreous System Co_3O_4-P_2O_5 and their Interpretation.* J. Non-Cryst. Solids **72** 281-108.

Higazy A A, Bridge B, Hussein A & Ewaida M A 1989. *Elastic Constants and Structure of the Vitreous System ZnO-P_2O_5.* J. Acoust. Soc. Am. **86** 1453-1458.

Hogarth C A & Khan M N 1990. *The Role of Rare Earth Ions in Electronically Conducting Glasses.* J. Non-Cryst. Solids **123** 339-343.

Holder J 1970. *Improvements on Pulse Superposition Velocity Measurements.* Rev. Sci. Instr. **41** 1355-1356.

Hughes D S & Kelly J L 1953. *Second Order Elastic Deformation in Solids.* Phys. Rev. **92** 1145-1149.

Hunklinger S 1974. *Proceedings Ultrasonic Symposium* (IEEE, New York) p. 493.

Hunklinger S 1977. *Acoustic and Dielectric Properties of Glasses at Low Temperatures.* (Festkörperprobleme) Adv. Sol. Stat. Phys. **17** 1-11.

Hunklinger S & Arnold W 1976. *Ultrasonic Properties of Glasses at Low Temperatures.* Physical Acoustics. Ed. Mason W P & Thurston R N Vol **12** 155-215.

Hunklinger S & Schickfus M v 1981. *Acoustic and Dielectric Properties of Glasses at Low Temperatures.* Amorphous Solids Low-Temperatures Properties, Topics in Current Physics, Vol. **24** Ed. W.A. Phillips (Springer-Verlag, Berlin) p. 81.

Hunklinger S 1982. *Phonons in Amorphous Materials.* J. Phys. (Paris) **43** 461-474.

Hunklinger S & Raychaudhuri A K 1986. *Thermal and Elastic Anomalies in Glasses at Low Temperatures.* Prog. Low Temp. Phys. Ed. Brewer D F Vol **9** 265-344.

Huntington H B 1958. *The Elastic Constants of Crystals.* Solid State Physics. Ed. Seitz F & Turnbull D (Academic, New York) Vol. **7**.

Ignatiev F N, Karpov V G & Klinger M I 1983. *Atomic Critical Potentials and Structure of Non-Single-Well Potentials in Glasses.* J. Non-Cryst. Solids **55** 307-323.

Ilisavskii Yu V & Kulakova L A 1988. *High-Temperature Acoustic Anomalies and Superionic Conduction in Multicomponent Phosphate Glasses.* Sov. Phys. Sol. Stat. **30** 1718-1723.

Ilisavskii Y V, Kulakova L A & Tikhonov VV 1989. *Mechanisms of Elastic Relaxation of Multicomponent Phosphate Glasses.* Sov. Phys. Sol. Stat. **31** 1363-1365.

Jäckle J 1972. *On the Ultrasonic Attenuation in Glasses at Low Temperatures.* Z. Phys. **257** 212-223.

Jäckle J 1981. *Low Frequency Raman Scattering in Glasses.* Amorphous Solids Low-Temperature Properties. Topics in Current Physics. Vol. **24** Ed. Phillips W A (Springer-Verlag, Berlin) p. 135.

Jagannathan A, Orbach R & Entin-Wohlman O 1989. *Thermal Conductivity of Amorphous Materials above the Plateau.* Phys. Rev. B **39**, 13465-13477.

Jagannathan A & Orbach R 1990. *Temperature and Frequency Dependences of the Sound Velocity in Vitreous Silica due to Scattering off Localized Modes.* Phys. Rev. B **41**, 3153-3157.

James B J 1987. *Determination of the Elastic and Dielectric Properties of Quartz.* PhD thesis. University of London.

Jayaraman A, Narayanamurti V, Bucher E & Maines R G 1970. *Continuous and Discontinuous Semiconductor-Metal Transition in Samarium Monochalcogenides Under Pressure.* Phys. Rev. Letts. **25** 1430-1433.

Jiang Y S, Zhang J H, Xu W J, Ma Z T, Ying X X, Mao H F, Mao S & Li J 1986. *Preparation Techniques For Phosphate Laser Glasses.* J. Non-Cryst. Solids **80** 623-629

Jørgensen C K 1955. *Effective Quantum Numbers in d- and f-Shells.* J. Inorg. Nucl. Chem. **1** 301-308.

Jones D P, Thomas N & Phillips W A 1978. *The Low-temperature Thermal Properties of Amorphous Arsenic.* Philos. Mag. B **38**, 271-288.

Karpov V G, Klinger M I & Ignatev F N 1983. *Theory of the Low-Temperature Anomalies in the Thermal Properties of Amorphous Structures.* Sov. Phys. JETP **57** 439-448.

Kittinger E 1977. *Correction for Transducer Influence on Sound Velocity Measurements by the Pulse Echo Method.* Ultrasonic **15** 30-32.

Kohli J T, Condrate R A & Shelby J E 1993. *Raman and Infrared Spectra of Rare Earth Aluminosilicate Glasses.* Phys. Che. Glasses **34** 81-87.

Kondo K, Iio S & Sawaoka A 1981. *Nonlinear Pressure Dependence of the Elastic Moduli of Fused Quartz up to 3GPa.* J. Appl. Phys. **52** 2826-2831.

Kordes E 1939. Z. Anorg. Allgem. Chem. **241** 171-2831.

Kordes E 1941. Z. Physik. Chem. (B) **50** 194.

Kordes E & Becker H 1949. Z. Anorg. Allgem. Chem. **260** 185.

Kordes E, Vogel W & Feterowsky R 1953. Z. Electrochemie **57(4)** 282.

Kowada Y, Adachi H, & Minami T 1993. *Electronic States and Chemical Bonding in Phosphate Glasses.* J. Phys. Chem. **97** 8989-8992.

Krause J T 1971. *Variables Affecting the Acoustic Loss and Velocity of Vitreous Silica from 4 to 300oK.* J. Appl. Phys. **42** 3035-3037.

Krause J T 1973. *Anomalous Temperature-Frequency Dependence of Acoustic Properties of Vitreous Silica at Low Temperatures.* Phys. Lett. **43A** 325-326.

Krause J T & Kurkjian C R 1968. *Vibrational Anomalies in Inorganic Glass Formers.* J. Am. Cer. Soc. **51** 226-227.

Kul'bitskaya M N, Nemilov S V & Shutilov V A 1974. *Manifestation of Structure inhomogeneities in the Temperature Dependences of the Velocity of Sound in Glasses.* Sov. Phys. Sol. Stat. **16** 2319-2322.

Kurkjian C R, Krause J T, McSkimin H J, Andreatch P & Bateman T B 1972. *Amorphous Materials.* Ed. Douglas R W & Ellis B (Wiley, New York) p. 463.

Laird B B & Schober H R 1991. *Localized Low-Frequency Vibrational Modes in a Simple-Model Glass.* Phys. Rev. Lett. **66**, 636-639.

Lakkad S C 1971. *Temperature Dependence of the Elastic Constants.* J. Appl. Phys. **42** 4277-4281.

Lambson E F, Saunders G A, Bridge B & El-Mallawany R A 1984. *The Elastic Behaviour of TeO2 Glass Under Uniaxial and Hydrostatic Pressure.* J. Non-Cryst. Solids **69** 117-133.

Lambson E F, Saunders G A & Hart S 1985. *The Second and Third Order Elastic Constants of Tellurite Glasses.* J. Mat. Sci. **4** 669-673.

Lambson E F 1988. *The Elastic Behaviour of Glasses Under High Pressure.* M. Phil. Thesis. University of Bath.

Lasjaunias J C, Ravex A, Vandorpe M & Hunklinger S 1975. *The Density of Low Energy States in Vitreous Silica: Specific Heat and Thermal Conductivity Down to 25 mK.* Sol. Stat. Comm. **17** 1045-1049.

Leibfried G & Ludwig W 1961. *Theory of Anharmonic Effects in Crystals.* Solid State Physics, Ed. Seitz F & Turnbull D (Academic, New York) Vol. **12** 275.

Long M, Galison P, Alben R & Connel G A N 1976. *Model for the Structure of Amorphous Selenium and Tellurium.* Phys. Rev. B **13** 1821-1829.

Mackenzie A P 1993. *Recent Progress in Electron Probe Microanalysis.* Rep. Prog. Phys. **56** 557-604.

Malinovsky V K & Sokolov A P 1986. *The Nature of Boson Peak in Raman Scattering in Glasses.* Sol. Stat. Comm. **57** 757-761.

Malinovsky V K, Novikov V N, Parshin P P, Sokolov A P & Zemlyanov 1990. *Universal Form of the Low-Energy (2 to 10 meV) Vibrational Spectrum of Glasses.* Eur. Phys. Lett. **11** 43-47.

Mandelbrot B B 1977. *Fractals, Form, Chance and Dimension.* (Freeman, San Francisco).

Marion J E & Weber M J 1991. *Phosphate Laser Glasses.* Eur. J. Sol. Stat. Inorg. Chem. **28** 271-287.

Martin S W 1991. *Review of the Structure of Phosphate Glasses.* Eur. J. Sol. Stat. Inorg. Chem. **28**.163-205.

Mason W P 1958. *Physical Properties and the Properties of Solids* (D Van Nostrand Company, Inc. Princeton).

Matsubara E, Waseda Y, Ashizuka M & Ishida E 1988. *Structural Study of Binary Phosphate Glasses with MgO, ZnO, and CaO by X-ray Diffraction.* J. Non-Cryst. Solids **103** 117-124.

Matz W, Stachel D & Goremychkin E A 1988. *Structure of Alkaline-Earth Metaphosphate Glasses Investigated by Neutron Diffraction.* J. Non-Cryst. Solids **101** 80-89.

May J E Jr 1958. *Precise Measurements of Time Delay.* IRE Nat. Conv. Rec. **6** 134.

Maynell C A 1972. *Ultrasound Propagation in the Sodium Borosilicate Glass System.* PhD. Thesis. University of Bath.

Maynell C A, Saunders G A & Scholes S 1973. *Ultrasound Propagation in Glasses in the Metastable Immiscibility Region of the Sodium Borosilicate System.* J. Non-Cryst. Solids **12** 271-294.

McSkimin H J 1961. *Pulse Superposition Method for Measuring Ultrasonic Wave Velocities in Solids.* J. Acoust. Soc. Am. **33** 12-16.

McSkimin H J 1965. *Variations of the Ultrasonic Pulse Superposition Method for Increasing the Sensitivity of Delay-Time Measurements.* J. Acoust. Soc. Am. **37** 864-871.

McSkimin H J & Andreatch P 1962. *Analysis of the Pulse Superposition Method for Measuring Ultrasonic Wave Velocities as a function of Temperature and Pressure.* J. Acoust. Soc. Am. **34** 609-615.

McWhan D B 1967. *Linear Compression of α-Quartz to 150kbar.* J. Appl. Phys. **38** 347-352.

Mierzejewski A, Saunders G A, Sidek H A A & Bridge B 1988a. *Vibrational Properties of Samarium Phosphate Glasses.* J. Non-Cryst. Solids **104** 323-332.

Mierzejewski A, Saunders G A, Sidek H A A, Hampton R N & Al-Mummar I J 1988b. *Valence Instability of Samarium Ions in Phosphate Glasses.* J. Sol. Stat. Ion. **28-30** 778-782.

Miller P J 1979. *Low Frequency Raman Scattering and Glass Transitions in Alkali Metaphosphate Glasses.* J. Chem. Phys. **71** 997-1003.

Moeller 1973. *The Chemistry of the Lanthanides.* (Pergamon Press, UK) p. 6.

Morgan S H, Magruder III R H & Silberman E 1987. *Raman Spectra of Rare Earth Phosphate Glasses.* J. Am. Ceram. Soc. **70** C378-380.

Mozzi R L & Warren B E 1969. *The Structure of Vitreous Silica.* J. Appl. Cryst. **2** 164-172.

Murnaghan F D 1944. *Compressibility of Media Under Extreme Pressure.* Proc. Natn. Acad. Sci. **30** 244.

Musinu A, Piccaluga G & Pinna G 1990. *Structural Properties of Lead-Iron Phosphate Glasses by X-ray Diffraction.* J. Non-cryst. Solids **122** 52-58.

Nelson B N & Exarhos G J 1979. *Vibrational Spectroscopy of Cation-site Interactions in Phosphate Glasses.* J. Chem. Phys. **71** 2739-2747.

Nemanich R J 1977. *Low Frequency Inelastic Light Scattering from Chalcogenides Glasses and Alloys.* Phys. Rev. B **16**, 1655-1674.

Nga P T, Prod'homme M & Dao N Q 1991. *Studies of Lanthanide Phosphate Glasses.* Eur. J. Sol. Stat. Inor. Chem. **28** 567-579.

Nye J F 1985. *Physical Properties of Crystals* (Oxford University Press, New York).

Orbach R 1986. *Dynamics of Fractal Networks.* Science **231** 814-819.

Papadakis E P 1964. *Ultrasonic Attenuation and Velocity in three Transformation Products in Steel.* J. Appl. Phys. **35** 1474-1482.

Papadakis E P 1966. *Ultrasonic Diffraction Loss and Phase Change in Anisotropic Materials.* J. Acoust. Soc. Am. **40** 863-876.

Papadakis E P 1967. *Ultrasonic Phase Velocity by the Pulse-Echo-Overlap Method Incorporating Diffraction Phase Corrections.* J. Acoust. Soc. Am. **42** 1045-1051.

Parshin D A 1993. *Soft Potential Model and Universal Properties of Glasses.* Proc. 13th Conf. of Condensed Matter Division, European Physical Society, Germany, Regensberg, March 1993.

Parshin D A & Sahling S 1993. *Heat Release in Glasses at Low Temperatures.* Phys. Rev. B **47** 5677-5688.

Peselnick L, Meister R & Wilson W H 1967. *Pressure Derivatives of Elastic Moduli of Fused Quartz to 10 kb.* J. Phys. Chem. Solids **28** 635-639.

Piché L, Maynard R, Hunklinger S.& Jäckle J 1974. *Anomalous Sound Velocity in Vitreous Silica at Very Low Temperatures.* Phys. Rev. Lett. **32** 1426-1429.

Phillips W A 1972. *Tunnelling States in Amorphous Solids.* J. Low Temp. Phys. **7** 351-360.

Phillips W A 1981. *The Thermal Expansion of Glasses.* Amorphous Solids Low-Temperatures Properties. Topics in Current Physics, Ed. Phillips W A (Springer-Verlag, Berlin) Vol. **24** p. 53.

Phillips W A 1987. *Two Level States in Glasses.* Rep. Prog. Phys. **50** 1657-1708.

Phillips W A 1990. *Vibration and Relaxation in Glasses.* in Phonons 89. Ed. Hunklinger S, Ludwig W & Weiss G (World Scientific, Singapore) 367-374.

Pohl R O 1981. *Low Temperature Specific heat of Glasses.* Amorphous Solids Low-Temperatures Properties, Topics in Current Physics, Ed. Phillips W A (Springer-Verlag, Berlin) Vol. **24** p. 27.

Pollard H F 1977. *Sound Waves in Solids* (Pion Ltd.).

Posselt D, Kjems J K, Bernasconi A, Sleator T & Ott H R 1991. *The Thermal Conductivity of Silica Aerogel in the Phonon, the Fracton and the Particle Mode Regime.* Eur. Phys. Lett. **16**, 59-65.

Ramos M A, Gil L, Bringer A & Buchenau U 1993. *The Density of Tunnelling and Vibrational States of Glasses within the Soft-Potential Model.* Phys. Stat. Sol. A **135** 477-492.

Ravaine D 1985. *Ionic Transport Properties in Glasses.* J Non-Cryst. Solids **73** 287-303.

Rawson H 1991. *Glasses and Their Applications* (Institute of Metal, UK).

Raychaudhuri A K & Hunklinger S 1984. *Low-Frequency Elastic Properties of Glasses at Low Temperatures - Implications on the Tunnelling Model.* Z. Phys. B **57** 113-125.

Runciman W A 1958. *Absorption and Fluorescence Spectra of ions in Crystals.* Rep. Progr. Phys. **21** 30-57

Sales B C & Boatner L A 1984. *Lead-Iron Phosphate Glass: A Stable Storage Medium for High-level Nuclear Waste.* Science **226** 45-48.

Sales B C, Abraham M M, Bates J B & Boatner L A 1985. *Structural Properties of Lead-Iron Phosphate Glasses.* J. Non-Cryst. Solids **71** 103-112.

Sales B C, Ramsey R S, Bates J B & Boatner L A 1986. *Investigation of the Structural Properties of Lead-Iron Phosphate Glasses Using Liquid Chromatography and Raman Scattering Spectroscopy.* J. Non-Cryst. Solids **87** 137-158.

Sales B C 1990. *Structural Relaxation Dynamics of Phosphate Glasses: The Effects of Network Topology on the Glass Transition.* J. Non-Cryst. Solids **119** 136-150.

Samara G A & Giardini A A 1964. *High Pressure Manganin Gauge with Multiple Internal Calibrants.* Rev. Sci. Instrum. **35** 989-992.

Sato Y & Anderson O L 1980. *A comparison of the acoustic and thermal Grüneisen parameters for three glasses at elevated pressure.* J. Phys. Chem. Solids **41** 401-410.

Saunders G A, Senin H B, Sidek H A A & Pelzl J 1993. *Third-Order Elastic Constants, Vibrational Anharmonicity, and the Invar Behavior of the $Fe_{72}Pt_{28}$ Alloy.* Phys. Rev. B **48** 15801-15806.

Schmetzer K, Bank H & Gübelin E 1980. *The alexandrite effect in minerals; chrysoberyl, garnet, corundum and fluorite.* Neues Jahrb. Miner. Abh. **138** 147-164.

Schober H R & Laird B B 1991. *Localized Low-Frequency Vibrational Modes in Glasses.* Phys. Rev. B **44**, 6746-6754.

Scott V D & Love G 1983 (Eds). *Quantitative Electron-Probe Microanalysis.* (Ellis Horwood Limited, Chichester).

Senin H B, Wang Q, Saunders G A & Lambson E F 1993. *Non-linear Acoustic Properties of Samarium Phosphate Glasses.* J. Non-cryst. Solids **152** 83-96.

Shull H E 1969. *Higher Order Elastic Constants and Anharmonic Properties of Cubic Crystals with Application to NaI, KI and Vitreous Silica.* Ph.D thesis. Pennsylvania State University.

Shuker R and Gammon R W 1970. *Raman-Scattering Selection-rule Breaking and the Density of States in Amorphous Materials.* Phys. Rev. Lett. **25** 222-225.

Sidek H A A, Saunders G A, Hampton R N, Draper R C J & Bridge B 1988. *Samarium-ion Valence Instability in a Glassy Matrix.* Philos. Mag. Lett. **57** 49-53.

Simon I 1957. *Structure of Neutron-Irradiated Quartz and Vitreous Silica.* J. Am Ceram. Soc. **40** 150-153.

Slater J C 1939. *Introduction to Chemical Physics.* (McGraw-Hill, Inc. New York).

Soga N 1969. *Pressure derivatives of the Elastic Constants of Vitreous Germania at 25°C, -78.5°C and -195.8°C.* J. Appl. Phys. **40** 3382-3385..

Soules T F 1990. *Computer-Simulation of Glass Structures.* J Non-Cryst. Solids **123** 48-70.

Stokowski S E, Martin W E & Yarema S M 1980. *Optical and Lasing Properties of Fluorophosphate Glass.* J. Non-cryst. Solids **40** 481-487.

Strakna R E 1961. *Investigation of Low-Temperature Ultrasonic Absorption in Fast-Neutron Irradiated SiO_2 Glass.* Phys. Rev. **123** 2020-2026.

Strakna R E & Savage H T 1964. *Ultrasonic Relaxation Loss in SiO_2, GeO_2, B_2O_3 and As_2O_3 Glass.* J. Appl. Phys. **35** 1445-1450.

Sun K & Risen W M, Jr 1986. *Rare Earth Phosphate Glasses.* Sol. Stat. Comm. **60** 697-700.

Susman S, Volin K J, Price D L, Grimsditch M, Rino J P, Kalia R K, Vashishta P, Gwanmesia G, Wang Y & Liebermann R C 1991. *Intermediate Range Order in Permanently Densified Vitreous SiO_2 - A Neutron-Diffraction and Molecular Dynamics Study.* Phys. Rev. B **43** 1194-1197.

Suzuki K & Ueno M 1985. *Experimental Discrimination Between Bridging and Non-bridging Oxygen Phosphorus Bonds in P_2O_5, Na_2O glass by Pulse Neutron Total Scattering.* J. De Phys. **46** C8 261-265.

Tarasov V V 1963. *New Problems in the Physics of Glass,* Chapt. 5, Israel Program for Scientific Translations Ltd. Jerusalem (p. 153).

Thurston R N 1964. Physical Acoustics. Ed. Mason W P Vol **1A** 155-215.

Thurston R N & Brugger K 1964. *Third-Order Elastic Constants and the Velocity of Small Amplitude Elastic Waves in Homogeneously Stressed Media.* Phys. Rev. **133** A1604-A1610.

Tielbürger D, Merz R, Ehrenfels R & Hunklinger S 1992. *Thermally Activated Relaxation Processes in vitreous silica: An Investigation by Brillouin Scattering at High Pressures.* Phys. Rev. B **45** 2750-2760.

Toratani H, Meissner H E, Izumitani T & Stokowski S E 1987. *Phosphate Laser Glass Of Absorption Loss of 10^{-4} cm^{-1}.* J. Non-Cryst. Solids **93** 701-708

Truell R, Elbaum C & Chick B B 1959. *Ultrasonic Methods in Solid State Physics* (Academic Press, New York).

Tu Hailing, Saunders G A & Bach H 1984. *Elastic Behaviour under Pressures of Semiconducting SmS.* Phys. Rev. B **29** 1848-1857.

Van Wazer J R 1958. *Phosphorous and its compounds,* Vol.1 (Interscience Publishers, New York).

Vacher R, Courtens E, Codden G, Pelous J & Woignier T 1989. *Neutron Spectroscopy Measurement of a Fracton Density of States.* Phys. Rev. B **39** 7384-7387.

Vukcevich M R 1972. *A New Interpretation of the Anomalous Properties of Vitreous Silica.* J. Non-cryst. Solids **11** 25-63.

Walter G, Kranold, Stachel D & Götz W 1990. *Structural Studies of Metaphosphate Glasses Using Small Angle X-ray Scattering Techniques.* Phys. Chem. Glasses **31** 188-195.

Wang Q, Saunders G A, Lambson E F, Bayot V & Michenaund J P 1990. *Vibrational Anharmonicity of Vitreous Samarium Phosphate.* J. Non-Cryst. Solids **125** 287.

Wang Q, Saunders G A, Senin H B & Lambson 1992. *Temperature Dependences of the Third Order Elastic Constants and Acoustic Mode Vibrational Anharmonicity of Vitreous Silica.* J. Non-cryst. Solids **143** 65-74.

Warren B E and Biscoe J 1938. *Fourrier Analysis of X-ray Patterns of Soda-Silica Glass.* J. Amer. Ceram. Soc. **21** 259-265.

Waterman P C 1959. *Orientation Dependence of Elastic Waves in Single Crystals.* Phys. Rev. **113** 1240-1253.

Weber M J 1990. *Science and Technology of Laser Glass.* J. Non-cryst. Solids **123** 208-222.

Wells A F 1975. *Structural Inorganic Chemistry* (Clarendon Press, Oxford).

Wentorf R H 1962. *Modern Very High Pressure Techniques* (Butterworth, London).

Westman A E R 1960. *Constitution of Phosphate Glasses* in: Modern Aspects of the Vitreous State. Ed. Mackenzie J D (Butterworths, London) p. 63-91.

Weyl W A 1959. *Coloured Glasses* (Society of Glass Technology).

White G K 1964. *Thermal Expansion of Silica at Low Temperatures.* Cryogenics **4** 2-7.

White G K & Birch J F 1965. *Phys. Chem. Glasses* **6** 85

White G K 1975. *Thermal Expansion of Vitreous Silica at Low Temperatures.* Phys. Rev. Lett. **34** 204-205.

White W B, Roy R & Crichton J M 1967. *The 'alexandrite effect': An optical Study.* Amer. Mineral. **52** 867-871.

William J & Lamb J 1958. *On the Measurement of Ultrasonic Velocity in Solids.* J. Acoust. Soc. Am. **30** 308.

Winterling G 1975. *Very-Low-Frequency Raman Scattering in Vitreous Silica.* Phys. Rev. B **12** 2432-2440.

Wong J & Angell C A 1976. *Glass: Structure by Spectroscopy* (Dekker).

Wright A C 1990. *Diffraction Studies of Glass Structure.* J. Non-Cryst. Solids **123** 129-148.

Yogurtcu Y K, Lambson E F, Miller A J & Saunders G A 1980. *An Apparatus for High Precision Measurements of Ultrasonic Wave Velocity.* Ultrasonics **18** 155-159.

Yost W T & Breazeale M A 1973. *Adiabatic Third-order Elastic Constants of Fused Silica.* J. Appl. Phys. **44** 1909-1910.

Zachariasen W H 1932. *The Atomic Arrangement in Glass.* J. Am. Chem. Soc. **54** 3841-3851.

Zarzycki J 1991. *Glasses and the Vitreous state* (Cambridge).

Zeller R C & Pohl R O 1971. *Thermal Conductivity and Specific Heat of Noncrystalline Solids.* Phys. Rev. B **4** 2029-2041.

APPENDIX I

COMPUTER PROGRAMME: TOECUNI.FOR

This programme is for the computation of the third order elastic stiffness tensor components, hydrostatic pressure derivatives and the long-wavelength acoustic mode Grüneisen parameters for an isotropic material from 77K-300K. The input data are the longitudinal v_L and shear v_S ultrasonic wave velocities, and the uniaxial pressure derivative $\{(1/W)dW/dP\}_{P=0}$ for three mode configurations listed in Table 3.1. The programme was written in FORTRAN 77, has been operated in a 486-PC with the aid of the Microsoft FORTRAN Compiler V5.0.

The primary variables used are:

den, VL, VS	Density, longitudinal and shear ultrasonic wave velocities
C11, C12, C44	SOEC
YM, BW, PR	Young's modulus, bulk modulus, Poisson's ratio
M1, M2, M3	Uniaxial stress derivatives $\{(1/W)dW/dP\}_{P=0}$
C111, C112, C123, C144, C155, C456	TOEC
DC11DP, DC12DP, DC44DP, DBDP	Hydrostatic pressure derivatives of the SOEC and bulk modulus
GL, GS, AVG, AVG1	Longitudinal, shear, and means (high and low temperature) acoustic mode Grüneisen parameters

```
c    program TOECUNI.FOR
c    program to calculate TOEC using 3 modes of uniaxial stress
c    from 293-77K
     real T(100),C11(100),C44(100),M1(100),M2(100),M3(100)
     real C12(100),YM(100),BM(100),PR(100),VL(100),VS(100)
     real DWG1(100),DWG2(100),DWG3(100),E1(100),E2(100),E3(100)
     real C123(100),C144(100),C456(100),C111(100),C112(100)
     real C155(100),DC11DP(100),DC12DP(100),DC44DP(100)
     real DBDP(100),GL(100),GS(100),AVG(100),AVG1(100)
     real A1(100),A2(100),B3(100),C3(100),D1(100),D2(100),D3(100)
     real den
     integer i,N
     character file1*15,file2*15

     print *,""
     print *," TO CALCULATE THE THIRD ORDER ELASTIC CONSTANTS,"
     print *," HYDROSTATIC PRESSURE DERIVATIVES AND GRÜNEISEN"
     print *," PARAMETERS FOR AN ISOTROPIC MATERIAL"
     print *," USING THREE MODES OF UNIAXIAL STRESS"
     print *," written by HB SENIN"
     print *," 22 October 1992"
     print *,""

     PRINT *,'How many sets of data? '
     read *,N
     PRINT *,'what is the density? '
     read *,den

10   print *,'1. Input file m123.dat'
     read(*,'(a)')file1
     open(1,file=file1,err=10,status='old')
     do 30 i=1,N
20   read(1,*,end=40)T(i),VL(i),VS(i),M1(i),M2(i),M3(i)
     M1(i)=M1(i)*1E-11
     M2(i)=M2(i)*1E-11
     M3(i)=M3(i)*1E-11
30   CONTINUE

C    SAVE THE RESULTS
40   print *,"2. ENTER FILE NAME FOR OUTPUT"
     read(*,'(a)')file2
     open(2,file=file2,err=40,status='new')

C    TO CALCULATE THE ELASTIC MODULI
     do 50 i = 1,N
      C11(i)=VL(i)*VL(i)*den
      C44(i)=VS(i)*VS(i)*den
      C12(i)=C11(i)-2*C44(i)
      BM(i) =(C11(i)+2*C12(i))/3
      YM(i)=(3*C11(i)*C44(i)-4*C44(i)*C44(i))/(C11(i)-C44(i))
     PR(i)=(C11(i)-2*C44(i))/(2*C11(i)-2*C44(i))
50   CONTINUE
```

```
C    TO CALCULATE THE THİRD ORDER ELASTIC CONSTANT
     do 60 i = 1,N
     DWG1(i)=2*C11(i)*M1(i)
     DWG2(i)=2*C44(i)*M2(i)
     DWG3(i)=2*C44(i)*M3(i)
     A1(i)=2*PR(i)-1
     A2(i)=2*(4*PR(i)-1)
     B3(i)=2*(PR(i)-1)
     C3(i)=4*PR(i)
     D1(i)=YM(i)*DWG1(i)-2*PR(i)*C11(i)
     D2(i)=YM(i)*DWG2(i)+2*C44(i)
     D3(i)=YM(i)*DWG3(i)-2*PR(i)*C44(i)
     E1(i)=D1(i)/A1(i)
     E2(i)=A2(i)*(B3(i)*D3(i)-D2(i)*C3(i))/(C3(i)*A1(i)**2-B3(i)
    + *A1(i)**2)
     E3(i)=2*C3(i)*(D2(i)-D3(i))/(A1(i)*C3(i)-A1(i)*B3(i))
      C123(i)=E1(i)+E2(i)+E3(i)
        C123(i)=C123(i)
      C144(i)=(D2(i)*C3(i)-D3(i)*B3(i))/(A1(i)*C3(i)-A1(i)*B3(i))
        C144(i)=C144(i)
      C456(i)=(D3(i)-D2(i))/(C3(i)-B3(i))
        C456(i)=C456(i)
      C111(i)=C123(i)+6*C144(i)+8*C456(i)
      C112(i)=C123(i)+2*C144(i)
      C155(i)=C144(i)+2*C456(i)
60   CONTINUE

C    TO CALCULATE THE HYDROSTATIC PRESSURE DERIVATIVE
      do 70 i = 1,N
      DBDP(i)=-(C111(i)+6*C112(i)+2*C123(i))/(9*BM(i))
      DC44DP(i)=-(6*C11(i)-6*C44(i)+C111(i)-C123(i))/(6*BM(i))
      DC11DP(i)=DBDP(i)+4*DC44DP(i)/3
      DC12DP(i)=DC11DP(i)-2*DC44DP(i)
70   CONTINUE

C    TO CALCULATE THE GRÜNEISEN PARAMETERS
     do 80 i = 1,N
      GL(i)=-(3*BM(i)+2*C11(i)+C111(i)+(2*C112(i)))/(6*C11(i))
      GS(i)=-(3*BM(i)+2*C44(i)+ (C111(i)/2) - (C123(i)/2))/(6*C44(i))
       AVG(i)=(GL(i)+2*GS(i))/3
       AVG1(i)=(GL(i)/VL(i)**3 + 2*GS(i)/VS(i)**3) /(1/VL(i)**3 +
   + 2/VS(i)**3)
80   CONTINUE
C    PRINT THE RESULTS
     do 90 i=1,N
     print 100,T(i),C11(i),C44(i),BM(i),YM(i),PR(i)
     print 120,T(i),C111(i),C112(i),C123(i),C144(i),C155(i),C456(i)
     print 130,T(i),DC11DP(i),DC44DP(i),DBDP(i),GL(i),GS(i),AVG1(i)
100  FORMAT(F10.0,4X,5E10.4/)
120  FORMAT(F10.0,4X,6E10.4/)
130  FORMAT(F10.0,4X,6E10.4/)
90   CONTINUE
```

```
C     Saving the calculated results
      do 150 i=1,N
      C11(i)=C11(i)/1E9
      C44(i)=C44(i)/1E9
      BM(i)=BM(i)/1E9
      YM(i)=YM(i)/1E9
      write (2,155)T(i),C11(i),C44(i),BM(i),YM(i),PR(i)
155   FORMAT(F10.0,2X,4F10.2,2X,1F10.3)
150   CONTINUE

      WRITE (2,*)' '
      DO 160 i=1,N
      C111(i)=C111(i)/1E9
      C112(i)=C112(i)/1E9
      C123(i)=C123(i)/1E9
      C144(i)=C144(i)/1E9
      C155(i)=C155(i)/1E9
      C456(i)=C456(i)/1E9
      write (2,165)T(i),C111(i),C112(i),C123(i),C144(i),C155(i),C456(i)
165   FORMAT(F10.0,2X,6F10.2)
160   continue

      WRITE (2,*)' '
      do 170 i=1,N
      write (2,175)T(i),DC11DP(i),DC44DP(i),DBDP(i),GL(i),GS(i),AVG(i)
     +,AVG1(i)
175   FORMAT(F10.0,3X,7F10.2)
170   continue
      close(1)
      close(2)
      stop
      end
```

APPENDIX II

COMPUTER PROGRAMME: FOEC.FOR

This programme is for the computation of the fourth order elastic stiffness tensor components for an isotropic material. The programme was written in FORTRAN 77, has been operated in a 486-PC with the aid of the Microsoft FORTRAN Compiler V5.0. The primary variables used are:

den, VL, VS	Density, longitudinal and shear ultrasonic wave velocities
C11, C12, C44	SOEC
YM, BW, PR	Young's modulus, bulk modulus, Poisson's ratio
krhoN	Planck's constant*density*the number of vibrational unit per unit mass.
C111, C112, C123, C144, C155, C456	TOEC
C1111, C1112, C1144, C1122, C1123, C1166, C1266, C1244, C1456, C4444, C4455	FOEC
DC11DT, DC44DT	Temperature derivatives of the SOEC
D2C11D, D2C44D	Second pressure derivatives of the SOEC

```
c     program FOEC.FOR
C     Calculation of FOEC using set of four linear equations
c     E1 = 9X+48Y+64Z+20V
c     E2 =    9Y+24Z+ 6V
c     E3 = (3X+16Y+32Z+16V)/2*C11 + (3Y+ 8Z+ 6V)/C44
c       = (3/(2*C11))X + (8/C11+3/C44)Y + (16/C11+8/C44)Z
c          + (8/C11+6/C44)V
c     E4 = (    3t2+ 8t3+ 8t4)/2*wl  + (5t2+16t3+24t4)/wt
C       = (3/2wl+ 5/wt)Y + (4/wl+16/wt)Z + (4/wl+24/wt)V

      REAL C111(50),C112(50),C123(50),C144(50),C155(50),C456(50)
      REAL X(50),Y(50),Z(50),V(50),E1(50),E2(50),E3(50),E4(50)
      REAL T(50),C11(50),C12(50),C44(50),BM(50),PR(50),YM(50)
      REAL DC11DP(50),DC44DP(50),DC12DP(50),DC11DT(50)
      REAL DBDP(50),DC44DT(50),D2C11D(50),D2C44D(50)
      REAL A1(50),A2(50),A3(50),A4(50),B1(50),B2(50),B3(50),B4(50)
      REAL wl(50),wt(50),GL11(50),GT11(50),GL23(50),GT23(50)
      REAL AA1(50),AA3(50),DD4(50),C3(50),C2(50),C1(50),C4(50)
      REAL XX1(50),XX2(50),XX3(50),XX4(50),YY1(50),YY3(50)
      REAL ZZ1(50),ZZ3(50),VV1(50),VV3(50),D1(50),D2(50),D3(50),D4(50)
      REAL C1111(50),C1112(50),C1144(50),C1122(50),C1123(50),C1166(50)
      REAL C1266(50),C1244(50),C1456(50),C4444(50),C4455(50)
      real krhoN
      integer i,N
      character file1*15,file2*15


      print *,""
      print *,""
      print *,"* CALCULATION OF THE FOEC USING ULTRASONIC DATA"
      print *,"* FOR AN ISOTOPIC MATERIAL"
      print *,"* 17  September  1992"
      print *,"* WRITTEN BY HB SENIN"
      print *,""
      print *,""
      PRINT *,'How many sets of data? '
      read *,N
      print *,'input k rho N '
      read *,krhoN
 10   print *,'1. FILE FOR INPUT DATA "FOEC.DAT"'
      read(*,'(a)')file1
      open(1,file=file1,err=10,status='old')
      do 30 i=1,N
 20   read(1,*,end=40)T(i),C11(i),C44(i),DC11DT(i),DC44DT(i),
     + D2C11D(i),D2C44D(i),C123(i),C144(i),C456(i)
      C11(i)=C11(i)*1E9
      C44(i)=C44(i)*1E9
      DC11DT(i)=DC11DT(i)*1E6
      DC44DT(i)=DC44DT(i)*1E6
      D2C11D(i)=D2C11D(i)*1E-9
      D2C44D(i)=D2C44D(i)*1E-9
      C123(i)=C123(i)*1E9
```

```
      C144(i)=C144(i)*1E9
      C456(i)=C456(i)*1E9
30    CONTINUE

c     SAVE THE RESULTS
40    print *,"4. ENTER FILE NAME TO SAVE THE RESULTS"
      read(*,'(a)')file2
      open(2,file=file2,err=40,status='new')

C     To Calculate Bulk and Young Moduli and Poisson's Ratio
      do 50 i=1,N
       C12(i)=C11(i)-2*C44(i)
       BM(i)=(C11(i)+2*C12(i))/3
       YM(i)=(3*C11(i)*C44(i)-4*C44(i)*C44(i))/(C11(i)-C44(i))
        PR(i)=(C11(i)-2*C44(i))/(2*C11(i)-2*C44(i))
50    CONTINUE
C     To Calculate the TOEC
      do 60 i=1,N
       C112(i)=C123(i)+2*C144(i)
       C155(i)=C144(i)+2*C456(i)
       C111(i)=C123(i)+6*C144(i)+8*C456(i)
60    CONTINUE
C     TO CALCULATE THE HYDROSTATIC PRESSURE DERIVATIVES
      DO 70 i=1,NY
       DBDP(i)=-(C111(i)+6*C112(i)+2*C123(i))/(9*BM(i))
       DC44DP(i)=-(6*C11(i)-6*C44(i)+C111(i)-C123(i))/(6*BM(i))
       DC11DP(i)=DBDP(i)+4*DC44DP(i)/3
       DC12DP(i)=DC11DP(i)-2*DC44DP(i)
70    CONTINUE

C     TO CALCULATE 9X+48Y+64Z+20V = E1
      do 80 i = 1,N
      E1(i) = 9*BM(i)*BM(i)*D2C11D(i) -(1+(3*DBDP(i)))*C11(i)
     + - (4+3*DBDP(i))*(C111(i)+2*C112(i))
80    CONTINUE
C     TO CALCULATE 9Y+24Z+6V = E2
      do 90 i = 1,N
      E2(i) = 9*BM(i)*BM(i)*D2C44D(i) -(1+3*DBDP(i))*C44(i)
     + -(4+3*DBDP(i))*(C144(i)+2*C155(i))
90    CONTINUE

C     TO CALCULATE E3
      do 92 i = 1,N
      GL11(i)=- (3*BM(i)+2*C11(i)+C111(i)+2*C112(i))/(6*C11(i))
      GT11(i)=- (3*BM(i)+2*C44(i)+C144(i)+2*C155(i))/(6*C44(i))
      E3(i)=(3*dC11dT(i))/(krhoN) +6*GL11(i)*GL11(i)+
     + 12*GT11(i)*GT11(i)-(5*C111(i)+2*C112(i))/(2*C11(i))
     + -(C111(i)+2*C112(i)+4*C155(i))/C44(i)

92    CONTINUE
C     TO CALCULATE E4
      do 93 i = 1,N
      wl(i)=(C11(i)+C12(i)+2*C44(i))/2
      wt(i)=(C11(i)+3*C44(i))/4
```

```
      GL23(i)= -(C44(i)+wl(i)+(2*C155(i)))/(6*wl(i))
      GT23(i)= -(C44(i)+wt(i)+C155(i)+C144(i)/2+(3*C456(i))/2)/
     + (6*wt(i))
      E4(i)=(3*dC44dT(i))/(krhoN)+6*GL23(i)*GL23(i)+
     + 12*GT23(i)*GT23(i)-(2*C144(i)+7*C155(i)+2*C456(i))/(2*WL(i))
     + -(2*C144(i)+9*C155(i)+3*C456(i))/(2*wt(i))
93    CONTINUE

C     The operation of determinant
      do 94 i = 1, N
       A1(i) = 9
       A2(i) = 0
       A3(i) = 3/(2*C11(i))
       A4(i) = 0
       B1(i) = 48
       B2(i) =  9
       B3(i) = (8/C11(i) + 3/C44(i))
       B4(i) = (3/(2*wl(i)) + 5/(4*wt(i)))
       C1(i) = 64
       C2(i) = 24
       C3(i) = (16/C11(i) + 8/C44(i))
       C4(i) = (4/wl(i) + 4/wt(i))
       D1(i) = 20
       D2(i) =  6
       D3(i) = (8/C11(i) + 6/C44(i))
       D4(i) = (4/wl(i) + 24/(4*wt(i)))
94    continue

c     Calculation of 4 independents fourth order elastic
c     constants
c     X(i), Y(i), Z(i) and V(i)
c     Since A2 and A4 = 0 ; hence
      do 95 i = 1, N
       AA1(i) = A1(i)*B2(i)*C3(i)*D4(i)-A1(i)*B2(i)*C4(i)*D3(i)
     +  -A1(i)*B3(i)*C2(i)*D4(i)+A1(i)*B3(i)*C4(i)*D2(i)
     +  +A1(i)*B4(i)*C2(i)*D3(i)-A1(i)*B4(i)*C3(i)*D2(i)
       AA3(i) = A3(i)*B1(i)*C2(i)*D4(i)-A3(i)*B1(i)*C4(i)*D2(i)
     +  -A3(i)*B2(i)*C1(i)*D4(i)+A3(i)*B2(i)*C4(i)*D1(i)
     +  +A3(i)*B4(i)*C1(i)*D2(i)-A3(i)*B4(i)*C2(i)*D1(i)

c     DD4(i) is the denominator
      DD4(i) = AA1(i) + AA3(i)

c     calculation of X(i)
      XX1(i)=E1(i)*B2(i)*C3(i)*D4(i)-E1(i)*B2(i)*C4(i)*D3(i)
     + -E1(i)*B3(i)*C2(i)*D4(i)+E1(i)*B3(i)*C4(i)*D2(i)
     + +E1(i)*B4(i)*C2(i)*D3(i)-E1(i)*B4(i)*C3(i)*D2(i)
      XX2(i)=E2(i)*B1(i)*C3(i)*D4(i)-E2(i)*B1(i)*C4(i)*D3(i)
     + -E2(i)*B3(i)*C1(i)*D4(i)+E2(i)*B3(i)*C4(i)*D1(i)
     + +E2(i)*B4(i)*C1(i)*D3(i)-E2(i)*B4(i)*C3(i)*D1(i)
      XX3(i)=E3(i)*B1(i)*C2(i)*D4(i)-E3(i)*B1(i)*C4(i)*D2(i)
     + -E3(i)*B2(i)*C1(i)*D4(i)+E3(i)*B2(i)*C4(i)*D1(i)
     + +E3(i)*B4(i)*C1(i)*D2(i)-E3(i)*B4(i)*C2(i)*D1(i)
      XX4(i)=E4(i)*B1(i)*C2(i)*D3(i)-E4(i)*B1(i)*C3(i)*D2(i)
```

```
     + -E4(i)*B2(i)*C1(i)*D3(i)+E4(i)*B2(i)*C3(i)*D1(i)
     + +E4(i)*B3(i)*C1(i)*D2(i)-E4(i)*B3(i)*C2(i)*D1(i)
      X(i) = (XX1(i) - XX2(i) + XX3(i) -XX4(i))/DD4(i)

c     calculation of Y(i)
      YY1(i)=E2(i)*A1(i)*C3(i)*D4(i)-E2(i)*A1(i)*C4(i)*D3(i)
     + -E3(i)*A1(i)*C2(i)*D4(i)+E3(i)*A1(i)*C4(i)*D2(i)
     + +E4(i)*A1(i)*C2(i)*D3(i)-E4(i)*A1(i)*C3(i)*D2(i)
      YY3(i)=E1(i)*A3(i)*C2(i)*D4(i)-E1(i)*A3(i)*C4(i)*D2(i)
     + -E2(i)*A3(i)*C1(i)*D4(i)+E2(i)*A3(i)*C4(i)*D1(i)
     + +E4(i)*A3(i)*C1(i)*D2(i)-E4(i)*A3(i)*C2(i)*D1(i)
      Y(i) = (YY1(i) + YY3(i))/DD4(i)

c     calculation of Z(i)
      ZZ1(i)=E3(i)*A1(i)*B2(i)*D4(i)-E4(i)*A1(i)*B2(i)*D3(i)
     + -E2(i)*A1(i)*B3(i)*D4(i)+E4(i)*A1(i)*B3(i)*D2(i)
     + +A1(i)*B4(i)*E2(i)*D3(i)-A1(i)*B4(i)*E3(i)*D2(i)
      ZZ3(i)=A3(i)*B1(i)*E2(i)*D4(i)-A3(i)*B1(i)*E4(i)*D2(i)
     + -A3(i)*B2(i)*E1(i)*D4(i)+A3(i)*B2(i)*E4(i)*D1(i)
     + +A3(i)*B4(i)*E1(i)*D2(i)-A3(i)*B4(i)*E2(i)*D1(i)
      Z(i) = (ZZ1(i) + ZZ3(i))/DD4(i)

c     calculation of V(i)
      VV1(i)=A1(i)*B2(i)*C3(i)*E4(i)-A1(i)*B2(i)*C4(i)*E3(i)
     + -A1(i)*B3(i)*C2(i)*E4(i)+A1(i)*B3(i)*C4(i)*E2(i)
     + +A1(i)*B4(i)*C2(i)*E3(i)-A1(i)*B4(i)*C3(i)*E2(i)
      VV3(i)=A3(i)*B1(i)*C2(i)*E4(i)-A3(i)*B1(i)*C4(i)*E2(i)
     + -A3(i)*B2(i)*C1(i)*E4(i)+A3(i)*B2(i)*C4(i)*E1(i)
     + +A3(i)*B4(i)*C1(i)*E2(i)-A3(i)*B4(i)*C2(i)*E1(i)
      V(i) = (VV1(i) + VV3(i))/DD4(i)
       X(i) = X(i)/1E9
       Y(i) = Y(i)/1E9
       Z(i) = Z(i)/1E9
       V(i) = V(i)/1E9
      print 110,X(i),Y(i),Z(i),V(i)
110    format (4E20.4)
95     continue

c     Calculation of a complete set of the fourth order elastic
c     constants
      DO 96 I = 1, N
      C1111(i) = X(i) + 12*Y(i) + 32*Z(i) + 12*V(i)
      C1112(i) = X(i) + 6*Y(i) + 8*Z(i)
      C1144(i) = Y(i) + 2*V(i)
      C1122(i) = X(i) + 4*Y(i) + 4*V(i)
      C1123(i) = X(i) + 2*Y(i)
      C1166(i) = Y(i) + 4*Z(i) + 2*V(i)
      C1266(i) = Y(i) + 4*Z(i)
      C1244(i) = Y(i) + 2*Z(i)
      C1456(i) = Z(i)
      C4444(i) = 3*V(i)
      C4455(i) = V(i)
      print *,T(i),C1111(i),C1112(i),C1144(i),C1122(i),C1123(i)
     + ,C1166(i)
```

```
      PRINT *,' '
      PRINT *,T(i),C1266(i),C1244(i),C1456(i),C4444(i),C4455(i)
 96   CONTINUE

C     Saving the calculation
      do 98 i=1,N
      WRITE (2,97)T(i),C111(i),C112(i),C123(i),C144(i),C155(i),C456(i)
 97   FORMAT(F10.1,2X,6E10.3)
 98   CONTINUE
      write (2,*)' '
      do 135 i=1,N
      write (2,138)T(i),X(i),Y(i),Z(i),V(i),E1(i),E2(i),E3(i),E4(i)
 138  format (1x,1F10.0,2x,8E10.4)
 135  continue
      write (2,*)' '
      do 140 i=1,N
      WRITE (2,150)T(i),C1111(i),C1112(i),C1144(i),C1122(i),C1123(i)
     + ,C1166(i)
 150  FORMAT(2X,1F10.0,2X,6F15.4)
 140  CONTINUE
      write (2,*)' '
      DO 160 i = 1, N
      WRITE (2,170)T(i),C1266(i),C1244(i),C1456(i),C4444(i),C4455(i)
 170  FORMAT(2X,1F10.0,2X,5F15.4)
 160  CONTINUE
      close(1)
      close(2)
      stop
      end
```

PAPERS PRESENTED AT SCIENTIFIC CONFERENCES

1. Vibrational Anharmonicity of Vitreous Samarium Phosphate. Wang Qingxian, **H B Senin,** G A Saunders, E F Lambson, V Bayot & J-P Michenaud. 11th *Condensed Matter Division Annual General Conference*, European Physical Society, University of Exeter, UK, 8-11 April 1991.

2. Ultrasonic Studies of Rare Earth Phosphate Glasses. **H B Senin,** Q Wang, G A Saunders, R C J Draper, H M Farok, P J Ford, W Poon, H Vass & B Bridge. *Developments in Acoustic and Ultrasonics Conference*, University of Leeds, UK, 24-25 September 1991.

3. Ultrasonic Studies of Rare Earth Phosphate Glasses. **H B Senin,** Q Wang, G A Saunders, R C J Draper, H M Farok, P J Ford & B Bridge. *Annual Conference of Solid State Physics (Malaysia) - 1993*, Universiti Pertanian Malaysia, 24-26 October 1991.

4. Acoustic and Optical Properties of Rare Earth Phosphate Glasses. **H B Senin,** H M Farok, G A Saunders, Q Wang, R C J Draper, M Cankurtaran, P J Ford, W Poon, H Vass & B Bridge. *Condensed Matter Division Annual General Conference - 1991*, University of Birmingham, UK, 17-19 December 1991.

5. Linear and Nonlinear Acoustic Optical Properties of Rare Earth Phosphate Glasses. **H B Senin,** Q Wang, R C J Draper, G A Saunders, P J Ford, M Cankurtaran & W A Lambson. *12th General Conference of the Condensed Matter Division, Europium Physical Society*, Praha, Czechoslovakia, 6-9 April 1992.

6. Nonlinear Acoustic Properties of Rare Earth Phosphate Glasses. **H B Senin,** Q Wang, G A Saunders, R C J Draper, E F Lambson, M Cankurtaran, P J Ford, H A A Sidek & W A Lambson. *Annual Conference of the Progress in Physical Acoustics and Ultrasonics*, University of Oxford, UK, 22-23 September 1992.

7. Anomalous Elastic Behaviour Under Pressure - and with Temperature near 220K in $YBa_2Cu_3O_{7-x}$ and Related High Tc Superconductors. M Cankurtaran, G A Saunders,.P J Ford, D P Almond, Q Wang, E F Lambson, W A Lambson, **H B Senin** & R C J Draper. *Annual Conference of the Progress in Physical Acoustics and Ultrasonics*, University of Oxford, UK, 22-23 September 1992.

8. Manufacture and Physical Properties of Rare Earth Phosphate Glasses. **H B Senin,** Q Wang, G A Saunders, R C J Draper, E F Lambson, M Cankurtaran, P J Ford, H M Farok, H A A Sidek & W A Lambson. *Symposium on Science & Art in Glass*, Royal Institution, London, UK, 19-21 October 1992.

9. The Effect of Temperature and Pressure upon Acoustic Properties of Rare Earth Phosphate Glasses. **H B Senin,** H A A Sidek & G A Saunders. *National Symposium in Physics - 1992*, University of Malaya, Malaysia, 24 October 1992.

10. Elastic and Nonlinear Acoustic Properties of Neodymium and Samarium Phosphate Glasses. **H B Senin,** H A A Sidek, G A Saunders, P J Ford, Q Wang, R C J Draper & W A Lambson. *Advances in Amorphous State Chemistry Conference*, Scientific Societies Lecture Theatre, London, UK, 1st December 1992.

11. Nonlinear Acoustic Properties of Nd, Eu and Sm Phosphate Glasses. **H B Senin,** H A A Sidek, G A Saunders, P J Ford, Q Wang & R C J Draper. *Condensed Matter and Materials Physics Annual General Conference- 1992*, University of Sheffield, UK, 15-17 December 1992.

12. Nonlinear Acoustic Properties and Invar Behaviour of $Fe_{72}Pt_{28}$. **H B Senin,** H A A Sidek, G A Saunders, Q Wang, Ll Manosa, P J Ford & J Pelzl. *Condensed Matter and Materials Physics Annual General Conference - 1992*, University of Sheffield, UK, 15-17 December 1992.

13. Comparison of Elastic Behaviour with Temperature and Under Pressure in $YBa_2Cu_3O_{7-x}$ and $YBa_2Cu_4O_8$ High T_c Superconductors. M Cankurtaran, G A Saunders, P J Ford, D P Almond, Q Wang, E F Lambson, W A Lambson, **H B Senin** & R C J Draper. *Condensed Matter and Materials Physics Annual General Conference - 1992*, University of Sheffield, UK, 15-17 December 1992.

14. Optical and Acoustic Properties of Europium Phosphate Glasses. **H B Senin**, H M Farok, G A Saunders, P J Ford, W Poon & H Vass. *13th General Conference of the Condensed Matter Division, European Physical Society,* Universität Regensburg, Germany, 29 March - 2 April 1993.

15. Ultrasonic Studies of Nd^{3+} Phosphate Glasses. H A A Sidek, **H B Senin** & G A Saunders. *3rd General Conference of Industrial Physics*, University Kebangsaan Malaysia. 20-22 April 1993.

16. Nonlinear Acoustic Properties of Gadolinium Phosphate Glasses. **H B Senin,** P J Ford, G A Saunders & H A A Sidek. *National Conference on Physics - 2nd decade of UPM (Malaysia)*, University Pertanian Malaysia. 6-8 July 1993.

17. Magnetic Properties of Nd^{3+} Phosphate Glasses: Static Susceptibility. J M Keartland, I P Goudemond, M J R Hoch, **H B Senin,** P J Ford & G A Saunders. *39th South African Institute of Physics (SAIP) Conference*, Stellenbosch, South Africa. 6-9 July 1993.

18. Magnetic Properties of Nd^{3+} Phosphate Glasses: Spin Dynamics. I P Goudemond, J M Keartland, M J R Hoch, **H B Senin,** P J Ford & G A Saunders. *39th South African Institute of Physics (SAIP) Conference*, Stellenbosch, South Africa. 6-9 July 1993.

19. Magnetic Properties of Nd^{3+} Phosphate Glasses. J M Keartland, I P Goudemond, M J R Hoch, **H B Senin,** P J Ford & G A Saunders. *XX International Conference on Low Temperature Physics*, University of Oregon, Department of Physics, Eugene, USA, 4-11 August 1993.

20. Nonlinear Acoustic Properties of the Ternary $(La_2O_3)_x(Sm_2O_3)_y(P_2O_5)_{(1-x-y)}$ Phosphate Glasses. **H B Senin,** H A A Sidek & G A Saunders. *10th Annual General Conference of Solid State Science (Malaysia),* Nuclear Energy Unit, Malaysia, 9-10 November 1993.

21. The Effects of La^{3+} and Sm^{3+} Modifiers on the Elastic and Nonlinear Acoustic Properties of Phosphate Glasses. **H B Senin,** G A Saunders, G Carini, G D'Angelo, M Federico & G Tripodo. *Condensed Matter and Materials Physics Annual General Conference - 1993,* University of Leeds, UK, 20-22 December 1993.

22. Acoustic Mode Softening in Terbium metaphosphate Glasses. **H B Senin,** H A A Sidek & G A Saunders. *To be presented in An International Conference on Recent Advances in Materials and Mineral Resources (RAAM '94),* University Sains Malaysia. 3-5 May 1994.

PAPERS PUBLISHED IN SCIENTIFIC JOURNALS AND CONFERENCE PROCEEDINGS

1. Temperature Dependences of the Third Order Elastic Constants and Acoustic Mode Vibrational Anharmonicity of Vitreous Silica. Q Wang, G A Saunders, **H B Senin** & E F Lambson. *J. Non-Cryst. Solids* **143** 65 (1992).

2. Ultrasonic Studies of Rare Earth Phosphate Glasses. **H B Senin,** Q Wang, G A Saunders, R C J Draper, H M Farok, P J Ford, W Poon, H Vass & B Bridge. *Developments in Acoustic and Ultrasonics*, ed. M. Povey and J. McClements, Institute of Physics, London, pp. 197 (1992).

3. Ultrasonic Studies of Rare Earth Phosphate Glasses. **H B Senin,** Q Wang, G A Saunders, R C J Draper, H M Farok, M Cankurtaran & P J Ford. *Proc. of the 8th Ann. Solid State Science (UPM)* pp. 157 (1991).

4. Non-Linear Acoustic Properties of Samarium Phosphate Glasses. **H B Senin,** Q Wang, G A Saunders & E F Lambson. *J. Non-Cryst. Solids* **152** 83 (1993).

5. Manufacture and Physical Properties of Rare Earth Phosphate Glasses. **H B Senin,** Q Wang, G A Saunders, R C J Draper, E F Lambson, M Cankurtaran, P J Ford, H M Farok, H A A Sidek & W A Lambson. *Glass Technology* **34** 75 (1993).

6. A Comparison Between the Elastic and Nonlinear Acoustic Properties of Neodymium and Samarium Phosphate Glasses. **H B Senin,** H A A Sidek, P J Ford, G A Saunders, Q Wang, R C J Draper & W A Lambson. *Advances in Amorphous State Chemistry*, Society of Glass Technology, UK, pp. 55 (1993).

7. Vibrational Properties of Europium Phosphate Glasses. **H B Senin,** H M Farok, H A A Sidek, G A Saunders & P J Ford. *Journal of Solid State Science and Technology (Malaysia)* **1** 18 (1993).

8. Effect of Temperature and Pressure on the Elastic Behaviour of Rare Earth Phosphate Glasses. H A A Sidek, S A Halim, **H B Senin** & G A Saunders. *Journal of Solid State Science and Technology (Malaysia).* **1** 50 (1993).

9. Third Order Elastic Constants, Vibrational Anharmonicity, and the Invar Behaviour of the $Fe_{72}Pt_{28}$ alloy. G A Saunders, **H B Senin**, H A A Sidek & J Pelzl. *Phys. Rev. B*, **48** 15801 (1993).

10. Magnetic Properties of Nd^{3+} Phosphate Glasses. J M Keartland, I P Goudemond, M J R Hoch, **H B Senin**, P J Ford & G A Saunders. *Low. Temp. Phys. Conf. Proc*, In press (1993).

11. Contrasting effects of Lanthanum and Samarium Modifiers on the Elastic and Nonlinear Acoustic Properties of Phosphate Glasses. **H B Senin,** G A Saunders, Li Jiaqiang & P J Ford. *J. Mat. Sci.* **29** 562-568 (1994).

Papers accepted for publication.

1. Pressure Induced Acoustic Mode Softening in Gadolinium Metaphosphate Glasses. **H B Senin**, G A Saunders, Li Jiaqiang & P J Ford. *Phys. Chem. Glasses.*

2. Temperature and Pressure Derivatives of the SOECs of Rare Earth Phosphate Glasses. **H B Senin,** H A A Sidek & G A Saunders. *Jurnal Fizik Malaysia (IFM).*

3. High Pressure Ultrasonic Studies on Neodymium Phosphate Laser Glass (Kajian Ultrasonik Tekanan Tinggi ke atas Kaca Laser Neodymium Fosfat) H A A Sidek, **H B Senin,** G A Saunders & P J Ford. *Bulletin Fizik (UTM) Malaysia* (In Malay).

4. The Acoustic Properties of Neodymium Phosphate Glasses Under Pressure. H A A Sidek, **H B Senin,** G A Saunders & P J Ford. *Jurnal Fizik Malaysia (IFM).*

5. Optical and Acoustic Properties of Europium Phosphate Glasses. H M Farok, **H B Senin,** G A Saunders, W Poon & H Vass. *J. Mat. Sci.*

6. Magnetic Investigation of Rare Earth Phosphate Glasses. P J Ford, C D Graham Jr, G A Saunders, **H B Senin** & J Cooper. *J. Mat. Sci. Lett.*

Papers submitted for publication.

1. The effects of Lanthanide ions Modifiers on the Local Motion of Relaxing Particles in Phosphate Glasses. G Carini, G D'Angelo, M Federico, G Tripodo, G A Saunders & **H B Senin.**